Dottorato in Ingegneria Geotecnica – *XV Ciclo*
Consorzio tra le Università di Roma *La Sapienza* e Napoli *Federico II*

Diaphragm walls to mitigate ground movements induced by tunnelling

Experimental and numerical analysis

Emilio Bilotta

A thesis submitted for the degree of Dottore di Ricerca

Supervisor:	Prof Carlo Viggiani	(Università di Napoli *Federico II*)
Co-Tutors:	Prof Renato Ribacchi	(Università di Roma *La Sapienza*)
	Prof David Nash	(University of Bristol, UK)
External Referees:	Prof Neil Taylor	(City University London, UK)
	Prof Sarah Stallebrass	(City University London, UK)

Roma, Aprile 2004

Dipartimento di Ingegneria Geotecnica – Università di Napoli *Federico II*

Contents

Acknowledgements

My research activity has been carried out under the guidance of Prof Carlo Viggiani, who proposed to me the topic to study. I am particularly indebted to him: in many occasions he stimulated my curiosity, encouraged my initiatives and gave me the right measure of things to do. Thanks to his support, the strong feeling of freedom in my work has always been tied to an agreeable sense of security.

I have carried out part of my research work in London at the Geotechnical Engineering Research Centre of the City University. The long time I spent there has been very fruitful for both my research and my personal experience. I strongly wish to acknowledge Prof Neil Taylor, Dr Sarah Stallebrass and Dr Andrew McNamara as they have always supported me with their brilliance, experience, competence, enthusiasm and good humour. My thanks also go to the technical staff, Keith Osbourne and Lloyd Martyka, for their patience and help. Among the research and degree students I met at City, I would like to give special thanks to David Mašín for our lunchtime discussions about numerical modelling and European eating habits. I would say that I am quite happy to feel a member of the widespread City-GERC family!

I wish to thank my co-tutors, Prof Renato Ribacchi of the University of Rome La Sapienza and Prof David Nash of the University of Bristol (UK). I am particularly grateful to Prof Ribacchi for the interest he has shown for my dissertation.

I also thank the Doctoral Board (Collegio dei Docenti) for giving me the possibility of developing part of my research abroad. Moreover, I particularly wish to remember the friendly support I have received at the Department of Geotechnical Engineering of the University of Naples.

In the followings, I would like to acknowledge some people in Italian, as I inevitably feel more comfortable in that!

Una tesi di Dottorato non sembra mai veramente finita… nello scrivere questi ringraziamenti, ponendo un termine al lavoro, i pensieri si allungano all'indietro sul periodo trascorso in questo Dipartimento, ai tanti volti che sono abituato a incontrare ogni mattina da ormai alcuni anni, a quelli che ero abituato a salutare più di frequente e ora vedo di rado. Mi piacerebbe indirizzarmi a ognuno, mi limiterò a ringraziare un campione limitato ma rappresentativo. Nell'ordine sparso che caratterizza i processi associativi del pensiero, vorrei ringraziare:

- Roberto Vassallo, per la sincera amicizia, ormai decennale, iniziata e cresciuta all'ombra della Meccanica delle Terre;

- Stefania Lirer, compagna di stanza, per la sua vitalità e il suo impagabile spirito positivo;
- Fiorenza de Sanctis, compagna di stanza, per la sua contagiosa tenacia;
- Luca de Sanctis, compagno di piacevoli trasferte, per le lunghe (ed estenuanti) discussioni serotine;
- Anna Scotto, Stefania Sica e Marco Nicotera, per i loro saggi e graditi consigli.
- Brunella Recinto e Gennaro Landi, per aver sopportato pazienti le prevaricazioni di un collega più anziano.

Vorrei inoltre ringraziare, per le sporadiche ma stimolanti discussioni, Alessandro Mandolini e Giulia Viggiani, alla quale devo anche il felice suggerimento di svolgere parte della mia ricerca alla City University.

Con due persone ho continuato a fare i conti in questo tempo: Alessandro Flora e Gianpiero Russo, e li ringrazio con particolare piacere. Ad Alessandro devo l'entusiasmo con cui mi sono appassionato alle "grosse grane" durante la tesi di Laurea e la scelta di iniziare il Dottorato. Nonostante non abbia poi proseguito il mio lavoro sul tema di ricerca a lui caro, ho avuto modo di apprezzare sempre di più nel tempo la sua opportuna, "sincera, preziosa, complicata" e liberale disponibilità. Gianpiero ha invece sopportato interminabili discussioni di metodo e ha condiviso con me l'interesse per molti aspetti della mia ricerca, spesso intervenendo con naturale, discreta, illuminata e comprensiva partecipazione. Con entrambi mi scuso per le intemperanze "di gioventù" di cui li ho talora resi vittime.

Vorrei infine ringraziare la mia famiglia, che mi ha sempre sostenuto nelle mie scelte, e in particolare mio padre, per non averle troppo contestate.

I. Introduction

Objectives

As the need of transportation has been increasing in our metropolises, the necessity of integrating the existing transport systems and developing new ones is becoming a bigger issue of interest for designers and contractors all over the industrialised world. Crossing densely urbanised areas with fast underground railways is one of the most commonly adopted solutions to reduce the environmental impact of the large number of people moving everyday across those areas. Many of our cities have been interested by the construction of new tunnels, generally located at a relatively shallow depth in the ground.

Tunnelling induces ground movements which affect the existing structures nearby and possibly damage them. This problem can be overcome for underground services by relocating them, but it becomes a very important issue of concern in the case of existing buildings or infrastructures. A reliable prediction of the movements induced by tunnelling is thus required during design, in order to recognise possible damages to the structures and, if needed, to adopt preventive measures to reduce these damages.

The purpose of this research is to present an experimental and numerical study of the effects of a diaphragm wall embedded between a shallow tunnel and a structure exposed to potential damage, in order to modify in a favourable sense the pattern of the movements induced by the excavation in a soft soil.

Methodology

The investigation of the problem was carried out by following two parallel ways:

- centrifuge modelling;
- numerical analysis.

Centrifuge modelling was used to measure the displacement fields occurring in different geometrical configurations of the problem. This method allowed collecting a rich data base of 'case histories'. This aspect seemed to be particularly important due to the lack in the technical literature of well documented cases in which similar techniques had been adopted. Therefore, the measurements from centrifuge tests on reduced scale models are useful, first of all, to better understand the mechanics of such a technique. They were also used to validate the numerical analyses which were performed.

Numerical analysis was used at three different stages. It was necessary to perform a set of preliminary finite element analyses in order to identify the main factors affecting the problem. This stage led to plan the following experimental work. A second set of numerical analyses was carried out after the experimental work with two main aims:

- comparing the prediction potential of two constitutive laws with the experimental measurements;
- integrating the set of configurations which had been studied in centrifuge with numerical simulation of configurations which had not been tested.

Finally, numerical analyses were performed to investigate the possibility of a limited generalisation of the results.

Outline of the dissertation

This dissertation is articulated in this introductive Chapter, four main Chapters and a Conclusions. Some Appendices are also reported at the end.

In Chapter II the background of the problem is presented. The existing methods of assessing ground movements (empirical, analytical and numerical methods) are described. A section is devoted to analyse the main soil constitutive issues which influence the ground response to tunnelling: non-linearity, small strain stiffness, anisotropy, stress path and recent stress history. The most common methods for assessing the damage induced to structures by tunnel excavation are also discussed in a part of the Chapter. Finally, the available techniques aimed to reduce the damage induced by tunnelling to an existing structure are overviewed. The set of protective measures is not exhaustive at all but it has been obtained by selecting case histories from the most recently published. Particular care was taken to choose the cases where the ground conditions and the constructing processes had been well described and data on the effectiveness of the adopted measures were available. Concerning this point, it is worth noticing that, although it can be helpful in general to find information in the literature about the effectiveness of the actions which can be undertaken to optimise design process, the number of cases that have been adequately monitored and documented fell short of expectations.

In Chapter III the experimental work and the test results are presented. The aim of the experimental work performed at City University was to study the effectiveness of the embedded diaphragm wall as a barrier against the ground movements induced by the excavation on model tunnel in centrifuge. As described in the Chapter, small scale models of circular tunnels were tested in centrifuge. A diaphragm of different geometrical characteristics had been embedded in them: its location, length, thickness and interface with the soil were varied. Totally, fourteen successful centrifuge tests were carried out. As the centrifuge model reproduces the behaviour of a prototype in plane strain, by capturing images of the model front section during the test and processing them afterwards, it was possible to determine the displacement field in the model at various epochs of test. In the Chapter the measured displacement fields are commented in detail and the influence of the various factors is discussed. At the end of the Chapter, in Appendix A and B, the measurements have been extensively reported.

The numerical analyses are presented in Chapter IV. In a section of this Chapter the main results of the preliminary analyses have been reported and discussed and the choices made in planning the experimental programme were justified. This set of analyses was not intended to reproduce the behaviour of the test, as it was performed at a stage of the research when the details of the materials to be used in the model and the test procedure were not yet established. After the tests, therefore, a new set of finite element analyses was performed in order to reproduce the experiments and integrate those cases which had been excluded from the experimental campaign. These analyses were intended to verify the potential of the adopted constitutive laws of reproducing the observed experimental behaviour and to integrate the experimental findings. Two constitutive laws were used in these analyses (Cam Clay and 3-SKH) and the results have been compared and discussed in a section of Chapter IV. In a following section the numerical results have been compared to the experimental data. In the last section of the Chapter it has been discussed how the various geometrical factors influence the calculated displacements and strains.

In Chapter V the scope and limits of the performed study are discussed and the results are summarised in order to interpret the observed behaviours (both experimental and numerical) in a simple framework. A set of quantities which describe the efficiency of the diaphragm wall in modifying ground movements are therefore defined. The dependence of these efficiency parameters on the various factors is shown in a section of the Chapter, by comparing some values as they have been calculated from experimental and numerical results. Also, a limited extension of the study was attempted, as shown and discussed in terms of efficiency in the last section of the Chapter.

Finally, in Chapter VI the limitations of the work are discussed, leading to suggestions for further work, and the implications of the results are highlighted.

II. Background

Prediction of movements induced by tunnel excavation

Tunnel design in urban areas often requires a careful assessment of the movements induced by the underground excavation in order to prevent damages to the existing structures.

The displacement field induced by tunnel excavation in soft ground (Fig. II.1) is the result of various phenomena:

- face deformation due to stress release: this is a negligible quantity if Tunnel Boring Machines (*cf.* App.1) are used with a good pressure control;
- movements induced by shield advancing: these are due to the extra cutting (which is necessary to reduce friction between the shield and the ground) and to the shield pitching and yawing. These latter contributions are more evident for large shields and when the workmanship is not trained yet to the peculiar ground conditions;
- ground movements inside the gap between the lining and the shield tail: it can be reduced by grout injections;
- lining deflection due to the earth pressure: this is a negligible quantity;
- long term volume change due to the consolidation process induced in clayey soils.

Such ground movements can be predicted by different methods, whose results can be compared each other: empirical methods based on field measurements, simple analytical models, numerical models, physical models (mainly small scale centrifuge tests).

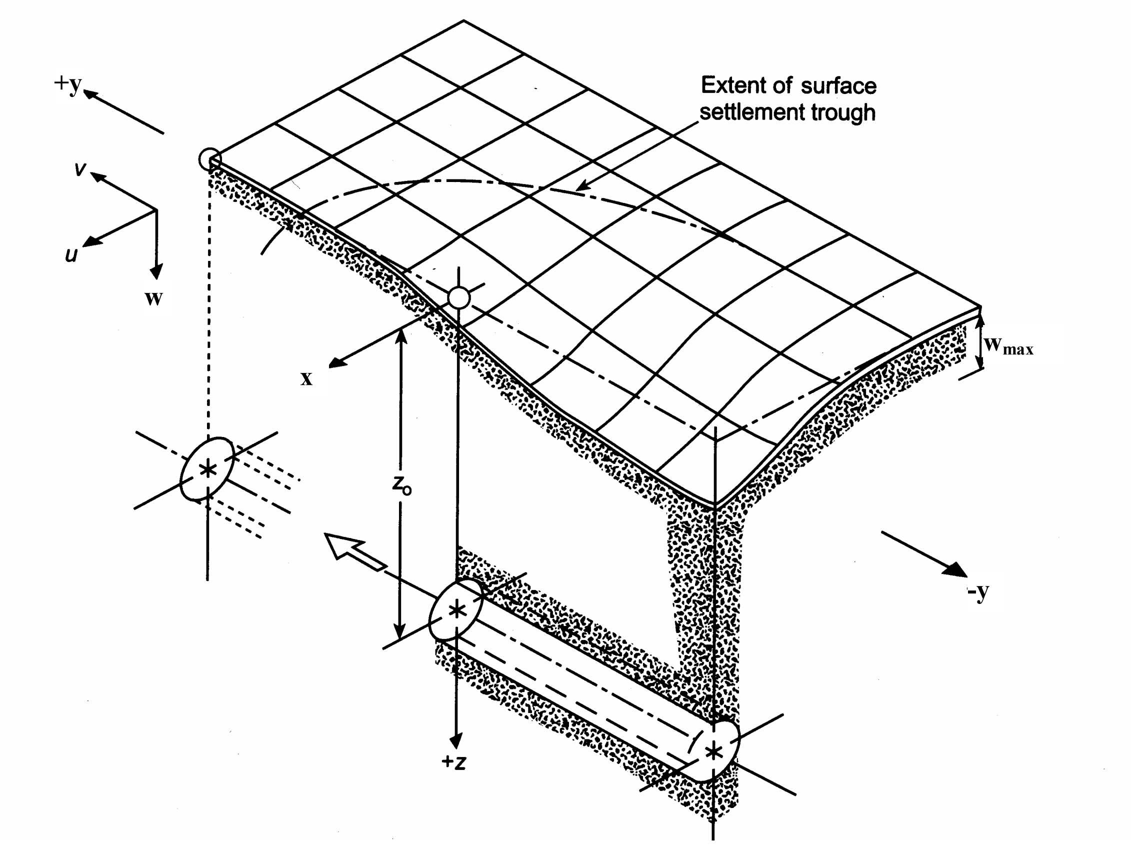

Figure II.1 – Ground movements induced by tunnel excavation (after Attewell et al.*, 1986)*

Empirical methods

Peck (1969) showed that the transverse settlement trough induced by a single tunnel excavation, in 'greenfield' conditions (without structures at the surface above), is closely described by a normal Gaussian distribution (Fig. II.2):

$$w(x) = w_{\max} \exp^{\left(\frac{-x^2}{2i^2}\right)} \tag{II.1}$$

$$\text{where } w_{\max} = \frac{0.31V'D^2}{i} \tag{II.2}$$

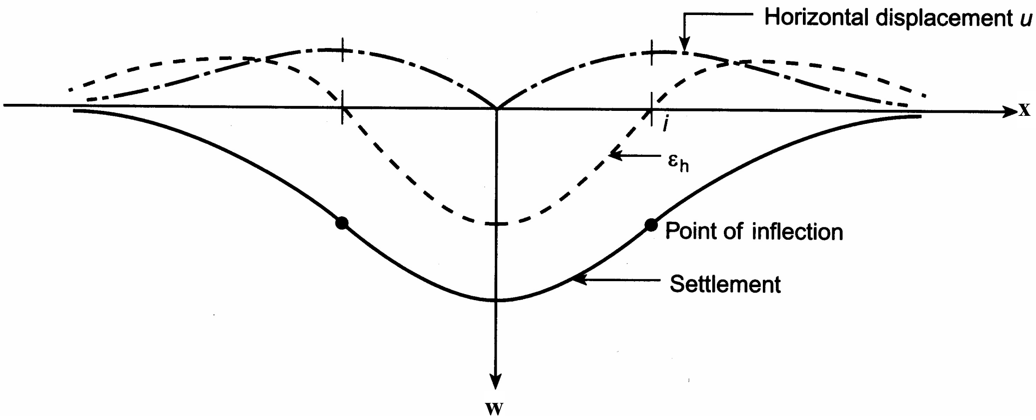

Figure II.2 – Transverse Gaussian distibution of settlements and relevant horizontal displacements and strains

A large number of site measurements justify the use of an empirical method based on the Gaussian distribution. One of the first cases in which the induced ground movements were widely measured is reported by Attewell and Farmer (1974). A 4.15m diameter circular tunnel was driven in London Clay at 29.3 m (axis depth). A segmented cast-iron lining was erected at the shield tail and the gap between the lining and the ground was filled by a low pressure grout injection. Three transverse lines along the tunnel, about 9 m apart, where monitored: surface settlements and horizontal displacements were measured by precise optical levelling, inclinometers and magnetic rings located along the inclinometer access tubes allowed to measure subsurface movements. The wide number of available data also permitted the Authors to draw interesting remarks on the various amounts of volume loss coming from different sources.

In fact, the parameter V' (volume loss) is the volume of ground which has been excavated in excess to the theoretical tunnel volume, expressed as a percentage of the latter. It is commonly assumed that the surface trough volume equals the volume loss. This assumption is likely to occur in clay at short term, whilst consolidation occurs in clay at long term. In dense granular soil, the trough volume reduces because dilatancy occurs.

The amount of V' depends on the type of ground and on the excavation method. Mair and Taylor (1997) revised a wide series of case histories and concluded that:

- in open face excavations in stiff clay, V' ranges between 1% and 2%
- if a sprayed concrete lining is adopted, its values reduce to a range between 0.5% and 1.5%
- in excavation with Tunnel Boring Machines, V' can be lower than 0.5% in sand whilst it is between 1% and 2% in soft clay.

The parameter i represents the half-width of the sagging part of the settlement trough. O'Reilly and New (1982) showed that this parameter is approximately linear with the depth z_o of the tunnel axis, and proposed:

$$i = 0.43 z_o + 1.1 \qquad \text{for cohesive soils} \qquad \text{(II.3)}$$

$$i = 0.28 z_o - 0.1 \qquad \text{for granular soils} \qquad \text{(II.4)}$$

However, they suggest to assume:

$$i = K z_o \qquad \text{(II.5)}$$

which is now common practice. The choice of K depends largely on the type of ground: Mair and Taylor (1997) analysed a large number of case histories which confirm the conclusions by O'Reilly and New (1982) on the values assumed by K, which generally varies between 0.4 and 0.6 for cohesive soils. Values above 0.5 which often occur in soft clay can be justified by the major difficulty in isolating the consolidation settlements which can be a more important component than in stiff clay (Samarasekera and Eisenstein, 1992). For granular soils, Mair and Taylor (1997) observed that K ranges between 0.25 and 0.35, with a larger scatter than for clays, but without a clear distinction between soils above and below the groundwater, in spite of what suggested by Peck (1969).

The displacement field at a given depth z, which can affect buried structures, can be evaluated with the empirical method by adopting again a gaussian distribution with:

$$i = K(z_o - z) \quad \text{(II.6)}$$

On the basis of both field measurements and centrifuge tests, Mair *et al.* (1993) showed that K is not constant but increases non-linearly with depth:

$$K = \frac{0.175 + 0.325(1 - z/z_o)}{(1 - z/z_o)} \quad \text{(II.7)}$$

The empirical method can be adopted also to predict the movement field in the three-dimensional problem of an advancing tunnel. In this case, the longitudinal profile of settlement can be fitted by a cumulative normal distribution as suggested by Attewell and Woodman (1982). They analyse two problems: ground loss in a point and ground loss along a line. In fact the second problem is solved by integrating the solution of the first one between the two edges y_i and y_f of the line. This means to integrate the normal distribution curve thus obtaining the cumulative normal distribution function:

$$G(\alpha) = \frac{1}{\sqrt{2\pi}} \int_{-\infty}^{\alpha} \exp\left(-\frac{\beta^2}{2}\right) d\beta \quad \text{(II.8)}$$

The generic settlement can be expressed as:

$$w = w_\infty \left[G\left(\frac{y - y_i}{i}\right) - G\left(\frac{y - y_f}{i}\right) \right] \quad \text{(II.9)}$$

where w_∞ is the settlement at y when the initial and final edge are at infinite distance and can be calculated following (II. 2).

By observing that G(0)=0.5 and G(∞)=1, it follows from (II.9) that the settlement at the excavation front equals 0.5 w_∞. The Authors also reported the measured settlements in six case histories: the comparison show that the less cohesive were the soil, the lower was the settlement at the front compared to the predicted 0.5 w_∞. This can be justified, according to the Authors, with other observations which are available in literature (e.g.

those reported by Cording and Hansmire, 1975) that the volume loss in clay, particularly without face support, mainly occurs at the front, whilst in sand and silt it occurs prevalently over the shield and at the shield tail. This means that in the latter case a lower V' should be adopted in predicting the front settlement.

The method proposed by Attewell and Farmer is usually applied to single tunnels in homogeneous (non-layered) ground, or even multiple tunnels if they do not interact each other, in greenfield conditions (no structures at surface) and for short term 'undrained' settlement evaluation.

Hansmire and Cording (1985) report the results of a wide monitoring along a stretch of the twin tunnels of the Washington Underground. The two 6.4 m diameter tunnels were excavated by a TBM at an average depth of about 14 m and 15 m in a silty sand and gravel deposit and were lined by a primary support of steel ribs and a secondary support of cast-in-place concrete. They are able to observe a clear asymmetry in the displacement field above the twin tunnels and to justify it with the low distance between the two tunnels (about 1.5 diameters between the two axes).

Mair and Taylor (1997) report other case histories available in literature and conclude that when the tunnel are very closely spaced, the ground in which the second tunnel has to be constructed has already experienced non-negligible shear strains due to the construction of the first tunnel. Hence, the resulting reduced stiffness justifies the increase of volume loss when excavating the second tunnel.

Long term settlements can be evaluated in some cases by the empirical method, but it requires the knowledge of the lining permeability in order to make likely hypotheses on the induced excess pore-pressures around the excavation. A detailed numerical analysis of such excess pore pressures in normal-consolidated and over-consolidated clays is reported by Samarasekera and Eisenstein (1990).

In summary, increase in settlements only occurs at long term when tunnelling in normal-consolidated clay. The larger increase the higher the lining permeability relative to the ground permeability, i.e. the more the lining tends to act like a drain. But in any case, very small increases in distortions and horizontal strains are observed.

Analytical method

The tunnelling process can be assimilated to a theoretical problem of the excavation of a circular cavity in a continuum. The calculation of the displacement field in this plane strain boundary problem has been performed for a linear elastic-perfectly plastic continuum (i.e. Clough and Schmidt, 1981; Mair and Taylor, 1993). Such analyses lead to very similar closed form expressions of the displacement field $u(r)$ around the cavity when the supporting pressure reduces from an initial value $\sigma_{r,o}$ to a value σ_r:

$$\frac{u}{R} = \frac{u}{R}\left(\frac{R}{r}, \frac{c_u}{E_u}, \exp\left(\frac{\sigma_{r,o} - \sigma_r}{c_u}\right)\right) \tag{II.10}$$

where R is the tunnel radius.

These solutions have been found under the hypothesis of axi-symmetry, which is very unlikely for shallow tunnels. Nevertheless they can be used to predict the displacement in a limited area around the tunnel. Also, the hypothesis of isotropy of stress is an issue of concern when modelling an excavation in heavy overconsolidated clays, where the horizontal stress can be much greater than the vertical ones.

Mair and Taylor (1993) produced also a solution for a spherical cavity thus modelling the ground movements ahead an advancing tunnel.

A solution for a homogeneous isotropic linear elastic incompressible half-space has been proposed by Sagaseta (1987). The presence of the top free surface is considered by means of a virtual source/sink, symmetric around the boundary with the source of movement, and some results for the elastic half-space (Boussinesq's and Cerruti's solutions). In Fig. II.3 the framework of the analysis is shown: three solutions are superimposed in order to get the solution of the actual problem, only the third one involves the elastic behaviour of the medium.

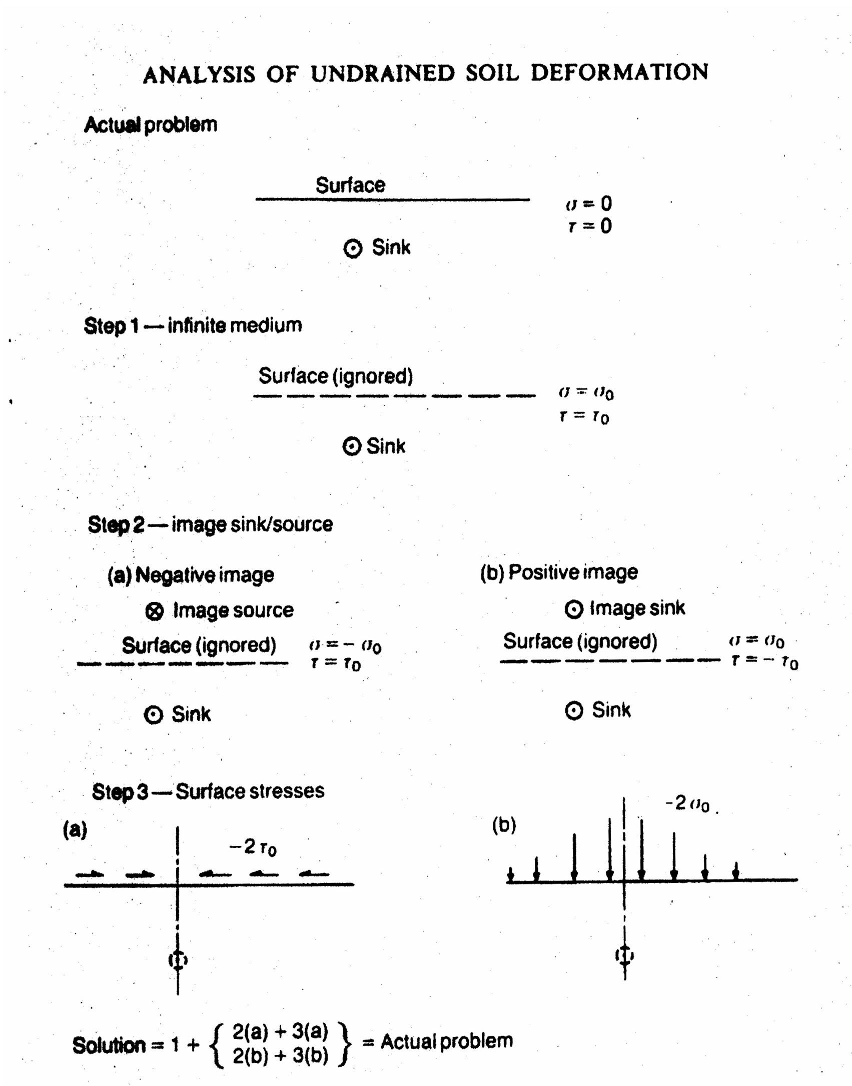

Figure II.3 – Framework of the analysis by Sagaseta (1987)

In plane strain conditions the horizontal (x direction) and vertical (z-direction) displacements at surface are:

$$u_{x,surf} = -V'\frac{D^2}{4}\frac{x}{x^2 + z_o^2} \tag{II.11}$$

$$u_{z,surf} = V'\frac{D^2}{4}\frac{z_o}{x^2 + z_o^2} \tag{II.12}$$

where D is the tunnel diameter, z_o the tunnel axis depth and V' the volume loss per unit length of excavation.

The Authors suggest to determine the amount of ground loss from direct observations in tunnels or from empirical correlations with other parameters, such as the stability ratio N.

Uriel and Sagaseta (1989) compared this solution with measurements by Cording and Hansmire (1975) at the Washington Metro. They are similar, but the observed trough appears narrower than the prediction. In the same paper the Authors extend the solution to include stiffness and stress anisotropy: it seems that the first is much less influent on the displacement field than the second one. In practice, they state that the solution for the isotropic case can be used with confidence for the analysis of ground movements in isotropic soils, whilst the coefficient of earth pressure has a significant effect on the displacement field and it should be conveniently taken into account in order to get realistic predictions.

Verruijt and Booker (1996) extend the Segaseta solution to a compressible soil and account for the ovalization of the cavity in the long term. A similar procedure as Sagaseta (1987) is adopted. The starting point is the solution for a singularity at a point of an infinite elastic medium: it is worth noticing that the elastic behaviour has to be considered in every step of the analysis, contrarily to Segaseta procedure, due to the medium compressibility. Two singularities have been imposed: the first is a uniform radial strain ε, which determines the ground loss, the second is a dimensionless parameter δ ruling the long-term purely distortional deformation (ovalization) of the tunnel boundary.

As a uniform contraction of the cavity is assumed, the parameter ε is half the volume loss per unit length V'. The complete expressions for the horizontal and vertical displacements in the half-plane will not be reported, their formal expression is:

$$u(x,z) = u(x,z,z_o,\varepsilon,\delta,\nu) \tag{II.13}$$

The compressibility of the soil is taken into account by the Poisson's ratio ν. If $\nu = 0.5$ (incompressible soil) and $\delta = 0$ (no long-term ovalization), the Verruijt and Booker solution degenerates in that by Segaseta (1987) and can be used to assess the short-term tunnelling-induced ground movements in clays.

Loganathan & Poulos (1998) modify the Verruijt and Booker solution, only for clays and undrained conditions, making an hypothesis on the contraction of the tunnel cavity. In their model the circular cavity contracts in a non-uniform way and the radial displacement varies from zero at the invert to g at the crown, where g is a 'gap' parameter as defined in Kerry Rowe and Kack (1983) and shown in Fig. II.4.

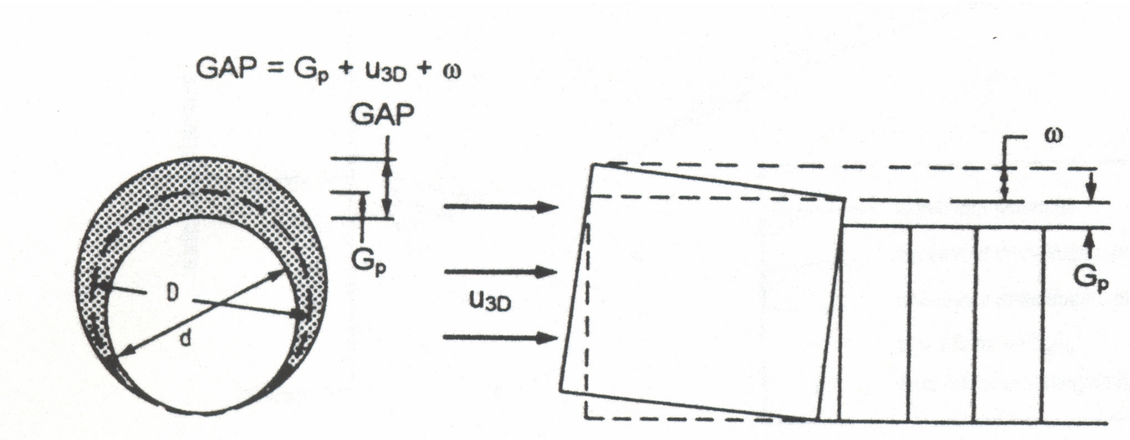

Figure II.4 – Definition of GAP parameter (Kerry Rowe and Kack, 1983)

This assumption leads to modify the expression for ε, which is not constant in the half-plane anymore:

$$\varepsilon(x,z) = \varepsilon_o \exp[-Ax^2 + B + C - Dz^2] \quad \text{(II.14)}$$

The parameter ε_o is equivalent to V' and it is defined through geometrical considerations on the shape of the radial deformation of the cavity boundary as:

$$\varepsilon_o = \frac{2gD + g^2}{D^2} \cong \frac{2g}{D} \tag{II.15}$$

The parameters A and B are determined by imposing that the surface settlement above the tunnel axis u(0,0) results from the whole volume loss $\varepsilon(0,0) = \varepsilon_o$ whereas the surface settlement at a horizontal distance H+R (or z_o+D/2) from the tunnel axis results from 25% of the whole volume loss: $\varepsilon(H+R,0) = 0.25\varepsilon_o$. The parameters C and D are determined by imposing $\varepsilon(x,H) = 0.5\varepsilon(x,0)$: this assumption follows from the shape of the non-uniform distribution of displacement at the tunnel boundary. A sketch of the boundary value problem is shown in Fig. II.5.

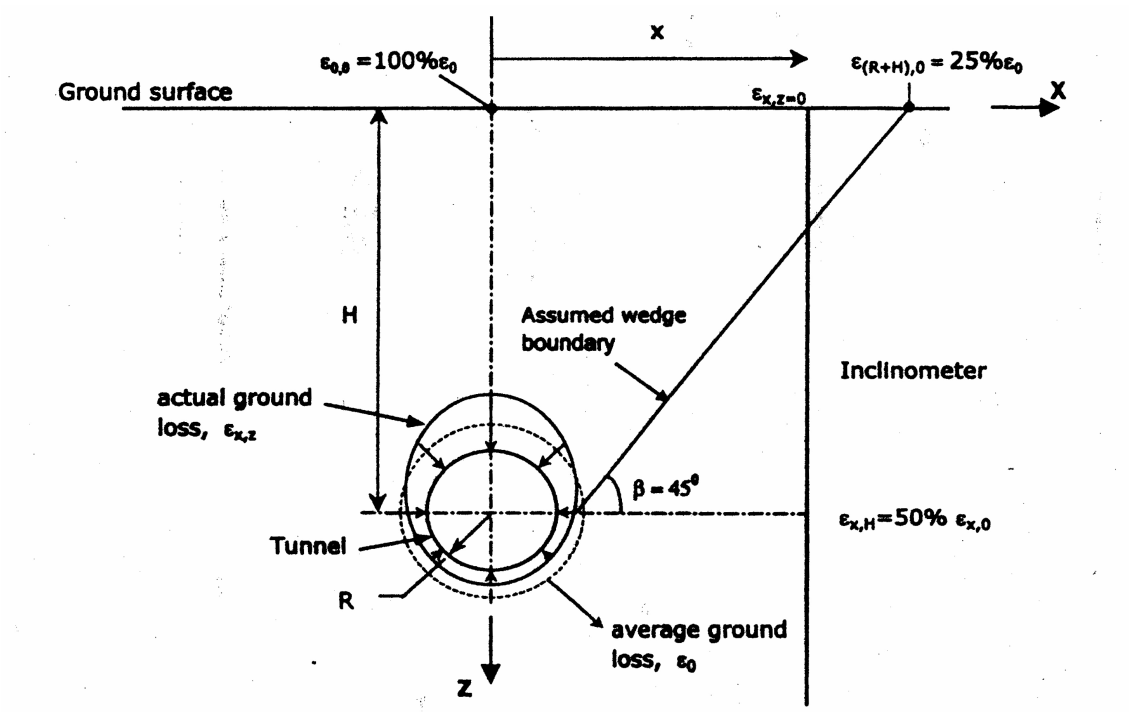

Figure II.5 – Sketch of the boundary value problem after Loganathan and Poulos (1998)

To model an undrained excavation in clay, Loganathan & Poulos (1998) assume that no long-term ovalization occurs, hence $\delta = 0$. Nevertheless they keep the dependency of the solution on the Poisson's ratio, as the only explicit soil parameter, even if in undrained conditions it is assumed $\nu = 0.5$.

The assessment of the parameter g is a crucial issue: this parameter permits to take empirically into account the excavation techniques, the three-dimensional effects and the non-linearity of the soil in a linear elastic closed form solution, provided that a sound engineering judgement is adopted.

This solution has been applied in the paper to five case histories previously published by various Authors. The settlement troughs predicted are slightly wider than those observed. Good agreement has been observed for subsurface settlements and horizontal displacements for uniform clays. Less satisfactory is the agreement with measurements in layered and sandy soils.

Numerical methods

Numerical methods, and particularly Finite Element Method, give the possibility to analyse several aspects of tunnel construction. Although the excavation process should be analysed in three dimensions and even if in the recent years a large progress in solving techniques occurred, bi-dimensional analyses are still the most common in practice. This is due essentially to the fact that a complete three-dimensional analysis requires a computational time which is still too high for design. For this reason a lot of efforts have been done in recent research to perform procedures to take into account three-dimensional effects in plane strain analyses.

A possible way is to use the ground reaction line (Panet and Guenot, 1982) which is a relationship between the radial stress applied at the tunnel boundary and the corresponding radial displacement. It characterizes the ground behaviour during the excavation: as soon as a degree of unloading inside the tunnel is allowed, the tunnel deforms and its deformation determines the volume loss around (Fig. II.6).

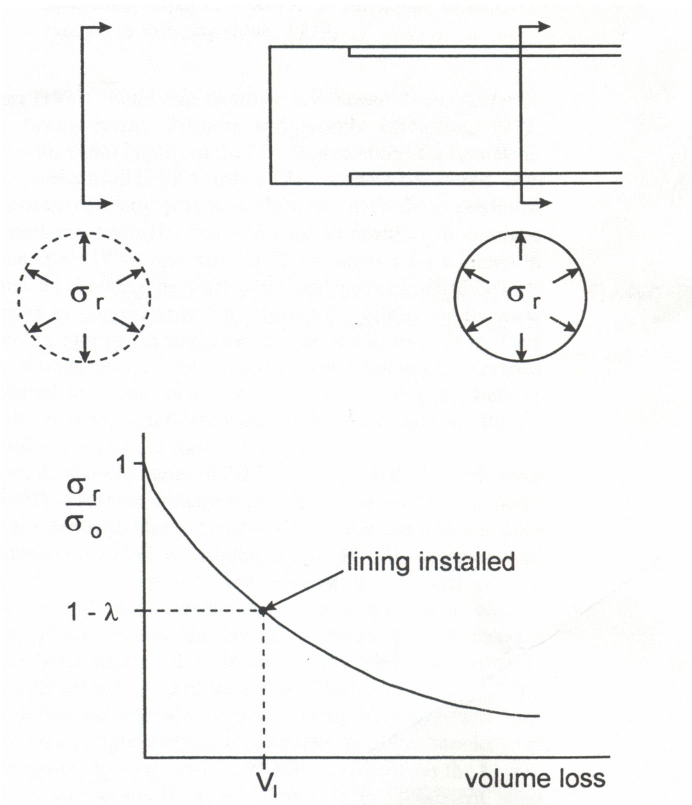

Figure II.6 – Ground reaction curve (Panet and Guenot, 1982)

The advantage of this method is that it is able to represent a three-dimensional problem of an advancing tunnel with a plane strain model. In fact, in a plane perpendicular to the tunnel axis which is located at a given distance ahead the tunnel, the stress level is not influenced by the excavation and equals the original one. On the other hand, if the cavity is able to self-sustain without lining, at a given section of the tunnel behind the heading the stress level around the cavity equals to zero and a new stress distribution around the cavity applies which is in equilibrium with the new boundary conditions.

In between these two locations, the stress around the cavity varies between the pre-existing one and zero: in terms of radial stress, σ_r varies between σ_o and 0. At a generic section in this span:

$$\sigma_r = (1-\lambda)\sigma_o \qquad \text{(II.16)}$$

where $\lambda=0$ when $\sigma_r=\sigma_o$ and $\lambda=1$ when $\sigma_r=0$.

By using a ground reaction curve, an amount of radial deformation, therefore an amount of volume loss, can be calculated for a given release $\lambda\sigma_o$ of the original radial stress. This means that a given volume loss can be achieved by installing a lining behind the heading of the excavation, which supports the cavity with a pressure $p=(1-\lambda)\sigma_o$.
In this way the three-dimensional problem can be modelled in plain strain conditions provided that an appropriate value is given to the parameter λ: this corresponds to assign a given load to the lining. Alternatively, a volume loss can be prescribed and the corresponding λ can be calculated. In fact the second procedure is more convenient when the design problem is focused on movement control. Both procedures depend on the adopted ground reaction line, which is itself a result of a model. Therefore care has to be taken to be sure that both the lining loads and the ground movements which have been calculated are consistent with measured loads and movements in similar ground and tunnel conditions. It has also to be noticed that this approach has been developed for deep tunnels, hence in axi-symmetric conditions (approximately constant stress state around the tunnel): the application to shallow tunnels, where these conditions are far to be realistic, requires considerable experience.
Alternatively, three-dimensional effects can be taken into account by using the 'gap' parameter proposed by Kerry Rowe *et al.* (1983) and modified by Lee *et al.* (1992a):

$$GAP = G_P + u_{3D}^* + \omega \tag{II.17}$$

In this definition, G_P is the physical clearance between the ground and the lining, u_{3D}^* is a term which accounts for the intrusion of soil from the excavation face, ω is an allowance for workmanship. In fact, this parameter represents an equivalent crown displacement in a plane strain model. It can be used to calculate a volume loss to be used in empirical methods, as in Lee *et al*. (1992b), or introduced in a finite element analysis as proposed by Kerry Rowe *et al*. (1983). In this latter case, an unlined tunnel analysis is performed until the soil does not come into contact with the lining. When the contact occurs, the lining limits the possible deformation of the soil, hence the interaction between the soil and the lining has to be analysed.

The main difficulty of this 'gap' approach is to assess a likely value for the GAP parameter. For cohesive soils Lee *et al*. (1992a) show a procedure for evaluating this parameter. The term G_P descends from the shield and lining sizes and it is determined once the machine-support system has been chosen. The term u^*_{3D} is evaluated by using the results of a parametric three-dimensional numerical analysis. In fact, this analysis has been performed for a circular tunnel in an elasto-plastic half space, excavated in undrained conditions, for given ranges of parameters (E_u/c_u between 200 and 800, H/D between 1.5 and 4.5, K_o between 0.6 and 1.4 and a given unit volume weight γ=20 kN/m^3). The results show that the value of the maximum axial intrusion at the tunnel face essentially depends on E_u, on the total stress removal at the tunnel face and on the stability ratio N. The Authors propose to express the term u^*_{3D} as a half the maximum axial intrusion at the tunnel face. Finally, they propose to relate the term ω to the elasto-plastic plane strain radial displacement at the crown *u* (which has been expressed in a closed form by various Authors, as previously mentioned) if the ground deformation at crown is not restrained by the lining; alternatively they relate ω to the physical gap G_P, if the lining constrain the ground deformation at crown. In practice, they assume:

$$\omega = \min\left(\frac{1}{3}u \quad , \quad 0.6G_p\right) \tag{II.18}$$

Physical models

A common way to study the main issues of a field problem is to use a physical model of it, generally at reduced scale.

The centrifuge is a powerful tool for testing reduced scale models when the appropriate scaling laws are respected (Schofield, 1980; Taylor, 1995). The main point concerning centrifuge testing is that a stress distribution can be created in the model in such a way that the stress level in every point is the same as in the homologous point in the prototype (*cf*. App. 2 for details). This feature is very useful in geotechnical models, as the mechanical behaviour of soil is stress dependent, and it is particularly important in problems dominated by self-weight effects, as is the case of movements induced by tunnel excavation. When the size of the model is equal to 1/N of the size of the prototype, the model has to be accelerated to N gravities in order to achieve the stress distribution which guarantees the mechanical equivalence between the model and the prototype.

In the centrifuge, both the longitudinal and the transversal settlement troughs caused by tunnel excavation can be investigated, depending on the way the excavation is simulated. As the sources of ground movement during tunnelling can be various (e.g. ground loss at face, around the shield, around the lining, movements induced by grouting between the lining and the surrounding soil) some approximations are unavoidable when modelling this process in the centrifuge.

Model tunnels both in sand and in clay have been tested in centrifuge. Potts (1976) and Atkinson *et al.* (1977) studied the stability of circular tunnels in dry sand at different ratios between the cover C and the diameter D in plane strain conditions. The stability in a longitudinal section of a tunnel in sand was studied by Chambon *et al.* (1991). Al Hallak *et al*. (2000) studied the movements and the stability of a bolt reinforced face in sand. A large number of centrifuge tests aimed to study the tunnel stability and the ground movements induced by tunnelling in clay was undertaken by Mair (1979). Among such tests, some were conducted in plane strain conditions and the same prototype of a shallow tunnel was modelled with geometrically similar models accelerated at different levels, thus performing a ‘modelling of models’. The observed settlements in similar models were in the same ratio of their accelerations in the centrifuge and this allowed to validate the centrifuge scaling laws for the studied problem. On the same line of research, several centrifuge tests have been performed since there on plane strain tunnel models both in clay and in sand: among them the work of Grant (1998) on modelling the pre-failure ground movements due to tunnelling in two layer ground conditions.

Tunnel-induced deformation of soft ground: some relevant constitutive issues.

Whatever approach is used to model the excavation of a tunnel, particular care is necessary in order to reproduce the main aspects of the field problem. Geometry, boundary conditions, initial state, mechanical properties of the soil have to be modelled as much accurately as possible. Nevertheless, the need for simplicity requires judging which issues the boundary problem is more sensitive to and spending many efforts in carefully incorporating them in the model.

The influence of the non-linear soil behaviour, the high stiffness at low strain levels, the stress path and the recent stress history on the deformation field around tunnels has been shown by many Authors.

It has been observed in several studies the effect of non-linearity and anisotropy on the width of the settlement trough. Kerry Rowe *et al.* (1983) performed a comparison between three simple models adopted to back-analyse the behaviour of a tunnel excavation in soft clay: a linear isotropic elastic, an anisotropic elastic, an anisotropic elastic-perfectly plastic model. The analyses were conducted in plane strain conditions. The linear elastic law is very sensitive to the reduction of weight due to the excavation: the ground tends to compensate the settlement due to the reduction of supporting forces at the tunnel boundary with the heave due to the soil removal. This second effect is the more important the wider is the distance between the invert of the tunnel and the bottom of the elastic stratum and it is because the stiffness is not dependent on the stress path (the same Young's modulus is assumed for loading and unloading). The result is that the settlements are under-predicted even if a low modulus is used. On the contrary this does not happen with an elasto-plastic law, provided that the elastic stiffness is not too low: in this case, in fact, the elastic strains which arise dominate over the plastic strains.

The predictions improve if a stiffness which increase with depth is used.

The use of a cross-anisotropic elastic law allowed the Authors to analyse the influence of the ratio between the horizontal and vertical moduli E'_h/E'_v : a marginally narrower settlement trough can be calculated by reducing this ratio. On the contrary the ratio of the independent shear modulus to vertical modulus G_{vh}/E'_v (G_{vh} is the most uncertain anisotropic elastic parameter and sophisticate techniques are needed to measure it) appears the most significant. Both in elastic and in elasto-plastic analyses, by decreasing the independent shear modulus the maximum calculated settlement increase and the shape of the settlement trough tends to be narrower.

Addenbrooke *et al*. (1997) draw very similar conclusions by comparing the results of plane strain analyses with linear and non linear, isotropic and anisotropic elastic perfectly plastic models. In Figs. II.7–II.8 a the computed settlement troughs are compared with field data at St James's Park (Standing *et al.*, 1996) for a single tunnel and a twin tunnel excavations. Model L4 is a non-linear isotropic elastic perfectly plastic model by Burland and Puzrin (1996) whilst J4 is a non-linear isotropic elastic perfectly plastic model by Jardine *et al*. (1986): both the models are able to consider the non-linear behaviour at small strains by calibrating bulk and shear moduli decay with strain level on triaxial results, L4 with a logarithmic function, J4 with a trigonometric one. L4 is also able to simulate in a simplified way the effect of the recent history on the soil behaviour by switching to a high stiffness at load reversal. Model AJ4 is a non-linear cross-anisotropic elastic perfectly plastic model obtained by modifying J4: the five cross-anisotropic elastic parameters keep a constant ratio with the relevant two isotropic elastic parameters. This allows reproducing the moduli decay with the same functions as in J4.

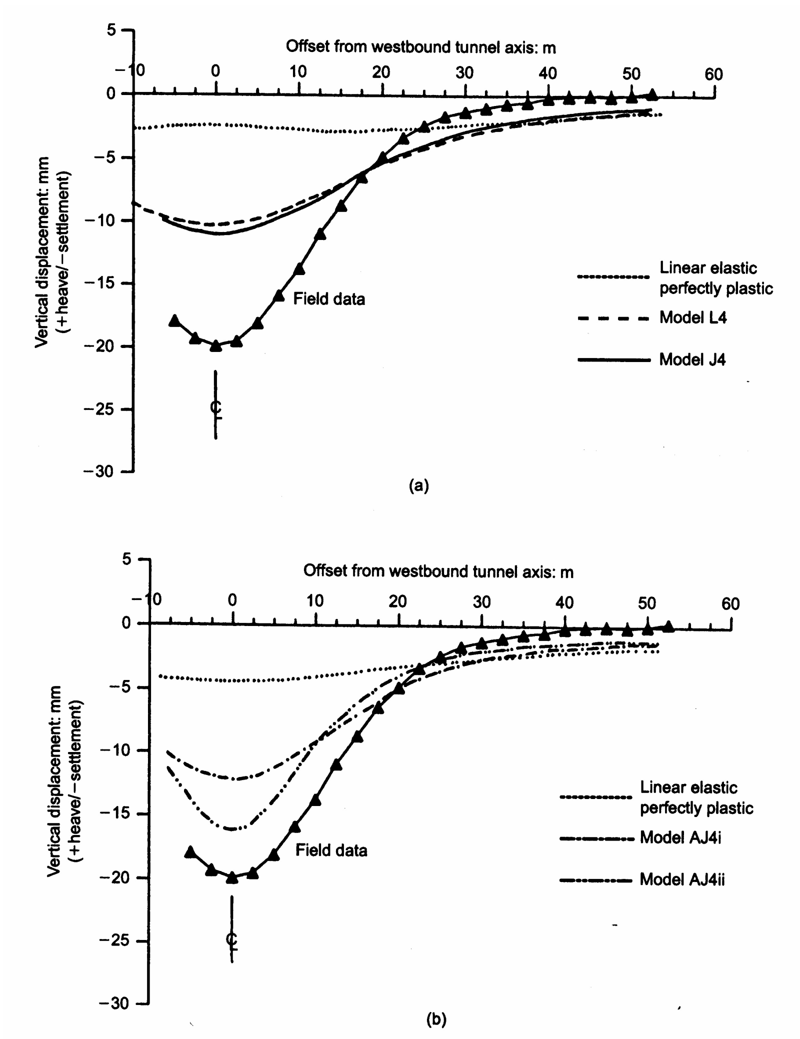

Figure II.7 – Computed and measured settlement at St James's Park, single tunnel (Addenbrooke et al.*, 1997)*

It can be observed in Fig. II.7-a that the linear isotropic model prediction for single tunnel is far away from the field measurements, whereas the two non-linear isotropic L4 and J4 give practically the same results and predict narrower profiles than the linear model, but still underestimate the maximum and predict a wider profile than measured. The prediction of the non-linear anisotropic AJ4 (Fig. II.7-b) is a narrower trough: in AJi the elastic parameters are based on field and laboratory data for London Clay, whilst in AJii the independent shear modulus G_{vh} has been assumed considerably lower. By introducing the 'true' value of G_{vh} modulus (AJi), the prediction is only slightly improved, compared to non-linear isotropic models. On the contrary, the use of a very soft G_{vh} (AJii) is a device which allows to improve noticeably the prediction of the surface trough. However, as the Authors observe, such a soft independent shear modulus is unrealistic and cannot be justified from laboratory or field test data for London Clay. The reason for this expedient is that it modifies the pattern of movements around the tunnel and increases the horizontal displacements in the whole ground: in this way the soil softening due to the face deformation can be taken into account in a plane strain analysis. It has to be verified if such an approach is still valid for predicting subsurface ground movements, ground and lining stresses and pore water pressure distributions. Moreover, further information is needed from the experimental side on how G_{vh} varies with the strain level.

In Fig. II.8-a the twin-tunnel trough shows the influence of the stress path reversal due to the excavation of the second tunnel: the L4 model predicts a trough closer to the measured one and better than J4 and AJ4i: this can be attributed to the fact that it takes account of the load reversal. In fact, in this case load reversal was observed above and below the second tunnel and in between the two tunnels. As J4 and AJ4 are not able to model any increase in stiffness due to the recent stress history, the Authors analysed the effect of a re-invoked high stiffness before the second excavation (the stiffness was re-stated at the original value all over the mesh). The results, as shown in Fig. II.8-b, demonstrate the importance of this issue when construction processes involving sensible stress-path changes are undertaken.

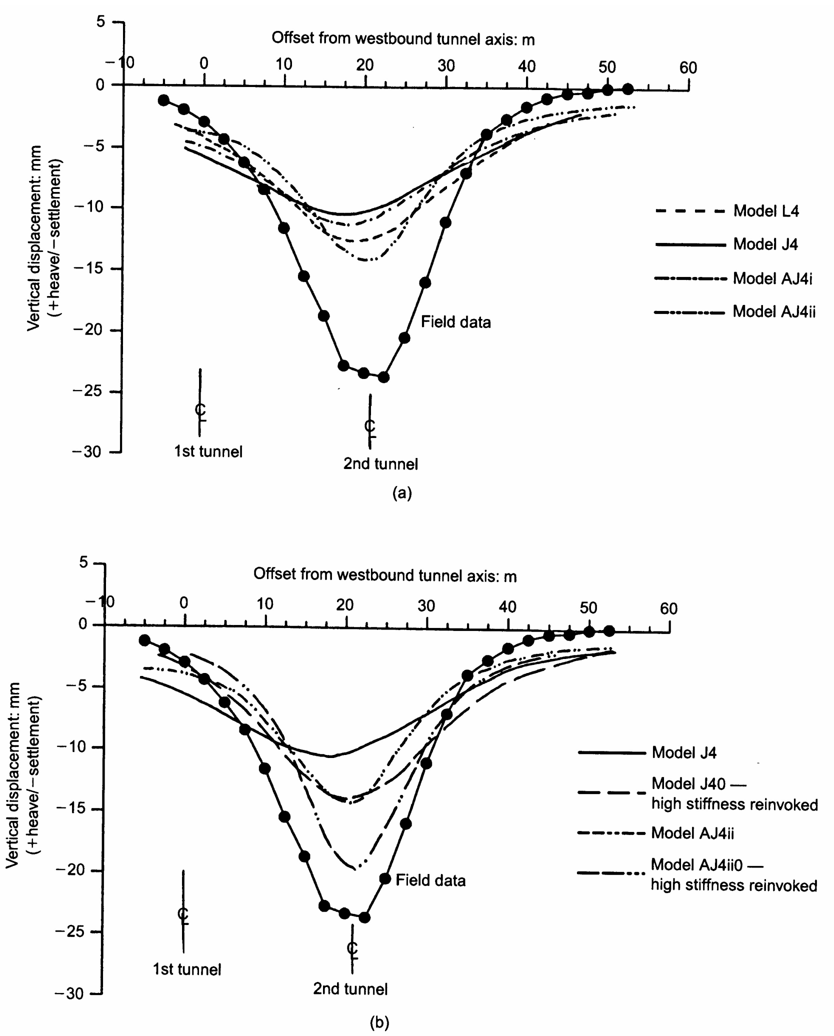

Figure II.8 – Computed and measured settlement at St James's Park, twin tunnels (Addenbrooke et al.*, 1997)*

The paper by Addenbrooke et al. (1997) leads to the conclusion that non-linearity of soil plays a major role than anisotropy in predicting the surface settlement trough induced by tunnelling, even if the role of the shear independent modulus is substantial. It has to be mentioned that other Authors (Simpson *et al.*, 1996) show results for similar ground conditions which indicate that also a linear model with a given degree of shear modulus anisotropy is able to reproduce the measured trough.

Another interesting issue is the anisotropy of the field stresses. The importance of the degree of anisotropy of the initial stress state around the tunnel is a topic to be carefully analysed: Gens (1995) observes that the influence of K_o on the excavation induced trough, although generally recognized, is not commonly considered in the analyses.

Kerry Rowe et al. (1983), in their parametric study, state that the effect of a change in K_o in an area immediately around the tunnel is significant because it influences the stress variations which occurs during the excavation and, consequently, the pattern of movement around the tunnel.

Addenbrooke (1996) proposed to reduce locally the value of K_o for over consolidated clays to take into account a three-dimensional effect in a plane strain analysis. In fact, three-dimensional analyses revealed that as far as the tunnel heading approaches a given transverse plane, the effective horizontal stress along this plane reduces at the side and increases above and below the tunnel. Therefore, by reducing the value of K_o to 0.5 (as for normal consolidated clay) over an area which extends from the invert to the crown for a distance about three times the radius of the tunnel at both sides, the effect of this three-dimensional stress change can be incorporated in a plane strain analysis. He performed analyses with linear and non-linear, isotropic and anisotropic models. In Fig II.9 some of the computed troughs are shown together with the relevant measured profile at Green Park (Attewell and Farmer, 1974). In particular, the curves in Fig II.9-a refer to an anisotropic linear elastic pre yield model, those in Fig. II.9-b and c to an isotropic non-linear elastic pre yield model (Jardine *et al.*, 1996). In Fig. II.9-a and b results are shown which refer to analyses where the K_o values were constant all over the mesh and equal to 1.5 (London Clay) and 0.5 (lowered value); in Fig. II.9-c the results refer to analyses in which K_o was set to 0.5 only in the area above defined and kept 1.5 all over the remnant mesh. It can be observed that the influence of K_o on the shape of the settlement trough is huge (Fig II.9-a) because, obviously, the plastic zones for low K_o onset before at sides, whereas for high K_o they develop first at tunnel crown and invert. Besides, even a linear model (which takes into account anisotropy with the 'true' independent shear modulus) is able to fit the experimental data provided that a convenient K_o is adopted. Furthermore, the anisotropic linear model predicts better the field trough than the isotropic non-linear one, for the same amount of effective stress ratio (*cf.* Fig II.9-a and b). Fig. II.9-c show how the prediction of the isotropic non-linear model can be improved by reducing K_o locally around the tunnel.

It has to be highlighted that this is also an arbitrary device, as questionable as setting up an unrealistically low G_{vh} modulus. The fact that the soil ahead the heading experienced a stress relief thus showing a lower K_o is in contrast with the assumption of a high stiffness in a non-linear model, which assume that no straining have occurred around the heading. In many problems, however, a great difficulty is encountered when assessing a likely distribution of K_o.

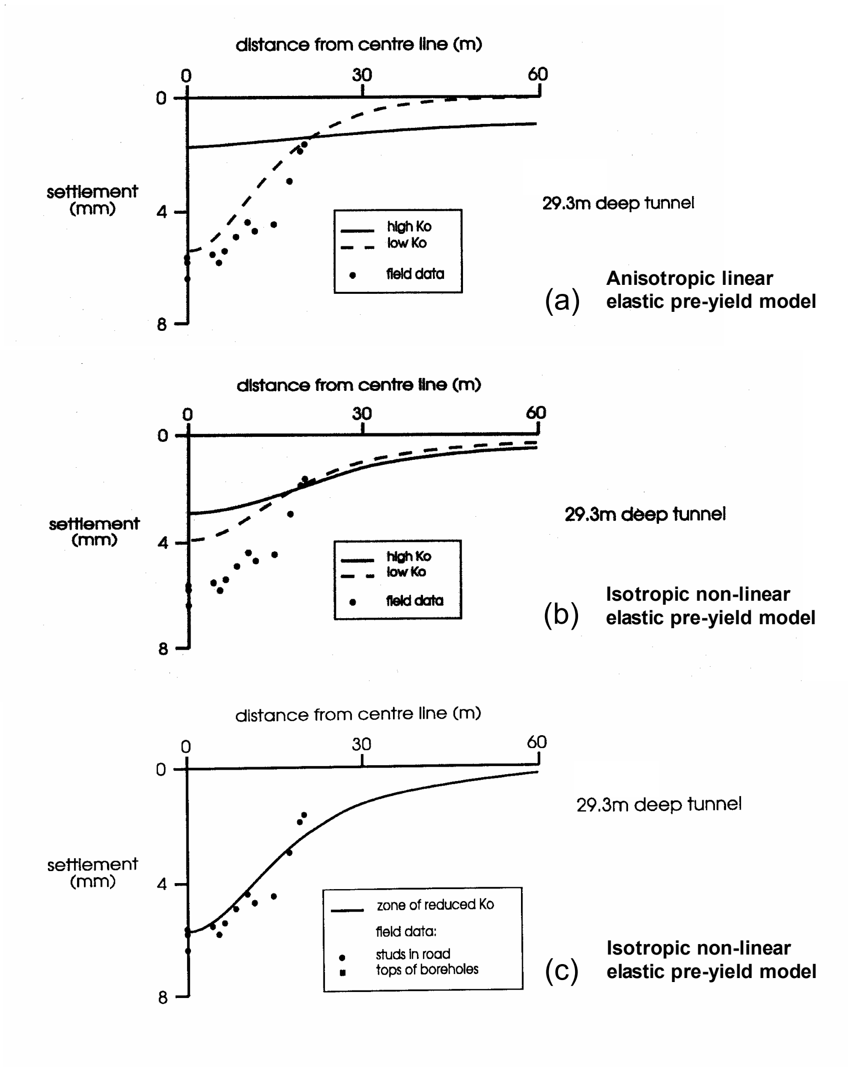

Figure II.9 – Computed and measured settlement at Green Park (Addenbrooke, 1996)

The dependence of the effective stress ratio before the excavation as well as of the small strain stiffness on the recent stress history can be issues of concern. Particularly in the case of stiffness parameters, as they have to be calibrated on laboratory tests which almost never reproduce correctly the stress history that the field soil experienced. The ability of modelling the stress history of the soil appears then a useful feature for a constitutive law. To include the effect of the recent stress history in a critical state mechanics framework, Stallebrass (1990) incorporated in the standard Modified Cam Clay two additional kinematic yield surfaces: this model was called 3-SKH (Three Surfaces Kinematic Hardening) and it is illustrated in App. 3. A parametric study has been carried out by Stallebrass *et al.* (1994a) in order to investigate the influence of the recent stress history on the deformations around tunnels excavated in overconsolidated soils, by using the 3-SKH model. In Fig. II.10 surface settlement profiles for shallow (a) and deep (b) tunnels are reported: they correspond to four different recent stress histories of the soil, described by anisotropic unloading or reloading. The recent stress histories is represented by the relative position of the three surfaces. It was not possible to simulate different stress history without changing the K_o profile, but the Authors reports a maximum difference between the profiles of 17% near ground level up to less than 5% at the deep tunnel level. In practice, the differences in the settlement profiles can be ascribed only to the different distributions of the soil stiffness around the tunnel boundary before the excavation, which arise from different histories. The effect of K_o has also been studied by varying the overburden stress: the results show that the lower K_o the narrower and deeper the settlement trough, consistently with those obtained by Addenbrooke (1996) with different models.

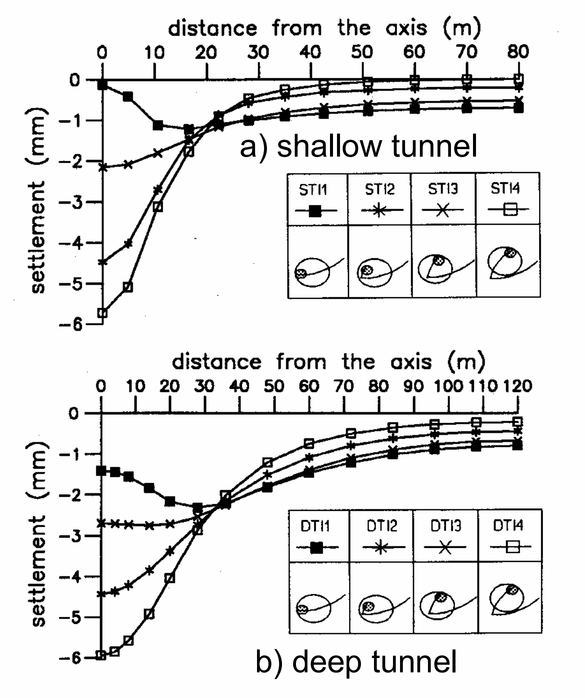

Figure II.10 – Effect of the recent stress history on the settlement profiles (Stallebrass et al.*, 1994a)*

Effects of tunnelling on buildings: damage assessment.

Assessment of a building damage can be a very subjective issue. A classification of damage is therefore a necessary instrument to measure objectively the degree of damage suffered by a structure.

Most of the existing classifications are based on the crack width in masonry. Cracking usually results from tensile strain. Polshin and Tokar (1957) and Burland and Wroth (1974) introduced the concept of 'critical' tensile strain, as that strain associated with a clear and visible cracking. Burland *et al*. (1977) replaced the concept of 'critical' tensile strain with that of 'limiting' tensile strain, thus referring to a serviceability parameter. This idea was further developed by Boscardin and Cording (1989) who analysed the damage of a number of brick-bearing-wall and small frame buildings affected by excavation and related it to the attained limiting tensile strain. They highlighted the fact that building deforming for excavation induced ground movements are usually less tolerant of differential settlements and distortions than similar structures settling under its own weight. This happens because of the horizontal ground strains which the excavation develops. Burland and Wroth (1974) had proposed to study the damage of a building with an elastic deep beam under bending and shear (Fig. II.11): the critical or limiting tensile strain can be attained at the extreme fibre as $\varepsilon_{b,\max}$ if the beam tolerance to bending deformation is lower than its tolerance to shearing deformation; on the contrary, it is attained along diagonal lines as $\varepsilon_{d,\max}$.

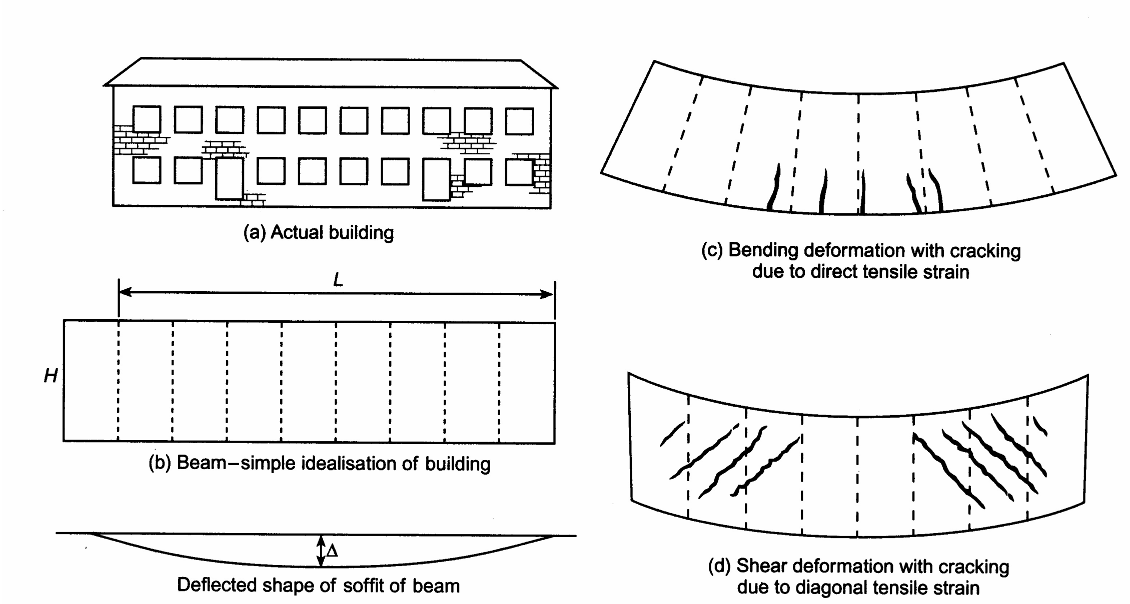

Figure II.11 – Cracking of a simple beam in bending and shear (Burland and Wroth, 1974)

By using the solution for a simply supported beam with a central load (Timoshenko, 1957), the deflection ratio Δ/L, i.e. the ratio between the mid-span deflection and the length of the beam, or, equivalently, the angular distortion β can be expressed under the assumption of isotropic elasticity and rectangular section, as functions of the limiting tensile strain $\varepsilon_{\lim}$, the ratios L/H and E/G and the position of the neutral axis. Two different functions are thus obtained, corresponding to the two conditions $\varepsilon_{b,\max} = \varepsilon_{\lim}$ (bending related tension cracking) and $\varepsilon_{d,\max} = \varepsilon_{\lim}$ (shearing related tension cracking): they have to be combined in order to define a limiting function which identifies the values of Δ/L for which a given level of cracking (defined by $\varepsilon_{\lim}$) occurs either for bending or shearing.

In order to account for the cracks induced by the horizontal ground tensile strains ε_h, which particularly develop close to excavations, Boscardin and Cording (1989) compose the abovementioned extreme fibre strain $\varepsilon_{b,\max}$ and diagonal strain $\varepsilon_{d,\max}$ with a constant horizontal strain ε_h: by equating these resultant maximum strains to the limiting strain $\varepsilon_{\lim}$, the limiting Δ/L or β become also functions of the horizontal ground strain ε_h.

Following Boscardin e Cording (1989), charts can be produced which allow to assess the level of damage induced by tunnelling to a given class of buildings, starting from the prediction of the quantities Δ/L (or β) and ε_h (Fig. II.12).

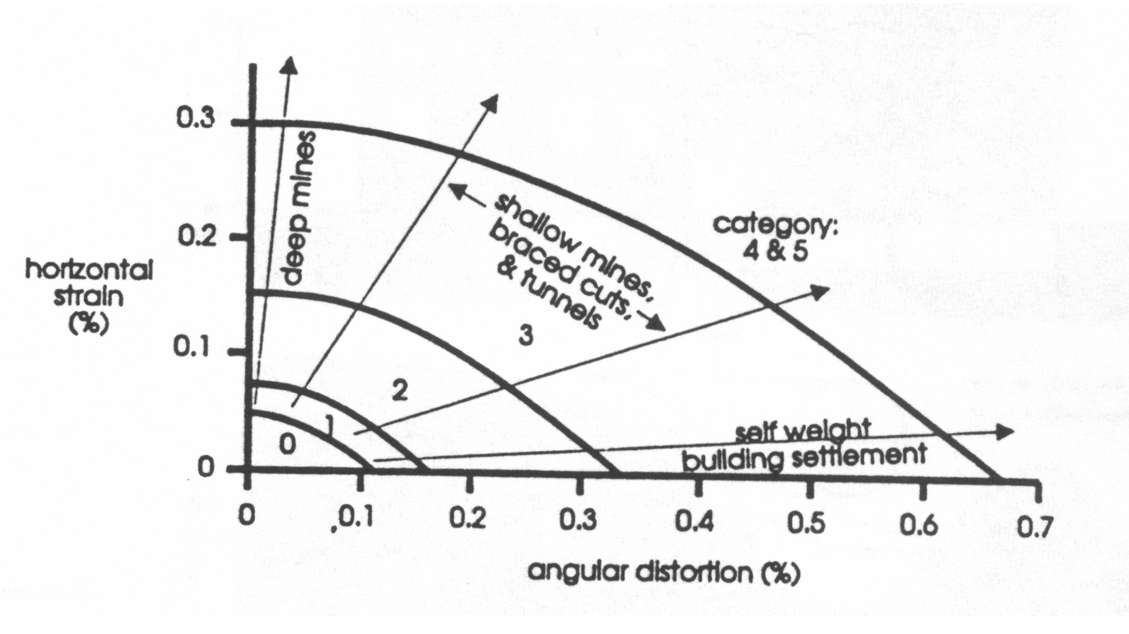

Figure II.12 – Building damage categories (Boscarding and Cording, 1989)

A rational methodology to analyse the damage induced to buildings has been widely adopted during the Jubilee Line Extension in London, as it has been described by Mair *et al.* (1996). It is based on the prediction of ground movements by using the empirical method, usually in plane strain conditions. A first level of analysis identifies those buildings which are located in areas where the greenfield prediction of the settlement exceeds 10 mm or in areas where the greenfield profile has a slope higher than 1/500. Only for these buildings a secondary stage of analysis is performed in which the category of damage of the building is defined by using the charts developed from the elastic deep beam model. At this level the analysis can be more accurate if the influence of the building of the induced ground movements is taken into account. In fact, it has been already observed that one of the limits of the empirical approach is not considering the beneficial effect of the building stiffness on the induced ground movements. As previously mentioned, Potts & Addenbrooke (1997) carried out a parametric study of the influence of building stiffness on ground movements induced by tunnelling using by a set of FEM analyses incorporating a non-linear elasto-plastic soil model in which the building is represented by an equivalent beam. They collected the results of such analyses to produce charts (Fig. II.13) in which modification factors to be applied to the deflection ratio Δ/L and the horizontal strain ε_h, as calculated from greenfield analyses, are plotted as functions of the relative axial stiffness α^* and bending stiffness ρ^* defined as follows:

$$\alpha^* = \frac{EA}{E_s(B/2)} \tag{II.19}$$

$$\rho^* = \frac{EI}{E_s(B/2)^4} \tag{II.20}$$

where E is the Young's modulus, A the cross-sectional area and I the moment of inertia of the equivalent beam, B is the width of the beam and E_s a representative soil stiffness. If such modification factors are applied to the empirical greenfield deflection ratios and horizontal strains, the assessed category of damage is more realistic.

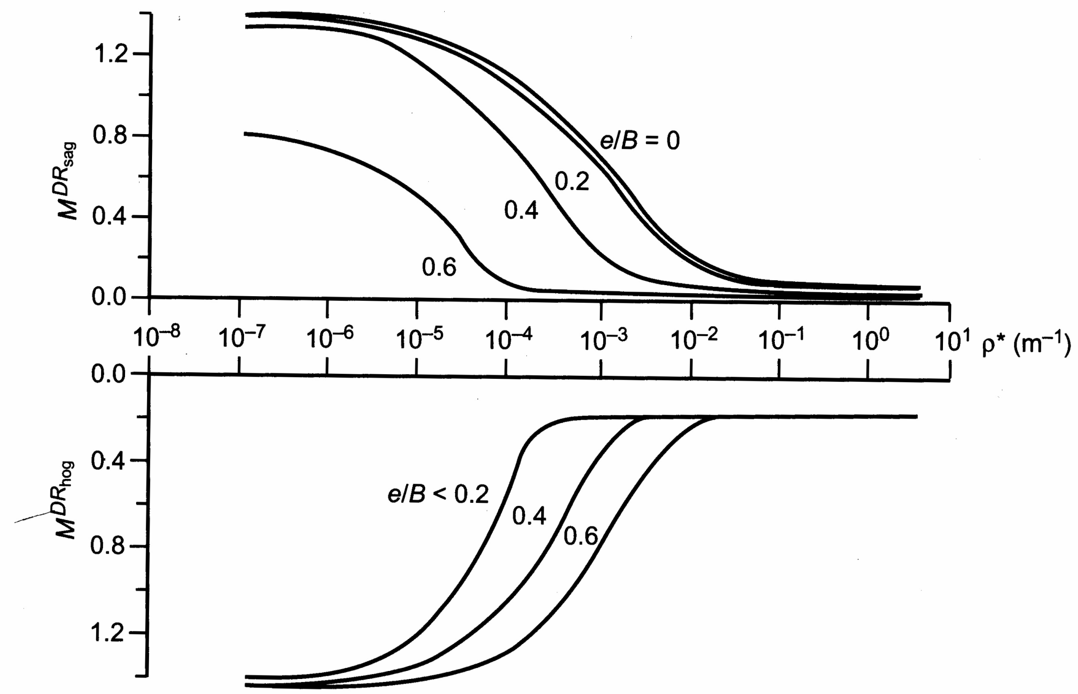

Figure II.13 – Modification factors for deflection ratio in sagging and hogging (Potts and Addenbrooke, 1997)

A more detailed analysis is then performed only for those buildings which potentially suffer limiting tensile strain higher than 0.15%. At this third level of analysis the problem is modelled in detail, by considering the interaction between the building and the ground and the three-dimensional effects.

Miliziano *et al.* (2002) performed a set of bi-dimensional numerical analyses aimed to model the soil-tunnel-structure interaction in order to predict as better as possible the amount of damage. The approach followed to model the masonry allowed the evaluation of number, frequency, pattern and width of the cracks.

Burd *et al.* (2000) performed a three-dimensional numerical study of settlement damage to buildings, with a multi-surfaces kinematic hardening model for soil and an elastic no-tension model for masonry. This study shows that the current assessment methods which apply a greenfield deformation to the building are conservative only for façades subjected to sagging deformation, whilst soil structure interaction effects are less significant when the building deforms in a hogging mode. In fact, the influence of the weight of the building is an increase of the magnitude of the settlements, whereas the building stiffness may act to reduce differential settlements: the resulting performance of the building depends on its position and orientation relative to the tunnel.

Protective measures.

In order to reduce the damage induced to an existing structure, a wide range of techniques is available. Harris (2001) suggested to group the techniques to protect structures during tunnelling operations into three classes: structural measures, in-tunnel actions and ground treatment methods. The distinction is sometimes difficult and somehow subjective because there are measures that can be seen as belonging to more than one class. A short review of some available case histories is reported.

Structural measures

This category is aimed to protect buildings from damages and comprises all the actions which reduce the impact of ground movements on the buildings by stiffening or strengthening them (e.g. using tie-bars, straps, reinforcing beams), by cutting joints to allow relative movements, by modifying the foundation system (e.g. deep underpinning) or by isolating the buildings from their foundations and controlling their movements (e.g. jacking). These measures are generally adopted when the existing defects of the buildings would require in any case repairs or partial renewal.

In-tunnel actions

It is recognised (Mair & Taylor, 1997) that the short term movements caused by tunnelling are the most significant causes of damage to the existing structures (with the only exception of tunnels with impermeable lining in soft clays, where the post-construction settlements can play an important role) and that they are mainly due to the ground deformation at the heading and around the excavated cavity before lining. Hence, the choice of the excavation method is crucial to reduce the impact on the existing buildings. Actually, this choice is strongly related to the soil conditions which affect the stability of the excavation. When closed face tunnelling is adopted, the face loss is close to zero and the ground movements are reduced. Nevertheless, sprayed concrete lining construction often achieves volume losses comparable or even lower than closed shield excavation (Mair & Taylor, 1997): this depends on the actions taken to reinforce the soil and to guarantee the stability of the heading during the excavation. At the same time these actions have the positive effect of reducing the movements at the source, being therefore also defined as in-tunnel protective measures (Harris, 2001). Among them, mechanical pre-cutting and pre-vaulting, radial and face injections, radial and face bolting can be mentioned. In most cases these measures are adopted in combination from a partial heading or pilot tunnel excavation. For instance, Maiorano and Viggiani (2003) report the excavation of a chamber in pyroclastic soil in Napoli where two tunnels (crown at about 20 m below the ground level) converge under a 3-storey masonry building (Fig. II.14).

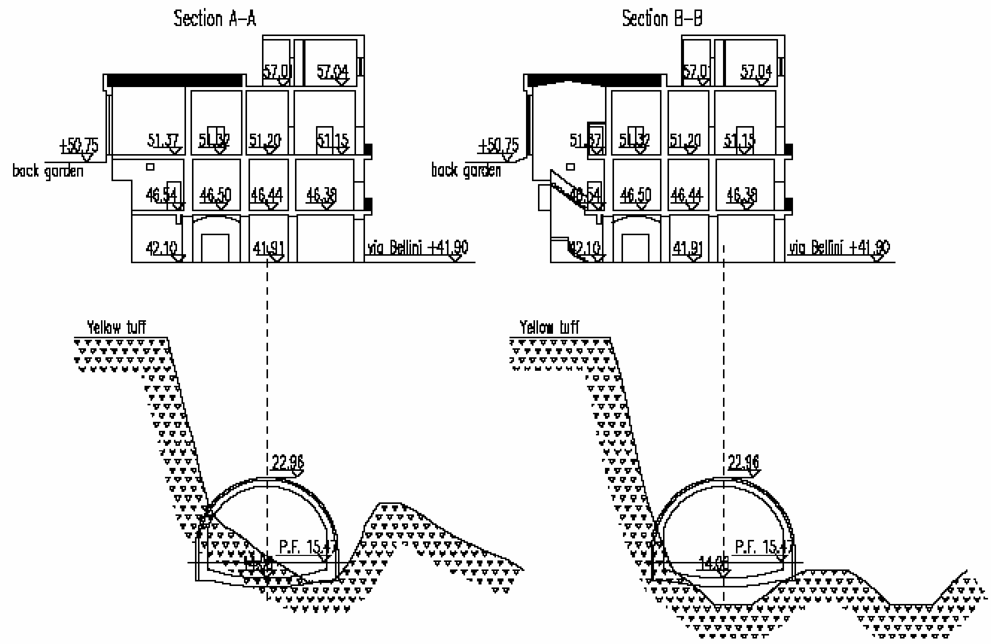

Sections through the building and the chamber

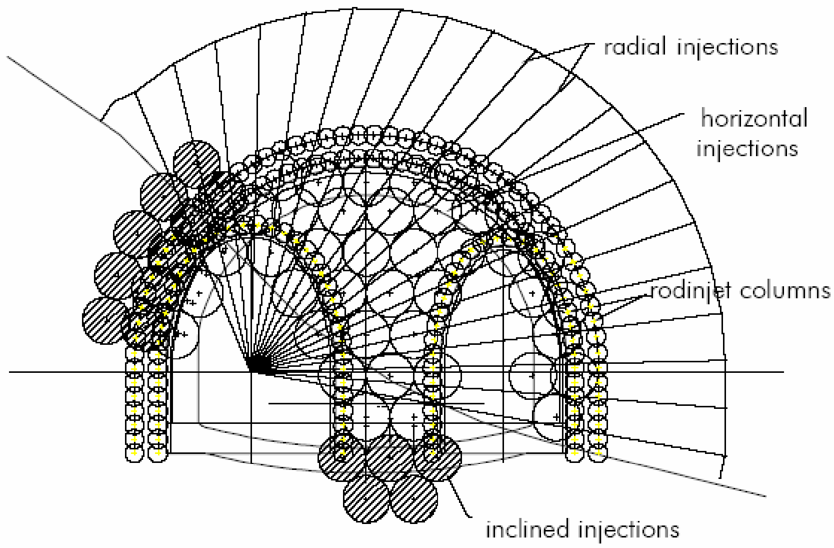

Ground treatment

Figure II.14 – In-tunnel actions in pyroclastic soil in Naples (Maiorano and Viggiani, 2003)

In this case a pilot tunnel was previously excavated under a jet-grouted vaulted arch from which radial and frontal chemical and cement injections were performed before excavating the whole section. Another typical combination of various in-tunnel measures is shown in Fig. II.15 and it was adopted during the excavation of the Frankfurter Kreuz Tunnel (10 m diameter, crown at 10 m depth) in sand and gravel under an existing highway (Quick *et al.*, 2003).

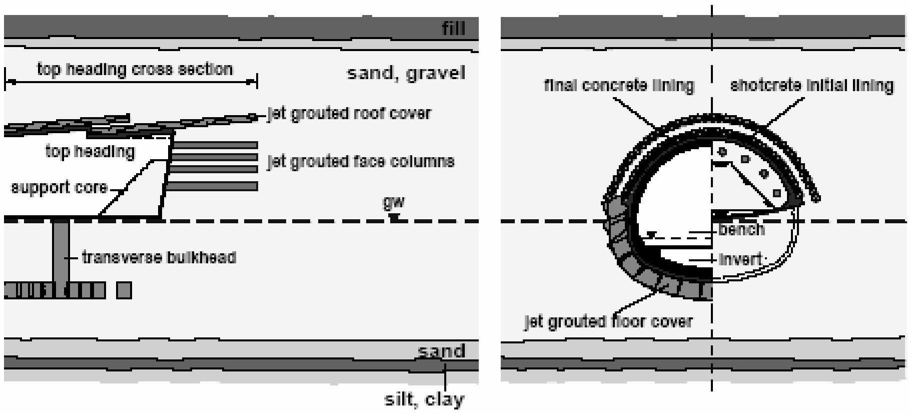

Figure II.15 – Construction details of Frankfurter Kreuz Tunnel (Quick et al.*, 2003)*

Ground movements were sensibly reduced by adopting a partial face excavation protected by jet grouted roof and face sides and by a watertight jet-grouted floor cover. The latter measure was adopted because the groundwater level was about at the tunnel axis and dewatering was not allowed. Different measures have been undertaken at the 'Baldo degli Ubaldi' Rome Underground Station, as reported by Lunardi & Focaracci (1998). A 21.5 m wide and 16 m high tunnel was there excavated in stiff clayey silts about 25 m bgl with separate headings: side drift, crown drift, bench and invert. In order to limit the settlements of a multi-storey building whose foundations lied only 2 m above the tunnel crown, the advance core was reinforced with fibre-glass rods 25 m long and a mechanical pre-cutting, filled by concrete, was performed before the crown excavation. Moreover, a pre-cast concrete segmented arch was installed at the crown and contrasted against the side lining walls through flat jacks housed in the key segment (‘active-arch’ system).

Ground treatment methods

Other methods which can be applied to reduce the damage of the structures by reducing the magnitude of the ground movements are based on ground treatment. This category includes both ground improvement and reinforcement which allow to modify the ground response to tunnelling. Moreover, a peculiar form of soil treatment which acts directly on the soil displacements is more and more adopted: compensation grouting.

Ground improvement techniques range from grouting to de-watering, soil compaction or replacement: all these methods have been used before excavation to stiffen and strengthen the ground. A widely used improvement technique is *permeation grouting*: it can be defined (Littlejohn, 2003) as “the introduction of low viscosity gelling solutions or particulate suspensions into the ground, e.g. clean sands and gravels or permeable discontinuities in rock, without disturbing the structure of the ground”. Permeation grouting has essentially two main effects: reduces the permeability of the soil and increases its strength and stiffness. The grout usually consists in silicate solutions, which reduce noticeably the soil permeability, and in micro-fine cement suspensions, which allow for stronger and stiffer results than silicate grouts. Permeation grouting has been adopted as a protective measure in various sites along the Jubilee Line Extension in London: generally, it created a sort of ‘slab’ in the layer of Terrace Gravel between the building foundation and the tunnel. In this way, the ground movements distribution was modified and the differential settlements of the affected building were reduced. In some cases it was used in combination with compensation grouting to give a more uniform response to grout injections.

Compensation grouting is defined in the current practice as “the introduction of a medium to high viscosity particulate suspension into the ground between a subsurface excavation and a structure, in order to negate or reduce the settlement of the structure due to ongoing excavation” (Littlejohn, 2003). Compensation grouting can be triggered when a threshold value of settlement or distortion of the structure is measured, or it can be adopted during the excavation following a pre-determined plan to limit the occurring settlement or distortion to a given value. In the first case it is called *observational* or *corrective* compensation grouting, in the second concurrent compensation grouting. Sometimes, a *pre-treatment* grouting (cement or chemical injections) is adopted to stiffen the soil and set up the fracture system before the actual compensation.

Compensation grouting can give rise to inclusions in the soil which have different shapes: *compaction grouting* is obtained with sand and silt mortar using large diameter grout tubes and consists in a series of injected bulbs; *fracture grouting* is obtained by hydro-fracturing the soil with relatively fluid grout injected from *tubes-à-manchettes* (TAMs).

Compaction grouting was applied for the first time to reduce settlements induced by tunnelling in the late 80's at the Bolton Hill Subway tunnels in Baltimore (Baker, MacPherson & Cording, 1980). The tunnel was excavated by a TBM in very dense sand and gravel and the injections were done every 1.5-3 m concurrently to the excavation and close to the tunnel between 1.5 and 4.5 m above the crown and about 1.5 m behind the tail of the shield. In this way the ground movement was reduced at its source and a series of one to four-storey buildings was protected, by limiting the maximum surface settlement to 12.5 mm.

One of the first use of fracture grouting during tunnelling was described by Pototschnik (1992). A station of Vienna Underground (30 m wide x 8 m high) was excavated by NATM 12 m below a 5-storey building in clay and silt sediments: the grout was injected at mid level between the excavation and the building (Fig. II.16). The maximum allowed settlement of 40 mm was exceeded due to dewatering but the deflection ratio of the structure was contained below the permitted value 1/1000.

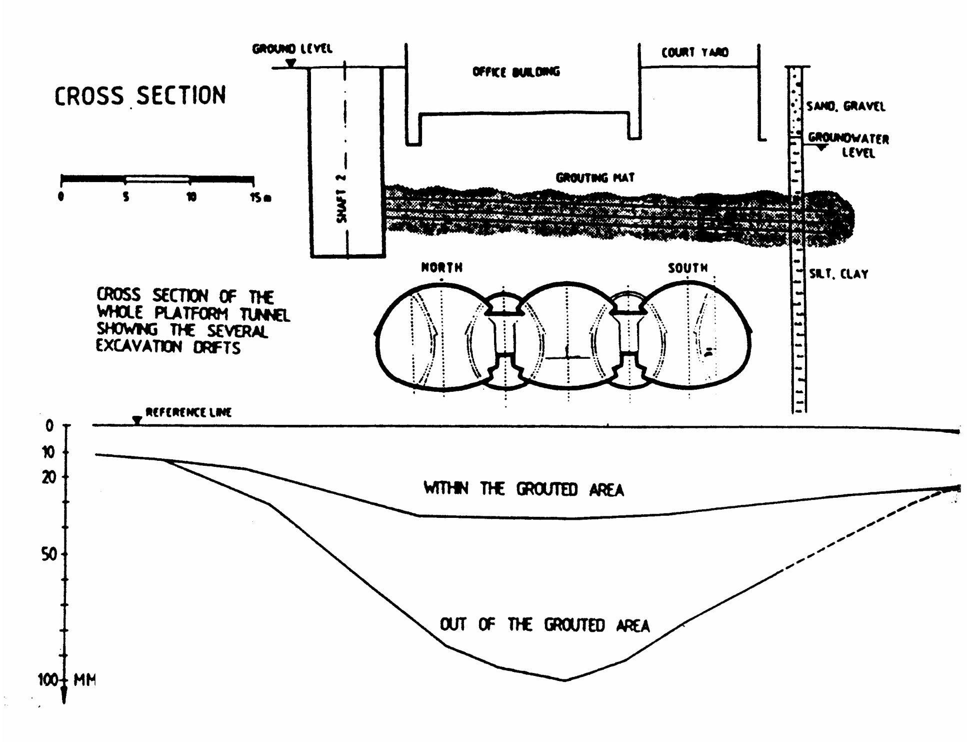

Figure II.16 – Comparison of settlement profiles for grouted and ungrouted area (Pototschnik,1992)

Fracture grouting in soft till (basically, a very heterogeneous clay with coarser inclusions) was applied to limit settlement under the Imperial Oil Research Building (Ontario, Canada) due to the excavation with an EPB shield of the St Clair River railway tunnel (9.2 m diameter, ~17 m axis depth) about 10 m below the building foundations (Forbes & Finch, 1996). In this case (Fig. II.17), pre-treatment grouting was performed which induced heave. Hence, the planned concurrent grouting was not necessary to respect the limiting maximum settlement of 10 mm (in fact, the actual net movement after tunnelling was a small heave), nevertheless it was carried out in order to limit the angular distortion to 1/1500.

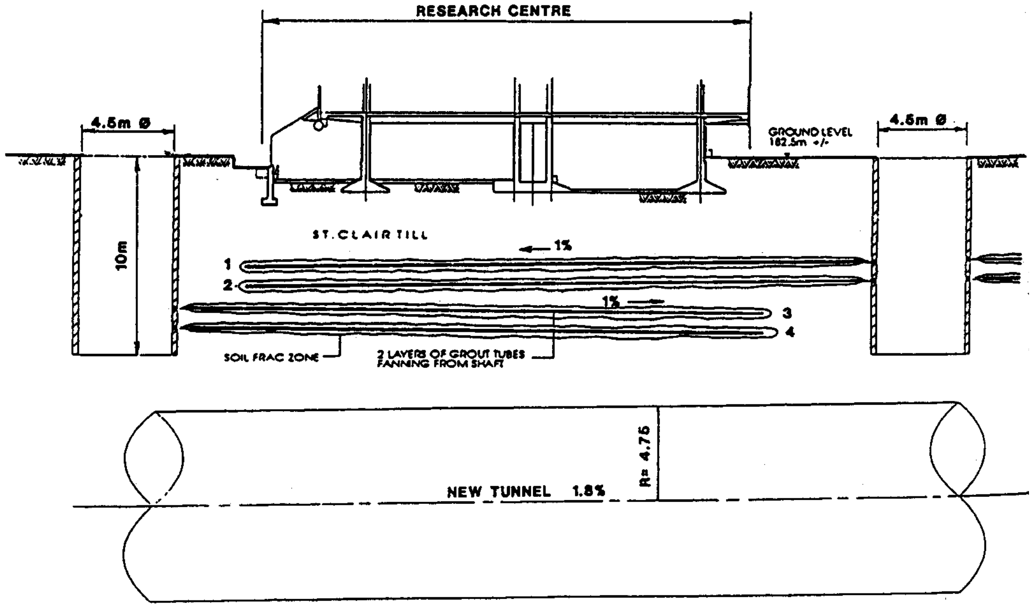

Figure II.17 – Fracture grouting in soft till (Forbes and Finch, 1996)

Before the excavation of the Jubilee Line Extension in London in the 90's, a few tests of compaction grouting in Thames Gravel and of fracture grouting in London Clay were carried out. It was decided not to run compaction grouting because it required to re-drill holes to inject again: fracture grouting, on the contrary, was performed at various locations along the 15.5 km of mainly twin 4.4 m internal diameter tunnels and 8 stations. An example of controlled ground movements by fracture grouting is reported in Fig. II.18.

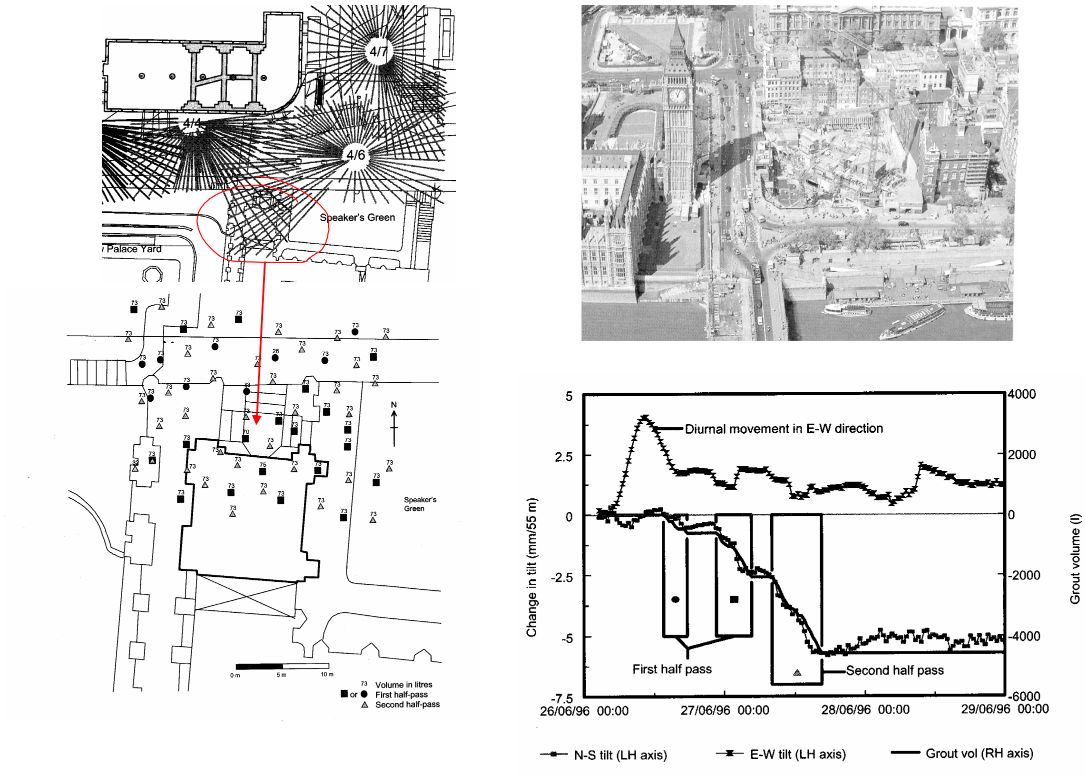

Figure II.18 – Fracture grouting at 'Big Ben' in London (Harris, 2003)

As London Clay is a heavy overconsolidated soil (K_o=0.8-2) and in hydro-fracturing methods the direction of the minor principal stress in the ground usually dictates the direction of the induced fractures, this method produced sub-horizontal fractures with opening up to 1-2 mm, thus inducing a controlled heave (Harris, 2001). Fracture grouting was used in the sequence: pre-treatment, concurrent grouting, corrective grouting beneath the Ritz Hotel, the Treasury Building and along Great George Street; the ground was pre-treated before concurrent grouting at the Royal Automobile Club and before corrective grouting along St. Thomas Street; concurrent grouting alone was used in the area of London Bridge whilst corrective grouting was used beneath Keetons Estate at Bermondsey, where a 'slab' in the Terrace Gravel overlying the clay layer was created by grouting before jacking the soil after tunnelling. With this strategy the damages to buildings were reduced everywhere to no more than slight (typical crack width up to 5 mm). In addition to this general requirement, for some buildings the settlement was limited to 25 mm; this limit was specified also for all the existing rail-carrying structures together with a maximum limit on their slope of 1/1000; for London Underground's existing tunnels the movements were limited to 10 mm and 0 mm for the escalators. A complete description of the protective measures (including compensation grouting) adopted along the JLE to meet all these requirements has been edited by Burland, Standing & Jardine (2001).

Lee et al. (1999) report a case of concurrent grouting in gravel beneath the Royal Hill Court, a 2-storey reinforced concrete frame building over the 2 tunnels (5.75 m diameter, ~11 m axis depth) of the Docklands Light Railway in London (Fig. II.19). The TAMs were installed about 2-3 m above the tunnel crown and the gravel was previously conditioned (pre-treatment grouting) to improve the efficiency of the following action.

The building settlements were lower than 15 mm and the angular distortions lower than 1/1000, thus satisfying the specified design criteria.

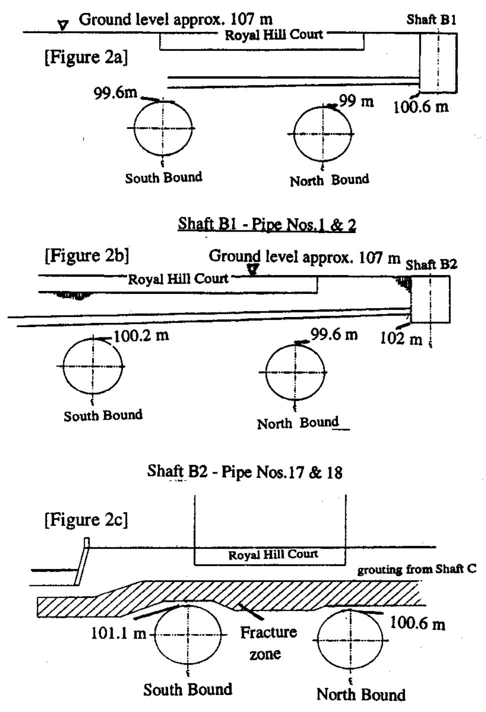

Figure II.19 – Typical grouting array at Royal Hill Court (Lee et al.*, 1999)*

Chambosse & Otterbein (2003) describe the protection of the Antwerp Central Station during the excavation of a tunnel (rectangular section, H=6 m, ~10 m roof depth) in a normally consolidated sand deposit (Fig. II.20). The tunnel was excavated with the Belgian method under a protective pipe umbrella roof located 5-6 m below the station foundations. The soil was pre-grouted to increase the horizontal stresses and its stiffness. The steel TAMs, located 3.5 m below the foundations, provided also a further strengthening of the ground. Concurrent fracture grouting was performed during piping and during tunnelling and resulted into about 2 mm heave of the building when the requirements were to restrict the vertical settlement to 5 mm and the slope to 1/2000.

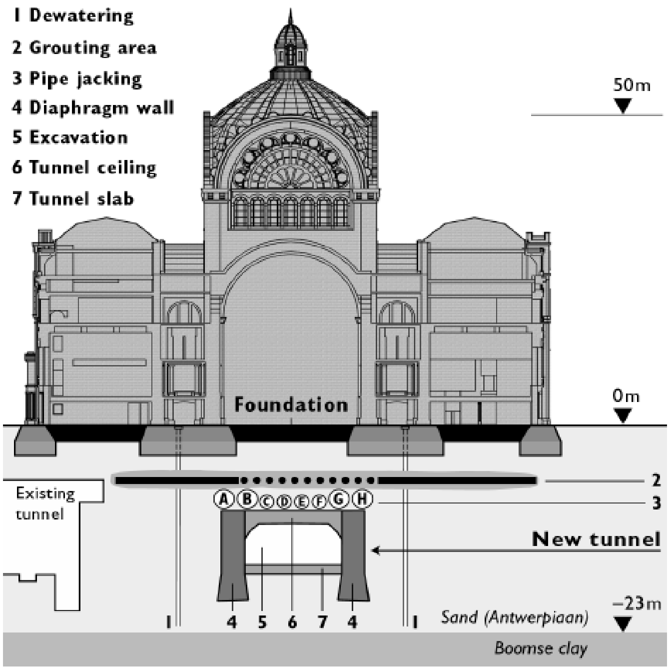

Figure II.20 – Antwerp Central station: construction details (Chambosse and Otterbein, 2003)

Sola, Monroe & Garcés (2003) report two cases of compensation grouting along the Lisbon Metro Line D extension (7- and 8-storey buildings on piles). The tunnel (10.5 m diameter, 27 and 25 m axis depth) was excavated with an EPB shield, mainly in calcarenite overlaid by 3-4 m of limestone (often containing voids) and about 10-13 m of clay. In one case permeation grouting was performed at the contact between the limestone and the clay to fill possible voids and concurrent grouting was carried out during the excavation. In the other one, the ground was pre-treated to increase its stiffness before tunnelling and concurrent grouting followed. In both cases the net result was a heave of a few millimetres, thus meeting the design requirements. It has to be mentioned that a jet-grouting portal around the tunnel section had been made to improve the very loose calcarenite before the arrival of the shield, thus reducing the risk of face instability.

Compensation grouting has been largely used as a protective measure during the first (1995-1999, 56.3 km of new line and 37 stations) and the second (1999-2003, 54.7 km and 26 stations) extensions of the Madrid Metro system. Melis *et al.* (2003) describe some cases of compensation grouting works undertaken during the last six years. All these cases are within Madrid and the local geology is very similar: about 7-8 m of fill and alluvium overlie about 10 m of dense sand with varying clay content. At some locations the tunnels were excavated in phases (Madrid method, 10.5 m diameter), at some others an EPB was used (9.38 m diameter). In some cases the compensation was concurrent, in the others it was necessary to perform corrective grouting to meet the requirements; pre-treatment grouting was not always needed. Other cases have to be mentioned: Melis *et al.* (1998) describe the first case of compensation grouting in Madrid (Fig. II.21) when protecting an existing tunnel by permeation grouting followed by concurrently fracture grouting and Sola, Guardia and Monroe (2003) illustrate in detail the case of two buildings in Vallecas (Madrid) which were protected by compaction grouting (Fig. II.22).

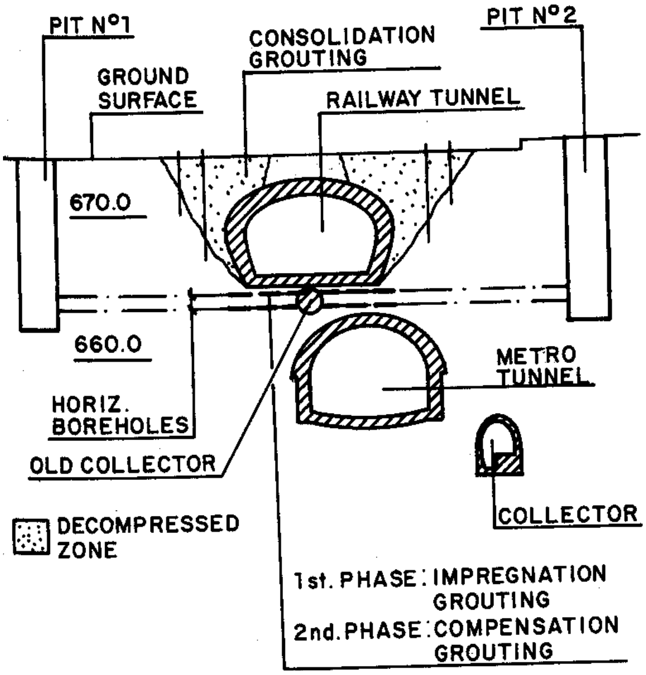

Figure II.21 – First case of compensation grouting in Madrid (Melis et al.*, 1998)*

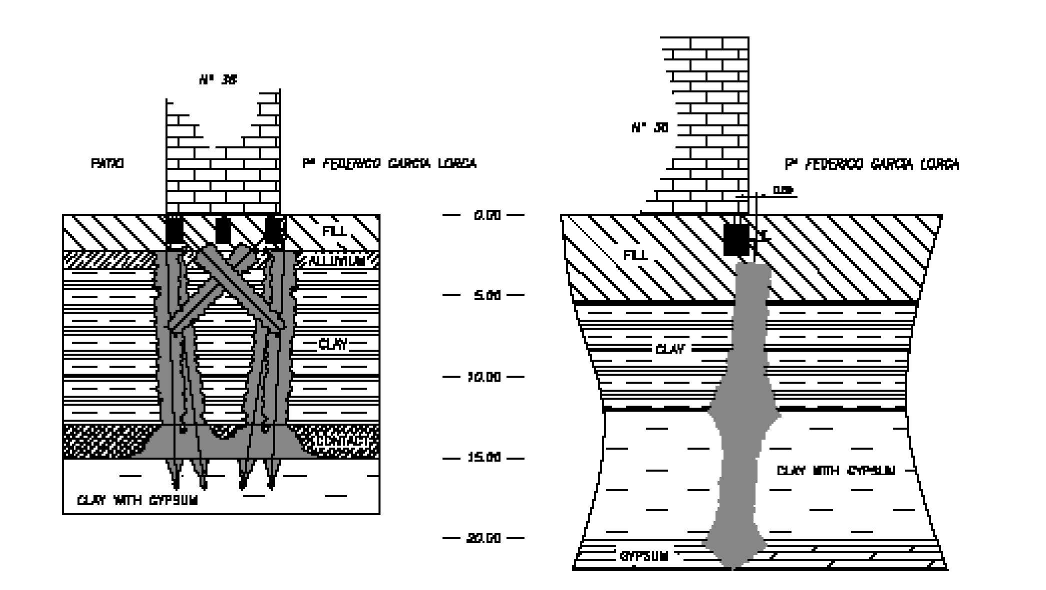

Figure II.22 – Buildings in Vallecas (Madrid): typical section of grouting works (Sola et al.*., 2003)*

Finally, it is possible to use structural <u>reinforcement of the ground</u> to reduce the damage to buildings in two ways: either the structural elements act to stiffen the soil thus reducing the magnitude of movements, or they act like a barrier against the ground movements by modifying the displacement fields.
An example of the first type is an 'umbrella' of steel pipes jacked above the crown of a tunnel, which is able to stiffen the soil when different actions are not feasible: this measure was adopted, for instance, beneath Bridge Street close to the Big Ben Tower during the JLE works. In the whole area compensation grouting was performed to control the movements of the tower; but installing very close spaced TAMs in the area beneath the street would have been too much problematic, thus inducing the contractor to adopt the structural umbrella solution (Harris, 2001).
During the excavation of the Yan An Dong Lu tunnel in Shanghai (Chen *et al.*, 1998), the ancient astronomical observatory, a building about 50 m high, needed to be protected from the excavation of a shield tunnel with 11 m diameter and 20 m axis depth, passing about 15 m away from the building foundation (Fig. II.23).

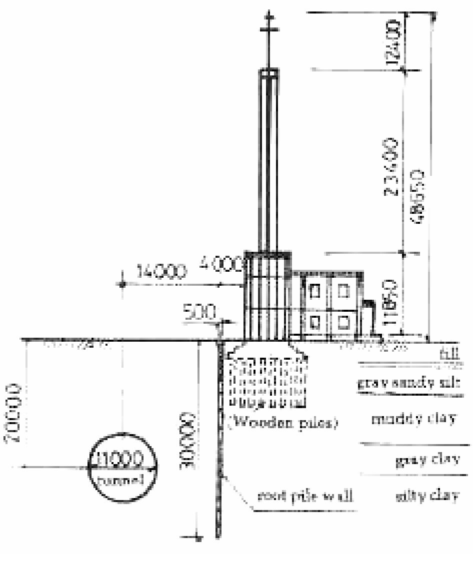

Figure II.23 – Root piles wall as a protective measure of the Shangai observatory (after Chen et al., *1998)*

This was a piled platform 14 m wide with probably 8÷10 m deep wooden piles. A root-pile wall about 30 m deep (the piles diameter was 20 cm) was constructed 14 m away from the tunnel axis and capped by a reinforced concrete beam. This beam was tied at its edges by tension cables which extended to the rear of the observatory and were anchored to blocks founded on additional root piles. The assessed tilt of the tower without root-piles ranged between 1/200 and 1/100 whilst the measured one was less than 1/1000.

A series of ground reinforcements has been carried out during the Madrid Metro tunnel construction by using jet-grouting. Essentially, three types of treatments have been performed to reduce ground movements, at the same time preventing instability phenomena: reinforcement by portals in jet-grouting columns, wall-type reinforcement and inverted V-type reinforcement. Sola, Monroe, Martin, Blanco & San Juan (2003) report 5 cases of jet-grouting portals, 6 cases of jet-grouting walls, 4 cases of inverted-V treatments which were undertaken along two lines of the Madrid underground between September 2000 and October 2001. An inverted-V treatment was carried out, for instance, beneath the access of the M-40 highway from Alcorcón where two parallel tunnels had to be excavated (Fig. II.24).

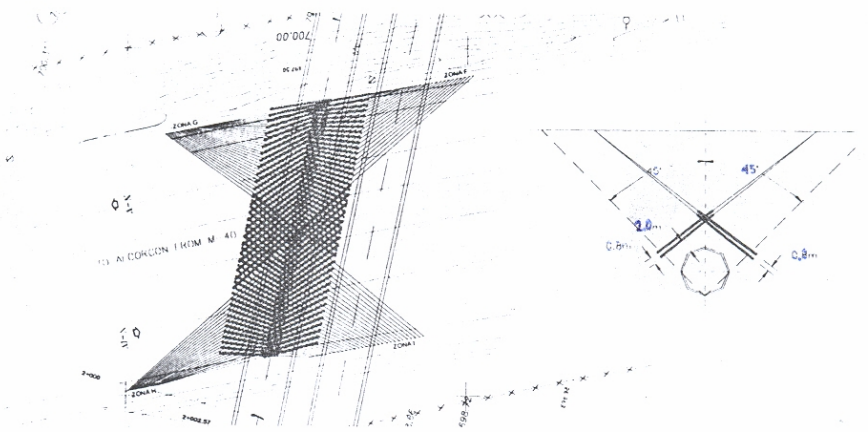

Figure II.24 – Inverted V-type jet grouting treatment (after Sola et al., *2003)*

The overburden clayey silty sands were 17 m thick. An inclined double wall of jet grouting columns was injected at each side of the first tunnel. These two walls converged and ended in a point above the tunnel crown while on the other edges they end on two 45° inclined lines from the invert. Hence, a sort of jet-grouting roof was protecting the excavation beneath: the Authors refer of movements induced by the excavation of both tunnels between 5 mm and 12 mm which were considered admissible.

The same Authors report a wall-type treatment to protect a 5-storey building located very close to a very shallow tunnel (Metrosur section X). The cover of the 10 m diameter tunnel was about 8 m thick and made of alluvial soils which in some zones were very soft. A discontinuous wall of 1.25 m spaced jet-grouting columns was constructed very close to the tunnel (less than one diameter from the centre at the tunnel axis level) between the tunnel itself and the building to be protected (Fig. II.25).

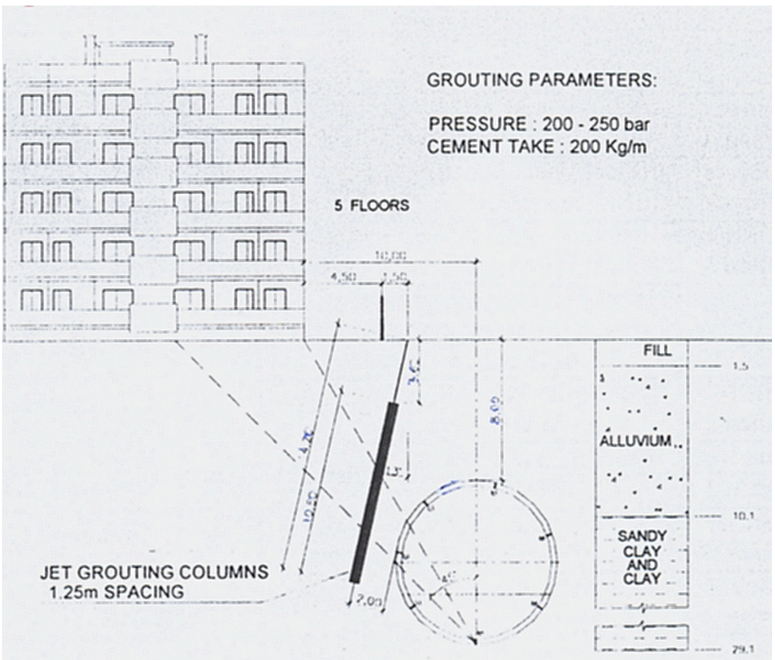

Figure II.25 – Wall-type jet grouting treatment (after Sola et al.*, 2003)*

The columns were inclined, as shown in the figure. They started at a depth of 3.60 m and ended at about midway between the tunnel axis and the invert. During jet-grouting the ground movements were less than 2 mm and after the tunnel construction the maximum settlement was about 2 mm, compared to the 10-12 mm which occurred in the nearby untreated zones. It has to be remarked that the softer zones of soil had been previously grouted to fill the voids thus improving the global effectiveness of the treatment.

A very similar action (Fig. II.26) had been undertaken close to the Madrid French Institute (Oteo *et al.*, 1999). In this case, a tunnel (8.4 m diameter, 14-15 m axis depth) was excavated by using an EPB shield partly in sand and partly in the overlying 10÷18 m fill cover. A building of the Institute was only 8-9 m away from the tunnel axis: two rows (70 cm spaced) of jet grouting columns (90 cm spaced) were made between the tunnel and the building, about 2 m away from the latter. The columns were interrupted at midway between the tunnel axis depth and its crown. The Authors measured settlements of about 5 mm beneath the building: this value was significantly lower than the values of 7-10 cm as predicted without treatment.

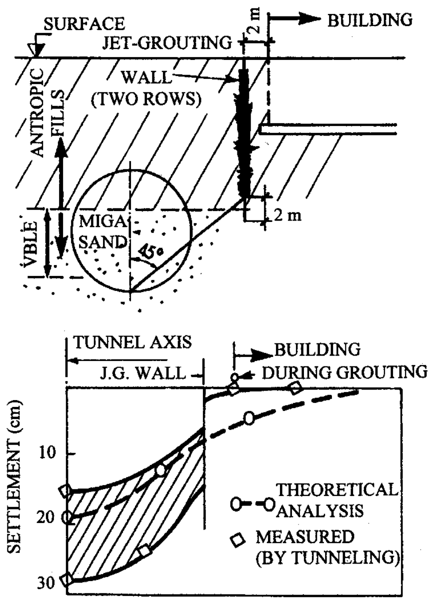

Figure II.26 – Madrid French Institute: protective measure and recorded settlements (after Oteo et al.*, 1999)*

At the end of this short overview, which does not intend to be exhaustive of all the possible solutions, it is worth noticing that the different technological solutions are usually adopted on the basis of some empirical or qualitative knowledge of their effects, much more than on the basis of a rational design process. This is largely due to the lack of field data and to the low research effort of modelling the effects of the most common protective actions. These observations were at the origin of the work presented in this dissertation on modelling one of the possible measures aimed to reduce the ground movements induced by tunnelling by inserting a vertical structural element as a barrier between the source of the movements (the tunnel) and the point to be protected.

III. Experimental work

Introduction

The aim of the experimental work carried out at the Centrifuge Laboratory of the City University London was to study the effectiveness of embedded diaphragm walls as a barrier to movements induced by the excavation of shallow tunnels in soft ground.

The basic idea being tested was whether or not a diaphragm wall embedded between the tunnel and an existing building was able to reduce ground movements behind the wall, thus reducing the possible damage to the building. The interest was focused on large and shallow circular tunnels, like those which are often excavated for underground railways. A wall was embedded into the models at different locations and its length, thickness and roughness were changed within the different tests that were performed. The image processing system of the centrifuge facility allowed determination of the displacement fields in the models.

The London geotechnical centrifuge testing facility

The London Geotechnical Centrifuge Centre is located in the premises of the City University London. The centrifuge facility is composed by a centrifuge room and an adjacent control room, as schematically shown in Fig. III.1.

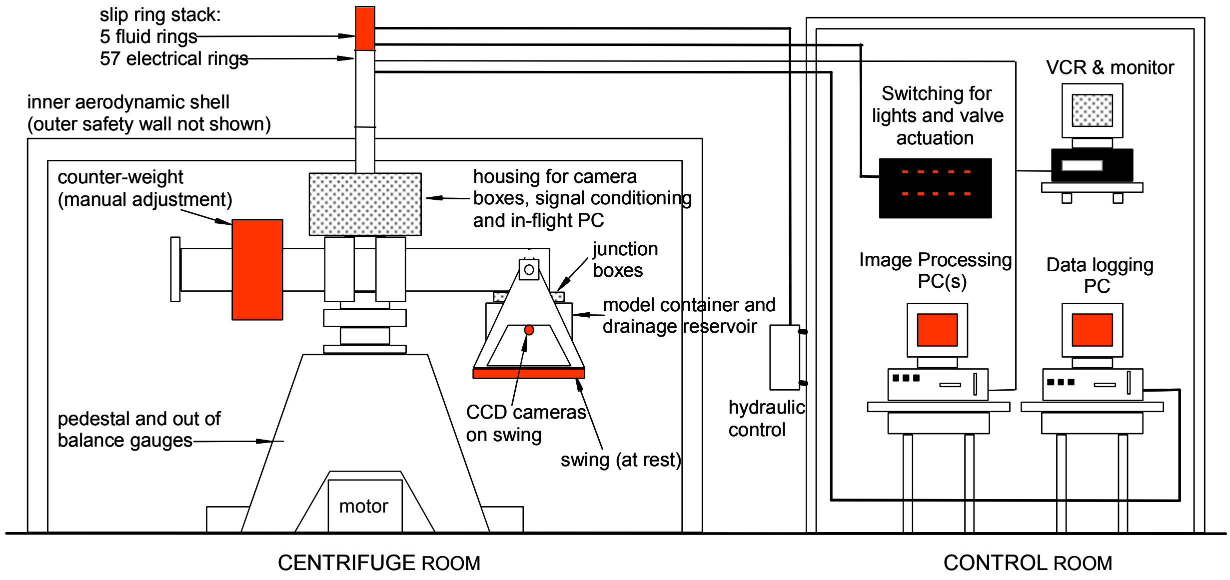

Figure III.1 - Sketch of the London Centrifuge facility (courtesy of Andrew McNamara)

The core of the London geotechnical centrifuge testing facility is an Acutronic 661 centrifuge. The radii to the base of the swinging basket in flight is 1.8 m which corresponds to working radius for soil models of about 1.5-1.6 m. Geometrical details are shown in Fig. III.2. The centrifuge has an operating capacity of 40 gravity tonnes and a maximum operating speed of 345 rpm, which results in 200g at 1.5m radius. As a consequence, a package up to 400 kg can be tested at 100 g or a package up to 200 kg at 200 g. The swinging basket has an available volume of 500 mm x 700 mm x 500 mm high.

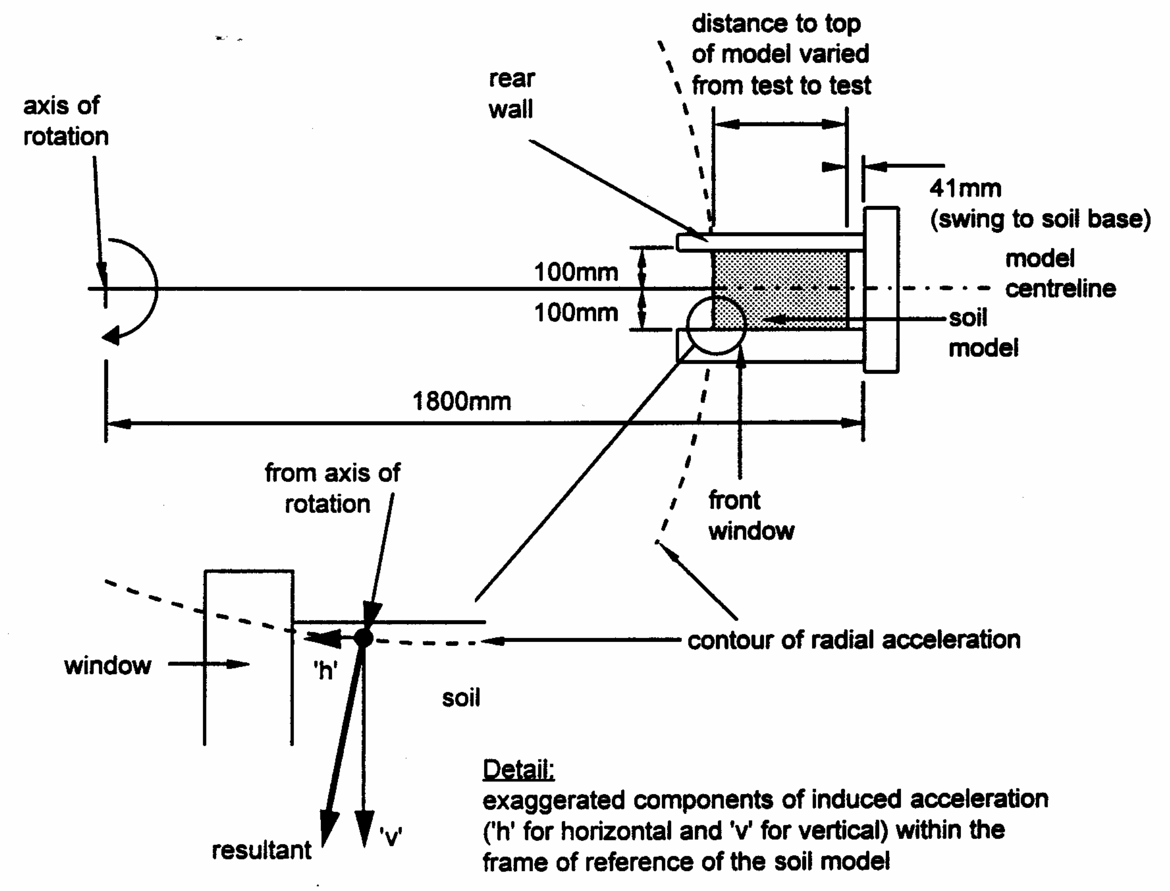

Figure III.2 – Centrifuge geometrical details (after Grant, 1998)

To minimise the energy dissipation during the flight, the rotating device is enclosed within an aerodynamic shell. A sacrificial wall surrounds the centrifuge chamber for safety reasons.

The centrifuge is balanced before every flight by means of a moveable counterweight. The out-of-balance forces are monitored during operation through four load cells which are located into the engine mount. As soon as an out-of-balance force reaches 20 kN, the system is automatically shut down. In this way it is possible to keep overnight operation without man control. However, the tests reported were conducted during day time and the monitored out-of-balance forces rarely exceeded 2 kN.

Electrical and fluid slip rings rotating together with the rotor arm allow electrical signals (power supply, transducers signals, CCTV system) to be relayed and water, compress air and oil to be supplied to the model during flight.

Onboard junction boxes permanently mounted on the centrifuge swing receive signals from the transducers and transmit them to an onboard signal conditioning unit to be filtered and amplified. These signals are then passed to a 16 bit analogue-to-digital converter and a computer, both housed near the centrifuge axis. This computer transfers the data through the slip rings as a single signal to a PC in the control room, which is provided of a data logging system. Data can be recorded at a rate close to 1 reading/s for each transducer, depending on the number of instruments to be logged.

Experimental procedure

In the followings, the experimental procedure adopted in the tests presented in this dissertation will be described. Details concerning used tools and equipments which can be found in Grant (1998) will not be reported.

Preparation of clay in the model

The models were prepared from a Speswhite kaolin slurry. Kaolin is used as a laboratory clay because of its relatively high permeability which allows for short consolidation time during sample preparation. It has been also widely used for centrifuge tests at City, particularly those in which an image processing of pictures taken during test was necessary, and the technique to set-up a model is well established.

Kaolin powder and distilled water were thoroughly mixed before each test to obtain homogeneous slurry at a water content of approximately 120% (about twice the liquid limit water content). As kaolin could be recovered after testing, part of the slurry was obtained by reusing kaolin from previous tests, with a water content of about 35%-40%. The whole mixing process took about four hours. Once ready, the slurry was carefully poured into a strong Duraluminium container (550 mm large x 200 mm width) ensuring that no air voids were trapped in the soil. The inner walls of the container had been lubricated with lithium grease in order to minimise friction. The base of the strong-box had a pattern of drainage channels communicating with two ports at the end of the box: this drainage system was kept clear from clay particles by lining the box bottom with a 3 mm porous plastic sheet and filter paper.

A porous plastic sheet and filter paper were positioned also on the top of the sample before it was placed under a consolidation press. This allowed the water drainage through holes in the loading plate from the sample top during consolidation.

The pressure was applied by an oil pressure loading ram which loaded the sample through a rigid plate and maintained (or adjusted) using a computer control. The sample was then one-dimensionally consolidated in the strong box to a vertical pressure p_{max} = 350 kPa and then swelled back to a pressure of 150 kPa. The value of p_{max} was chosen (after two trial tests, in the first of which p_{max} = 250 kPa) in order to get a model ground which was neither too strong nor too weak thus allowing large movements but preventing an early collapse during the test. The whole process took several days. The maximum pressure was not applied in a single step. First the sample was loaded up to 50 kPa and this pressure was kept for about twenty minutes in order to check the seal around the sample. Then the pressure was raised to 125 kPa, 200 kPa and 350 kPa in about a couple of days. The consolidation took two days and a half. At this point it was observed that vertical movements were negligible and the sample was swelled back to 150 kPa in one go. After about half a day two PDCR81 miniature pressure transducers with a porous stone, manufactured by Druck Limited, were embedded at two different points around the cavity, one at about 15 mm below ground level, the other at about 90 mm bgl, to check the pore pressure during the various phases of the test. The porous stones had been de-aired and saturated in a chamber filled by distilled water imposing a vacuum around 100 kPa for about 1 hour. These transducers were calibrated before most of the tests through the centrifuge data logging equipment up to 200 kPa against a Druck DPI101 Digital Pressure Indicator by applying a known pressure to the chamber using a Bishop ram. They were introduced from access ports in the rear wall of the strong-box. Holes in the ground were bored by an auger tube until about mid sample; the same tube was used as a guide to push the transducer inside the model. The tip of the transducer was previously dipped in de-aired slurry to improve the contact with the bedding clay. The same slurry was injected by means of a syringe to back-fill the gap behind the transducer and the port was sealed around the cable. The pressure was kept constant at 150 kPa for about one day and a half before testing.

Preparation of the model

On the day of test the taps of the bottom drainage were closed and the free water was sucked away from the top of the box. After that, the ram was lifted and the container was moved to the bench where the model was prepared. The front wall of the strong-box was removed and the front of clay sealed with silicone oil to prevent shrinkage. The extra height of clay was trimmed away and the top surface sealed with oil again. At that point, a circular tunnel cavity was cut by a previously lubricated thin walled stainless steel tube and a brass sampler which ran inside the tube. A jig was bolted onto the front of the box to hold in position and guide all the tools. A sketch of the details of tunnel cutting equipment is shown in Fig. III.3.

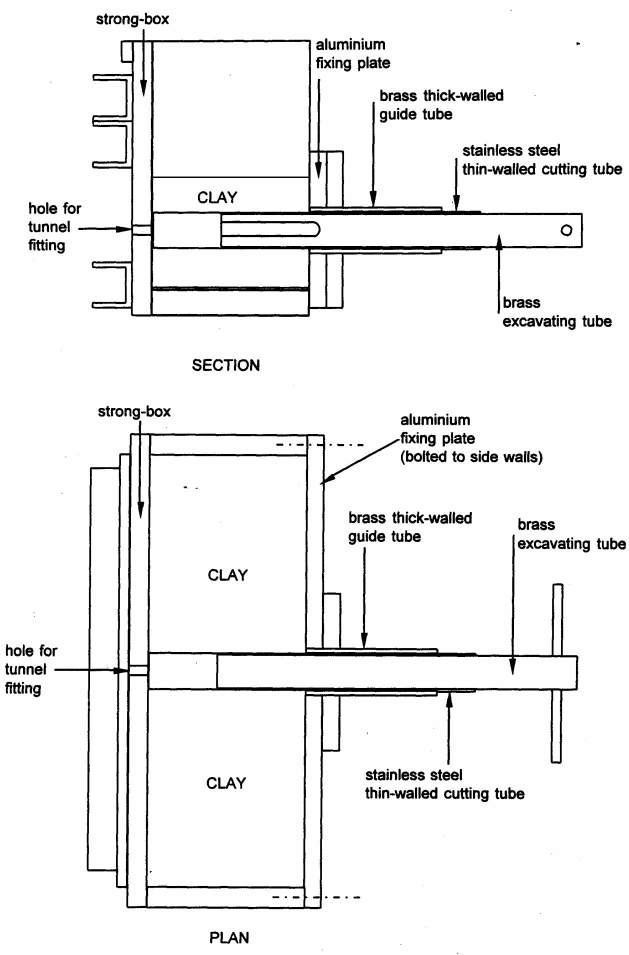

Figure III.3 – Details of tunnel cutting equipment (adapted after Grant, 1998)

This cavity was finally lined with a rubber bag provided with a special steel fitting at its back which allowed it to be supplied with pressurised air during the test. The lining membrane was 0.75 mm thick. The system fitting-bag was proved to be able to form an airtight seal against the box wall.

A regular grid (10 mm spaced) of black plastic targets (3 mm diameter cylinders) was then set up on the front face for image-processing and a Perspex window was bolted to the box to allow viewing by the CCTV camera. On the inner side of the window about 25 ml of viscous silicon grease were spread to minimise friction between the soil and the window. These operations were performed quickly with the drainage taps closed in order to minimise the clay swelling.

A third pore pressure miniaturised transducer was vertically installed from the top surface in a corner of the model at a distance of about 70 mm from both walls, by boring a hole and pushing it down with the same tube as the other two. The tip of the transducer, also spread with slurry, was located at a depth of about 50 mm bgl. Some slurry was used to backfill the hole together with some leftover consolidated clay to prevent excessive consolidation inside the hole during the flight. This third vertical transducer was originally thought to be used in addition to the other two, but due to its easier installation this was used in the later tests in place of the horizontal one located 15 mm bgl in axis with the tunnel.

Details on location and installation of the diaphragm walls will be given in the following section.

A plan view and three different sections of the model, as it was on the centrifuge swing platform, are shown in Fig. III.4.

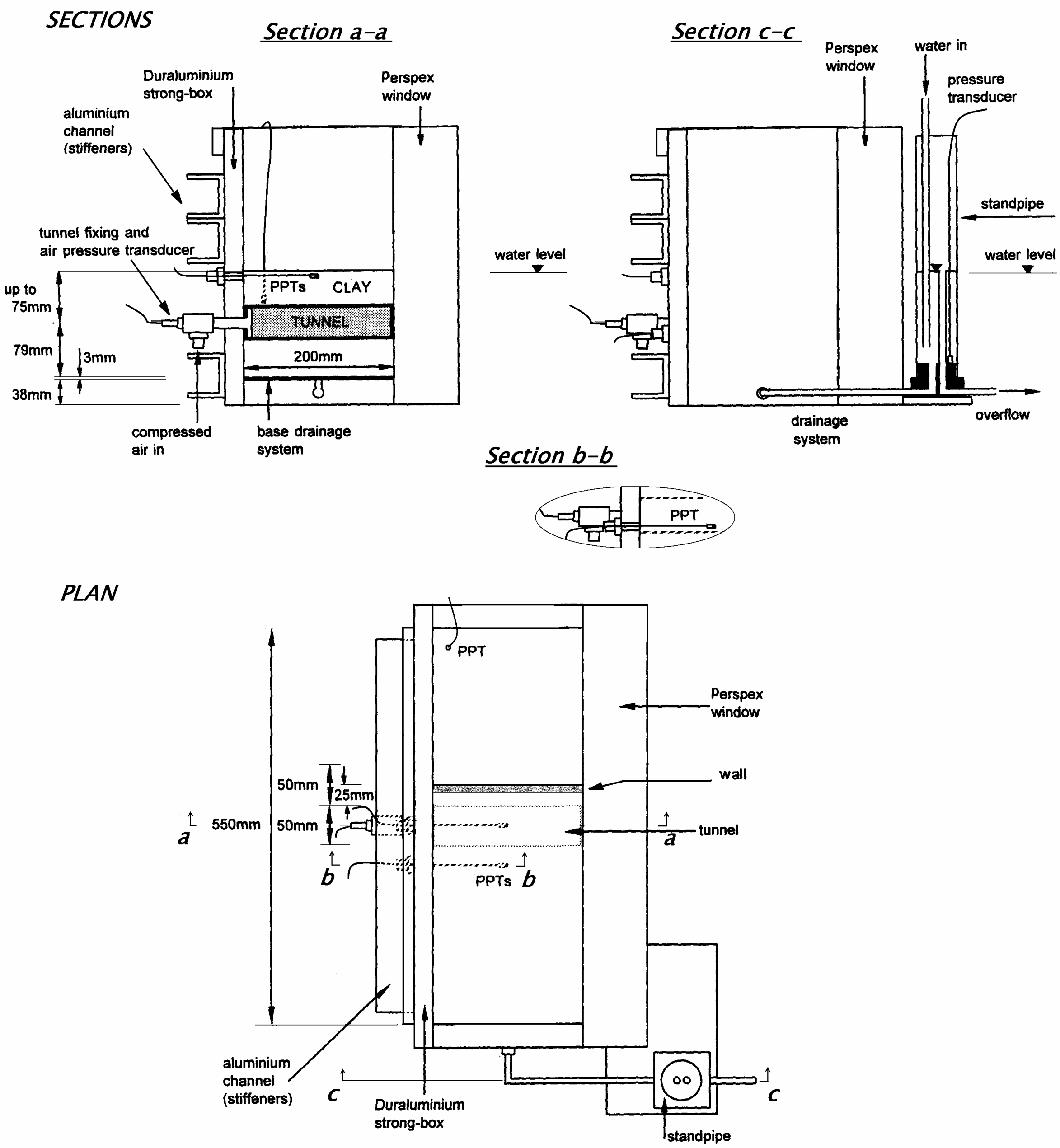

Figure III.4 – Sketch of a typical model

Experimental programme and tests set up

The research was aimed to study the effect of diaphragm walls as a measure of mitigation of movements induced by shallow tunnels in urban area. The investigation was limited to tunnels excavated in clay, mostly overconsolidated, resting on a rigid layer slightly more than one tunnel diameter beneath the invert. The effects of possible existing buildings, in terms of weight and stiffness, which have been discussed in Chapter II, were not taken into account in this work.

For shallow tunnels the value of the soil cover C is similar to the value of the tunnel diameter D; hence in the tests the ratio C/D=1 was chosen, although a few preliminary tests were carried out on models with C/D=0.9 (tests EB1÷3). The diameter D of the model tunnel was the same in all the tests and equal to 50 mm: following the relevant scaling law, to reproduce the behaviour of the excavation of an 8 m (at the prototype scale) wide tunnel, the model has to be tested at 160 g. This value was chosen as an average of tunnel diameters commonly adopted in excavations for underground urban light railways.

The characteristics of the sixteen tests which were carried out are shown in Tab. III.1 and their geometry is sketched in Fig. III.5. In the same table, in square brackets the relevant dimensions at the prototype scale are reported.

Table III.1 – Characteristics of the tests carried out (symbols as defined in Fig. III.5)

<table>
<tr><th>Test</th><th>p_{max}
(kPa)</th><th>C/D</th><th>L
(mm) [m]</th><th>t
(mm) [m]</th><th>d
(mm) [m]</th><th>Interface</th></tr>
<tr><td>EB1</td><td>250</td><td rowspan="3">0.9</td><td>-</td><td>-</td><td>-</td><td>-</td></tr>
<tr><td>EB2</td><td rowspan="15">350</td><td>-</td><td>-</td><td>-</td><td>-</td></tr>
<tr><td>EB3</td><td>70 [11.2]</td><td>0.8 [0.128]</td><td>50 [8]</td><td>no control</td></tr>
<tr><td>EB4</td><td rowspan="13">1</td><td>70 [11.2]</td><td>9.5 [1.52]</td><td>50 [8]</td><td>smooth</td></tr>
<tr><td>EB5</td><td>70 [11.2]</td><td>9.5 [1.52]</td><td>50 [8]</td><td>rough</td></tr>
<tr><td>EB6</td><td>-</td><td>-</td><td>-</td><td>-</td></tr>
<tr><td>EB7</td><td>70 [11.2]</td><td>9.5 [1.52]</td><td>75 [12]</td><td>rough</td></tr>
<tr><td>EB8</td><td>120 [19.2]</td><td>9.5 [1.52]</td><td>50 [8]</td><td>smooth</td></tr>
<tr><td>EB9</td><td>120 [19.2]</td><td>9.5 [1.52]</td><td>75 [12]</td><td>smooth</td></tr>
<tr><td>EB10</td><td>120 [19.2]</td><td>9.5 [1.52]</td><td>50 [8]</td><td>rough</td></tr>
<tr><td>EB11</td><td>120 [19.2]</td><td>9.5 [1.52]</td><td>75 [12]</td><td>rough</td></tr>
<tr><td>EB12</td><td>70 [11.2]</td><td>9.5 [1.52]</td><td>50 [8]</td><td>smooth</td></tr>
<tr><td>EB13</td><td>120 [19.2]</td><td>0.8 [0.128]</td><td>50 [8]</td><td>smooth</td></tr>
<tr><td>EB14</td><td>70 [11.2]</td><td>9.5 [1.52]</td><td>50 [8]</td><td>rough in trench</td></tr>
<tr><td>EB15</td><td>70 [11.2]</td><td>9.5 [1.52]</td><td>50 [8]</td><td>toothed</td></tr>
<tr><td>EB16</td><td>70 [11.2]</td><td>7.2 [1.15]</td><td>50 [8]</td><td>toothed</td></tr>
</table>

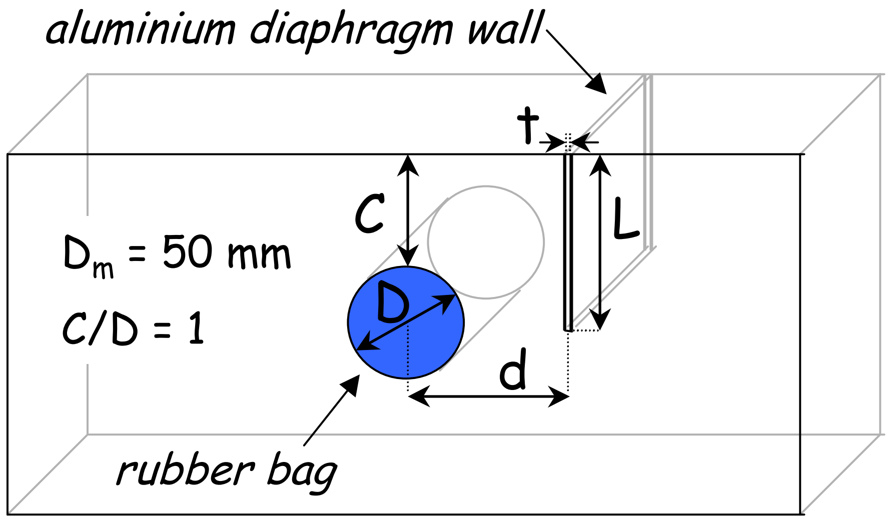

Figure III.5 – Sketch of the model

Tests EB4 and EB15 were unsuccessful because the model unexpectedly collapsed: in the former due to an automatic safety stop caused by a failure in the electrical equipments, in the latter probably due to a loss in air pressure. This was caused by a failure of the sealed connection between the air supply pipe and the tunnel fitting.

Reference test

A test without any wall is necessary in order to get a reference configuration: in tests EB1, EB2 and EB6 no wall was embedded in the model. Tests EB1 and EB2 were basically used to choose the amount of p_{max}: in the test EB1 the collapse occurred with a support pressure in the cavity of about 90 kPa whilst in the test EB2 this value reduced to about 60 kPa, thus enlarging the range of ground movements with reduction of support pressure. The consolidation pressure was not increased anymore in order to not to increase the soil stiffness.

The height of the model was in all the tests with C/D=1 equal to 157 mm: the height of the model was kept low to reduce the consolidation time, which was an issue particularly important in the re-consolidation phase during the centrifuge flight. The lateral rigid boundaries were 5 diameters away from the tunnels springs.

The water table was fixed at the soil surface. This was provided by feeding water to the base of the model through an external standpipe set at a constant water level. As the standpipe was offset from the model centreline by 234 mm, to take account of the curvature of the water table during the centrifuge test due to the radial acceleration field (Fig. III.2), its overflow level was fixed 15 mm above the groundwater level which means at 210 mm from the floor of the swinging basket. A pore pressure transducer without stone placed at the bottom of the standpipe measured the water pressure during the tests (*cf.* section c-c in Fig. III.4).

Tests with diaphragm walls

A series of tests was performed in which an aluminium wall was installed. Aluminium was chosen for its weight ($\gamma = 27$ kN/m^3) and stiffness (E = 7E4 MPa) which are similar to the values for reinforced concrete, more commonly adopted in practice. The walls which were embedded in the models are schematically shown in Fig. III.6. In the same figure details can be found on the location of the walls in the model.

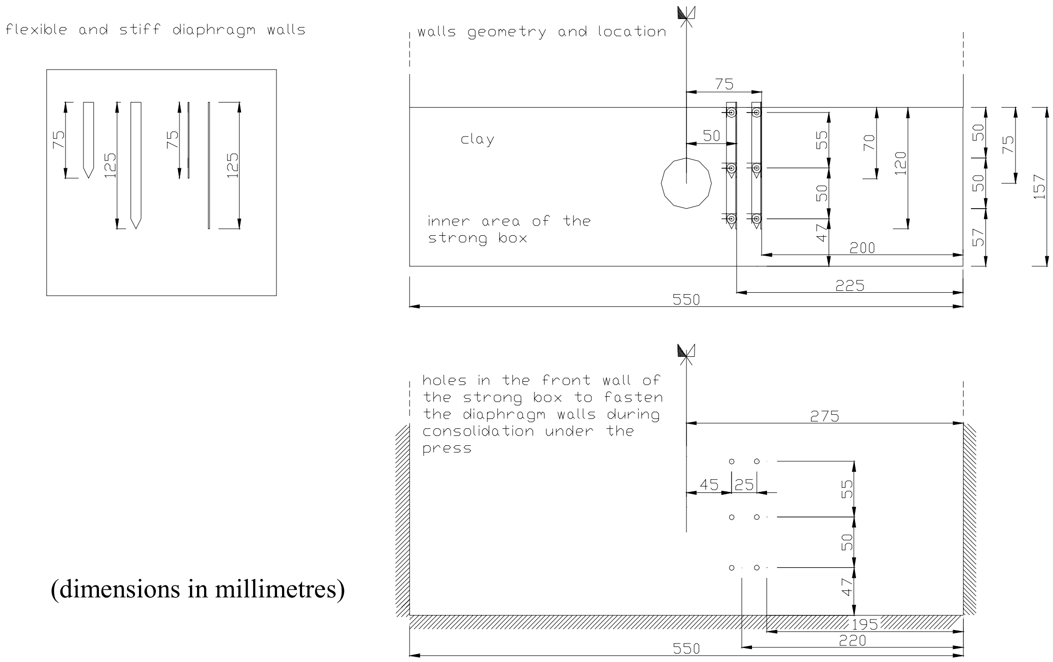

Figure III.6 – Sketch of the diaphragm walls geometry and location

In most of the tests the wall was inserted into the model before consolidation. In order to guarantee the wall did not move at this stage, it was bolted to the front wall of the strong-box through purposely drilled holes: their location in the front wall is also shown in the same Fig. III.6. In the tests EB14÷16 an alternative procedure was adopted with the wall installed after the soil had been consolidated in the press. In that case a trench in the model was excavated before cutting the tunnel cavity trough a specifically designed tool consisting in a steel cutter and guide as it is shown in the picture in Figs. III.7a-b. The wall was hence pushed into the trench from the front face of the model.

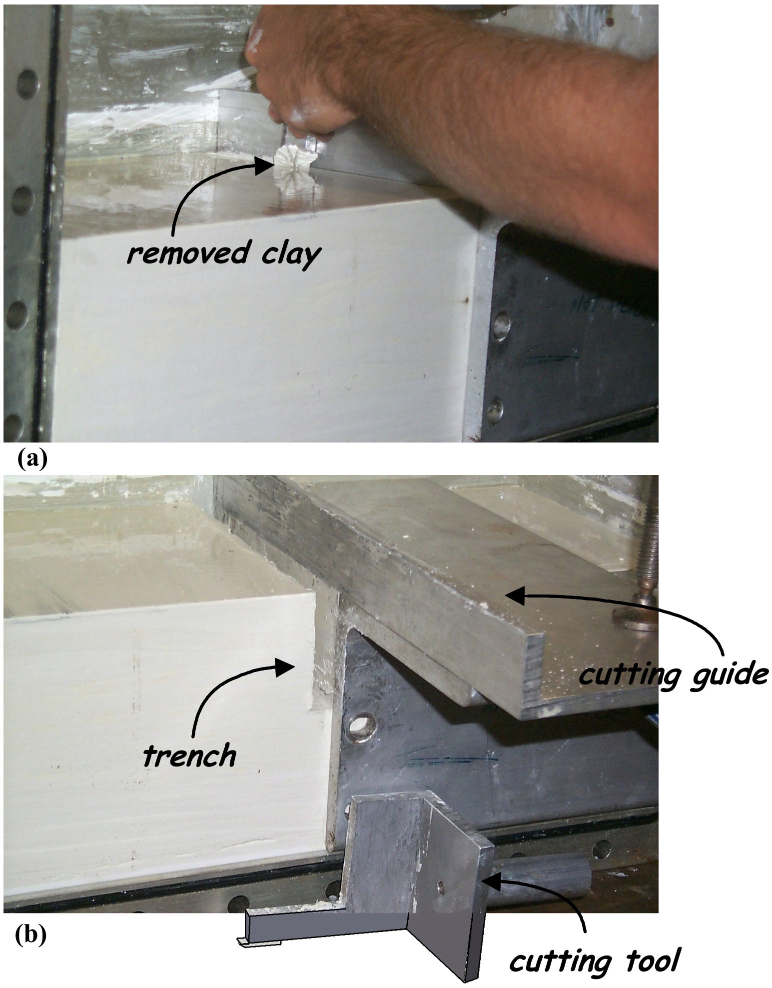

Figure III.7– Pictures of the trench excavation in tests EB14÷16

The wall geometry parameters (*cf.* Fig. III.5) varied over the set of models. In particular, the length of the wall L, its thickness t (which corresponds to a certain stiffness) and its offset d from the tunnel axis were varied as it can be seen in Tab. 1. Most of the walls were relatively thick and able to resist bending.

The length of the wall varied between two values corresponding to a *short* (about 1.5 C) and a *long* (about 2.5 C) wall. This choice originated from the assumption (which had been validated by preliminary numerical analyses) that a wall too short was ineffective whilst there was little addition of benefit by making the wall too deep.

The offset of the wall from the tunnel axis was either 1D or 1.5D: this distance includes the whole thickness of the wall. If we assume that the distance *i* of the inflection point of a typical settlement trough due to an undrained excavation in clay is given by the expression (II.5) $i = K(C + D/2)$ in which $K = 0.5$ (O'Reilly and New, 1982), it follows that in these tests $i = 0.75D$, hence the wall is located at about *i* and 2*i* from the tunnel axis. The reason for this choice is that the zone in between is usually subjected to ground movement profiles with high curvature, and there the damage on existing buildings could be high.

The two values of wall thickness correspond to a *very flexible* and a *nearly rigid* wall.

Furthermore, the influence of the roughness of the wall was investigated as well, by testing models with the same geometry but different interface with the clayey soil. For tests with a *smooth* interface, the wall surface was lubricated with lithium grease; in tests with *rough* interface, this was obtained by sticking with resin a layer of sand on the wall surface. In test EB3 the interface between kaolin and aluminium was not modified. In tests EB15 and EB16 the wall was shaped with teeth to obtain a rough interface. This trial was done to compare results to those from the model with sandy interface and check its effectiveness. A sketch of the tooth-shaped wall has been reported in Fig. III.8.

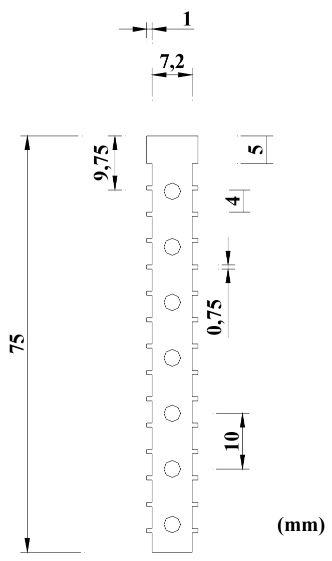

Figure III.8 – Tooth-shaped interface wall

Procedure of test

After the model package was ready, it was weighed and the position of the counterweight was calculated: the average weight of the package was usually around 119 kg. The model was placed onto the centrifuge swing and the piped connections were established. An air pressure transducer was inserted through the specially designed fitting between the air supply pipe and the tunnel lining bag (Section a-a in Fig. III.4). This transducer had been calibrated against the Druck DPI up to 300 kPa. A layer of silicone oil was then added to the top (about 250 ml) to prevent the evaporation of the pore water during the centrifuge run. After the standpipe had been positioned in the location shown in plan and section c-c in Fig. III.4, it was filled and connected to the drainage system by a flexible pipe: the tap provided on the fitting was opened only at the very last moment to limit swelling of clay. The water pressure transducer was installed in the standpipe and it was weighted down in order to keep the right position during flight. All the electrical connections were established and checked, including the CCTV camera and lights. Usually it was not necessary to relocate the camera since it kept the same position from the previous test. All the wires and tubes around the model had to be safely strapped together and to the frame of the swinging platform in order to reduce their fluctuations during the flight, thus allowing for lower loads on the connections. Only when all the checks were completed, the water was supplied to the model and the centrifuge shell closed. The safety door of the centrifuge room was shut and the centrifuge was ready to start.

All the operations since the strong-box had been removed from the consolidation press until this point took usually four hours about.

The model was then accelerated up to 50 g. After that the unbalance of the centrifuge arm was checked, the model was taken to 160 g. During the acceleration the air pressure inside the cavity was raised progressively by hand control to balance the increasing overburden pressure. This operation was performed through a Fairchild Model 10 regulator located in the control room. The final value of air pressure was slightly lower than the vertical stress at the tunnel axis (about 210 kPa in the tests with C/D=1) in order to avoid a too large uplift of the tunnel crown and it was arbitrarily set at 190 kPa in the tests with C/D=1 (at 170 kPa in test EB1 and 185kPa in tests EB2 and EB3 with C/D=0.9D). This pressure corresponds to an overburden stress at a depth of 68 mm, about midpoint between the cavity axis and crown. During spin-up, data were logged and stored with a high frequency (usually every second) for possible checking in case of problems and images were grabbed and stored every minute.

As spinning up increases the total stress distribution, a period of about six hours is needed to achieve the effective stress equilibrium. The steady state water table was fixed by supplying water into the model trough the standpipe and the equilibrium checked by the transducers embedded in the soil. During this re-consolidation stage, data were logged and stored with a low frequency (usually every 300 seconds), and images were grabbed and stored every 20 minutes.

After the equilibrium was reached, the excavation was simulated by reducing the air-pressure at the rate of about 100 kPa per minute, thus achieving a largely undrained response. During this phase, data were logged every second and pictures of the model were grabbed about every second and stored for the later image processing. Particular care was taken in order to be sure that every stored image could be univocally linked to a given air pressure inside the tunnel cavity.

Fig. III.9 shows the typical data recorded in a test (EB9) and referring to measurements of air pressure in the tunnel bag and of water pressure in the standpipe and in the clay. In the left part of the diagram it is easy to recognize the phase of spin up, characterised by a fast increase in pressure, after which consolidation in flight occurred. During consolidation, obviously, the pressure in the standpipe and in the tunnel cavity are constant, whilst the pore pressure transducers measure an increasing pressure, towards equalization with the imposed boundary conditions. The time scale is in second but a band in the lower part of the chart is reported which shows the corresponding time expressed in hours. In the right part of the diagram the following data are plotted at a different scale: the time band at bottom is now expressing time in minutes. By looking at the air pressure curve it can be identified the time when the excavation phase starts: the air pressure drops with a nearly constant rate in about two minutes. In the same time the standpipe pressure keeps constant, thus indicating that the centrifuge is still running at a constant spin. The drop in the standpipe pressure coincides with the spin down: at the end of it the pressure inside the standpipe corresponds to the earth gravity water head (1 g). The collapse of the cavity can be identified by the sudden jump in the air pressure trace and, at the same time, a kink can be observed in the diagram of pore water pressure at ppt1 (the pore pressure transducer closest to the tunnel). In fact, at this point a kinematic mechanism was clearly visible on the screen.

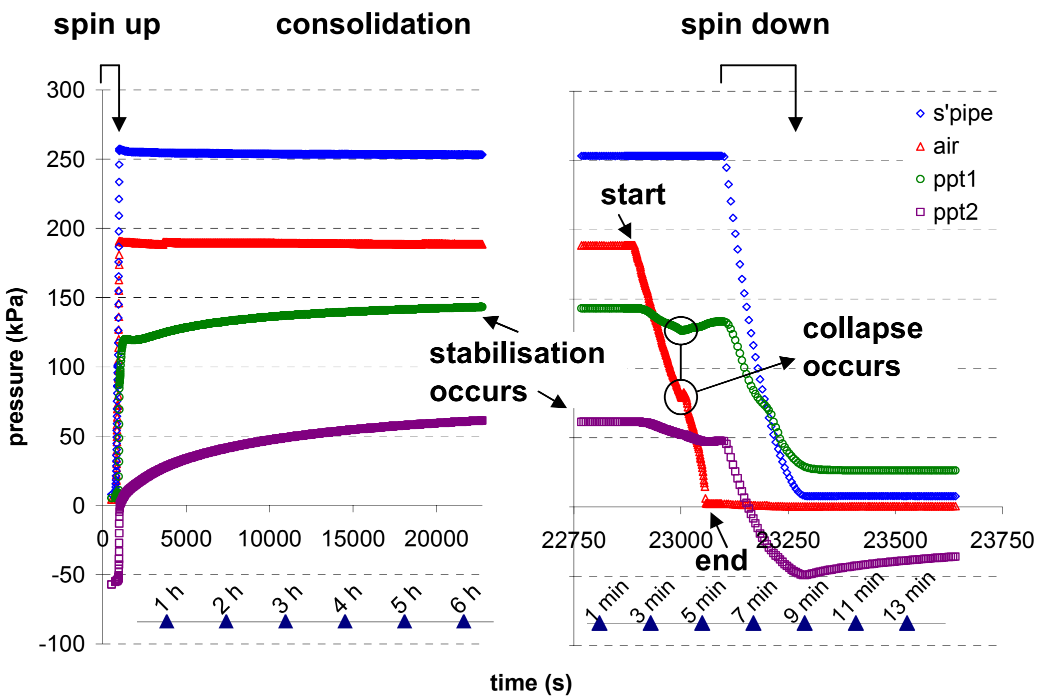

Figure III.9 – Typical data logged during a test (EB9)

Image processing

To determine the displacement fields in these plane strain models, as this was the main interest of the research, an image processing system was used. Basically, the ground movements are determined from the analysis of digital images obtained from the CCTV camera looking to the front Perspex window of the strong box during each test. In Fig. III.10 a typical image during a test is shown.

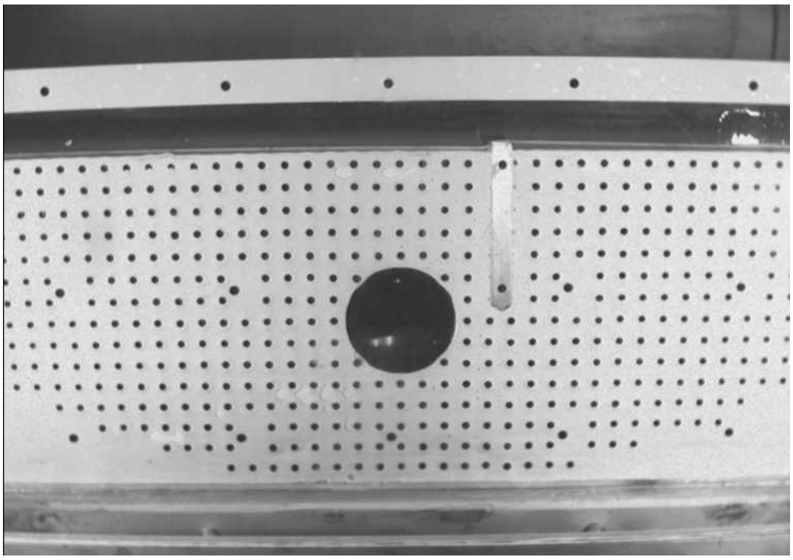

Figure III.10 – Typical image grabbed during a test (EB4)

The image processing system used during the tests has been developed at City University through a co-operation between the Geotechnical Engineering Research Centre and the Engineering Surveying Research Centre. It allows capturing, storing and digitally treating the pictures to know the co-ordinates of the target points on the front of the model at subsequent instants during the test; details can be found in Grant (1998) and Taylor et al. (1998).

The errors in measurements can be both systematic and random. The lower the systematic error, the more accurate the measurements; the lower the random error, the more precise they are.

The accuracy of the image processing was guaranteed by a careful calibration procedure (Taylor *et al.*,1998) performed by the software Digimet.

On the other hand, in order to know how precise were the measurements in the tests carried out, some checks have been done. By measuring the co-ordinates of all the target points in five subsequent images as captured during a test at a frequency of 1 per second when no movements were expected to occur, the deviations of the co-ordinates from their average values have been calculated. The more precise the measurements, the more these deviations should tend to zero. In Fig. III.11 these deviations have been subdivided in classes and their cumulative frequencies have been plotted: the maximum deviation of almost 90% of the vertical co-ordinates is less than ±5 μm, whilst more than 90% of the horizontal co-ordinates are measured with a precision of about ±15 μm. These values confirm previous observations (e.g. Grant, 1998). As the typical strain range in tunnel excavation is between 1 and 10 με (Mair, 1993), this precision was expected to lead to acceptable errors on the measured movements over a length of 150 mm (model depth).

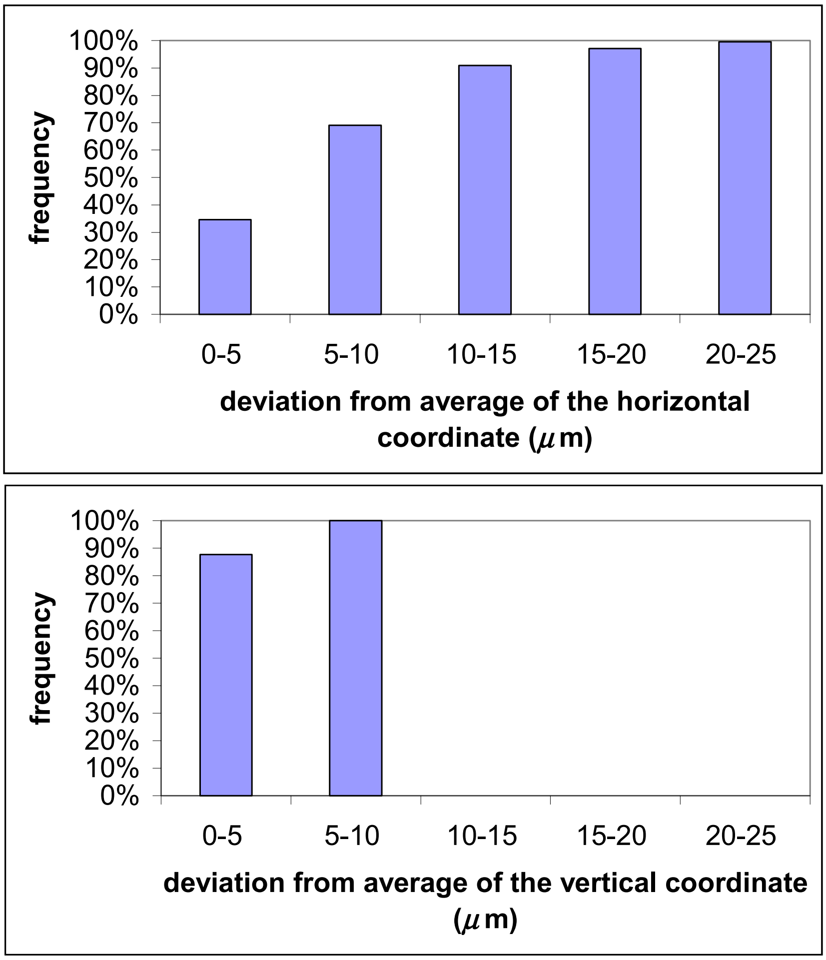

Figure III.11 – Vertical and horizontal deviations of the co-ordinates of the target points from their average values as calculated over five subsequent images.

Test results

Typical test paths

During each test the air pressure inside the cavity was progressively reduced thus simulating the stress release during a tunnel excavation. From the image processing of the pictures taken during the test, the settlement profile of the soil at various depths was determined. The first row of targets was usually located 5 mm below the ground surface and the movements of this row were assumed to represent the ground surface movements. As undrained conditions apply, the volume loss can be evaluated by numerical integration of the settlement trough.

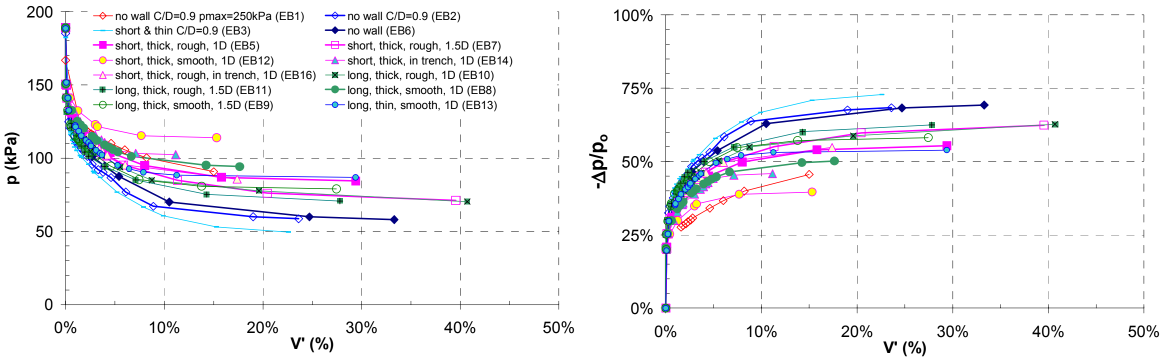

Figure III.12 - Supporting pressure p and relative pressure change -$\Delta p/p_o$ vs *V'(%).*

In Fig. III.12-a the supporting pressure inside the tunnel has been plotted against the volume loss expressed as a percentage of the tunnel volume; the horizontal asymptote of each curve is the collapse pressure of the tunnel. The collapse pressure of the tunnel without wall in tests with C/D=1 is lower than that obtained with a wall embedded in the model; in other words, the presence of a wall makes the tunnel less 'stable'. Hence, settlements can be maintained at the same magnitude as in the reference test by increasing the supporting pressure in the tunnel. This is not a problem itself, as far as ground movement control, rather than tunnel lining design, is the main goal of this protective measure. In Fig. III.12-b the relative pressure change -$\Delta p/p_o$ has been plotted along V'. The pressure which corresponds to the model failure has been evaluated as the asymptotic value of the (p:V') curves and in most tests it is not very far from the pressure value needed to achieve V'=20%. For each test, the collapse pressure has been reported in Tab. III.2.

In all cases the load factor (Mair *et al.*, 1981), that is the ratio between the stability ratio N at working conditions and the stability ratio at collapse:

$$LF = \frac{p_o - p}{p_o - p_{ult}} \tag{III.1}$$

has been calculated at various V' and plotted in Figs. III.13-III.14.

Table III.2 – Collapse pressures

Test	Collapse pressure (kPa)
EB1	88
EB2	59
EB3	49
EB5	84
EB6	58
EB7	71
EB8	94
EB9	79
EB10	70
EB11	69
EB12	114
EB13	87
EB14	102
EB16	82

Fig. III.12-a shows that, for a given geometry, the smooth walls lead to collapse before the rough ones, that is for lower volume losses, which correspond to higher supporting pressure in the tunnel. Moreover, the short walls are less 'stable' than the long ones, but this difference tends to minimise when the walls are far from the tunnel. By analysing the results obtained on the long and smooth walls (EB8 and EB13, respectively), it seems that the thinner (and lighter) one reduces the stability of the tunnel less than the thicker one. Even if the data are not enough to understand completely such evidences, it seems likely that tunnel stability is reduced by closer, shorter, heavier and smoother walls: in the set of the tests which have been carried out, this is the case of the test EB12, where in fact a supporting pressure almost twice larger than the in reference test EB6 (without wall) led the tunnel to collapse.

In Fig. III.13, it can be observed that the load factors calculated for all the tests without walls, corresponding to slightly different C/D values and different p_{max} (pre-consolidation pressure), vary almost in the same way with the volume loss V'. This is consistent with Mair *et al.* (1981).

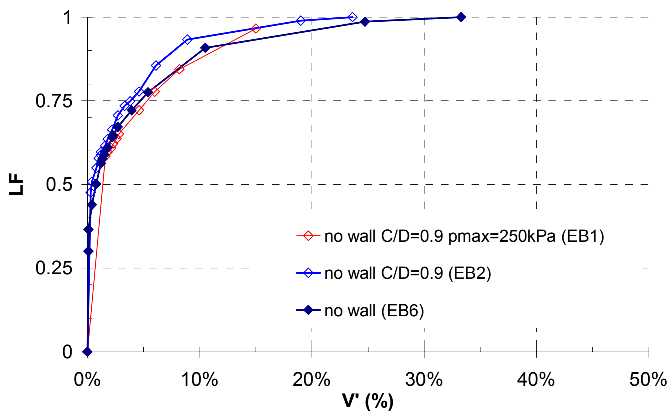

Figure III.13 - Profiles of load factors along volume loss for tests without wall.

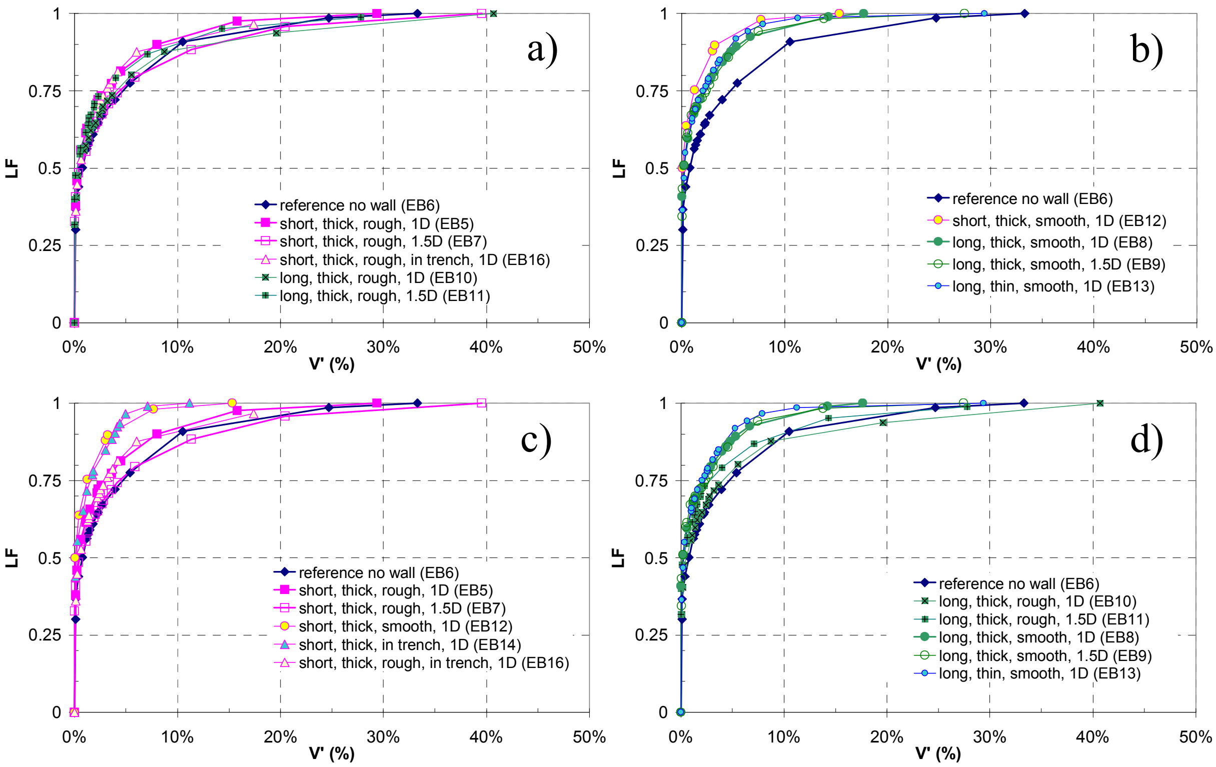

Figure III.14 - Profiles of load factors along volume loss for tests C/D=1 with wall compared to the reference no wall test EB6: a) rough walls, b) smooth walls, c) short walls, d) long walls .

In Fig. III.14 the LF profiles for tests with C/D=1 are plotted in four separate charts, to distinguish walls in classes by length and roughness and compare each class to the reference test without wall. It can be observed in Fig. III.14-a that all the rough wall profiles are very close each other and to the reference profile, all lying slightly above this at low volume losses (up to V'≅5%). This seems to indicate that rough walls affect the collapse pressure, but they do not affect the ratio $LF=N/N_c$. In fact, this would suggest that in this set of tests with rough walls, the increase of stress in the vicinity of the cavity due to the wall self weight should be taken into account when calculating the stability ratio N and its value N_c at collapse. On the other hand, the behaviour of smooth walls can be observed in Fig. III.14-b. The relevant LF profile are very close each others, and particularly those corresponding to the long walls are superimposed, but they lie all above the reference test profile. This means that the presence of a smooth wall in the model affects not only the collapse pressure, but also the load factor. In fact, the presence of such a strong shear discontinuity in a region very close to the cavity changes the 'boundary' conditions of the problem and this could justify such a different behaviour between smooth and rough wall models. A comparison between Figs III.14-c and d, where the models have been classed by the length of the wall leads to similar conclusions. As far as the degree of roughness achieved in tests EB14 and EB16 in concerned, it can be observed that the wall in test EB14 behaves like the smooth wall in test EB12; the wall in test EB16 behaves like the rough wall in test EB5.

Displacements fields

In Figs. III.A1÷A28, which have been reported at the end of this Chapter, the vertical and horizontal components of displacement as measured along some significant lines of the model face are shown. For each test, vertical and horizontal displacements along the vertical and the horizontal tunnel centre lines, horizontal displacements along vertical lines at tunnel sides and vertical displacements along three horizontal lines above the tunnel have been plotted at two different levels of supporting pressure. These pressures correspond to a settlement trough volume about 1.3% and 10% of the tunnel volume. These values have been chosen to compare patterns at a displacement level which is likely to occur in the field (V'=1.3%), and at a level where the measurements are less affected by errors (V'=10%). As it can be observed in Fig. III.12, in the former case the models are far away from failure whereas in the latter they are generally close to collapse.

In test EB1 an error was made in locating the grid to insert the target into the model. For this reason the vertical and horizontal displacements are shown along a vertical line about

3 mm left of the centre line. The displacement along the horizontal centre line have not been reported because the lines of targets were not in correspondence. In fact, a decision was taken to locate the first row of targets 5 mm below (0.8 m at prototype scale) the model top in order to measure displacements as closer as possible to the ground surface: a lower distance had not been guaranteed the success of the digital image processing for that row of target. As the tunnel cover was as low as 45 mm in this test, this choice led to locate the target rows 5 mm above and below the tunnel axis depth. In the same picture the settlements along the three target rows are shown: 5 mm, 25 mm and 45 mm below ground level, the first and the last charts are assumed to represent of the settlement trough at surface and at the crown level. The horizontal displacements with depth are plotted along vertical lines at about 50 mm and 80 mm left and right of tunnel centre. The general pattern of displacement appears to be similar at the two pressure levels as it is can be clearly observed in Fig. III.15 where the profiles of vertical and horizontal displacements are divided by the relevant maximum value and compared.

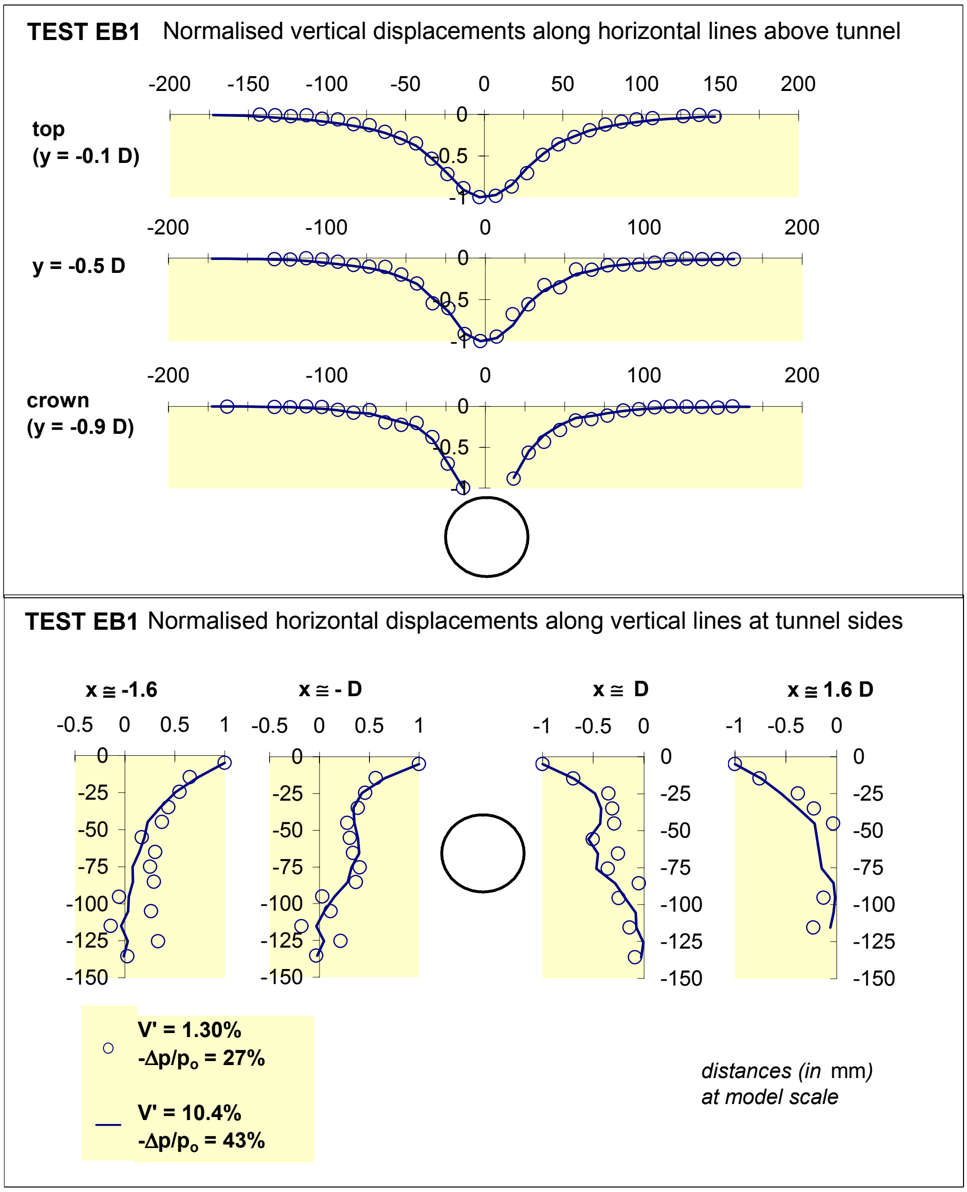

Figure III.15 - Profiles of vertical and horizontal displacements divided by the relevant maximum value

At low displacements (V'=1.3%) the normalised measurements show some scatter from the corresponding quantities at higher volume loss.

In test EB2 the first row of target was located 10 mm below the ground level: in this way a direct measurement of displacements at the horizontal tunnel centre line was available and it has been reported in the Figs. III.A3-4. In this test it was chosen to set the targets columns in order to have direct measurements at 1.5 D from the tunnel axis. In this way displacements were not measured along the vertical tunnel centre line. The horizontal displacements at 45 mm and 75 mm away from the tunnel axis are plotted with depth in the same figures. The settlements of the target rows located 10 mm, 30 mm and 40 mm bgl have also been plotted.

The maximum horizontal displacements can be observed at surface but it can also be noticed that the closest profiles to the tunnel show a clear increase in the magnitude of the horizontal displacements in the vicinity of the tunnel axis.

Also in this test the pattern of movements appears independent of the pressure level. By comparing the results of test EB1 and EB2 it can be observed that at the same volume loss the magnitude of displacements is the same all over the model and does not depend on the maximum previous compression, which is different (p_{max} = 250 kPa in EB1, p_{max} = 350 kPa in EB2), but a different supporting pressure is needed to reach the same volume loss.

In both cases the load factor (Mair *et al.*, 1981) as expressed in (III.1) has been calculated as reported in Tab. III.3.

Table III.3 – Loading factors for the displacement fields shown in Figs. III.A1÷4

Test	p_o (kPa)	p_{ult} (kPa)	p (kPa)	$-\Delta p/p_o$	LF	V'
EB1	166	88	120	27%	0.59	1.3%
			95	43%	0.91	10.4%
EB2	185	59	110	41%	0.59	1.25%
			65	65%	0.95	10.1%

The load factor corresponding to the same volume loss in each of the two test is the same, consistently with Mair *et al.* (1981) .

On the other hand a reduction of 43% of the original supporting pressure in test EB1 is able to attain a volume loss 10 times larger than a similar reduction of 41% in test EB2 as it corresponds to a loading factor about 1.5 times larger and approaching ultimate conditions (LF=1).

In test EB3 a thin and short diaphragm wall was embedded 50 mm away from the tunnel axis. Its interface was not treated, therefore this wall cannot be considered neither completely rough or completely smooth.

A column of targets was located along the vertical tunnel centre line and a row was also available along the horizontal centre line because the horizontal alignment of targets was the same as in test EB2. Therefore vertical and horizontal displacements have been plotted in Figs. III.A5-6 along these two lines. Horizontal displacements were also plotted along vertical lines at 50 mm and 80 mm away from the tunnel axis, as in test EB1. Vertical displacements along horizontal lines 10 mm, 30 mm and 40 mm deep were also reported.

A couple of targets were originally attached to the wall through welded supports. These supports were the same which were used during the consolidation stage under the press to keep the wall in position (Fig. III.5). Unfortunately, welding did not resist the shearing at the soil-wall contact during consolidation. Hence the measured displacements of such targets cannot be reliably attributed to the wall and have not been reported in the figures.

In Fig. III.16 vertical and horizontal displacements of test EB2 (bold line) and EB3 (thin line) have been compared at V'≅10%. It can be observed that the effect of this wall is not particularly evident. The settlement profiles at various depths show that the overall effect of the wall is slightly shifting the trough on the opposite side, giving an asymmetric shape to it.

This is testified also by the slight reduction of the horizontal displacements in the wall side of the model.

At the axis level the settlements close to the tunnel are larger in the model with wall than in that without wall. On the other hand, the settlement in the vicinity of the crown reduces in the test with wall. Therefore, it seems that the wall modifies the deformed shape of the cavity without affecting the overall deformation of the model.

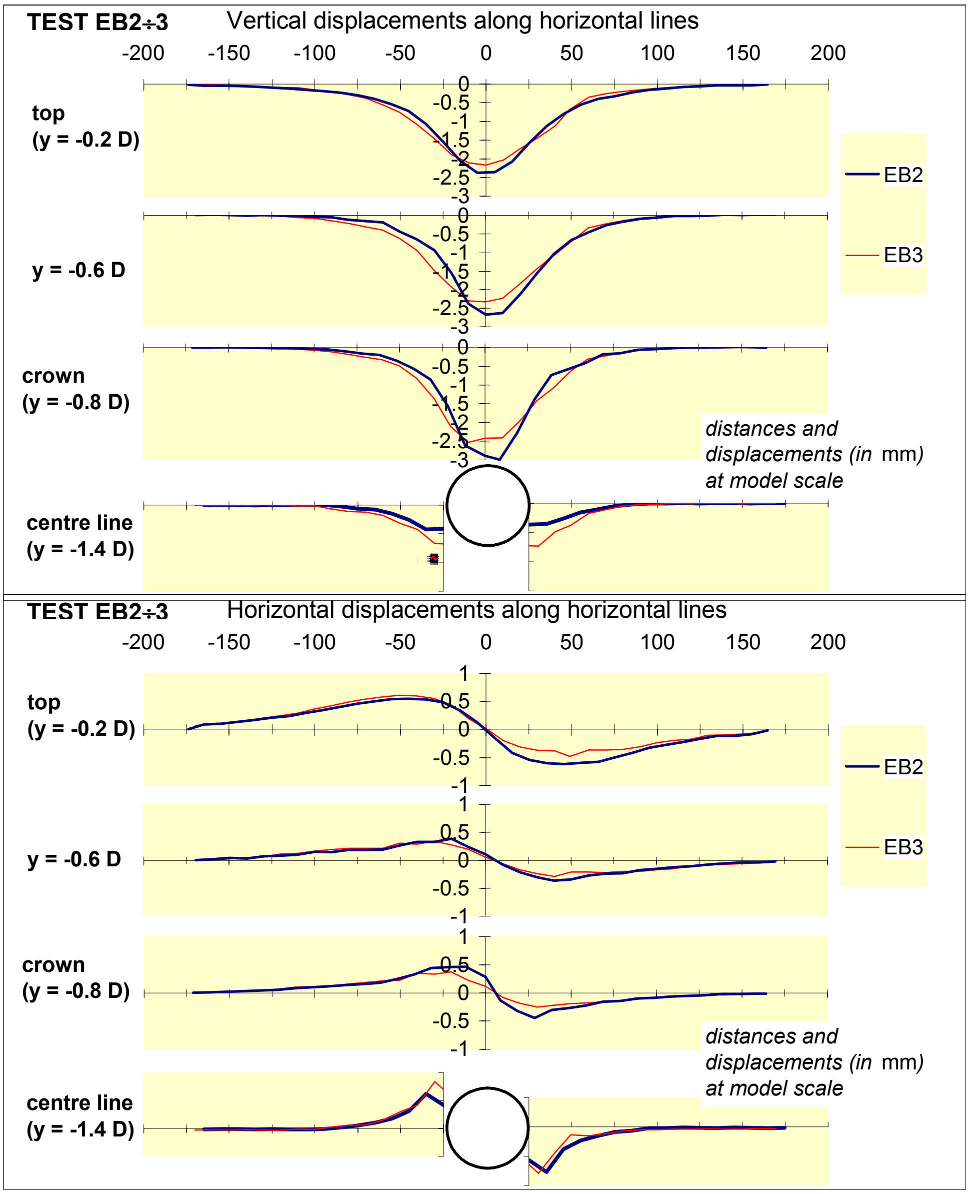

Figure III.16 - Profiles of vertical and horizontal displacements in tests EB2 and EB3 at V'≅10%.

In test EB5 a thick and short rough wall was embedded in the model: its outer edge was 50 mm away from the tunnel axis. Two targets were located along the wall axis, hence at 45 mm from the tunnel axis. The first row of targets was 5 mm deep: as the cover in this test was 50 mm, this setting allowed to have a row of targets at the tunnel axis level. A column of targets was also aligned with the vertical centre line. This configuration was also adopted in all the following tests.

The settlement profiles along the horizontal centre line, as reported in Figs. III.A7a-8a, show that the soil beneath the wall and in between the wall toe and the tunnel settles more than the soil behind the wall and on the other side of the tunnel. The corresponding horizontal displacement profiles (Figs. III.A7b-8b) show a similar increase in the same area. The increase in settlement below the wall toe corresponds to a larger settlement of the wall (Figs. III.A7d-8d) than the soil around. At the same time the horizontal displacements at x=D beneath the wall are larger than the wall horizontal displacements and than displacements along the symmetrical line. As far as the supporting pressure decreases and displacements increase, the wall rotates initially in anticlockwise direction, then in clockwise direction. At the same time, the soil beneath the wall tends to enter in the cavity: the magnitude of the horizontal displacements beneath the wall toe is higher than the corresponding one in the reference test (*cf.* the following EB6 test results). This could mean that the wall transfers a load to the ground in the toe area.

The soil above the tunnel crown up to surface tends to rotate to compensate for the downward movement of the wall and the soil nearby, as it appears by looking at the horizontal displacements which are reported in Figs. III.A7b-8b.

Test EB6 was performed as a reference test for models with C/D = 1. The geometry and the location of targets were the same as in test EB5 apart from the wall, which was not embedded in this model. The corresponding measured displacements have been reported in Figs. III.A9-10. It can be seen that vertical displacements along the vertical centre line increase with depth. The ratio $w_{\max}/w_c$ between the maximum surface settlement and the settlement at crown can be determined at both pressure levels equal to about 0.75 at V' =1.34% and about 0.8 at V'=10.5%. These values are very close to those calculated by an empirical correlation developed by Ng (1991) and based on 18 case histories. This is a linear relationship between the ratio $w_{\max}/w_c$ and the ratio $H/(D \cdot N)$, where H is the tunnel axis depth, D the tunnel diameter and N the stability ratio. By assuming an undrained strength $c_u = 40kPa$ (Ladd *et al.*, 1972), it follows N≅2 for p = 114 kPa (V'=1.34%) and N=3 for p = 70 kPa (V'=10.5%). Therefore, values of $H/(D \cdot N)$ equal to 0.75 and 0.5, respectively, can be calculated. For these values, the abovementioned relationship gives $w_{\max}/w_c$ equal to about 0.8 and 0.83.

The invert of the tunnel is subjected to a small amount of heave which is about 20% of the crown settlement at V'=1.34% and about 10% of it at V'=10.5%.

The horizontal displacements are zero along the vertical centre line as the trough is almost symmetrical about it.

The top target row settlement profile can be assumed to approximate the surface settlement trough. Hence, it can be fitted by a Gaussian curve. The volume loss V' can be easily evaluated at a given pressure level by integrating the settlement profile. In order to determine a value for the horizontal distance i of the inflexion point from the tunnel axis, various procedures can be adopted. In this case a least-squares estimation of i over the settlements measured in the range of $-\Delta p/p_o = 30\div50\%$ (V' = 0.4÷3.9%) within a distance d = ±2i from the axis was performed. The first guess for i can be assumed by using the expression (II.5) $i = K(C + D/2)$ in which $K = 0.5$ (O'Reilly and New, 1982). In Fig. III.17, the measured displacements have been reported in a plane in which the Gaussian function is plotted as a straight line. The linear regression, which is also shown, fits only the bold markers, which fulfil the condition $|d| = 2i$.

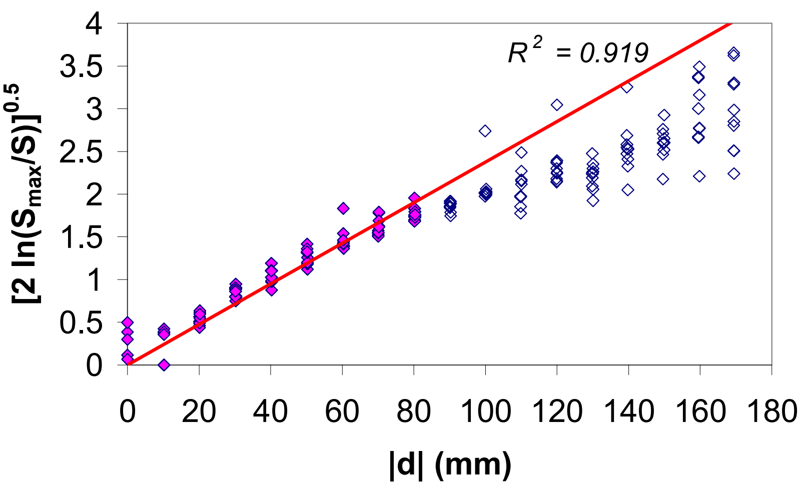

Figure III.17 – Linearised settlements at 'surface' in test EB6 in the range of $-\Delta p/p_o = 30\div50\%$

With this procedure a value of k=0.56 has been assessed, which is consistent with the indications for cohesive soils by O'Reilly and New (1982). In Fig. III.18 the vertical and horizontal displacements at surface have been divided by the maximum measured settlement and plotted together with the Gaussian fitting. The horizontal displacement fitting curve has been obtained under the hypothesis that the total displacement vectors are directed towards the tunnel axis.

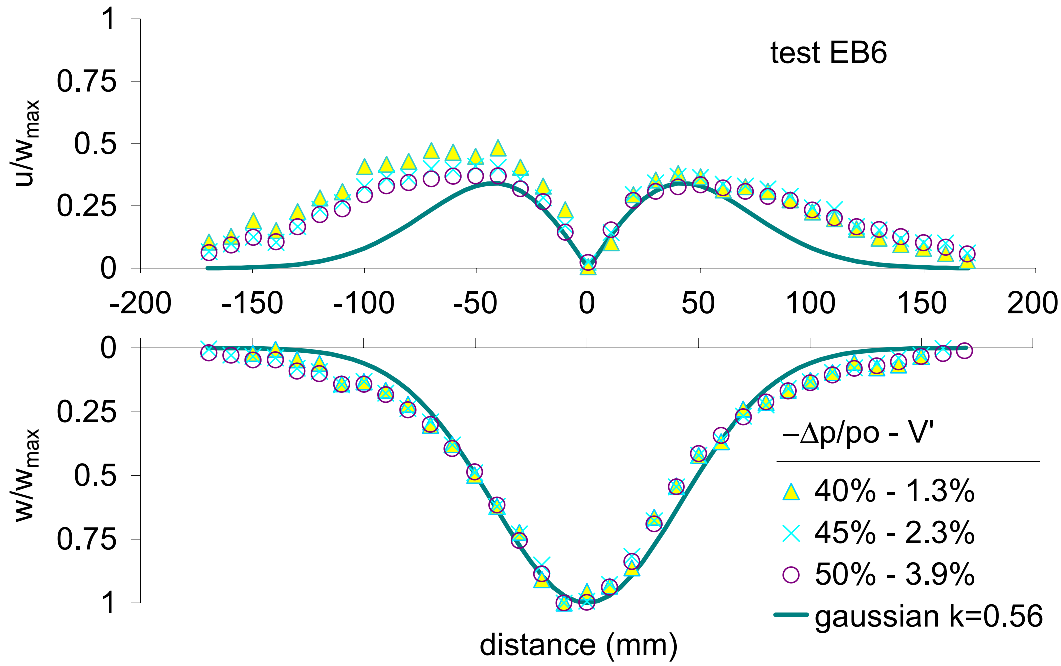

Figure III.18 – Displacement at 'surface' in test EB6 in the range of $-\Delta p/p_o$ = 40÷50% and curve fitting

The vertical displacements beyond 2i from the tunnel axis are underestimated by the Gaussian curve: this is a common evidence and a limit for the use of this fitting curve. The fitting appears also less accurate for horizontal displacements. The asymmetry in the measured horizontal movement distribution seems to reduce by increasing the magnitude of displacements and this is confirmed also in Fig. III.A9b-10b.

In test EB7 a thick and short rough wall was embedded in the model: its outer edge was 75 mm away from the tunnel axis. Two plastic targets were embedded in the wall as in test EB5, three more targets were painted in between them with the same spacing than the grid (10 mm).

It can be observed in Figs. III.A11-12, that the larger movements at the tunnel axis level occur in the area between the tunnel and the wall toe. The settlement profiles along the target rows above the horizontal centre line show that the soil in the vicinity of the wall on the tunnel side settles of the same amount than the wall. By moving towards the tunnel, the soil settlements increase and the maximum settlement occurs on the vertical centre line. This pattern is more clear at V'=9.6% than at V'=1.34%. It was not observed in test EB5, where the same wall was embedded closer to the tunnel: in fact, in that test the soil between the wall and the tunnel axis settled of the same amount of the wall itself from the tunnel axis level to the mid-cover, less than the wall from the mid-cover to the top. This further observation can be explained together with the pattern observed in test EB7 as the rough interface is able to restrain the movement of the soil nearby until a certain distance from the wall: in test EB5 the wall was closer to the cavity than in test EB7, hence the influence of the rough interface extended up to the tunnel, at the same time being the wall movements more affected by the excavation close to its toe. By observing the horizontal displacements profiles (Figs. III.A11c-12c) it can be noticed that the large inward movement to the cavity, as observed in test EB5, beneath the wall toe level and along the vertical line at 50 mm (x=D) have practically disappeared in test EB7 at 80 mm (x=1.6D), that is just behind the wall. This probably means that the local increase of load induced by the wall toe does not interact with the decrease of resistance which occurs as the cavity support pressure decreases. This can also explain why the wall rotates in anticlockwise direction since the beginning of the test without changing direction, as occurred instead during test EB5 in the same range of supporting pressures. It has to be noticed at this point that the lines which have been drawn in the figures for this and all the other tests over the points corresponding to the targets on the wall are only a schematic indication and they do not follow by any particular fitting rule.

Similarly to what observed in the test EB5, the soil above the tunnel crown up to surface tends to rotate in the same way as the wall, in this case being pushed by it.

In test EB8 the wall was smooth, thick and long, embedded 75 mm away (outer edge) from the tunnel axis. As it can be observed in Figs. III.A13-14, the vertical settlements above the tunnel are almost constant with depth. It follows that the ground above the tunnel settles without noticeable vertical strains. A clear discontinuity can be seen in displacement profiles which corresponds to the wall position. In fact the ground behind the wall does not move at all. The wall itself does not settle and its horizontal movements are negligible if compared to those of the ground along the symmetrical vertical line. Also the rotation of the wall is very small. Nevertheless, the horizontal displacements along the vertical centre line are positive at top (they are directed towards the wall, which, on the contrary, does not move) and decrease almost linearly with depth, showing a null point at crown. This behaviour depends likely on the lack of vertical support on the right side due to the smoothness of the wall. In fact, the wall acts similarly to a rigid smooth boundary along which vertical displacements are free and horizontal displacements are restrained. The soil above the tunnel tends to flow along this boundary more than just settle down: this could justify the positive horizontal components of displacement of the cover ground along the vertical tunnel centre line.

In test EB9 the same smooth, long and thick wall was embedded 75 mm away from the tunnel axis (outer edge). Its effect on the ground movements can be observed in Figs. III.A15-16. The wall provides again a discontinuity in shear stress transmission which causes a clear discontinuity in the settlement profiles at the location of the wall. Also, behind the wall the vertical and horizontal displacements are negligible. The wall itself has a very little initial settlement which is negligible. Its horizontal movements are very little (almost null) and directed towards the tunnel. Its rotation is negligible. The vertical displacements along the tunnel centre line increase with depth, similarly to all the previous tests apart from test EB8. The horizontal displacements along the same line are little and almost constant with depth. In between the wall and the tunnel, the horizontal displacements are concentrated nearby the tunnel level. The maximum settlement at surface is neither at the tunnel centre line (as in the reference test EB6) neither close to the wall interface (as in test EB8), but in between. Its distance from the tunnel centre line decreases with depth and it occurs on the centre line at the tunnel crown. It appears that the effect of the shear stress discontinuity on the overall pattern of movements is less important than in test EB8 because it is not so close to the tunnel as in that test. In fact, by predicting the displacement fields with the empirical method it can be verified that the wall is located very close to the boundary of the ground volume interested by movements induced by the excavation in no-wall conditions.

In test EB10 a long, thick and rough wall was embedded in the same location as in test EB8 (outer edge 50 mm away from the tunnel axis). Targets had been inserted or painted along its axis. By looking at Figs. III.A17-18, and particularly to the vertical displacement profiles, it can be observed that the rough interface provides a certain degree of restraint to the settlement of the soil nearby and particularly on the side towards the tunnel, but at the same time the whole right side of the model, where the wall is embedded, tends to settle more than the left side. A similar behaviour was observed in test EB5, where a shorter wall with similar characteristics was embedded; in this case the wall is longer and founded deeper in the ground. In fact both short and long rough walls seem to transfer part of the weight of the soil nearby to deeper ground ('negative skin friction'). Also the wall self-weight, which is about 50% higher than the soil unit weight, has to be considered in this transferred load. As the reduction of supporting pressure occurs very closely to the ground where the load is transferred, it can cause at the same time a reduction of the toe resistance: it is likely, then, that the 'wall side' of the model settles more than the 'no-wall side'.

The same wall was then embedded in the model for test EB11 in the same location as test EB9 (outer edge 75 mm away from the tunnel axis). The corresponding ground movements can be observed in Figs. III.A21-22. It is easy to observe that in this case the wall restrains the settlements of the ground nearby and the whole 'wall side' of the model settles less than the 'no-wall side'. The horizontal displacements in the 'wall side' are also reduced both behind the wall and in between the wall and the cavity. The wall rotates slightly in anticlockwise direction as far as the supporting pressure decreases. Differently from what happened in test EB10, the invert heave is low and even lower than in the reference test EB6; moreover, the horizontal displacements along the tunnel centre line beneath the invert are null. It can be stated that in this case the load due to the 'negative skin friction' effect and to the self weight of the wall is transferred to a ground zone which is far enough from the tunnel boundary, thus the toe resistance of the wall is not affected by the supporting pressure reduction.

In test EB12 a thick, short and smooth wall was embedded at the same location as in test EB5 (outer edge 50 mm away from tunnel axis); a set of 10 mm spacing targets was inserted in purpose drilled holes along its axis. In Figs. III.A21-22 the displacements are shown at two different volume losses. It is worth noticing that V'=9% corresponds to p≅115kPa which is the collapse pressure for this model. Similarly to test EB8 were a rough wall with the same geometry was embedded at the same location, the settlements above tunnel along the vertical centre line are almost constant with depth and no heave was observed at the invert. The horizontal displacements along the vertical centre line are generally positive and linearly decreasing with depth, as in test EB8. In this case it is evident that the ground above the tunnel moves towards right because it follows the wall movements. In fact the wall rotates in clockwise direction since the beginning of the test and, differently from test EB8 (rough wall) its horizontal translation is so negligible that the top wall horizontal displacement is negative. The wall settles, contrarily to test EB8 (smooth and long wall), and its vertical movement is comparable, but higher than in test EB5 (rough wall) at corresponding volume losses. All movements in the area behind the wall are negligible, as it occurred in test EB8.

The horizontal displacements beneath the wall toe are close to zero, whereas they increase in the area between the wall toe and the cavity. It is evident that, the wall shaft resistance being zero, as soon as the toe resistance decreases by reducing the support pressure in the close cavity, the wall tends to move down under its self weight.

In test EB13 a thin wall (0.8 mm thick) has been located with the outer edge 50 mm away from the tunnel axis. It was long and its interface was smooth. Three targets were attached to the wall with the same system used in test EB3. Their supports, used also to fix the wall during consolidation, did not detach from the wall during consolidation because the wall edge had been greased before and shear stresses were likely lower. Nevertheless, only two of them could be tracked by the image processing software, due to the presence of a target in the soil very close to the one at mid-span of the wall which interfered with it. For this reason, no indication on the bending of this flexible wall could be obtained from measurements. Some displacement profiles are reported in Figs. III.A23-24.

The vertical displacements above the tunnel and along the tunnel centre line increase as little with depth as in test EB8 (thick, smooth and long wall). The corresponding horizontal displacements are directed towards the wall and whereas they are almost constant with depth at low volume loss, they decrease linearly to almost zero at crown at higher volume loss. Below the invert, the horizontal displacements are zero, whereas a certain amount of local heave can be observed very close to the tunnel boundary. By looking at the horizontal profiles of settlements at various levels, and comparing the left and the right sides of the model each other, it can be observed that the wall provides a reduction of settlement at its back and induce an increase towards the tunnel. The same can be observed for horizontal displacements. This effects is more evident at a higher volume loss. In fact, the discontinuity is less marked than in test EB8, where the wall was stiffer. In this test the wall moves much more towards the tunnel, rotates in anticlockwise direction and it likely bends due to its flexibility, even if an evidence of this cannot be given, due to the lack of intermediate targets on the wall. As a consequence, the ground movement on the right side of the wall is not completely restraint.

In Figs. III.A25-26 measurements in test EB14 have been reported. In this test the same wall used in test EB5 (short and thick wall with a 'sandy' interface) was embedded in the model. The embedding procedure was different: a trench was cut after the soil had been consolidating and before cutting the tunnel cavity and the wall was pushed from the front of the model, as described before and shown in Fig.III.7. The aim was to check the roughness of the adopted interface and the effectiveness of the embedding procedure used in the previous tests.

In Figs. III.19-III.20 the measured ground movements in tests EB5, EB12 and EB14 at two volume losses have been plotted together for comparison. It is worth noticing that the three models differ only in the kind of interface and in the embedding procedure: the walls in EB5 and EB12 are embedded in the model before the consolidation under the press, EB14 is embedded afterward by trenching; the wall in EB5 and EB14 is the same and it has a rough interface obtained by sticking a layer of medium coarse sand on its surface, the wall EB12 has a smooth interface obtained by greasing its surface. By comparing the results it appears that at both volume losses, the displacements in the model EB14 are intermediate between those in the model EB5 and EB12. In fact, in the right (no-wall) part of the model the ground movements in tests EB5 and EB14 are almost the same. Also between the wall and the cavity, the ground movements in test EB14 are closer to those in test EB5; apart for the horizontal displacements above the tunnel along the centre line, which are closer to test EB12. The movements of the wall in EB14 are closer to those of the smooth wall in test EB12. Behind and beneath the wall the movements in test EB14 are similar to test EB12. Hence, the pattern of movements in test EB14 are similar to the model with a rough wall in the left part of the wall, closer to the model with a smooth wall in the right part. Therefore, the trenching procedure with a sandy interface wall leads to an uncontrolled interface, appearing that the front (tunnel side) interface of the wall behaves as rough whereas the back (boundary side) behaves as smooth. For this reason a new test was performed with a different interface.

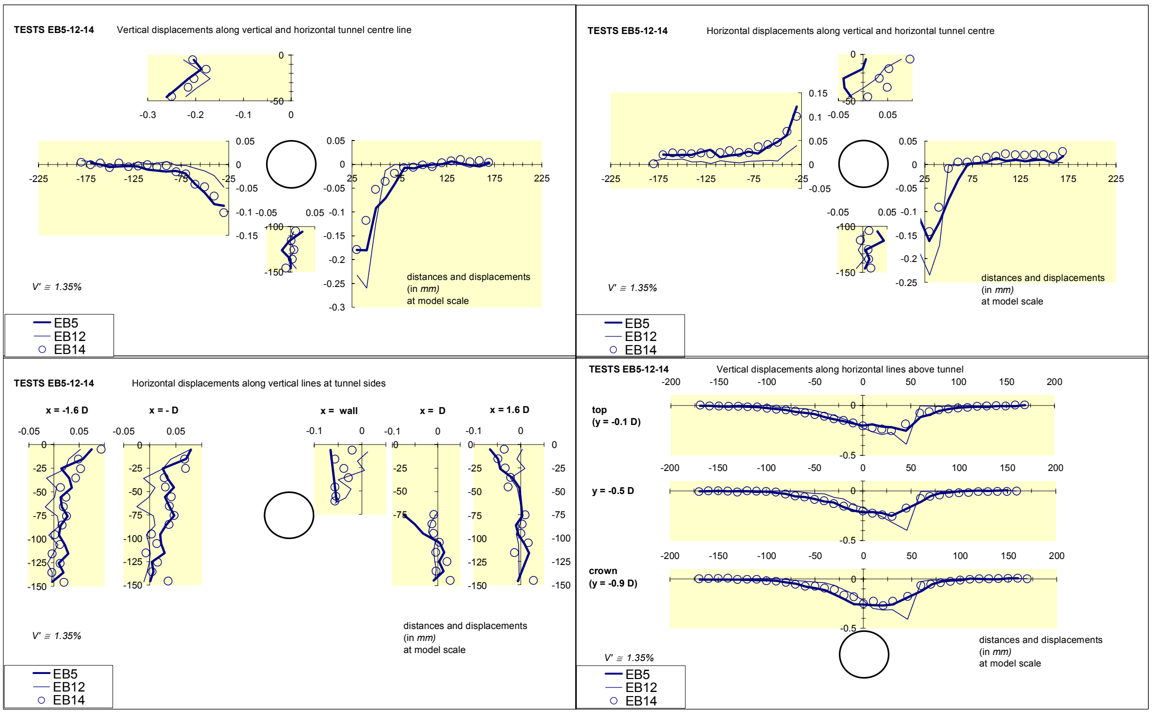

Figure III.19 – Ground movements in tests EB5, EB12, EB14 at V'≅1.35%

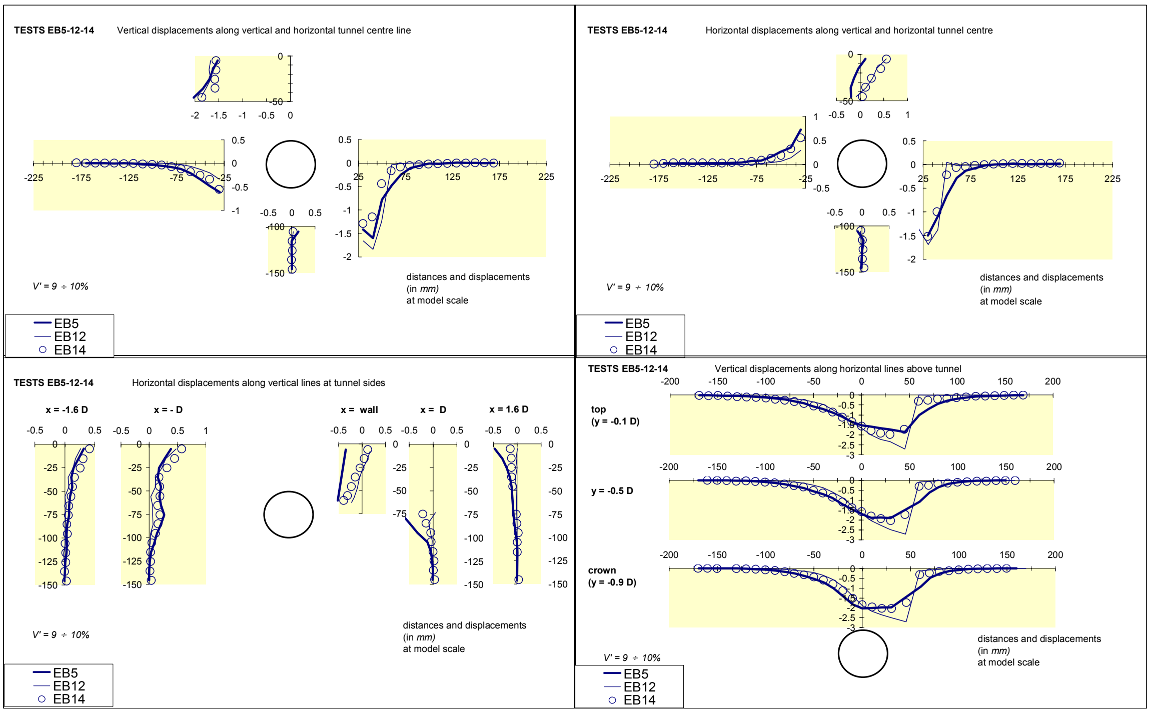

Figure III.20 – Ground movements in tests EB5, EB12, EB14 at V'=9÷10%

In test EB16 trenching was adopted again to insert the wall from the front of the consolidated ground. In this test a new wall was used: its edge was tooth-shaped in order to attain a high degree of roughness (details have been shown in Fig. III.8). The thickness of its web is 7.2 mm, hence the wall is sensibly more flexible than the other thick ones. Its length and location were the same as in test EB5. The relevant ground displacements are plotted in Fig. III.A27-28; the same are shown in Fig. III.21 together with those measured in test EB5. The measurements refer to V'≅10% but those at V'≅1.3% have the same pattern.

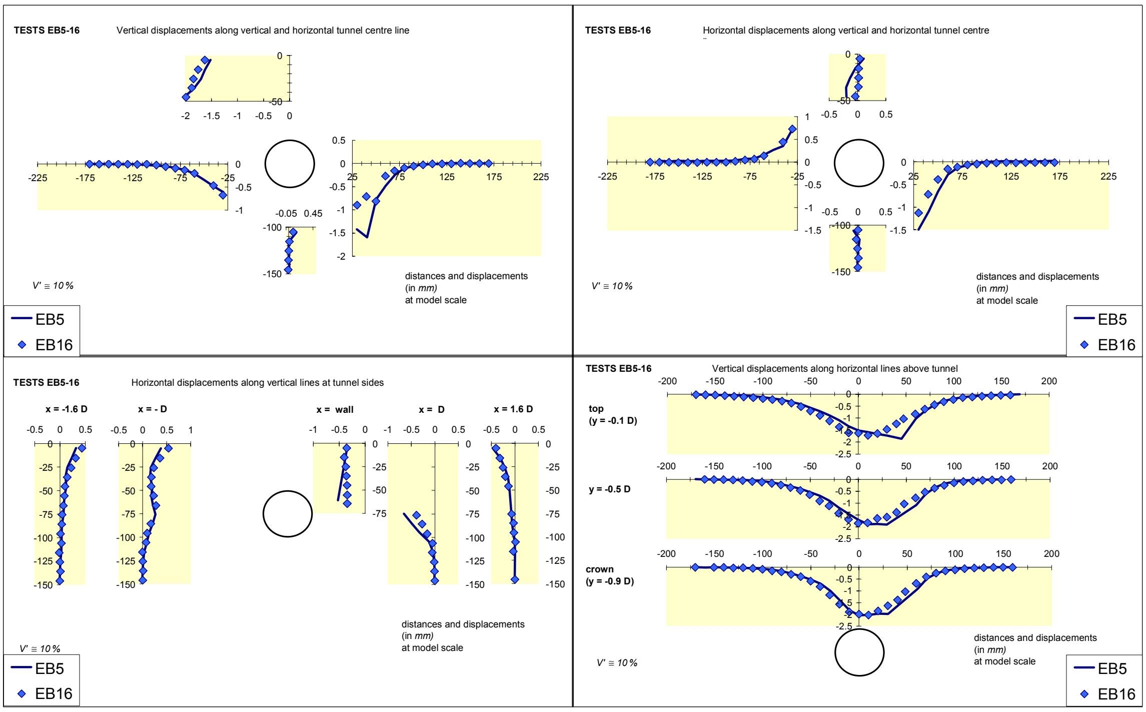

Figure III.21 – Comparison between test EB5 and EB16

As it can be observed in Fig. III.21 the ground movements in the two tests are almost the same.

A difference can be observed on the symmetry of the settlement trough and on the movements in the area between the wall toe and the tunnel. The troughs in test EB16 seem less asymmetric to the vertical centre tunnel line than in test EB5. The wall rotates and settles slightly more in test EB5 and the displacements between the tunnel and the wall toe are slightly higher. These differences could be attributed to the difference of weight of the wall between the test EB5 and EB16. On the other hand the substantial equivalence of the two sets of results induces to conclude that both the walling techniques give rise to the same effectiveness of rough interface.

A general pattern of the displacement fields in all the tests in vector form at the same relative pressure change ($-\Delta p/p_o$=40%) have been reported in Appendix III.B.

Undrained conditions

By integrating the vertical displacements along the horizontal lines at top, mid-cover and crown it is possible to evaluate their area. As it can be observed in Figs. III.A, these profiles extend enough to reach laterally zero values. Hence, by multiplying their area by the model width (200 mm) the volume of soil displaced below the corresponding level can be evaluated.

If undrained conditions occur, these calculated volumes should be the same at all levels, as no volume change is allowed. In fact in Tab. III.4 the calculated volumes of the troughs reported in Figs. III.A are shown. A part from test EB2 at low volume losses (V'≅1.35%), it can be verified that these volume are almost the same with a random error of a few percentage units. Therefore it can be stated that the cavity supporting pressure was likely reduced in undrained conditions.

Table III.4 – Calculated volumes of the settlement troughs at various depths

	V'≅1.35%			V'≅10%		
	Top	Mid-cover	Crown	Top	Mid-cover	Crown
	V_{trough}(mm^3)					
EB1	5103	4632	5181	40820	39289	39132
EB2	4906	3807	3336	39525	36346	36071
EB3	5299	4357	4553	38936	37916	37798
EB5	4985	4710	5456	37916	37445	38622
EB6	5260	4435	4553	41134	39407	40310
EB7	5260	5142	5417	35404	37484	38779
EB8	5103	4239	4553	37445	35364	35678
EB9	5142	4946	5181	39800	40545	40035
EB10	5456	5338	5809	38622	38897	39996

EB11	5456	5024	5691	37759	36934	39172
EB12	4867	4082	4632	35443	34187	35482
EB13	5220	4553	5024	40310	41409	41723
EB14	5024	4749	4592	35796	34462	34933
EB16	5024	4710	4828	38387	37719	37602

Influence of the wall length on the displacement fields

In Figs. III.22-III.24, some of the displacement fields at V'≅10% of two models with embedded walls and C/D=1 have been plotted together with the corresponding reference displacement fields (test EB6). The two walls have different length. The pattern of movements at V'≅1% is similar but less clear, as it has been observed in Figs. III.A.

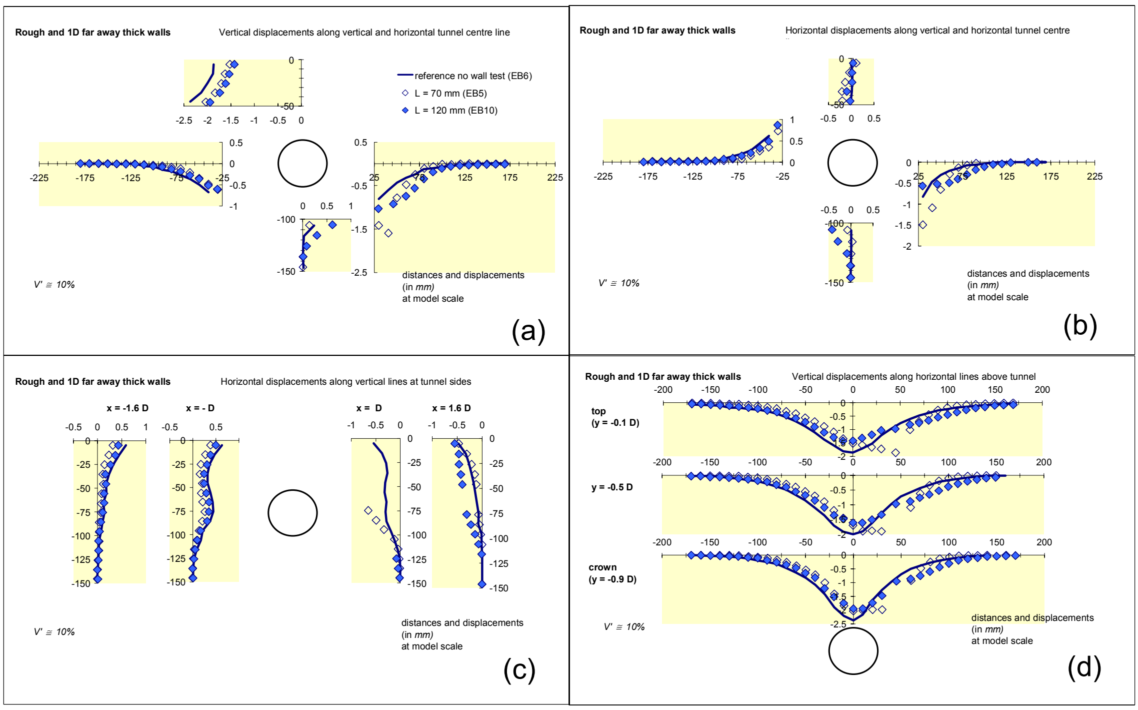

Figure III.22 – Comparison between test EB5, EB10 and EB6

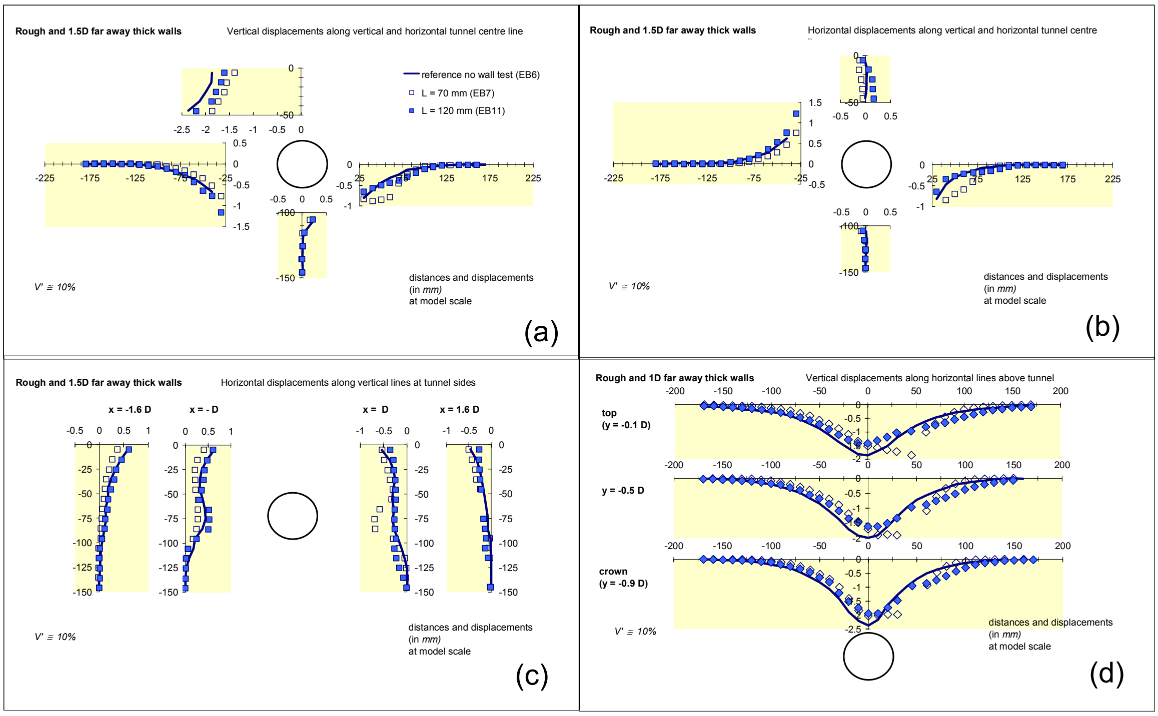

Figure III.23 – Comparison between test EB7, EB11 and EB6

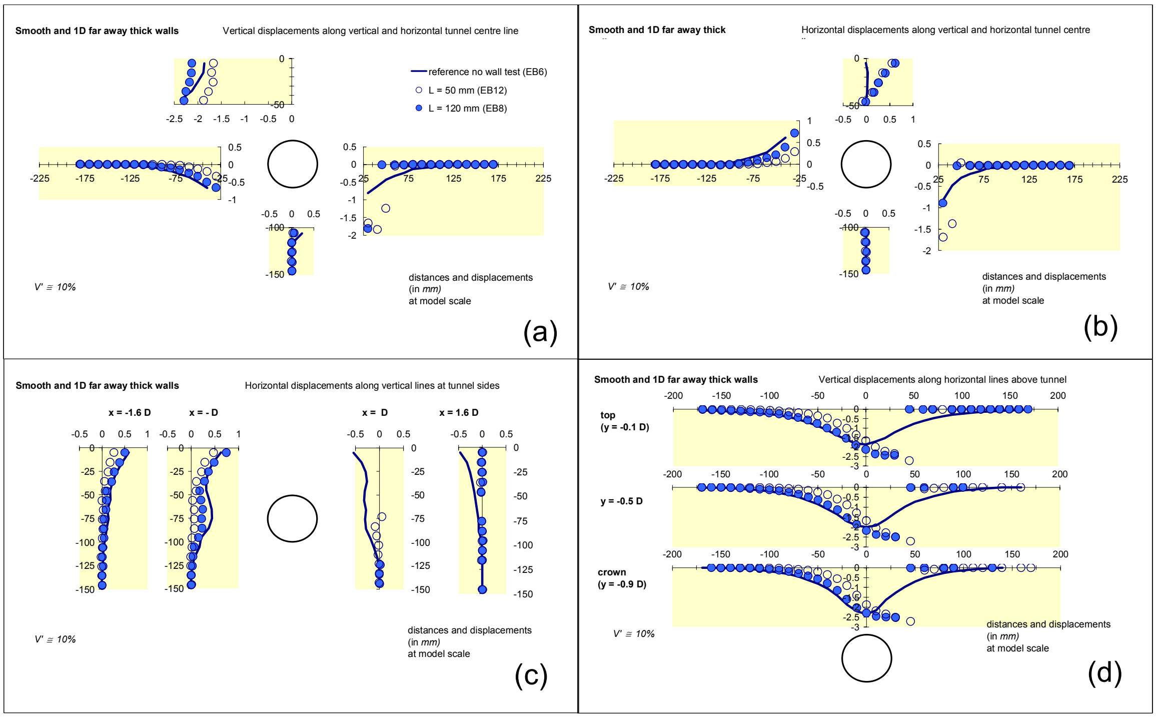

Figure III.24 – Comparison between test EB12, EB8 and EB6

In Fig. III.22 the measured ground movements in tests with rough and 1D faraway thick walls have been plotted. The differences between displacements pertaining to the model with the short wall and the model with the long one are very little and concentrated in the vicinity of the wall. The ground in this area settles more in the model with the shorter wall. A similar behaviour can be observed in Fig. III.23 where the same walls are embedded at 1.5D from the tunnel axis. In both cases it can be attributed to the fact that the wall transfers part of the soil load through its interface and its self-weight to the ground close to its toe: the longer wall toe is in deeper ground and this could justify the minor influence that the wall has on ground movements. As displacements at the same volume loss are compared, the increase in the magnitude of displacements in the wall part of the model corresponds to a decrease of it in the no-wall side. The comparison with the reference test shows that in both cases the measured displacements are not very different from those observed in the model without wall; moreover, the movements behind the wall are increased in many cases. In fact, the only test which provides a slight reduction of settlement is EB11, in which a long and thick wall was embedded at 1.5D from the tunnel axis (Fig. III.23d). In Fig. III.24 the ground movements in models with smooth and 1D faraway thick walls are shown. As a general comment it can be observed that both walls reduce ground movements behind: the displacements are very close to zero. On the other side of the wall the ground movements increase up to the tunnel vertical centre line. As the profiles correspond to the same amount of volume loss, the ground on the other side of the tunnel axis move less than in the corresponding area of the reference test. The shorter is the wall the more the settlement in the no-wall part of the model are reduced. Provided that the wall is long enough, the effects of its presence on the other side of the tunnel axis are negligible.

Influence of the wall thickness on the displacement fields

In Fig. III.25 the ground movements at V'≅10% in tests with a long and smooth wall close to the tunnel have been plotted together with the reference.

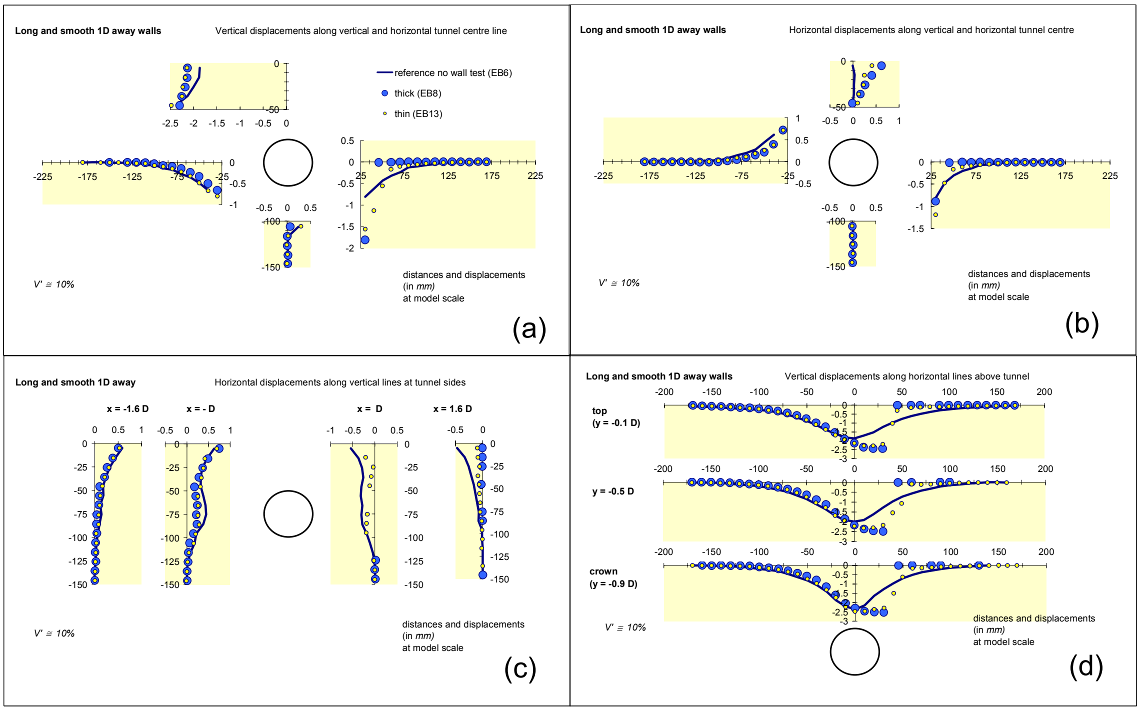

Figure III.25– Comparison between test EB8, EB13 and EB6

In test EB8 the wall was thick whereas it was thin in test EB13. The couples of corresponding profiles of displacements in the two tests are very similar each other. Therefore, at least for smooth walls, the influence of the wall thickness, hence of its stiffness, seems to be very little. This could be not true for a different roughness of the wall, as it was observed by comparing test EB2 and test EB3 that the thin wall with uncontrolled interface did not provide a significant change in the overall ground movements. Moreover, it has to be highlighted that at a lower volume loss (V’≅1%) the surface settlement trough of test EB13 is closer to the reference EB6 than to EB8 profile, as it can be seen in the following Fig. III.32.

Influence of the wall roughness on the displacement fields

In Figs. III.26-III.28 the ground movements of model with walls having the same size but different interface roughness have been compared each other and to the reference profiles at V’≅10%.

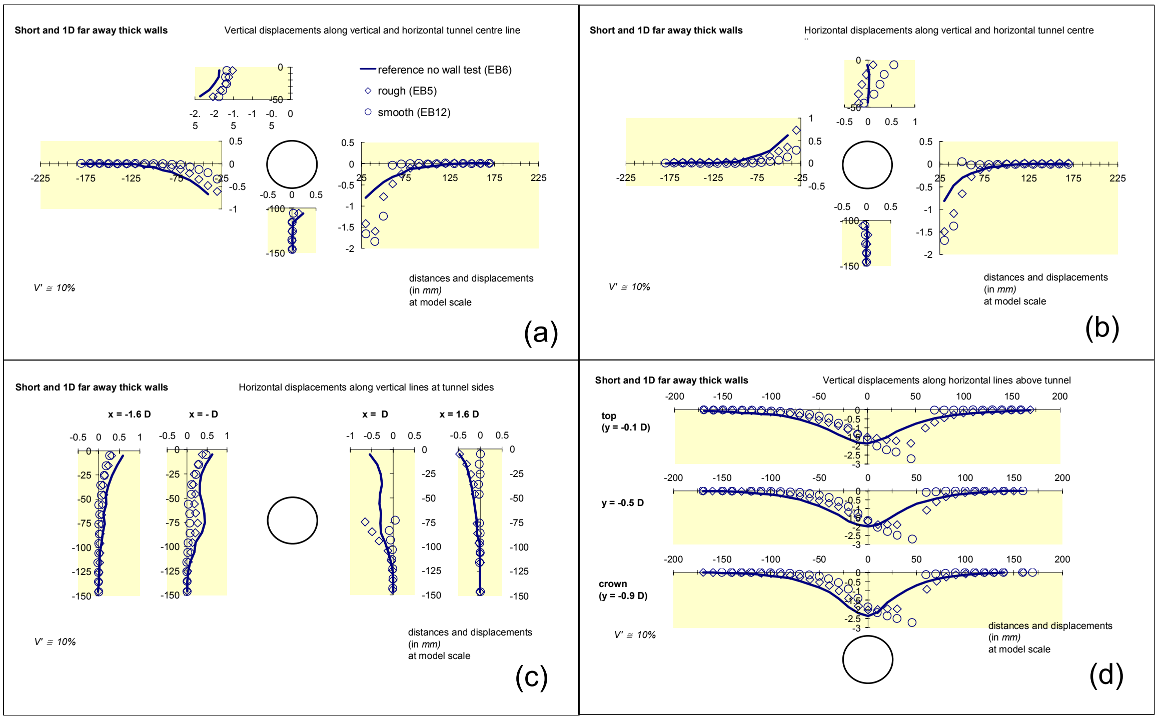

Figure III.26 – Comparison between test EB5, EB12 and EB6

In Fig. III.26 the two wall-model profiles refer to a short and thick wall embedded 1D away from the tunnel axis. In the zone of the model where the two wall reduce movements, the smooth wall provides generally a higher reduction than the rough wall. On the other hand, where the wall increases the ground movements they are larger in the model with the smooth wall. Behind the wall, the smooth wall reduces movements close to zero, whereas the rough wall does not provide such a reduction, on the contrary movements of the closer soil increase. Between the wall and the cavity both walls increase movements.

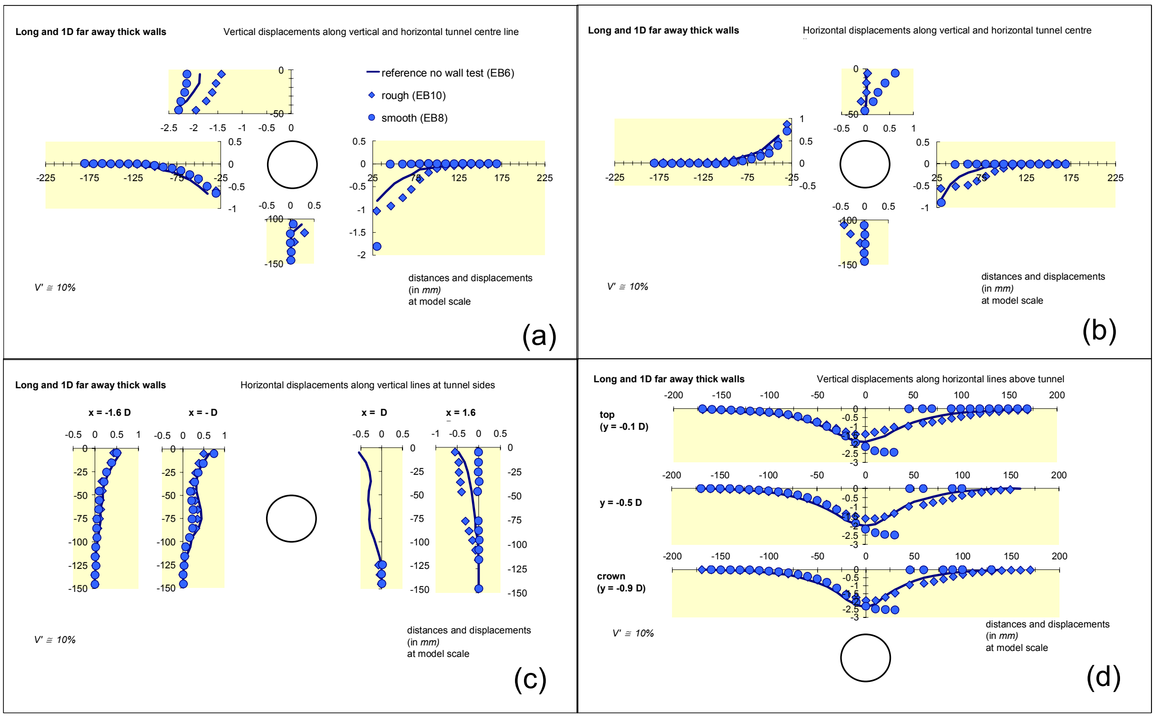

Figure III.27 – Comparison between test EB10, EB8 and EB6

In Fig. III.27 the profiles refer to long walls. In this figure a larger difference can be observed in ground movements in the wall side of the model between tests with rough and smooth wall than in the corresponding models with short walls. In fact, the profiles of settlements in the model with a rough wall are very close to the reference, whereas the smooth wall creates a strong discontinuity in the profiles. On the other side of the model, on the contrary, the effect of roughness is negligible and the displacement profiles pertaining to both rough and smooth wall tests are close to the reference.

In Fig. III.28 the profiles of the ground movements in tests with long and thick walls embedded 1.5D away from the tunnel axis are plotted with the reference profiles. The difference between profiles in the wall part of the model are less evident because the rough wall reduces the settlements of the soil nearby. In the no-wall part of the model the settlements in the rough wall model are close to the reference, whereas in the smooth wall model they are slightly lower. The effect on the horizontal displacements varies with depth: the rough walls reduce slightly the horizontal displacements at surface in the wall-side of the model, but this effect reduces with depth, and the relevant profile is close to the reference; on the other hand, the smooth wall reduces generally more the horizontal movements in the wall side of the model, apart from the area located around the tunnel axis level between the tunnel and the wall. In this area the ground moves towards the tunnel more than in the reference test and in the rough wall model test.

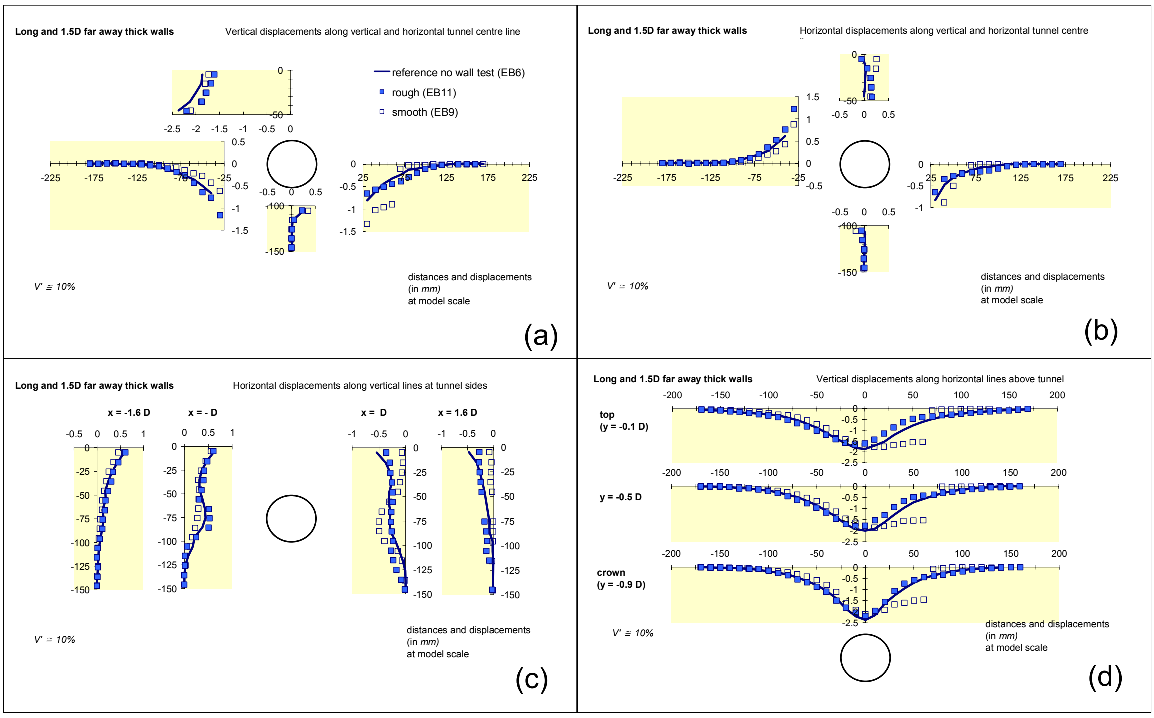

Figure III.28 – Comparison between test EB11, EB9 and EB6

In summary, smooth walls seems to be more effective than rough ones to reduce ground movements behind them, even if a major shortcoming is the increase of movements between the wall and the tunnel. Nevertheless, provided that a sufficient cavity support is guaranteed the volume loss can be controlled: the tests show that if the same volume loss is achieved as in the no-wall conditions, the settlement on the vertical tunnel centre line is almost the same with or without wall and the no-wall part of the model is almost unaffected by the presence of the wall.

Influence of the distance of the wall on the displacement fields

It has been noticed, at various points before, that the effect of a wall on ground movements are generally much more evident in the ground in the vicinity of the wall. In Figs. III.29-III.31 the results of tests in which the same wall (same length, thickness and roughness) was located in different positions are directly compared. In all cases, the wall modifies the pattern of movements in the same way, no matter its location. Particularly, in the no wall side of the model the curves pertaining to the same wall type at two different locations are almost superimposed: a major gap between the corresponding profiles can be observed for rough and long walls whereas the profiles of displacements in the models with smooth and long walls coincide.

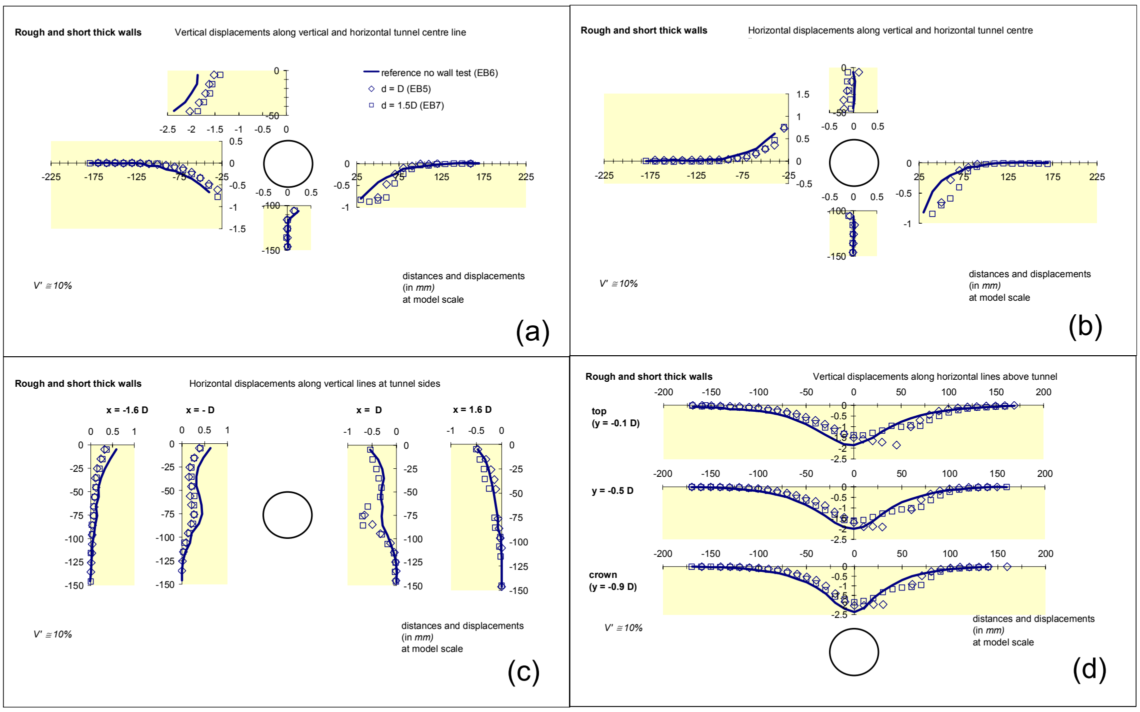

Figure III.29 – Comparison between test EB5, EB7 and EB6

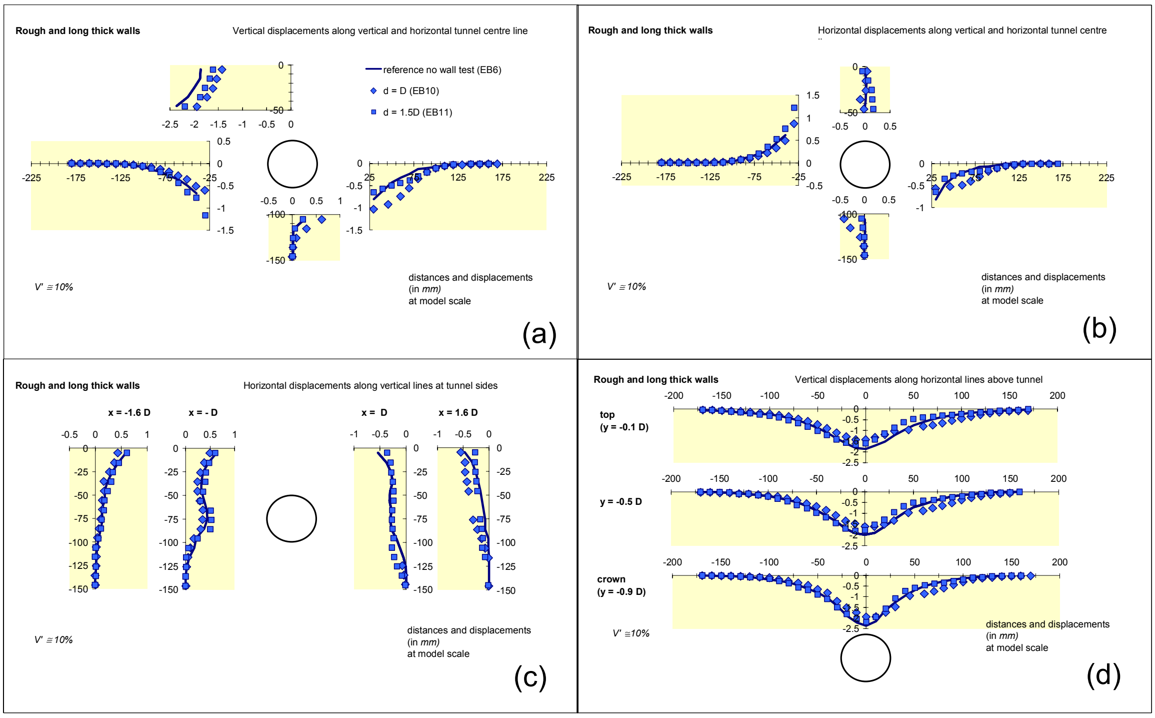

Figure III.30 – Comparison between test EB10, EB11 and EB6

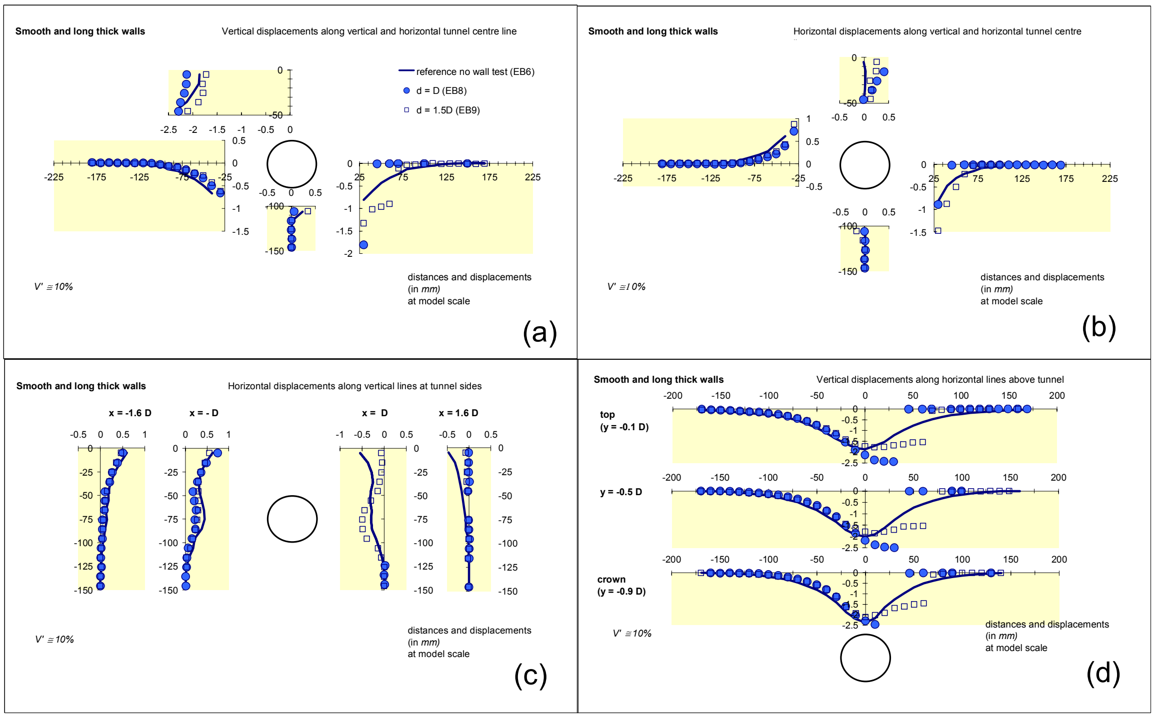

Figure III.31 – Comparison between test EB8, EB9 and EB6

Influence of the tunnel supporting pressure on the displacement fields

In Fig. III.32 the vertical and horizontal displacements at the 'surface' (first row of targets) are shown for tests with rough and smooth walls with C/D=1 at the same value of volume loss (around 1.35%). This volume loss is likely to occur in field practice but, as it has been shown, the pattern of ground settlements are very similar at different values of volume loss. Nevertheless, as already mentioned, the results pertaining to the long and smooth walls, with different thickness, at this low volume loss indicate that the stiff wall reduces the movements more than the flexible one. This could be expected but it does not results a higher volume loss (V'=10%).

In the reference test EB6 the value of V'=1.35% occurred at $-\Delta p/p_o$=40%. It seems hence interesting to compare the same type of curves at this value of pressure change, which corresponds to the same supporting pressure.

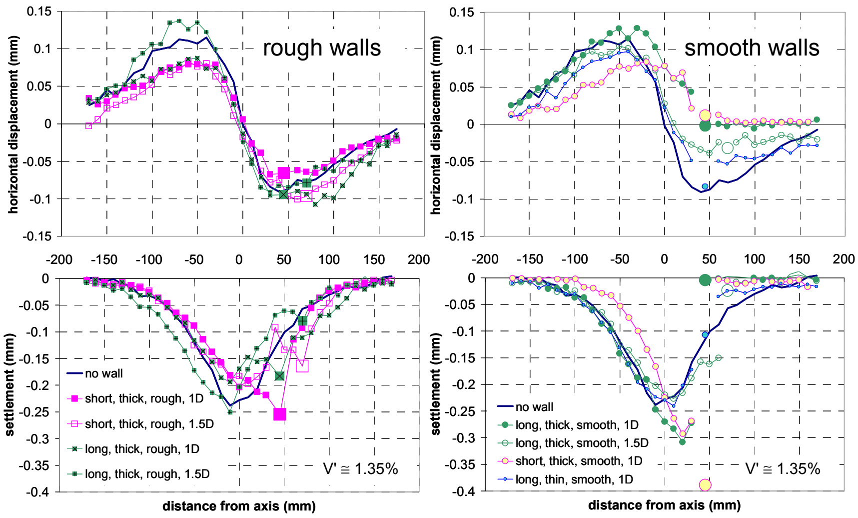

Figure III.32 – 'Surface' displacements at V'≅1.35% (the larger marker corresponds to the target on the wall)

Therefore, in Fig. III.33 similar curves are shown at 40% of pressure reduction. In these figures, the curves of the test EB12 have not been displayed for the sake of clarity, because the settlements were too high if compared to the other tests at the same pressure.

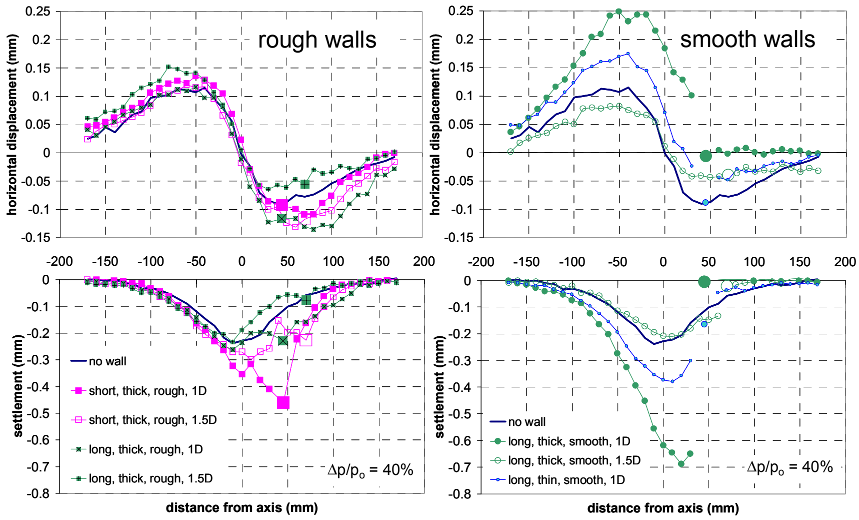

Figure III.33– 'Surface' displacements at 40% of supporting pressure reduction

From the charts shown in Fig. III.33 it can be observed that embedding a diaphragm wall between the tunnel and a (possible) building does not seem always a good measure of protection against large movements and severe damages if the same supporting pressure as in the no-wall condition is applied to the tunnel boundary. In particular, the rough diaphragm walls seem to behave worse than the smooth ones. On the other side, smooth walls provide a strong reduction of settlements behind them, but they increase settlements above the tunnel and in the ground on the opposite side of it.

APPENDIX A

Figures III.A1-III.A28

Figure III.A1

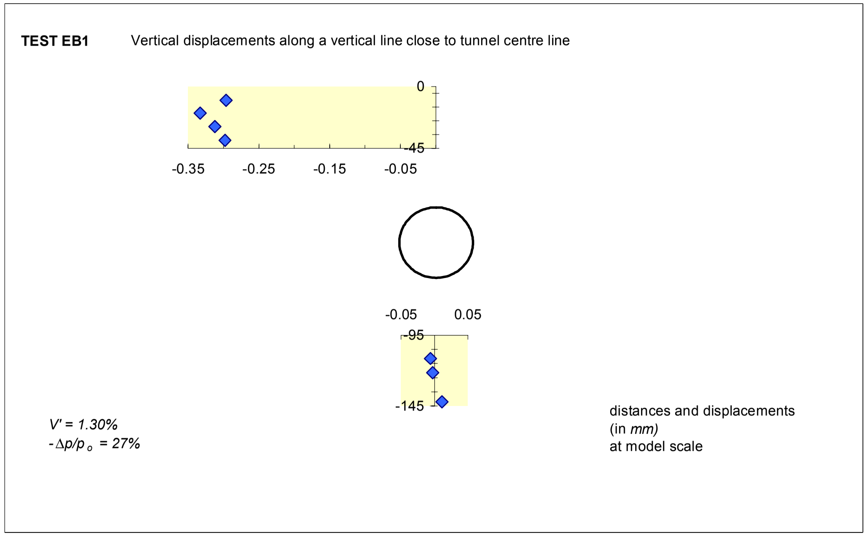

a)

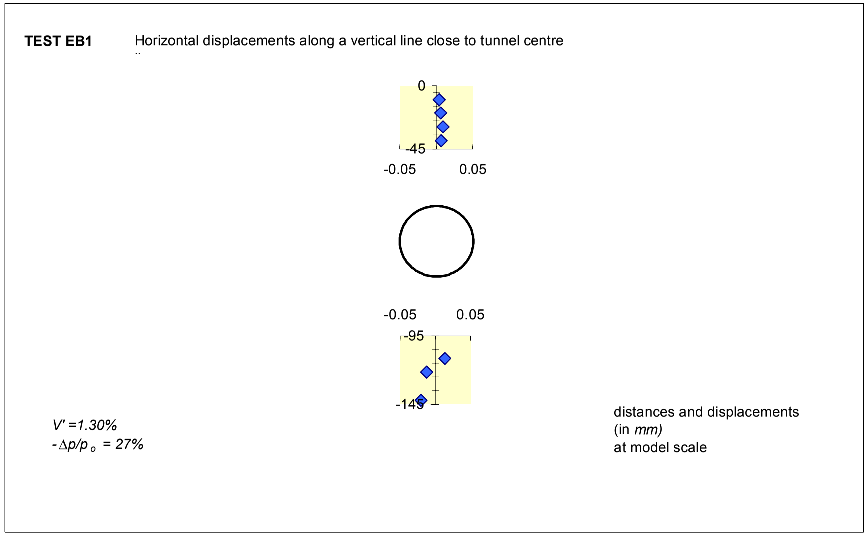

b)

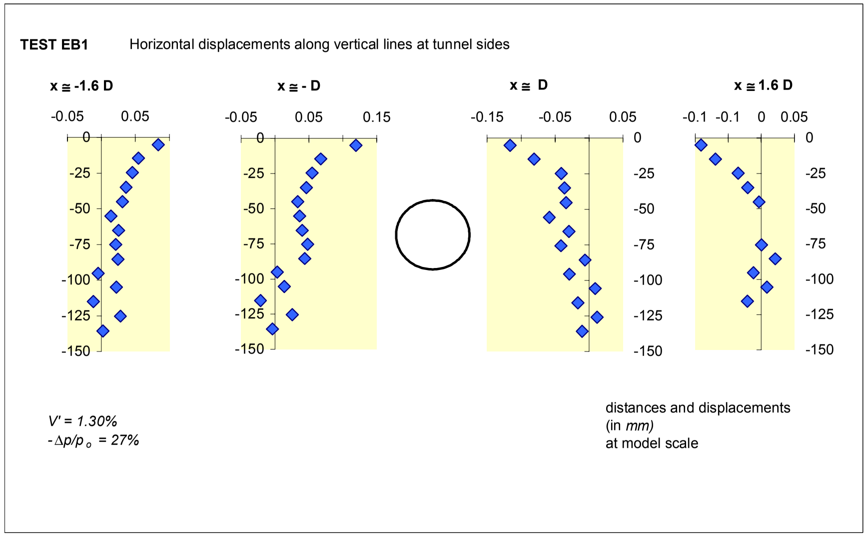

c)

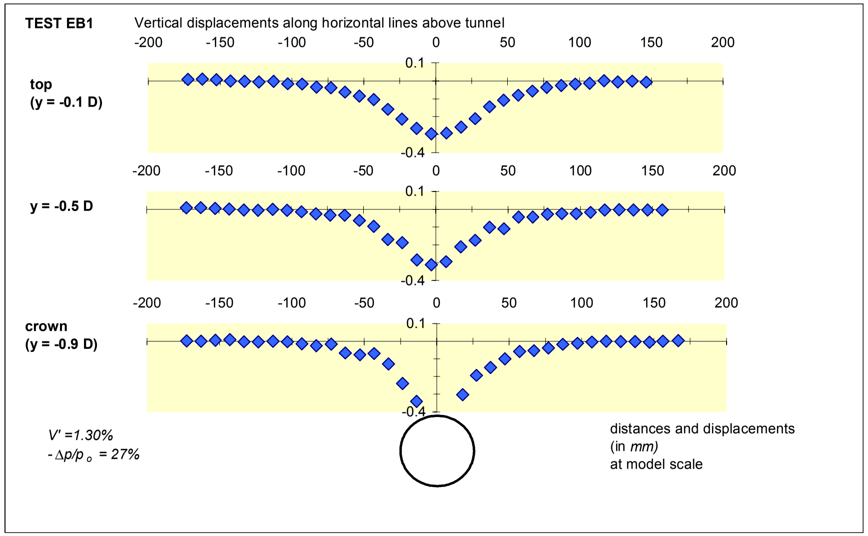

d)

Figure III.A2

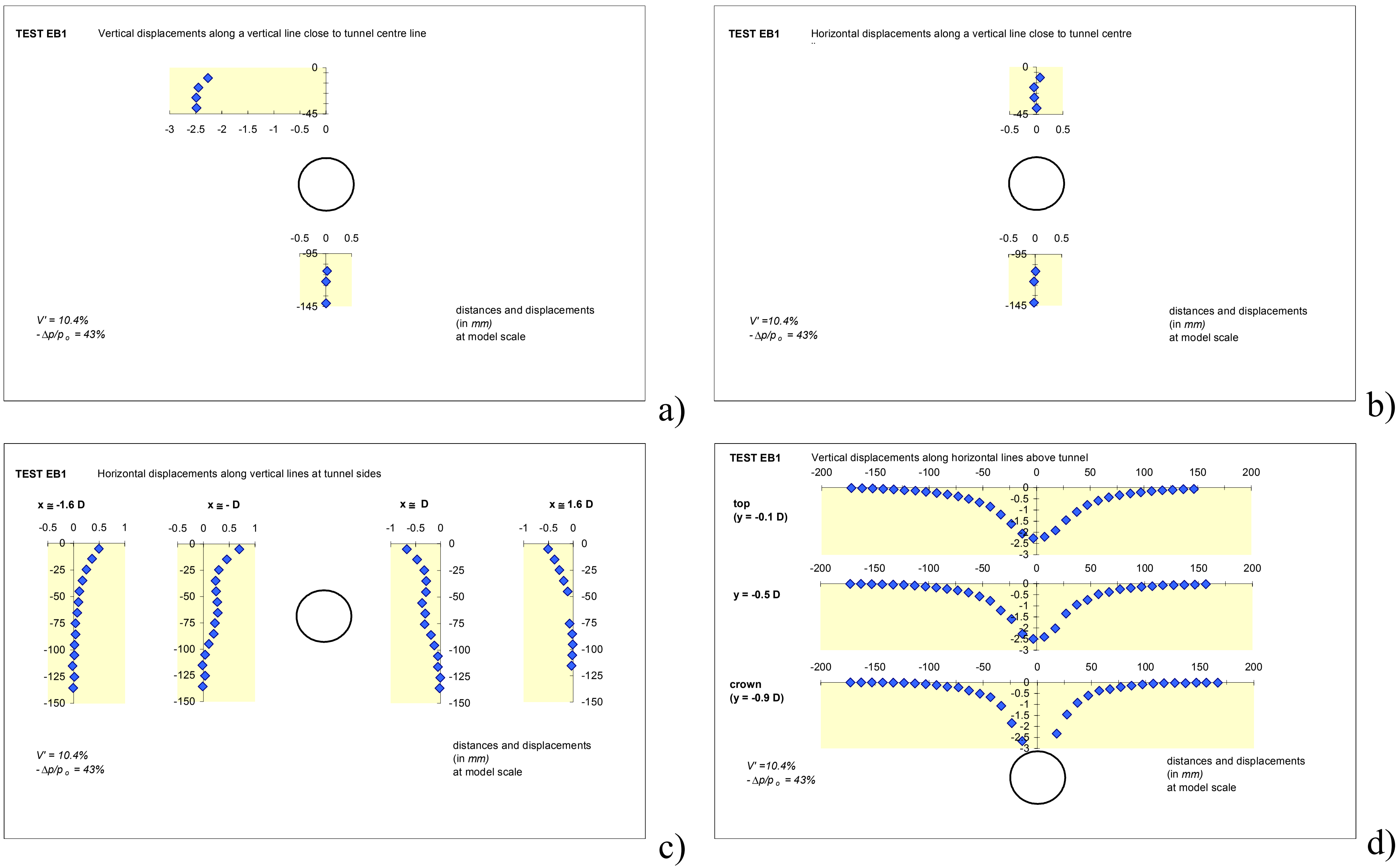

Figure III.A3

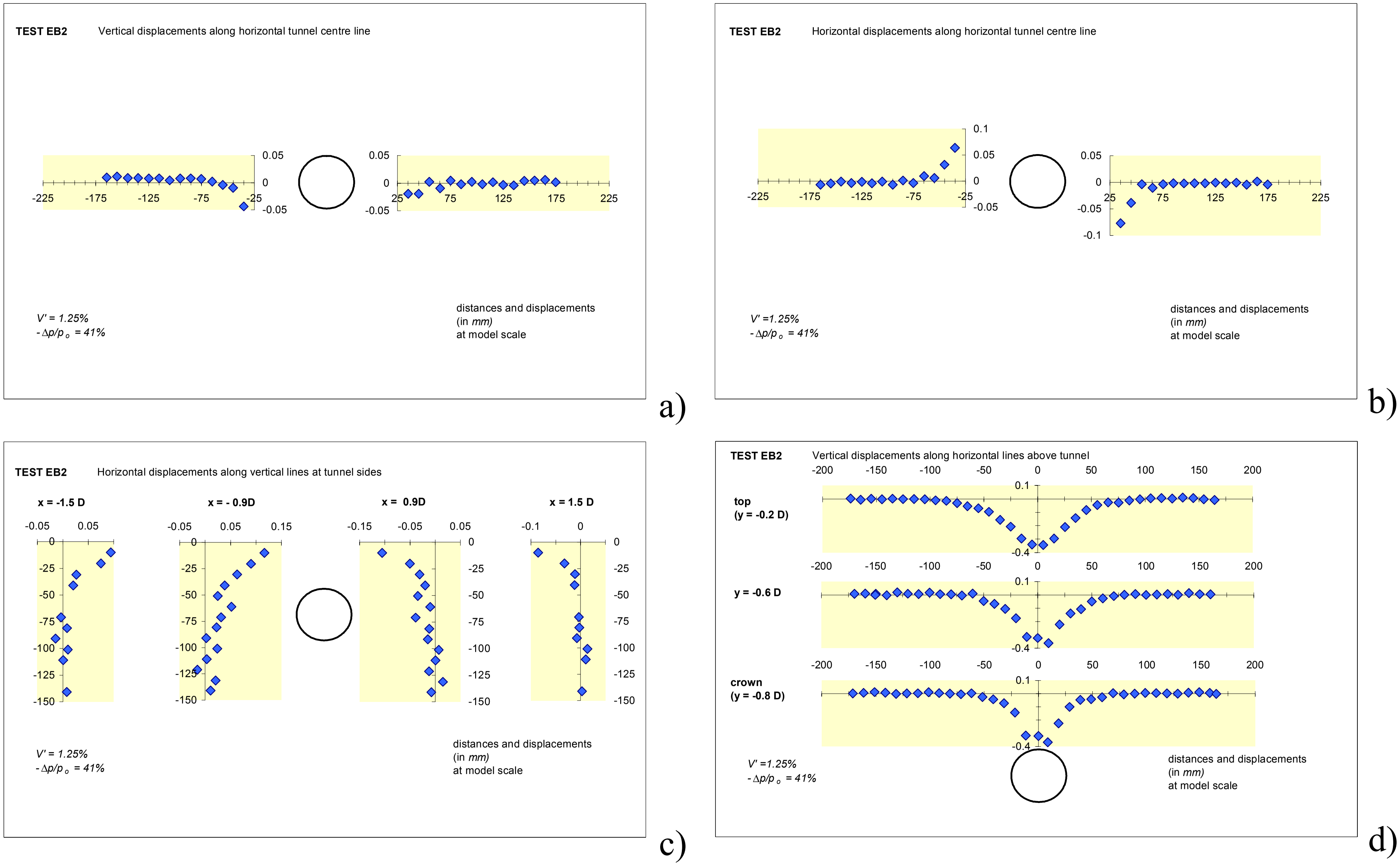

Figure III.A4

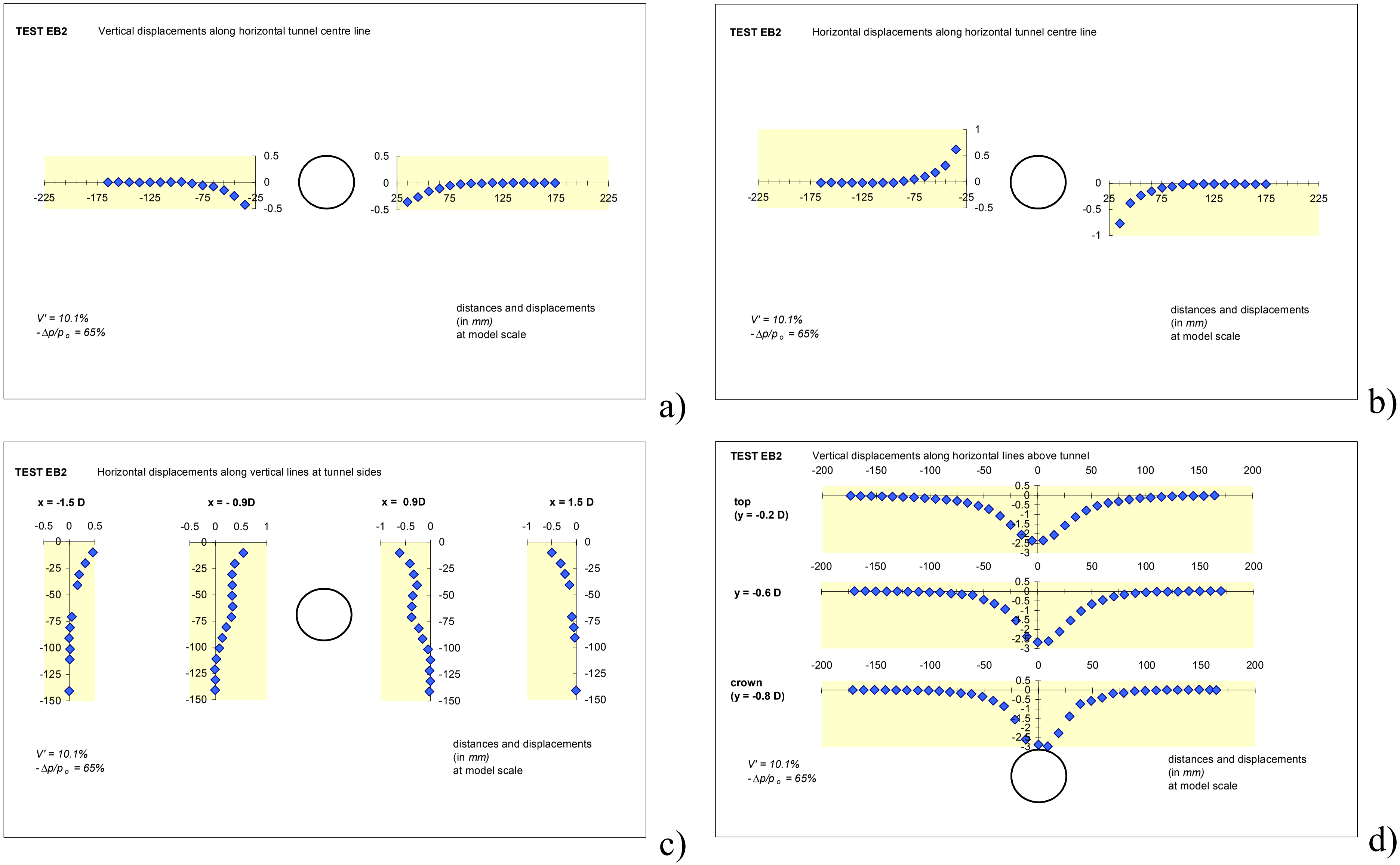

Figure III.A5

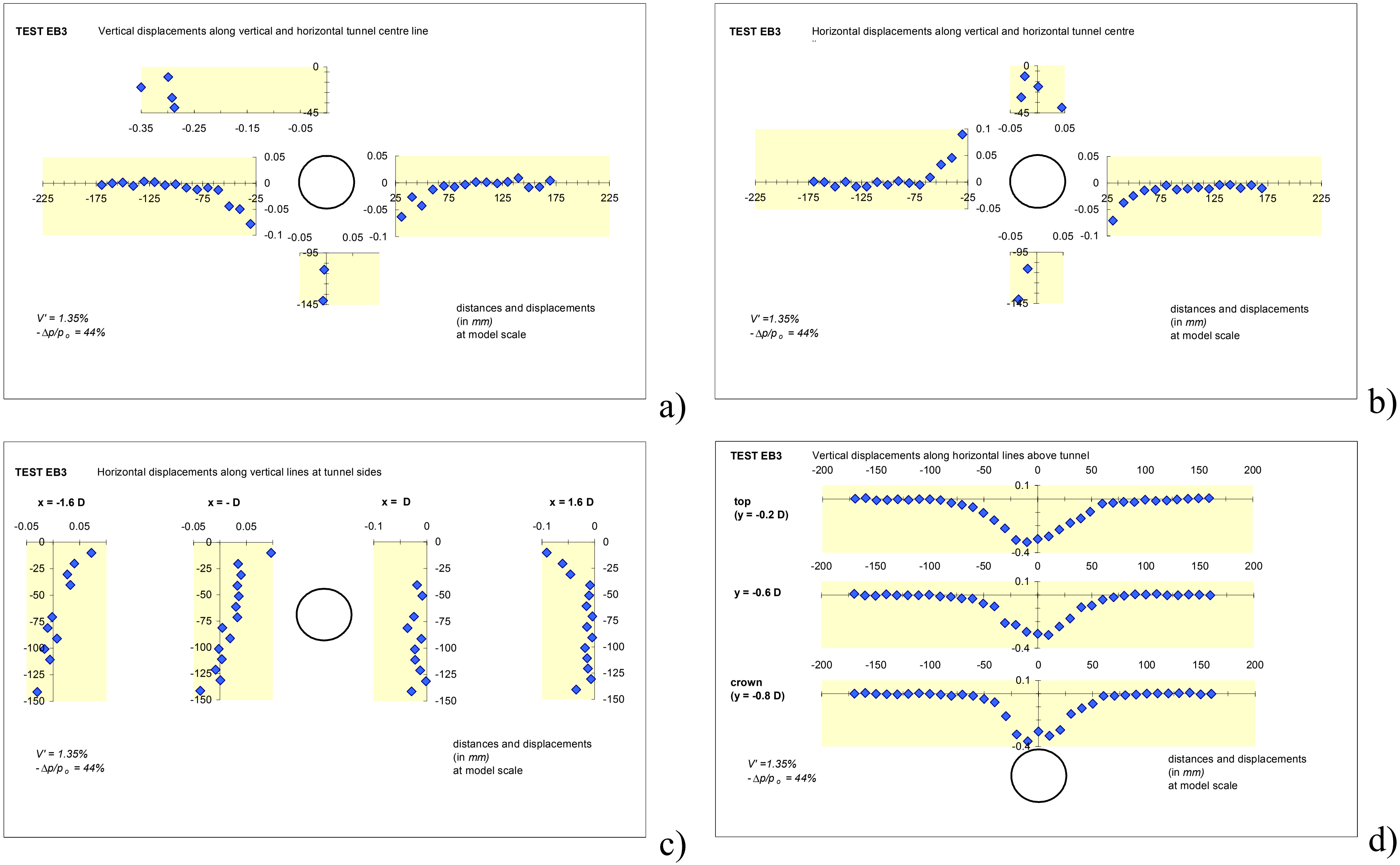

Figure III.A6

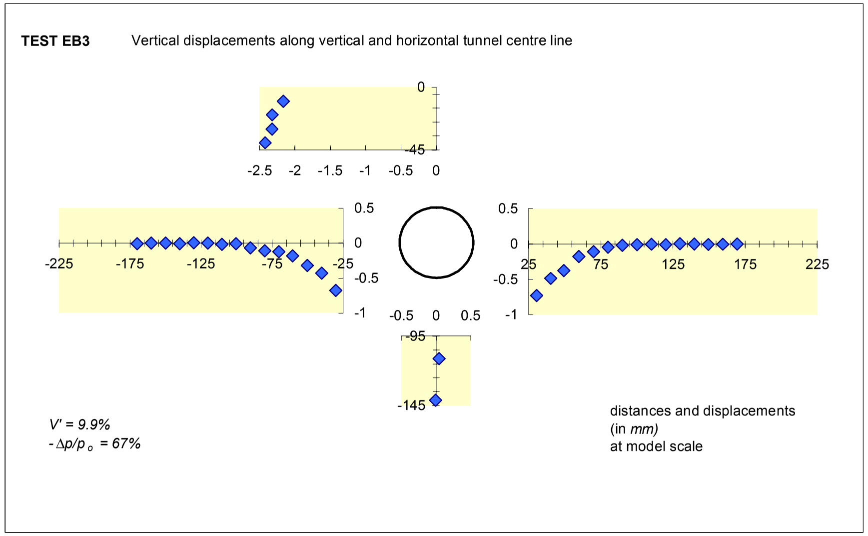

a)

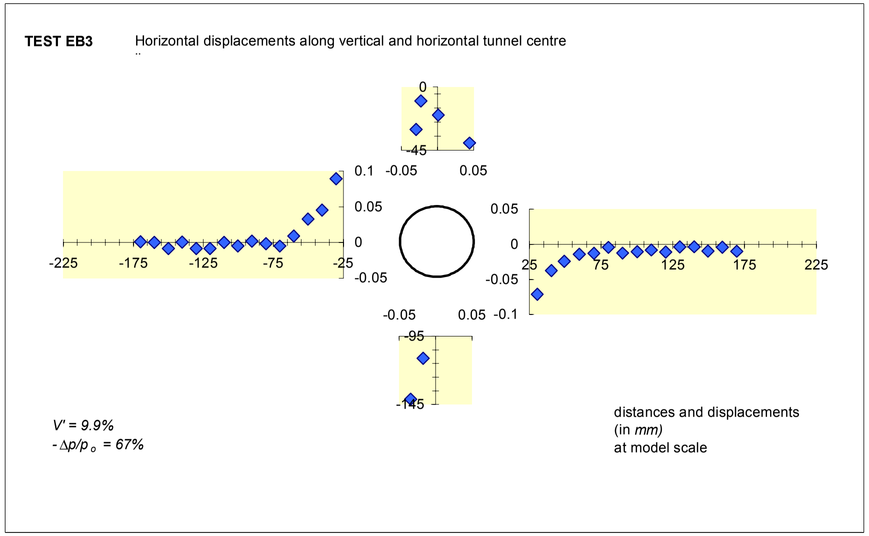

b)

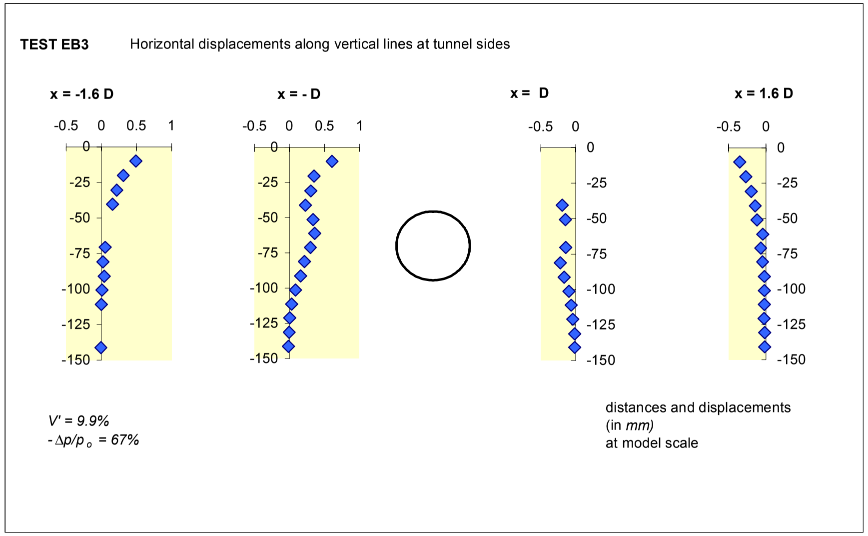

c)

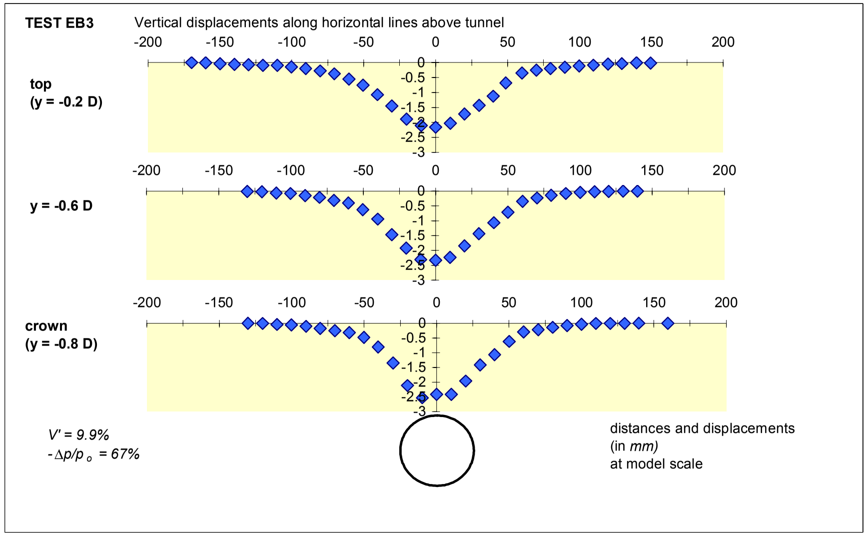

d)

Figure III.A7

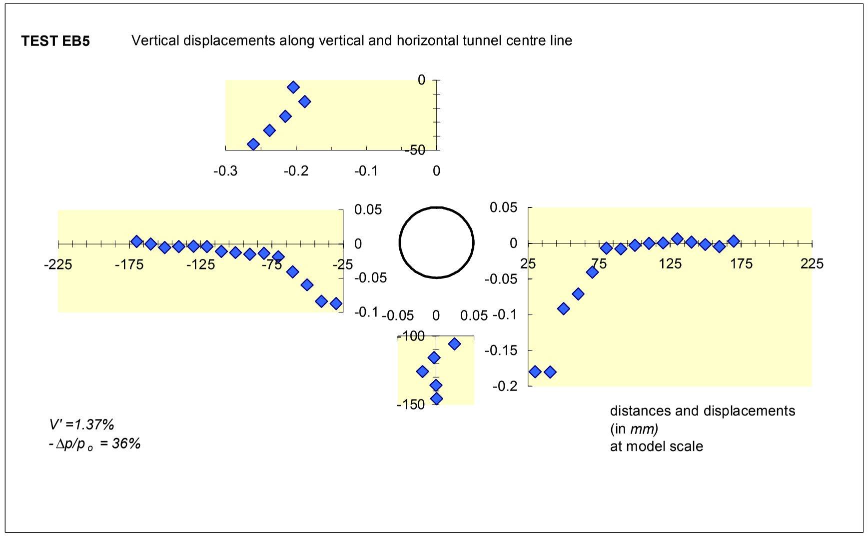

a)

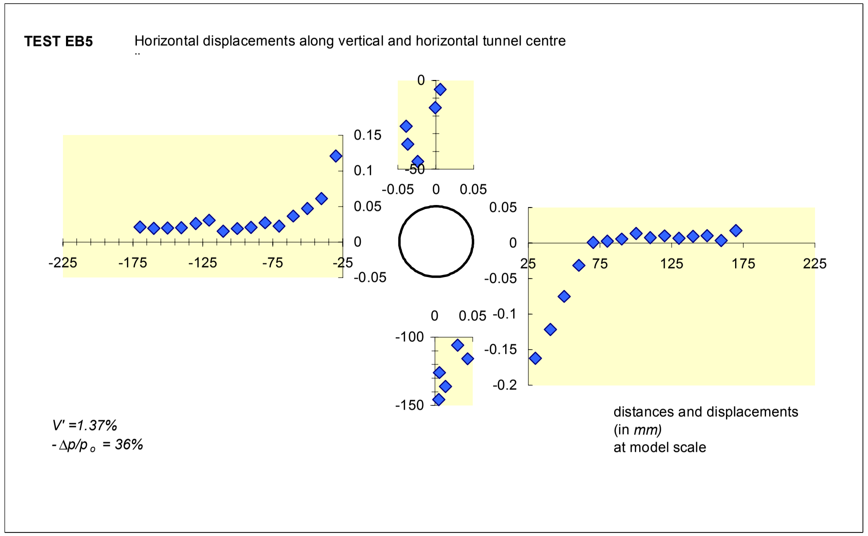

b)

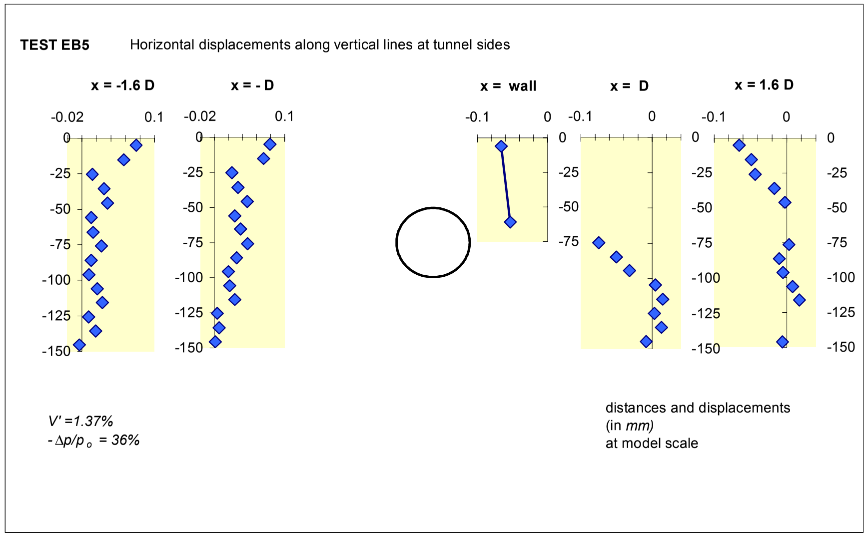

c)

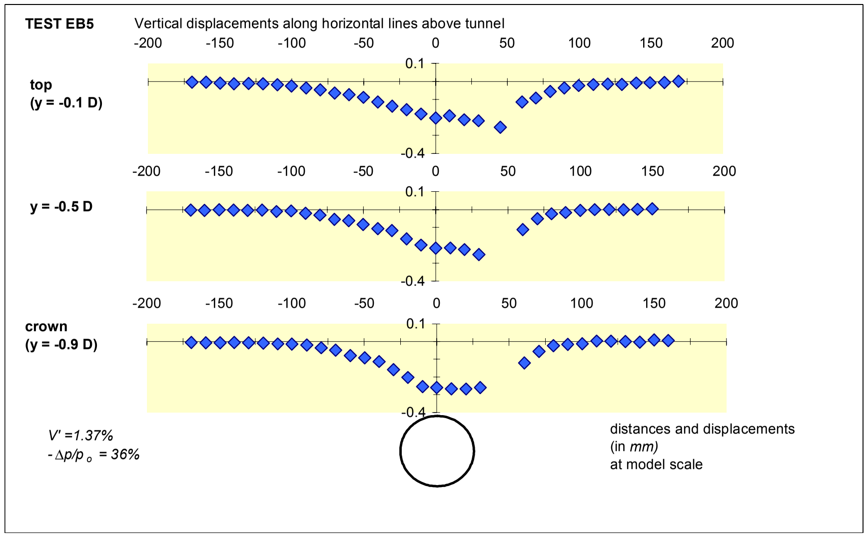

d)

Figure III.A8

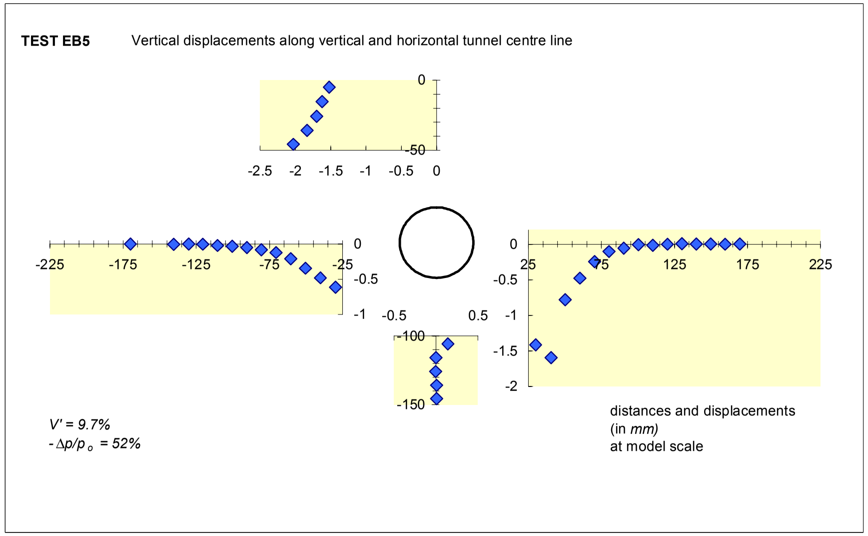

a)

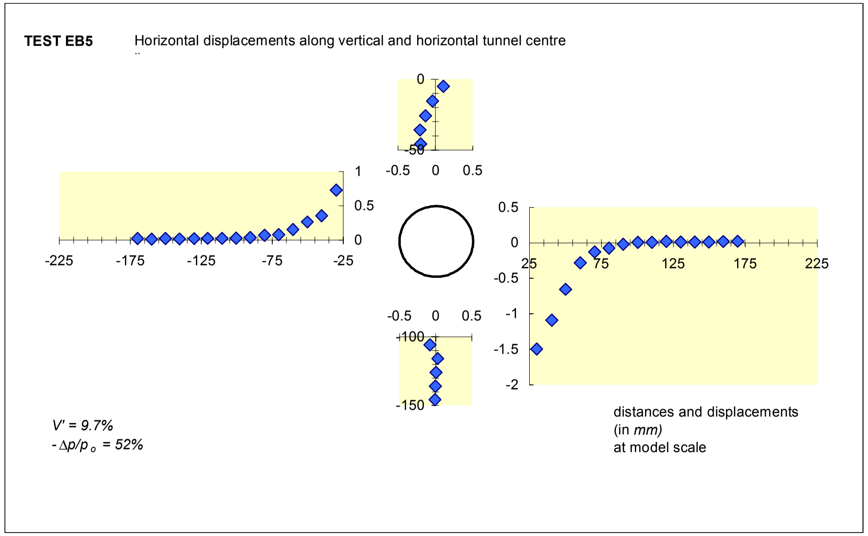

b)

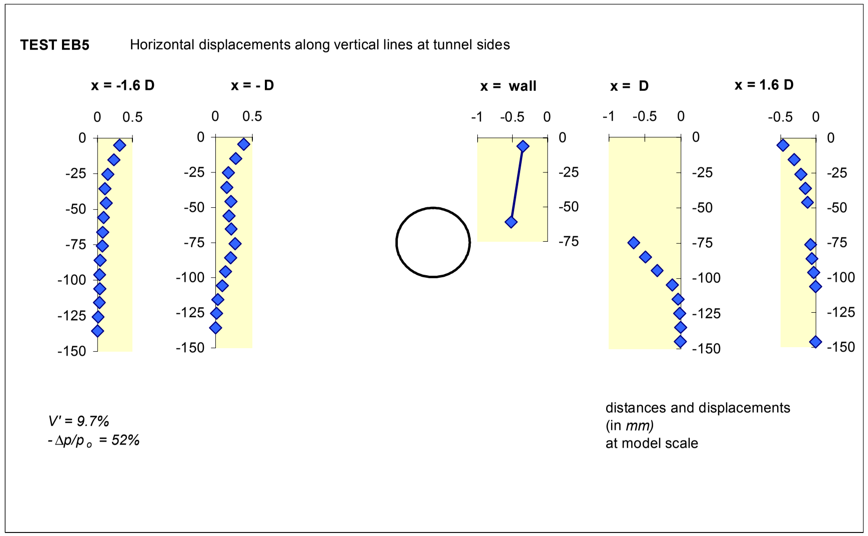

c)

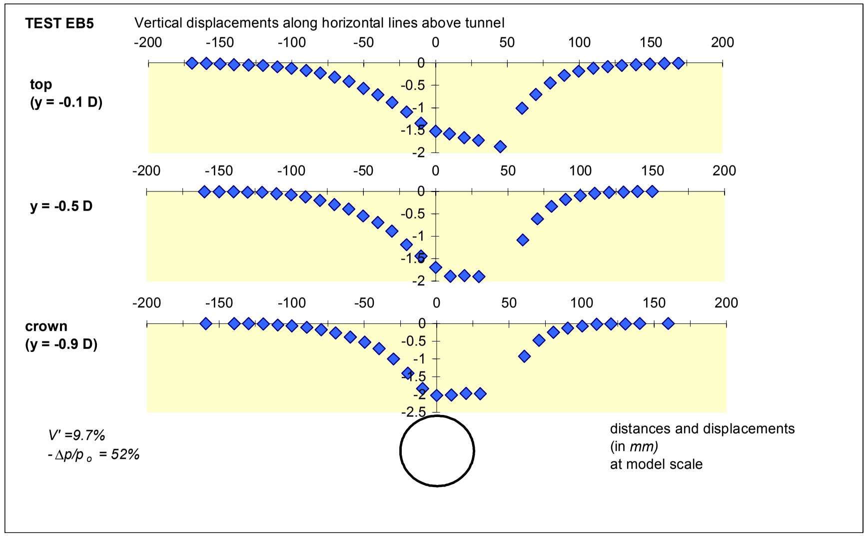

d)

Figure III.A9

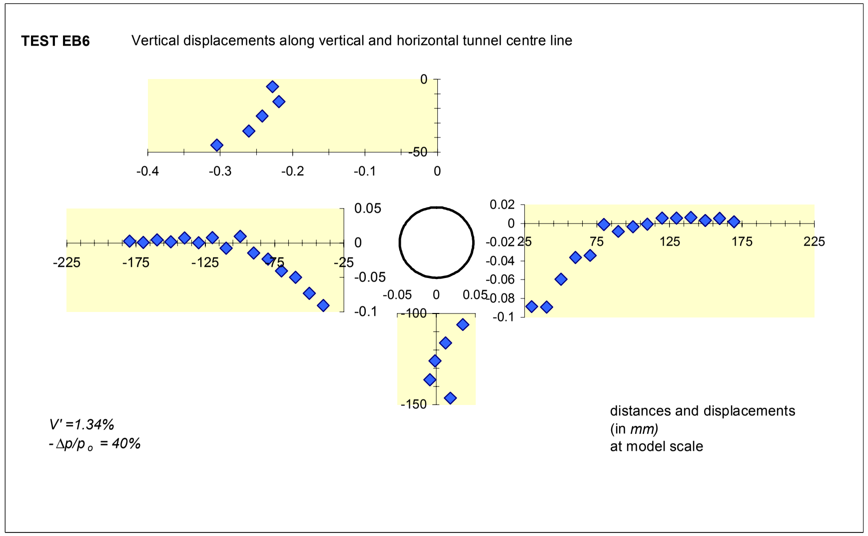

a)

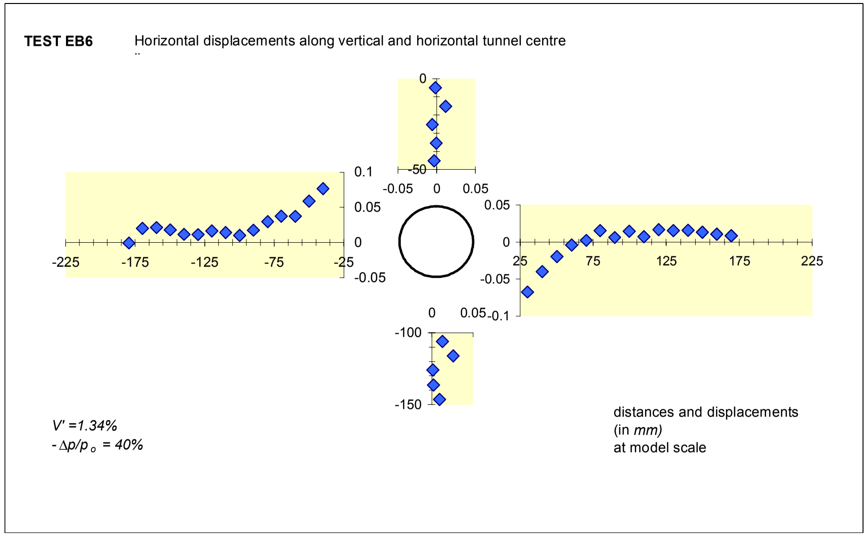

b)

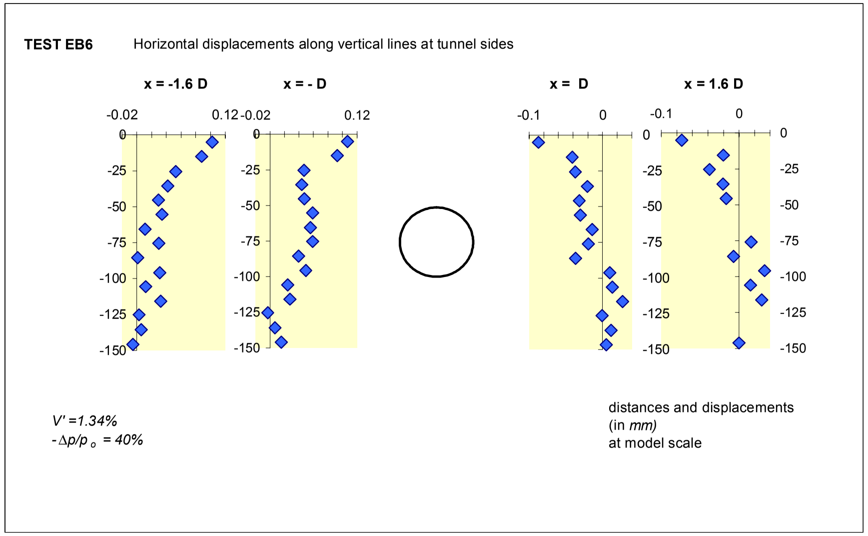

c)

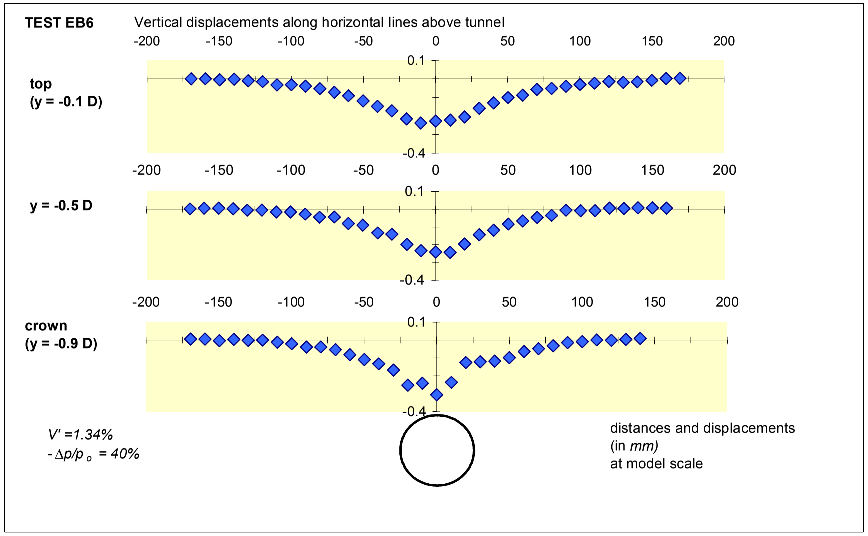

d)

Figure III.A10

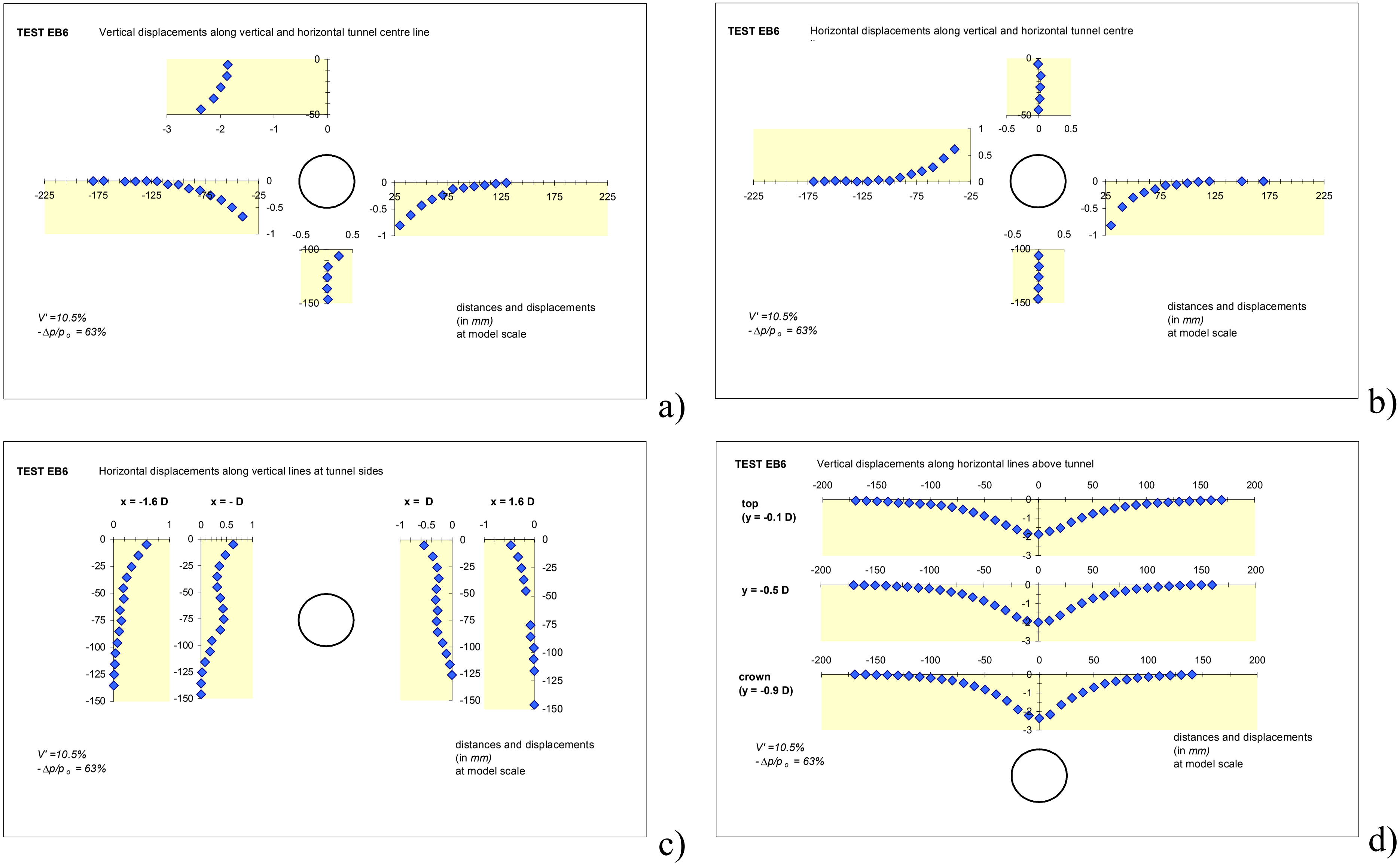

Figure III.A11

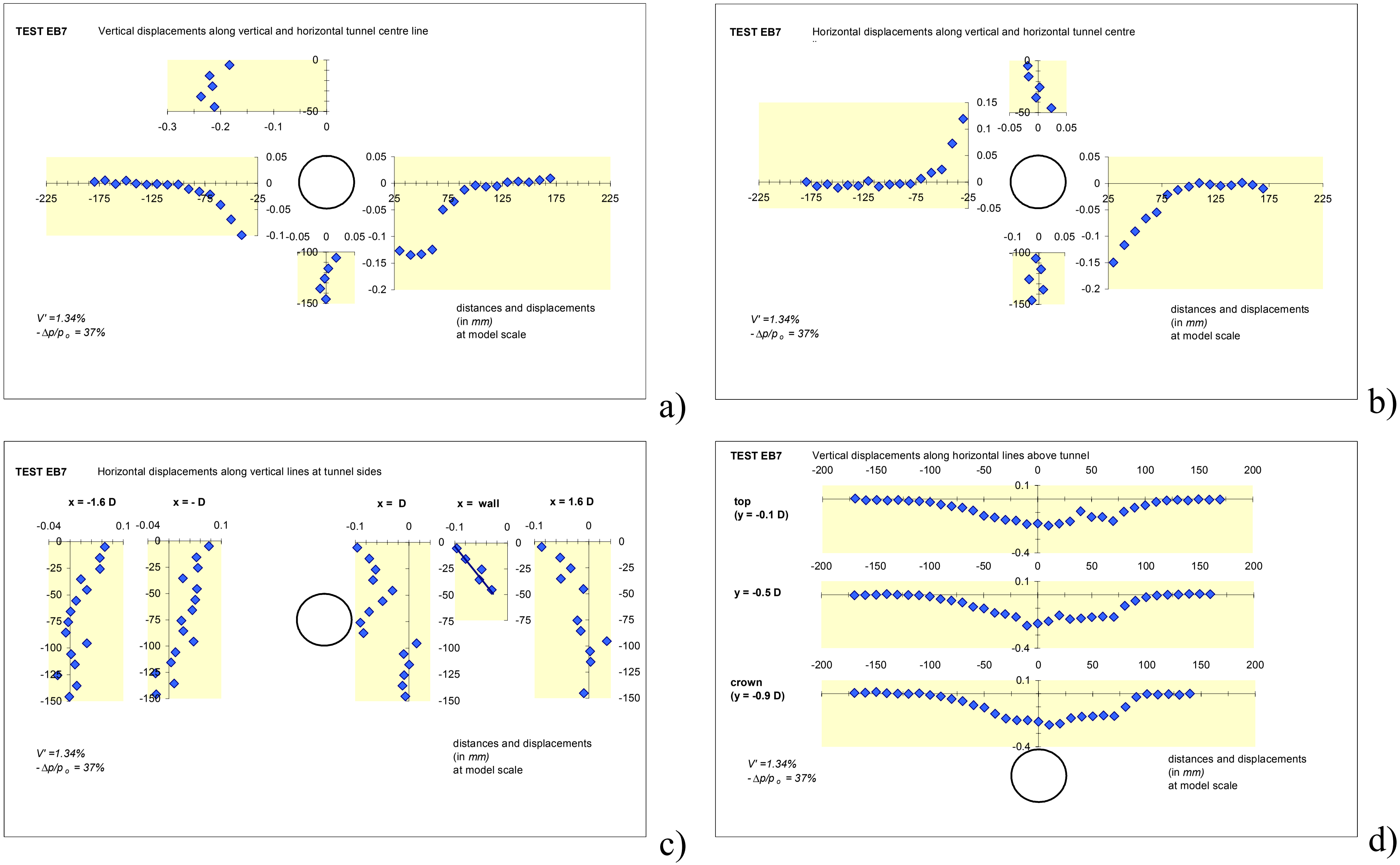

Figure III.A12

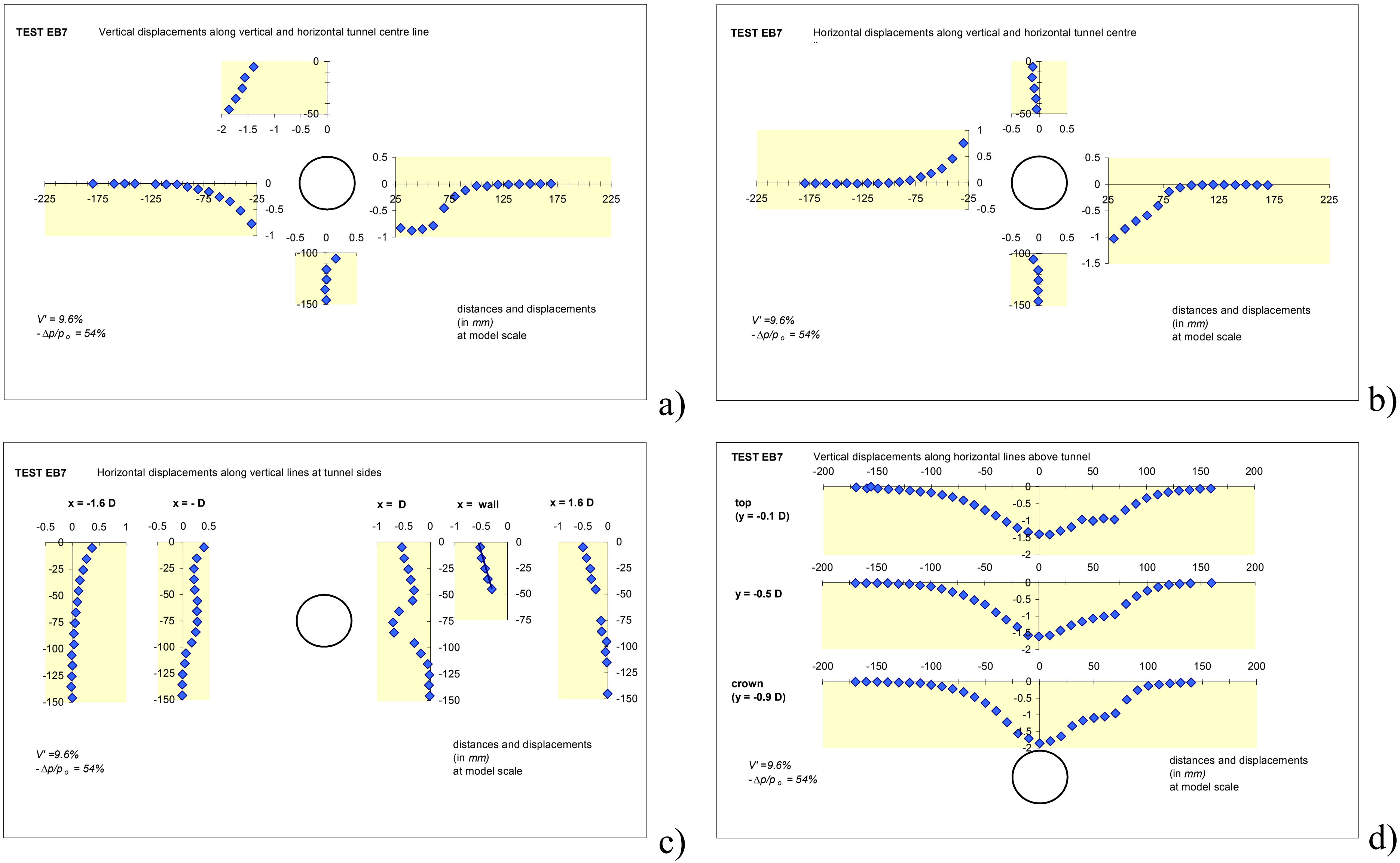

Figure III.A13

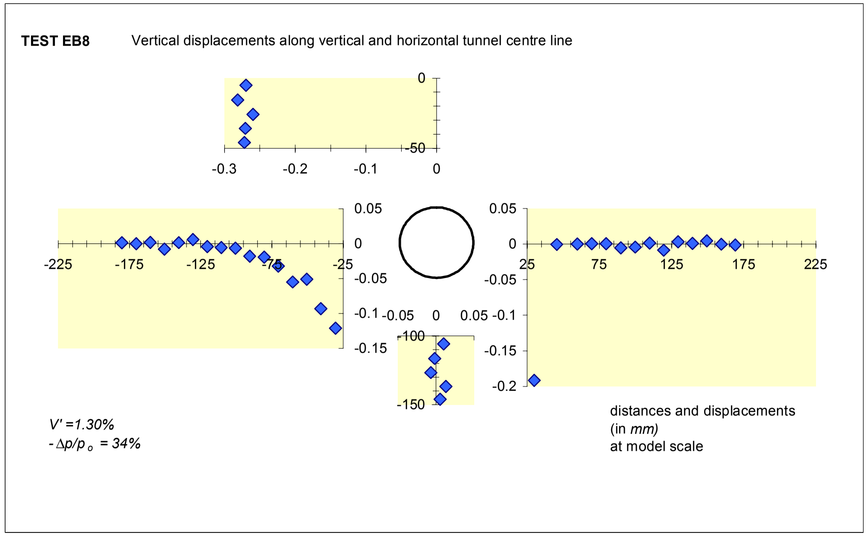

a)

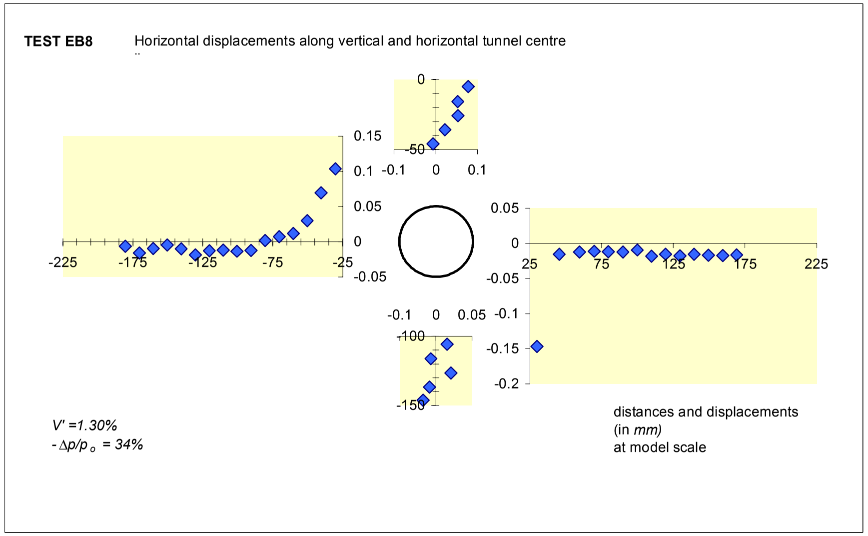

b)

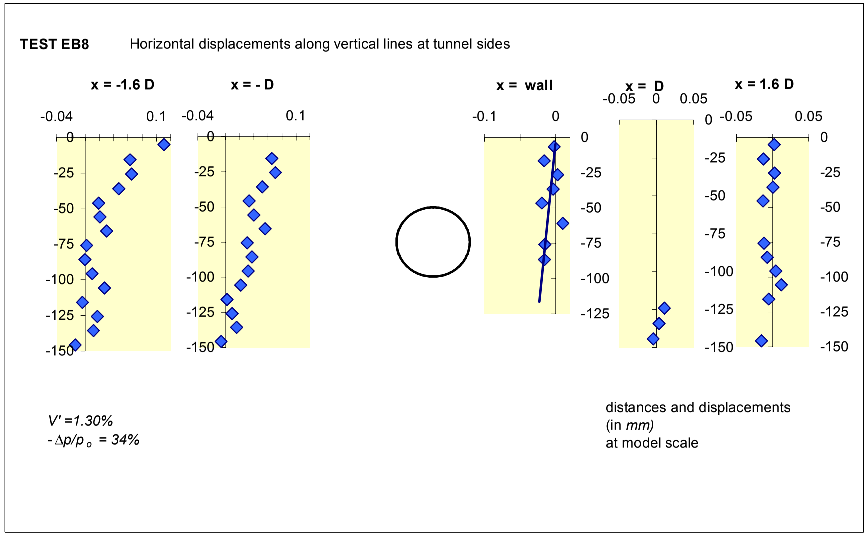

c)

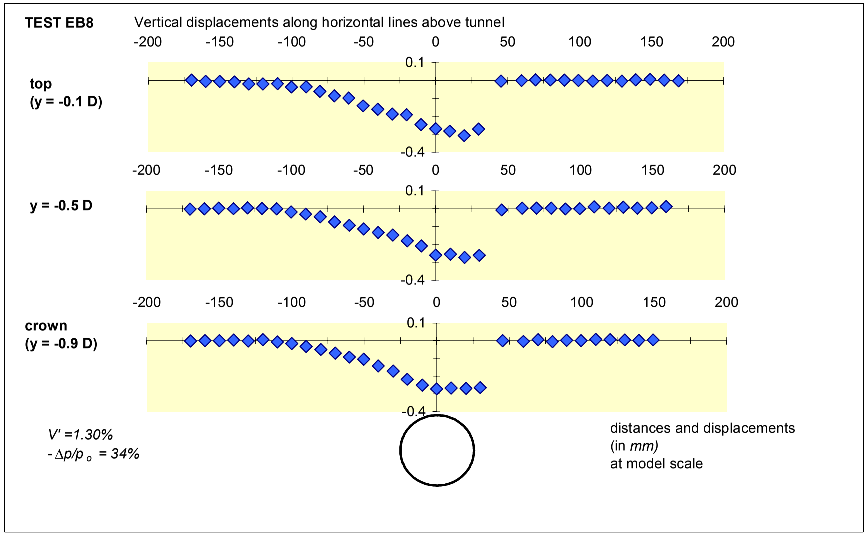

d)

Figure III.A14

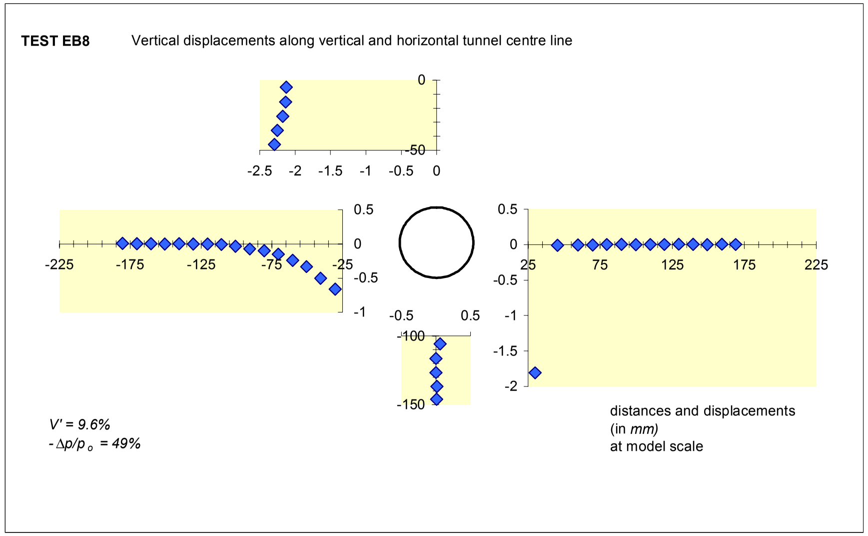

a)

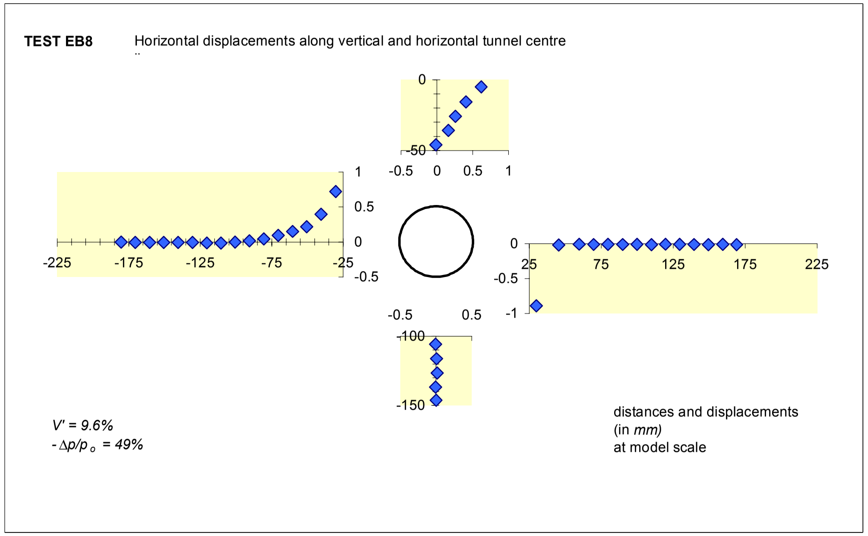

b)

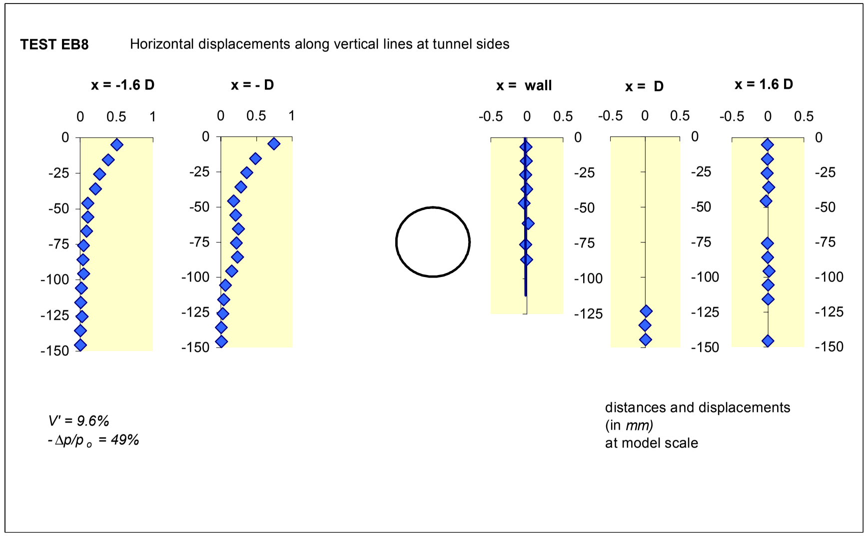

c)

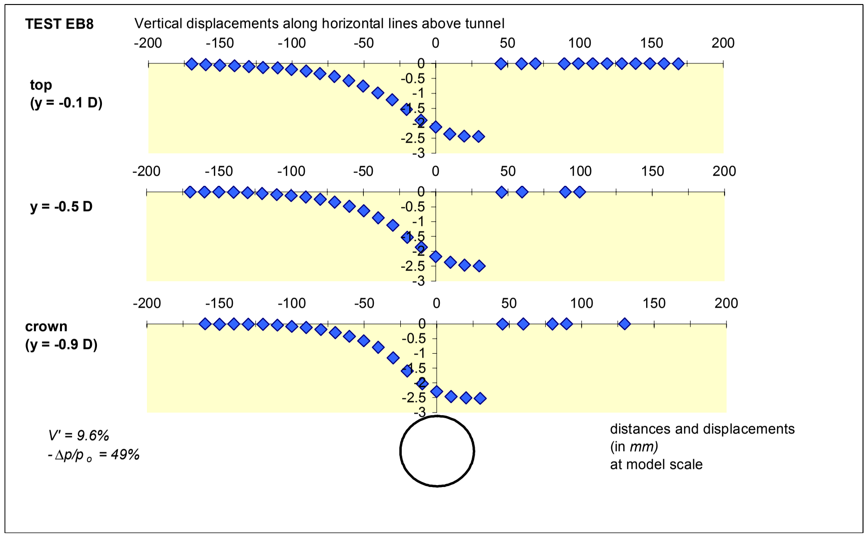

d)

Figure III.A15

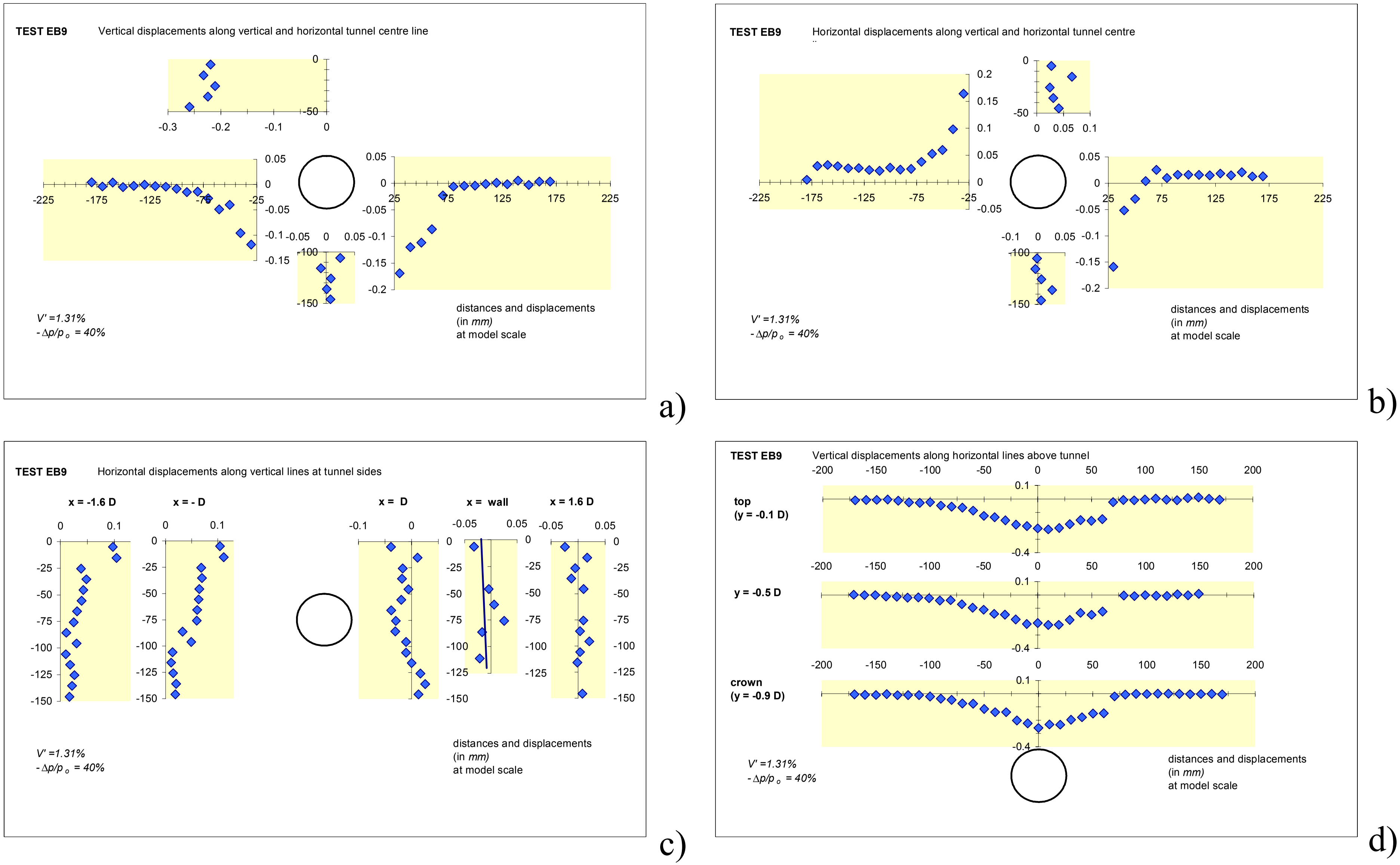

Figure III.A16

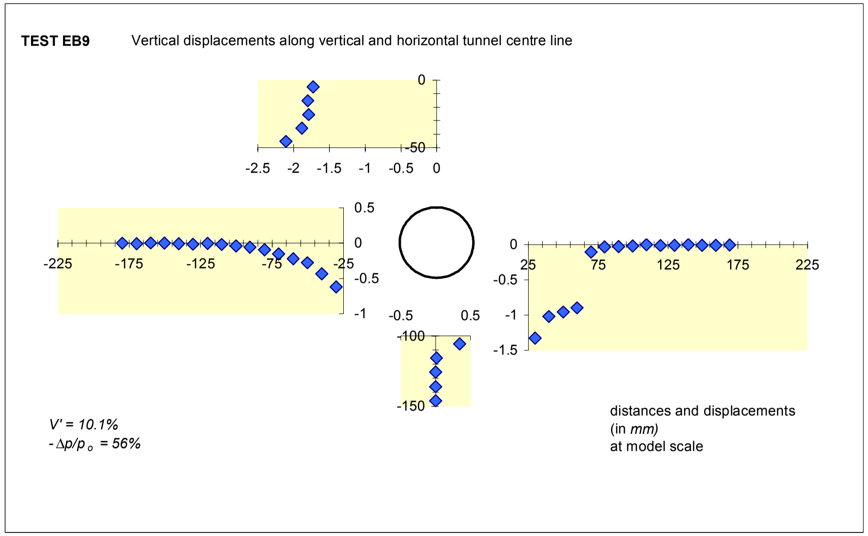

a)

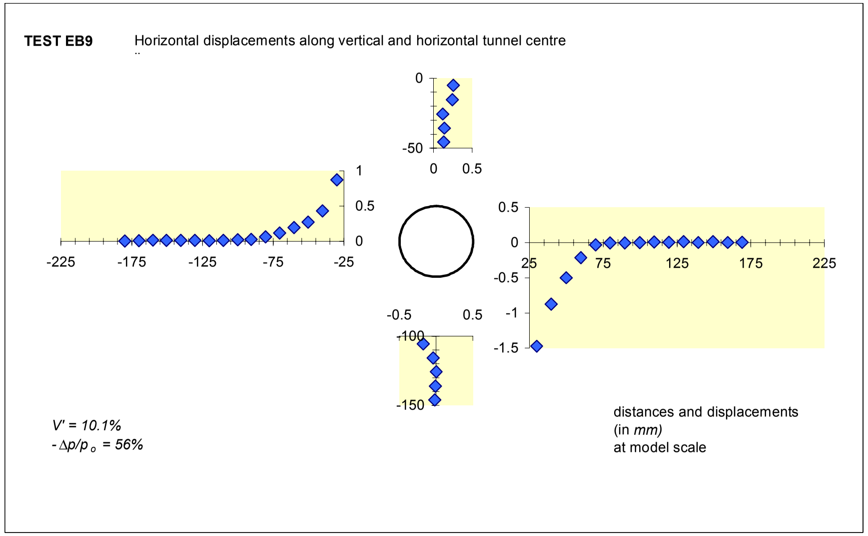

b)

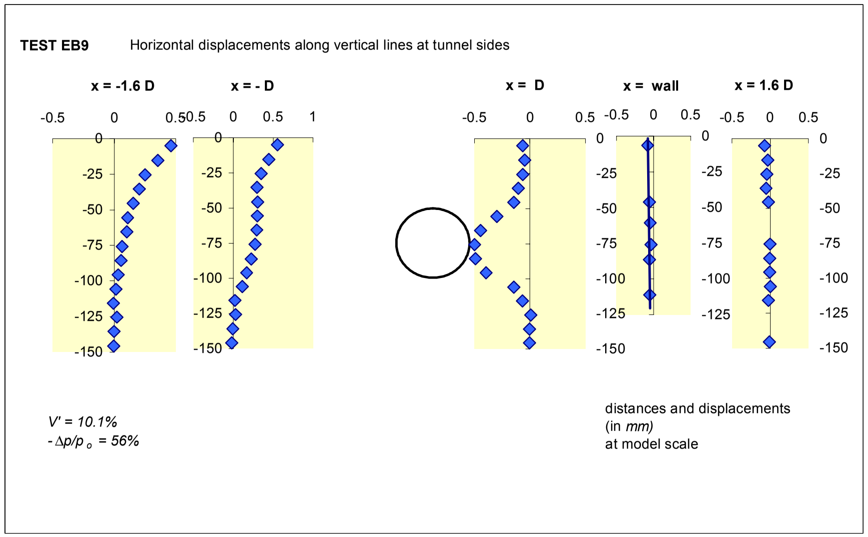

c)

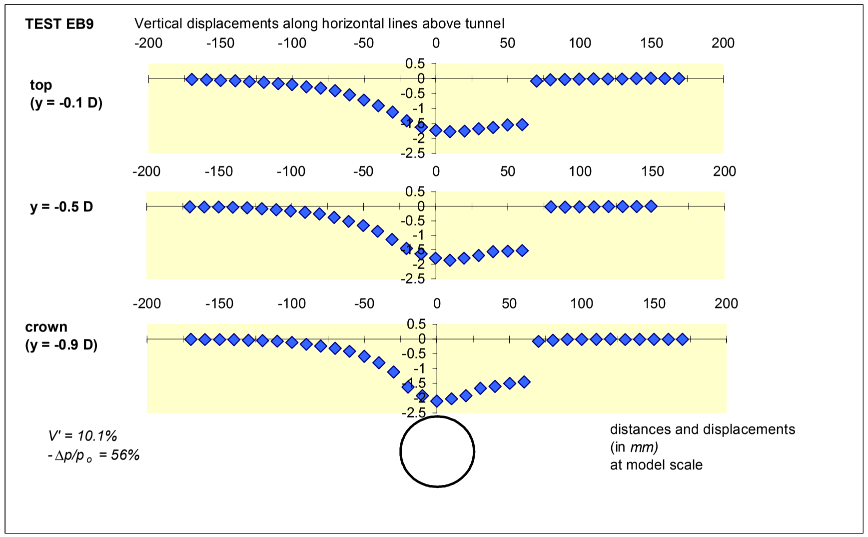

d)

Figure III.A17

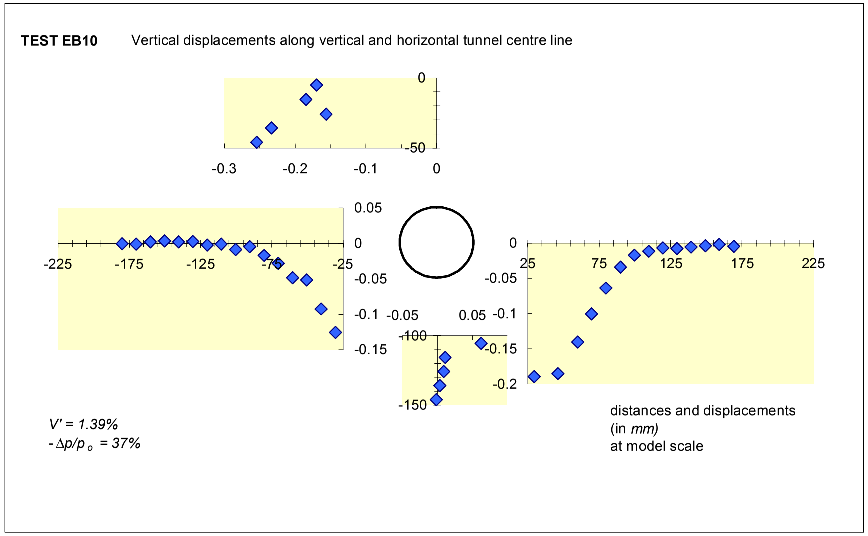

a)

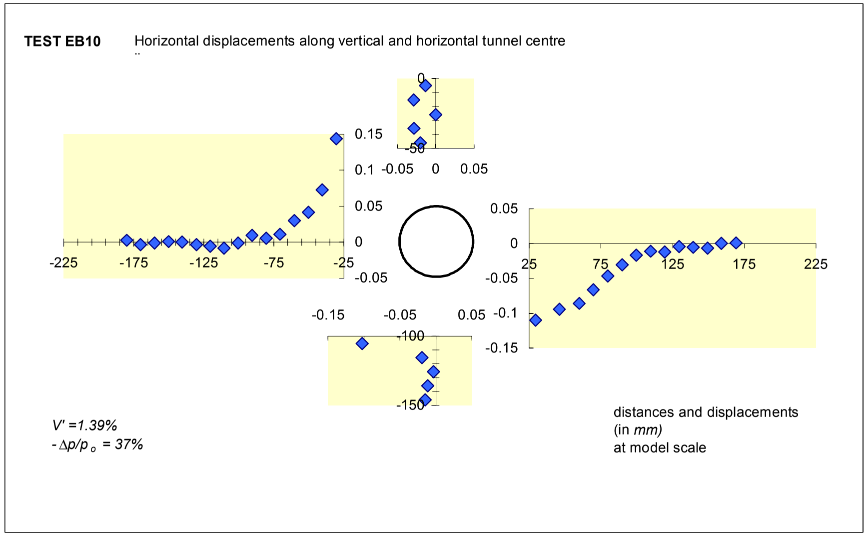

b)

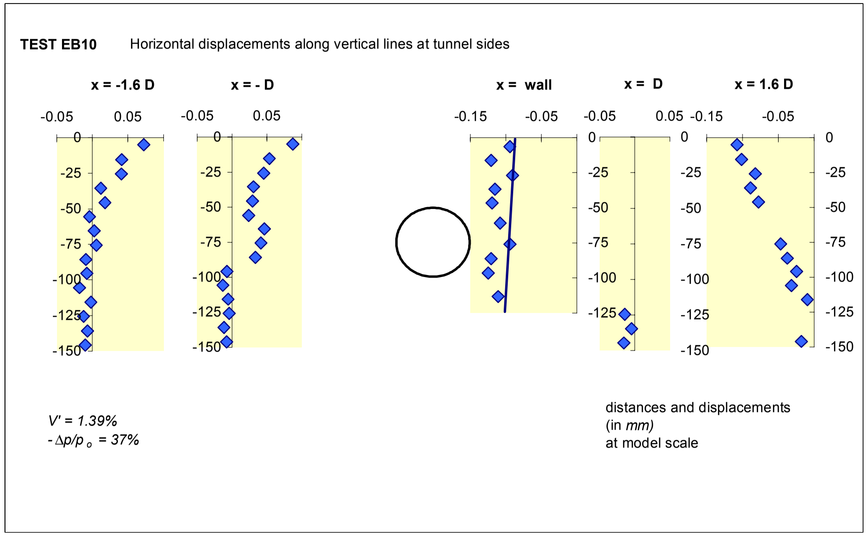

c)

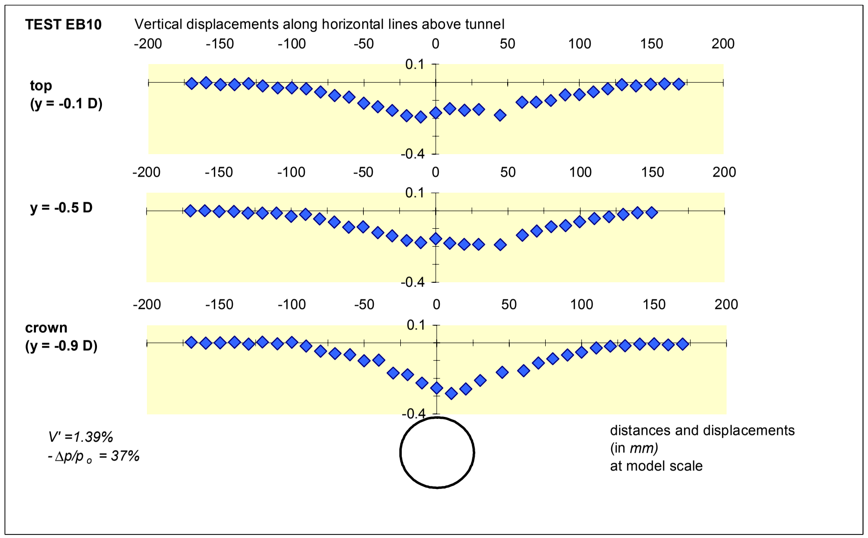

d)

Figure III.A18

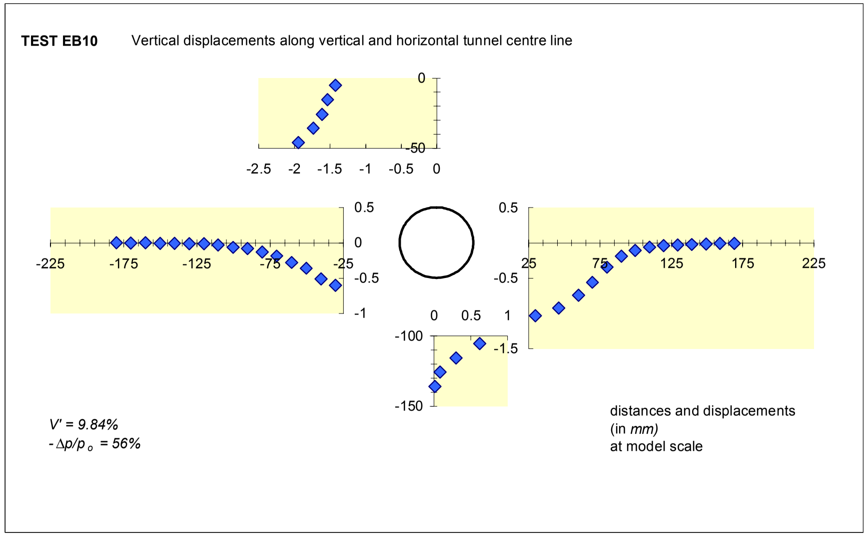

a)

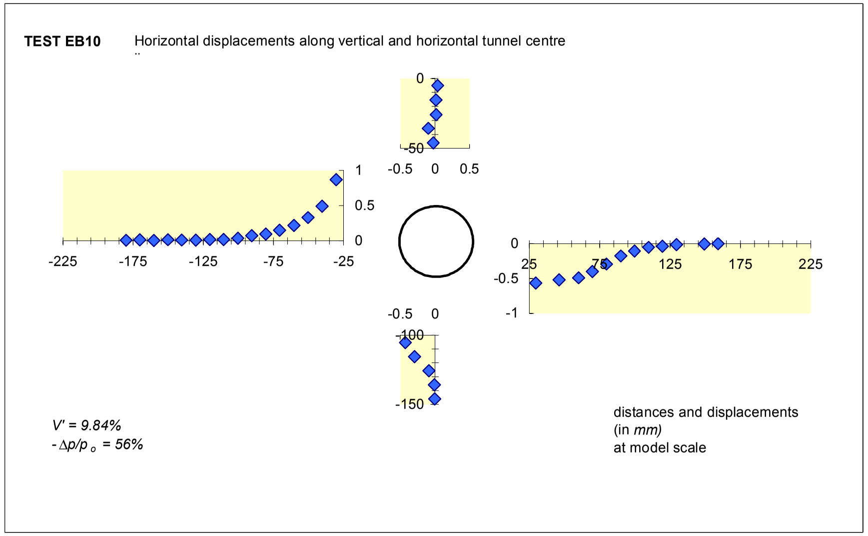

b)

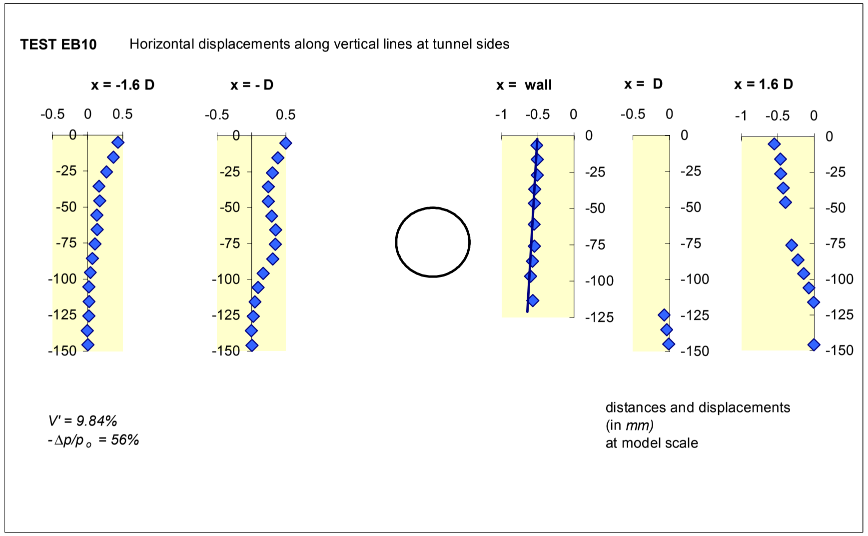

c)

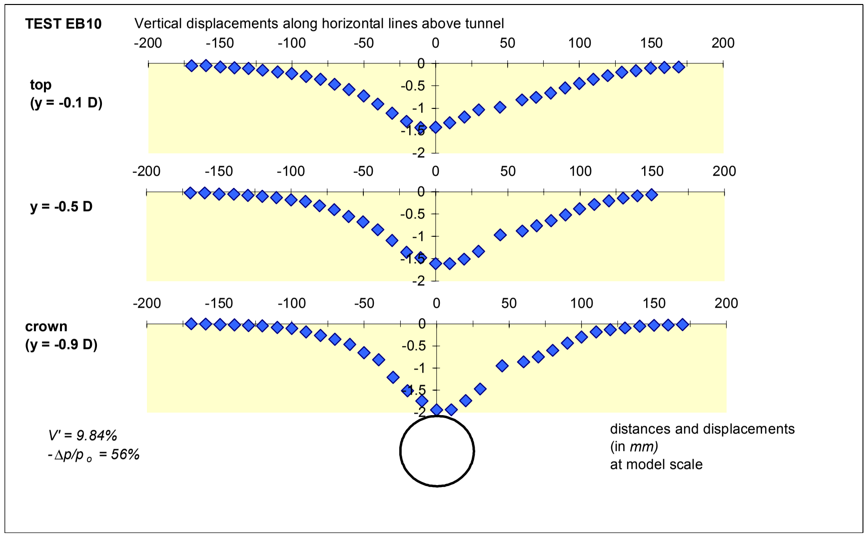

d)

Figure III.A19

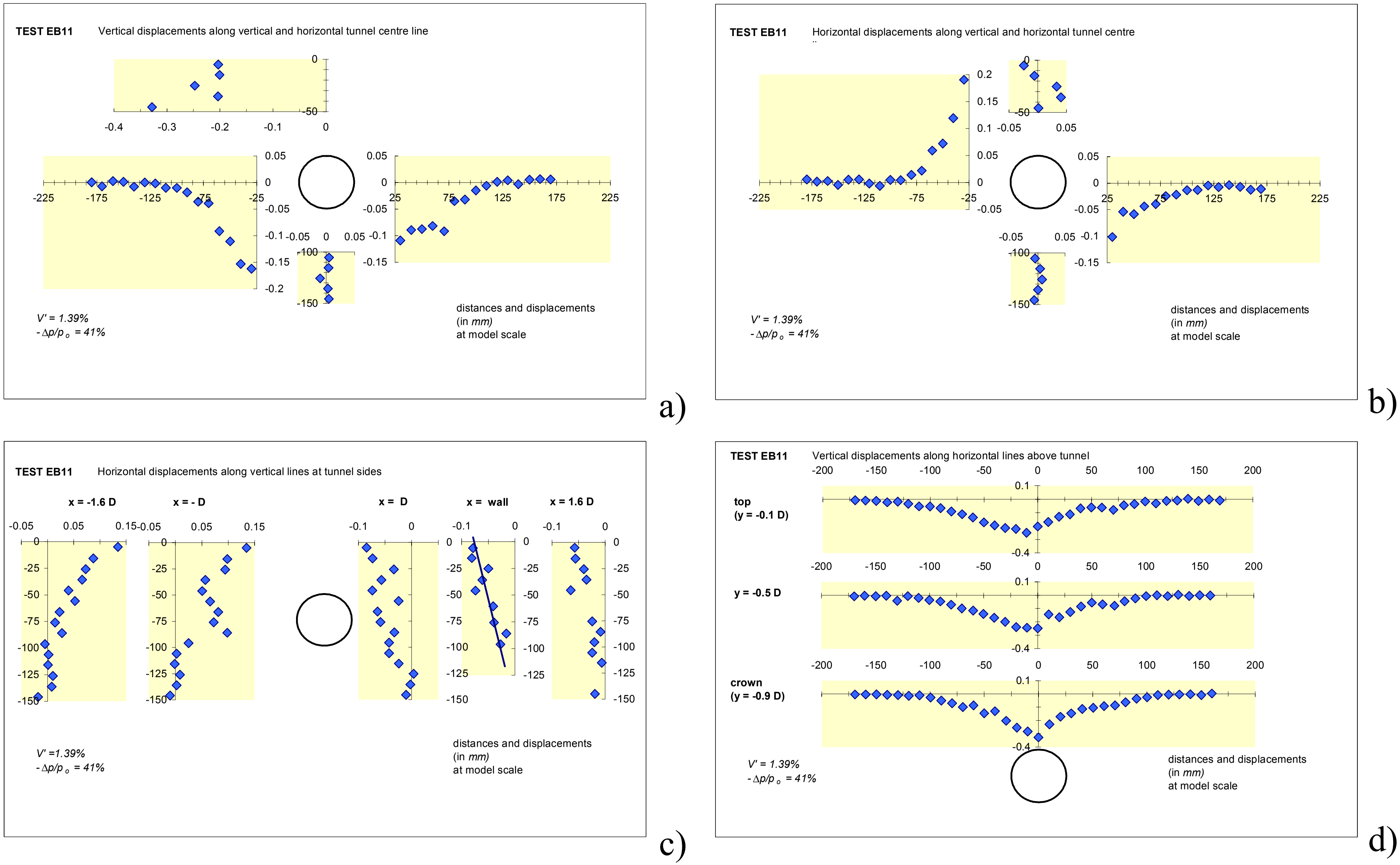

Figure III.A20

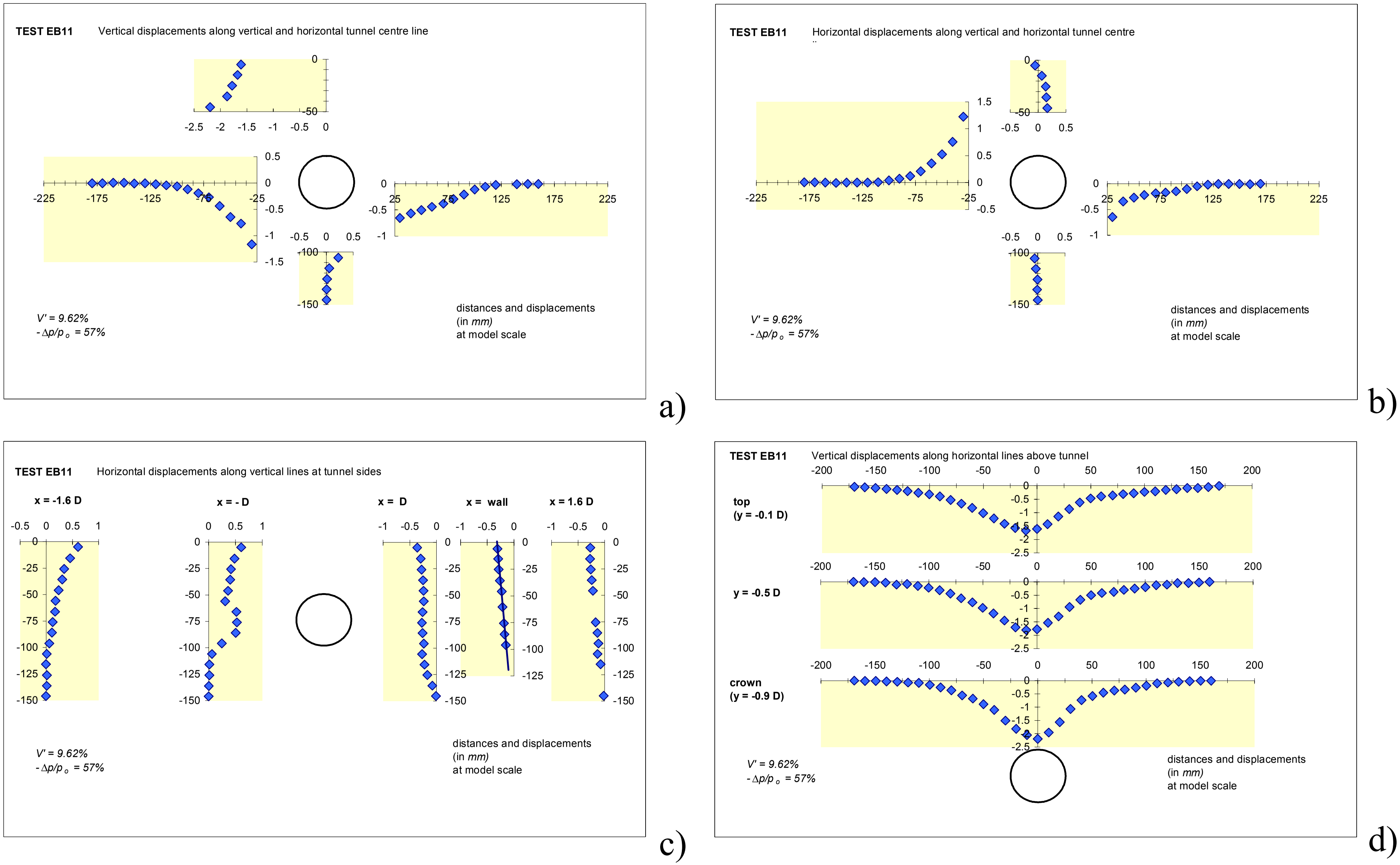

Figure III.A21

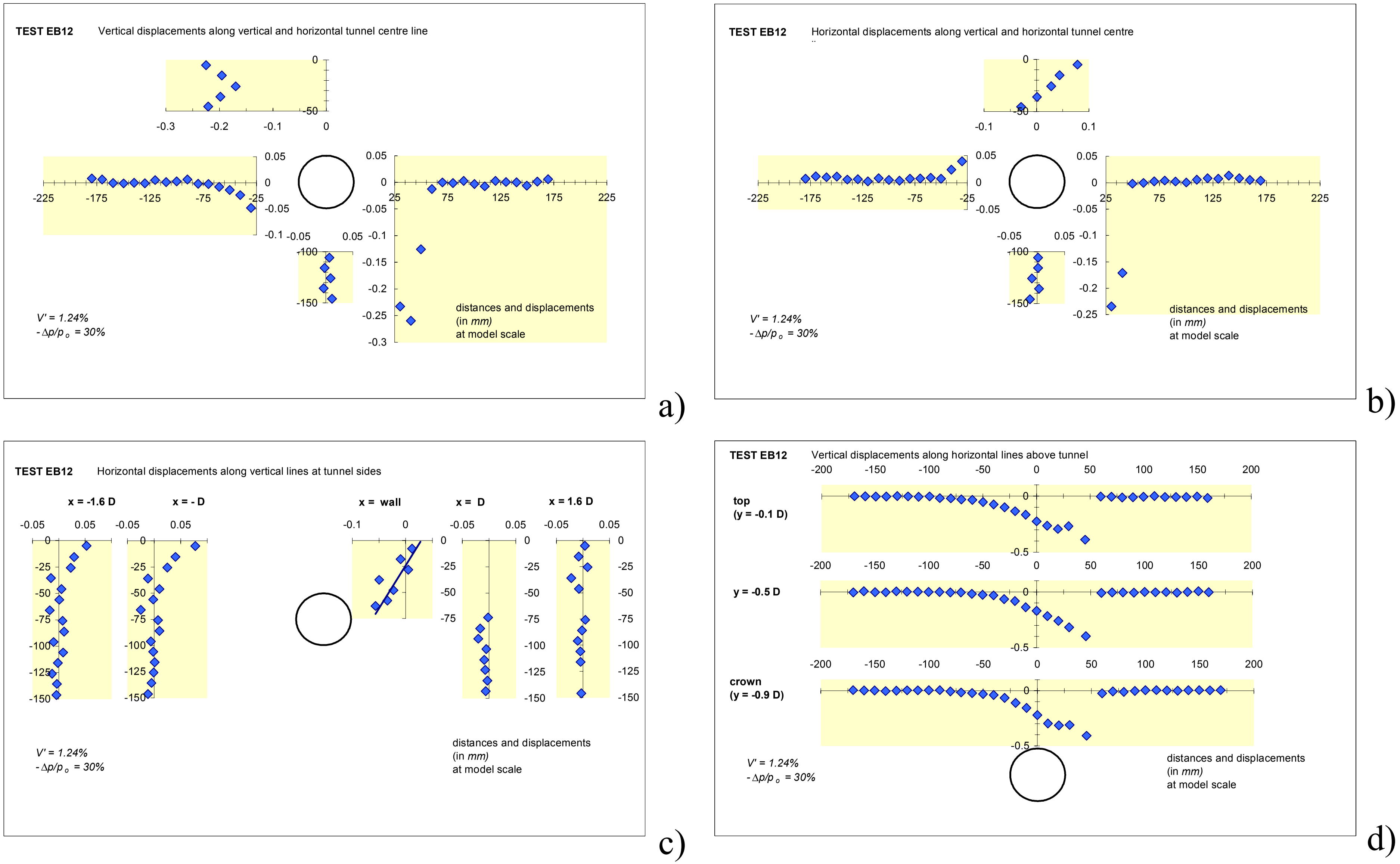

Figure III.A22

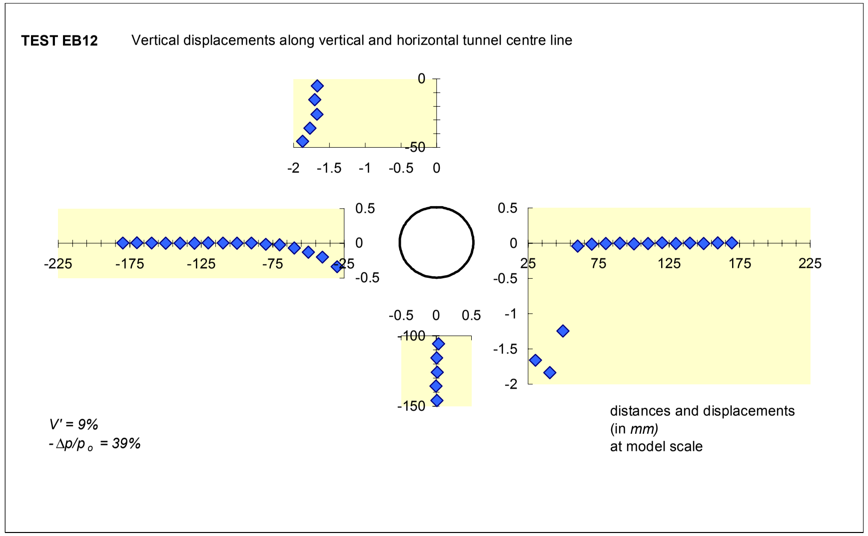

a)

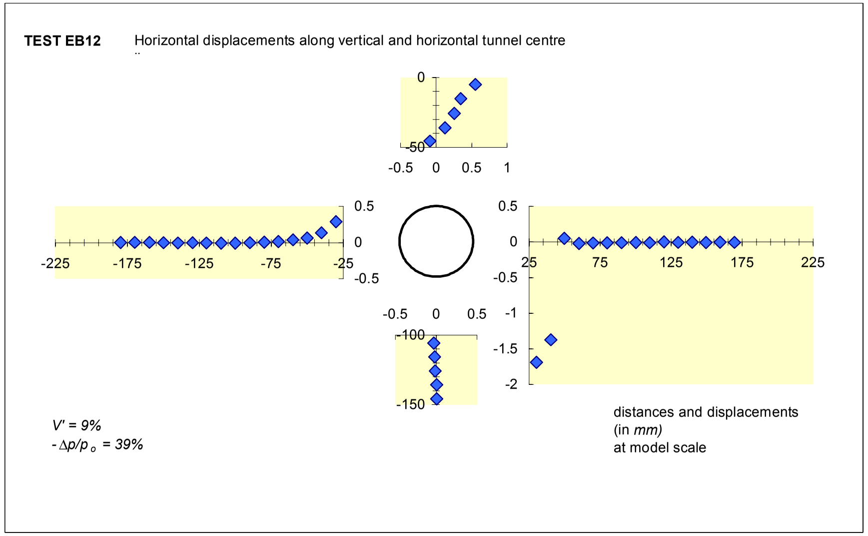

b)

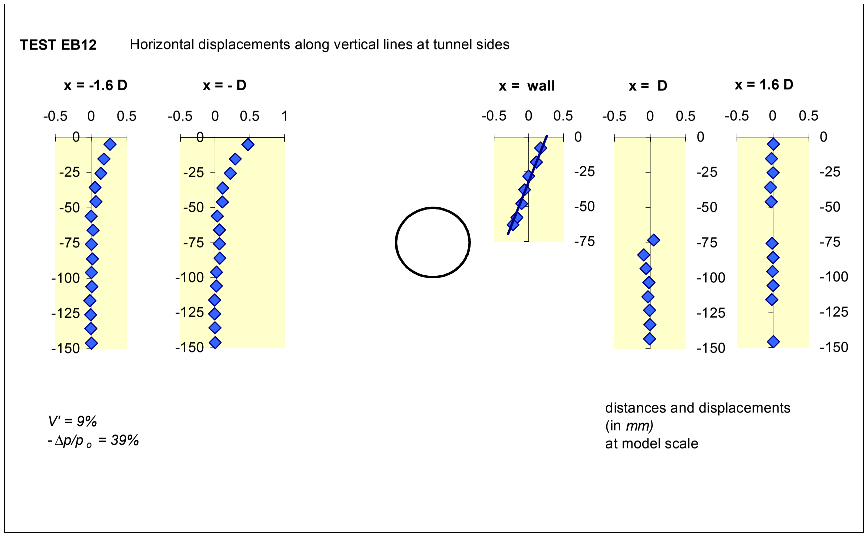

c)

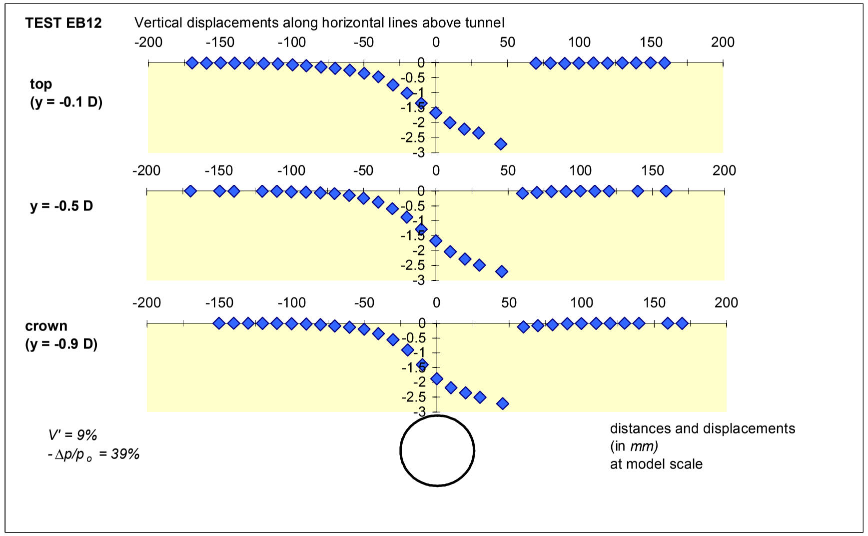

d)

Figure III.A23

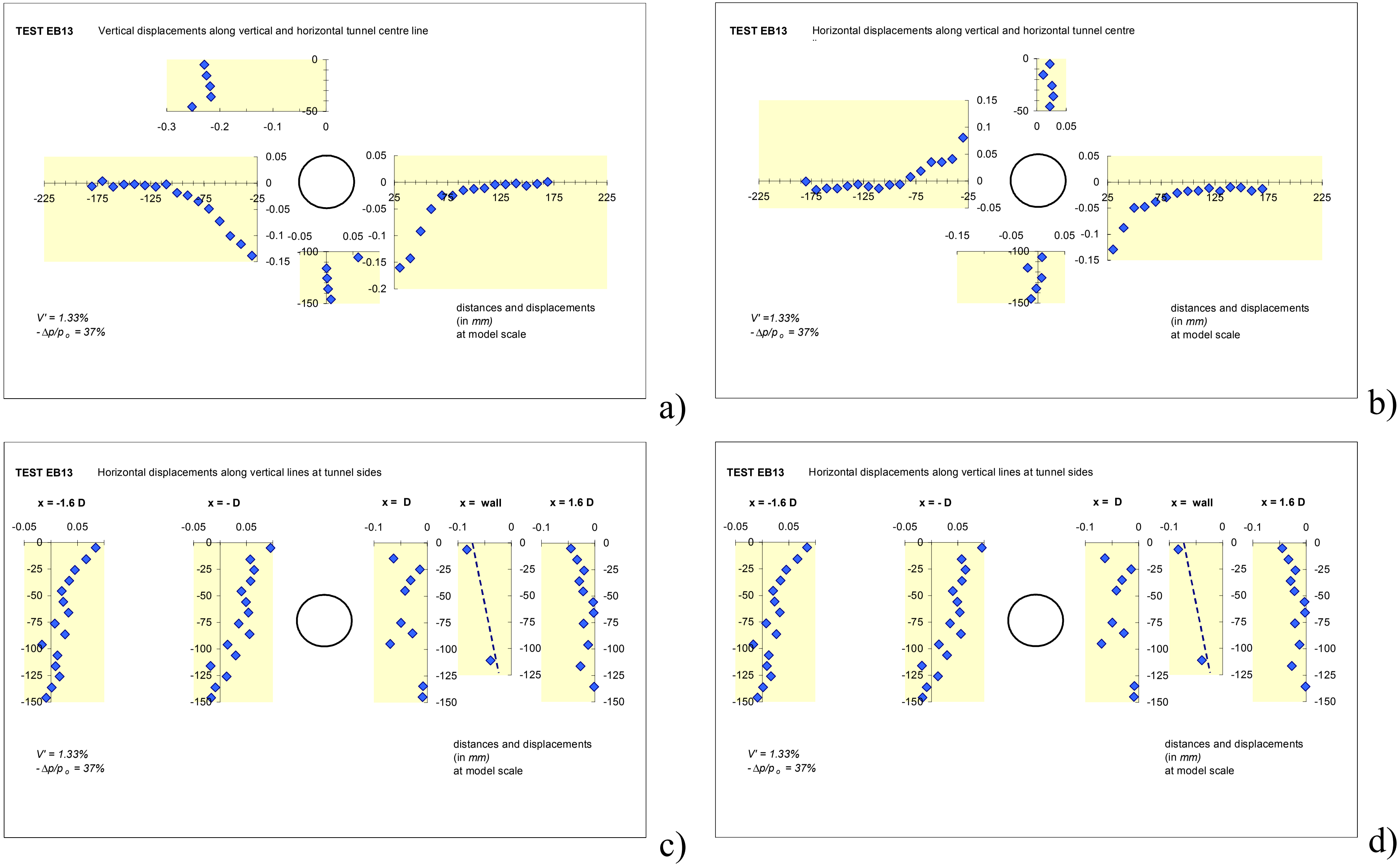

Figure III.A24

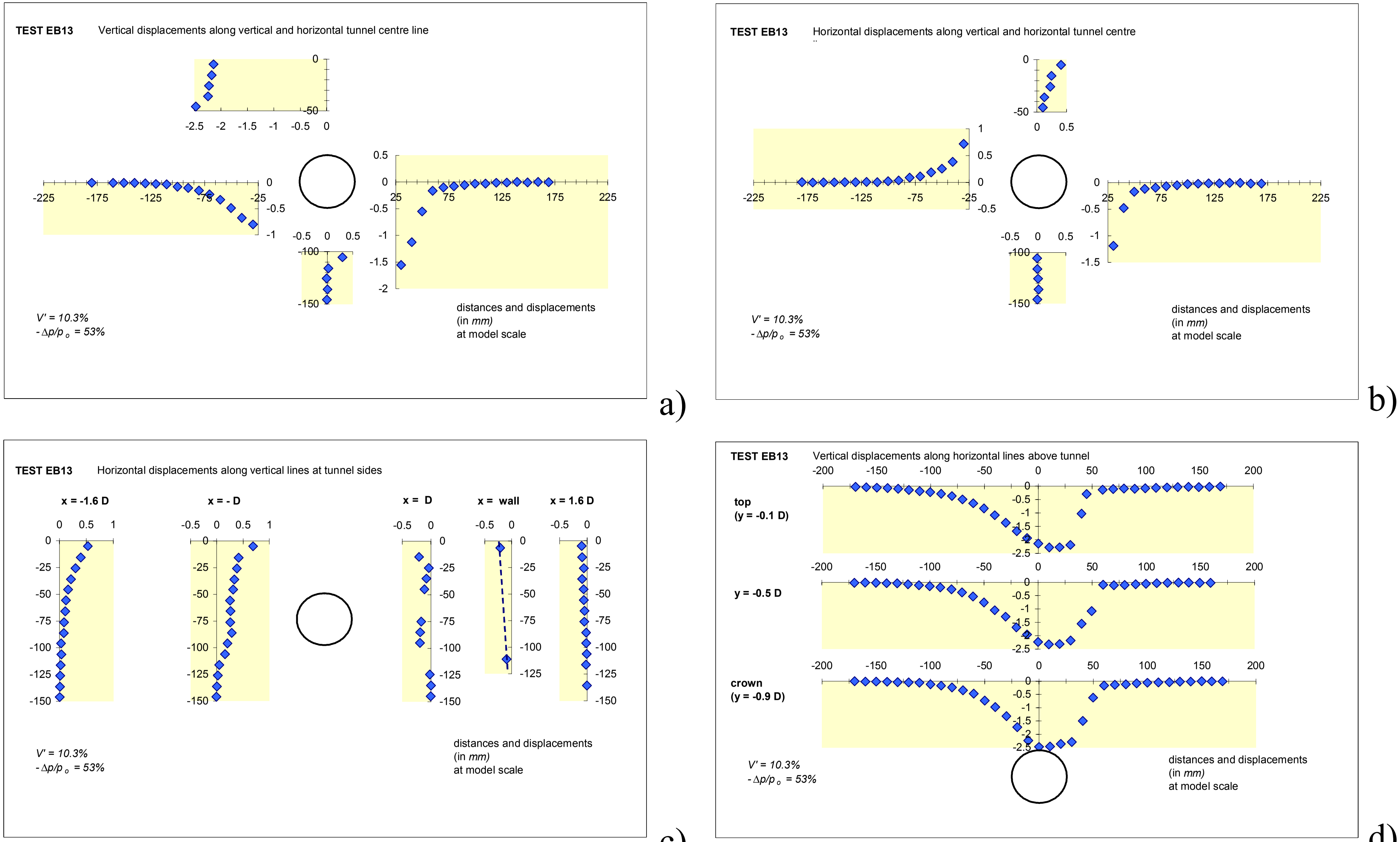

Figure III.A25

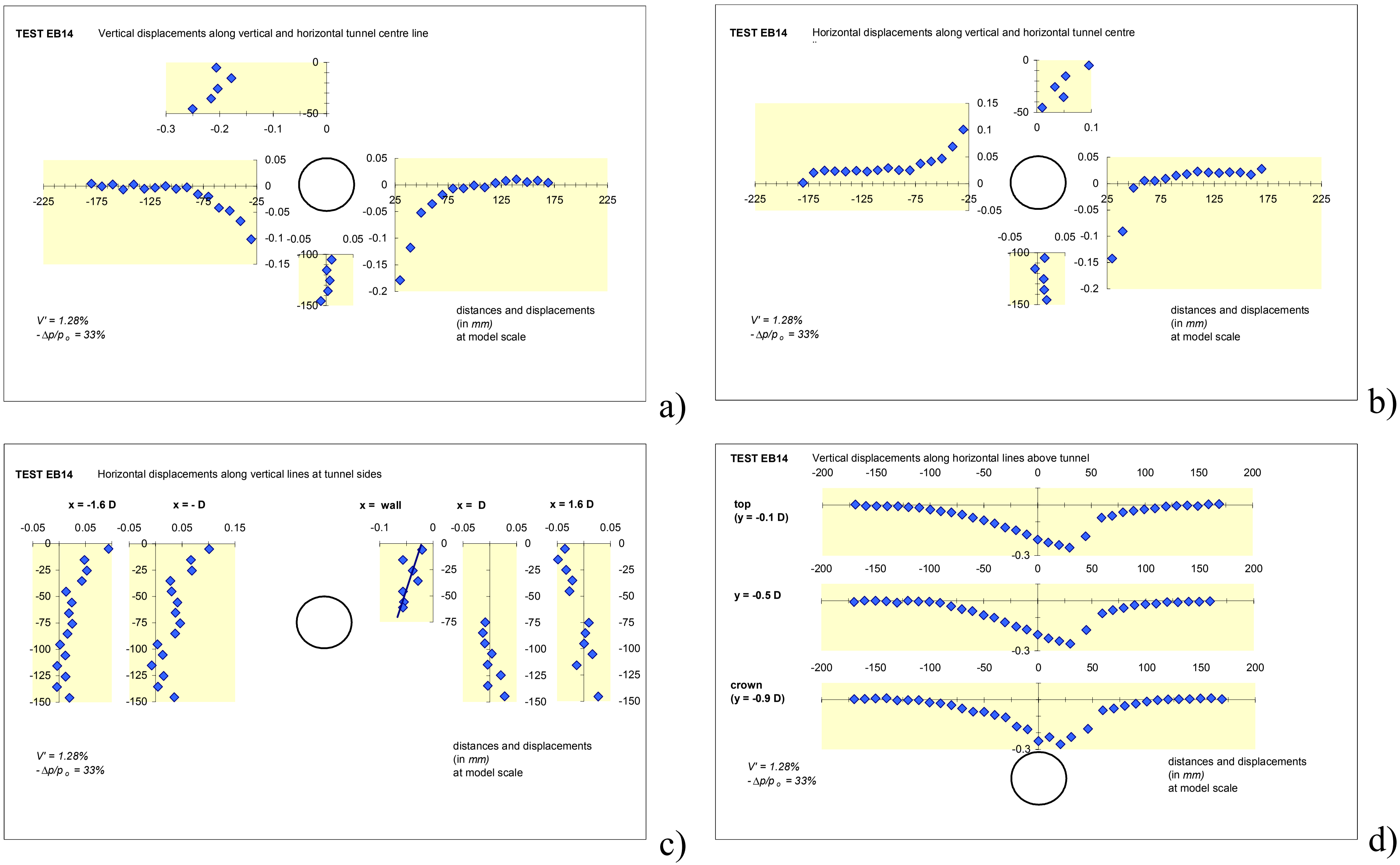

Figure III.A26

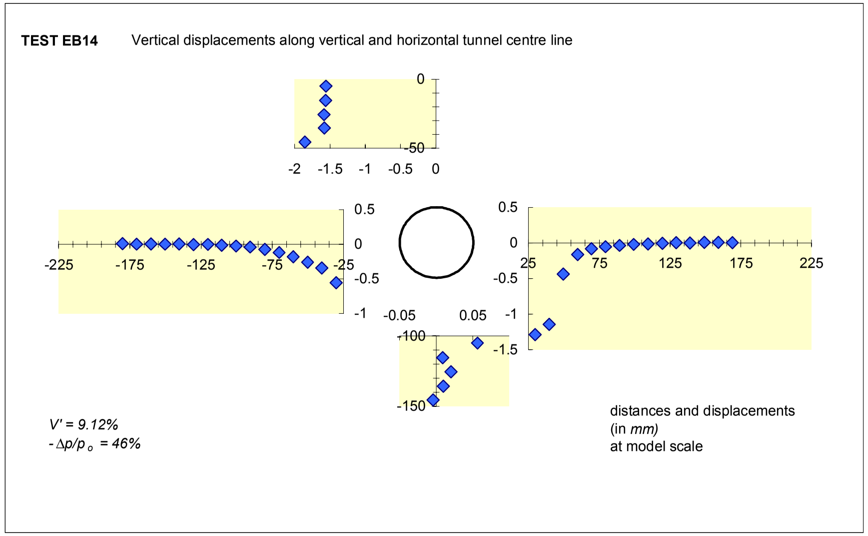

a)

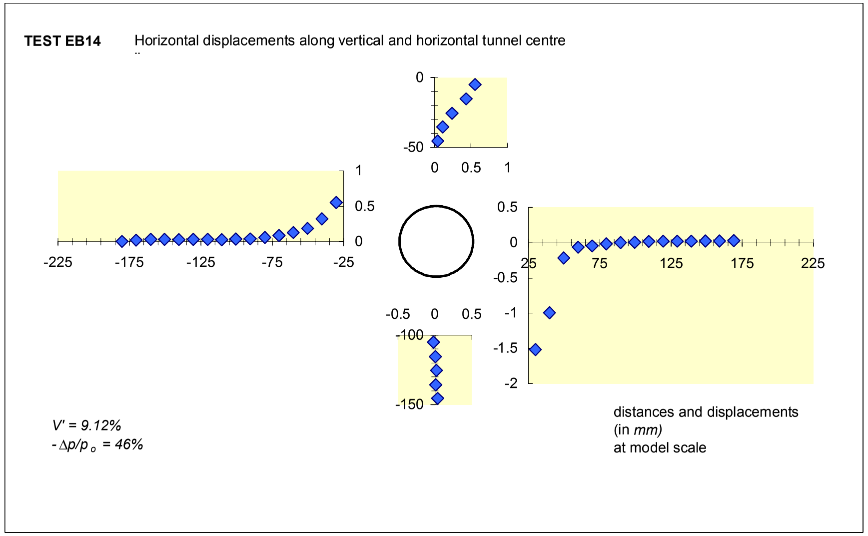

b)

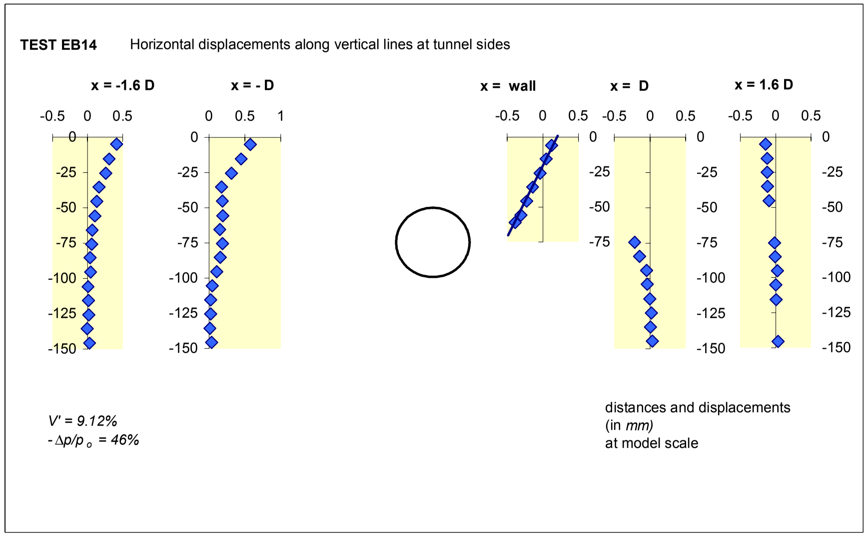

c)

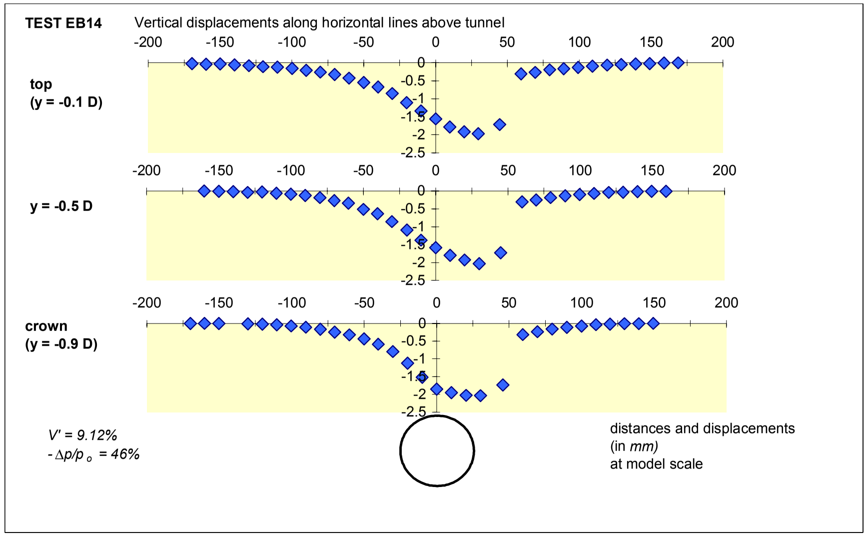

d)

Figure III.A27

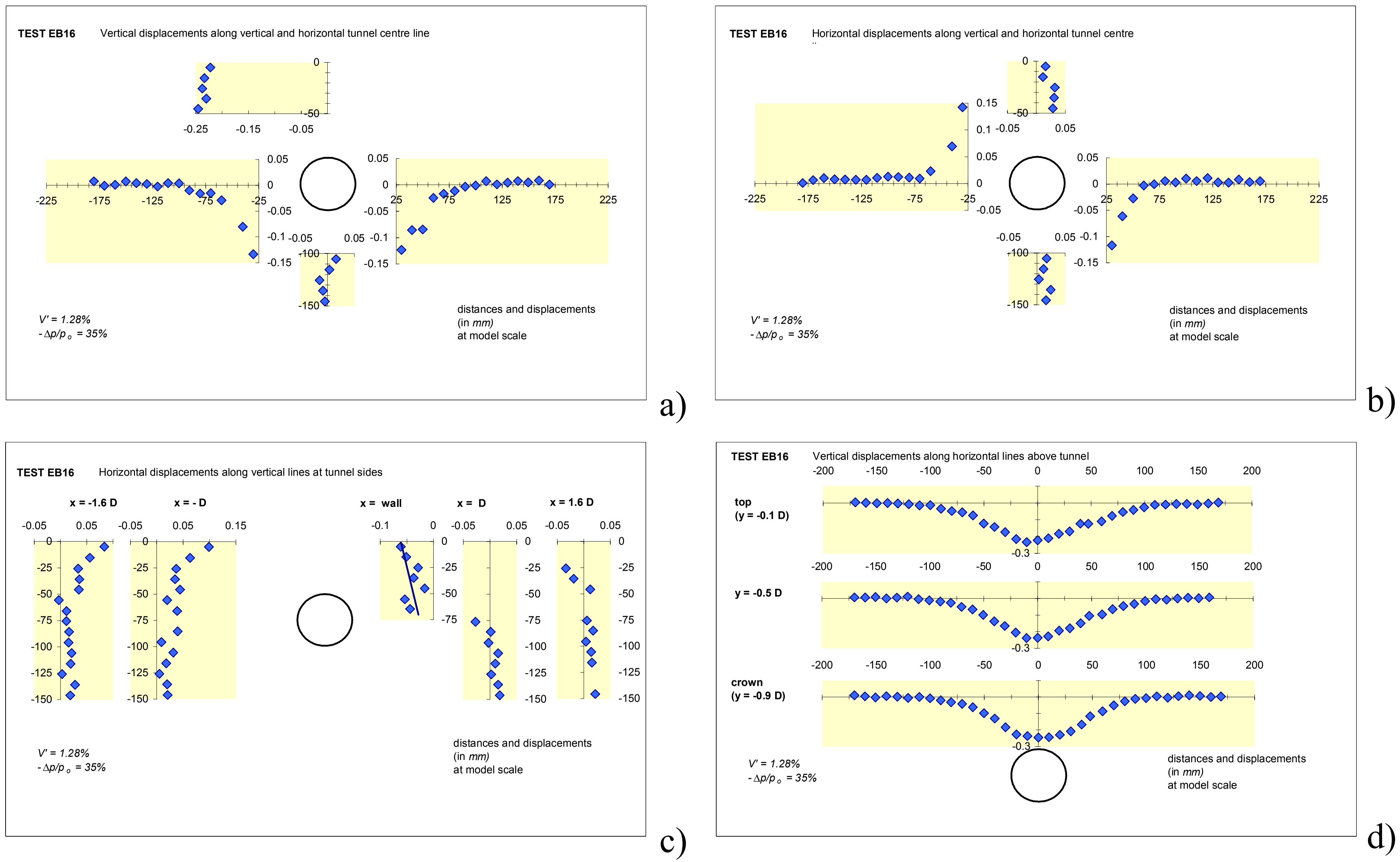

Figure III.A28

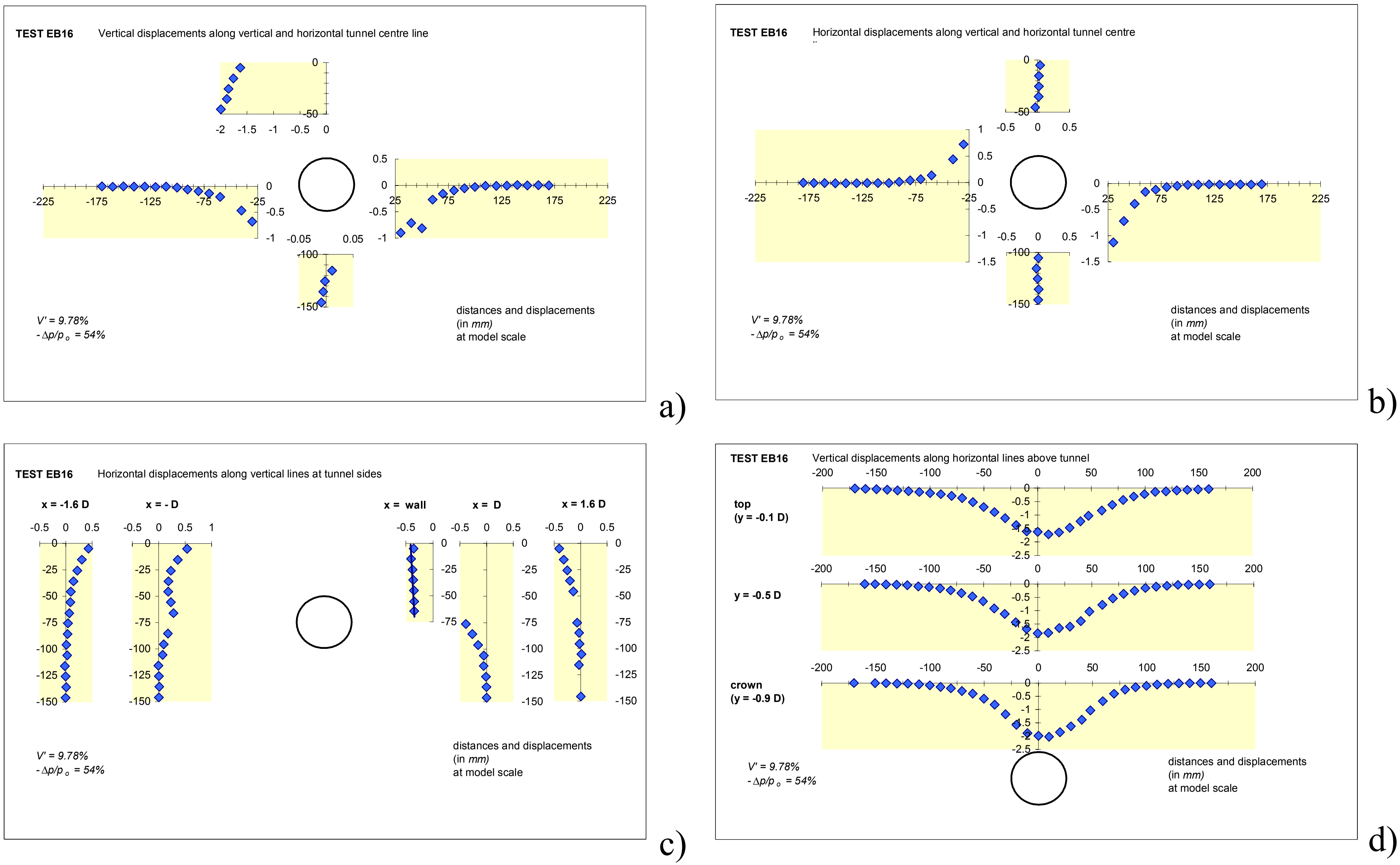

APPENDIX B

Displacement fields in the tests at a supporting pressure reduced of 40% of p_o

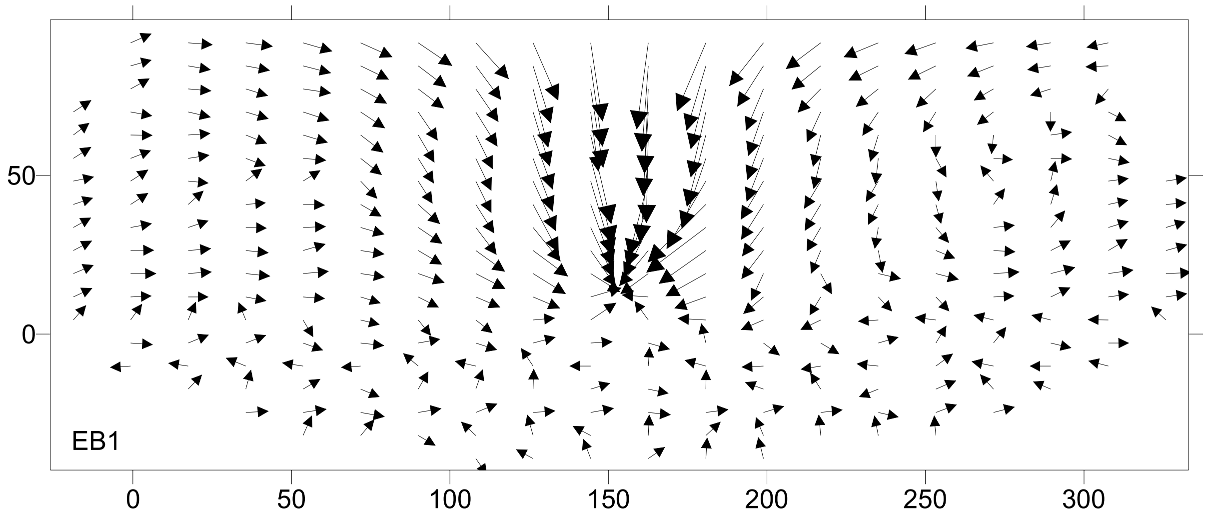
EB1
50
0
0
50
100
150
200
250
300

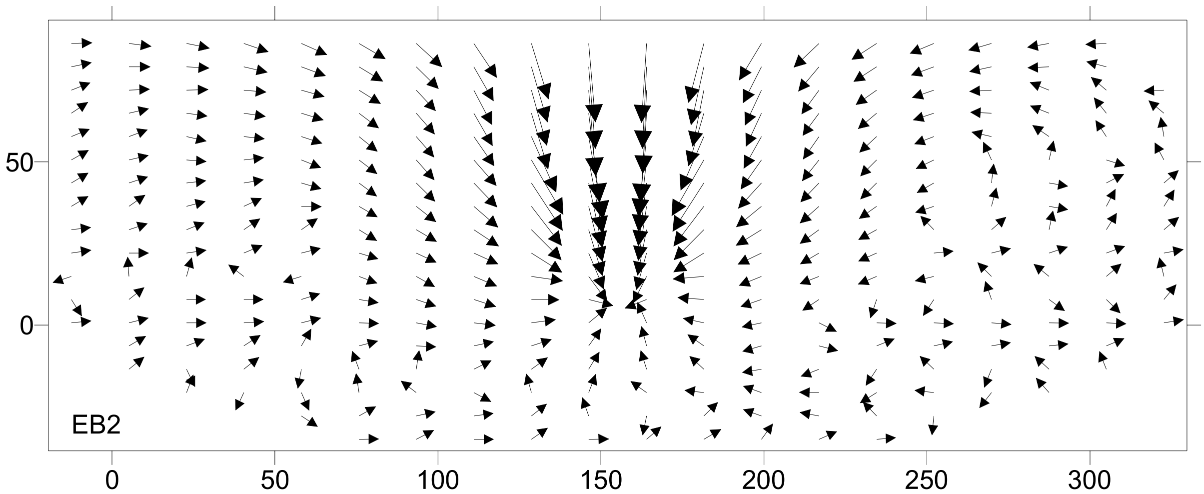
EB2
50
0
0
50
100
150
200
250
300

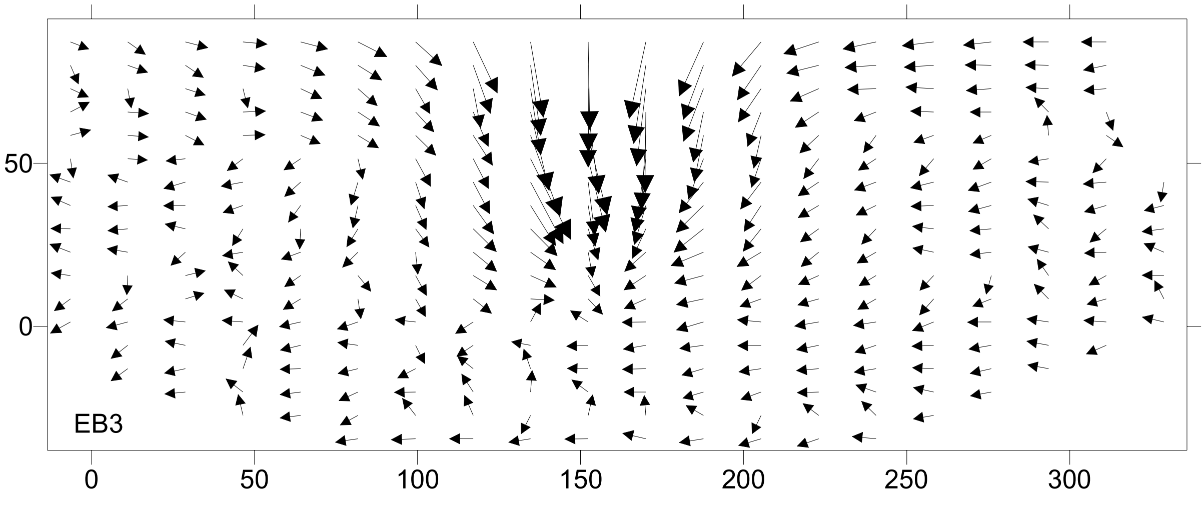
EB3
50
0
0
50
100
150
200
250
300

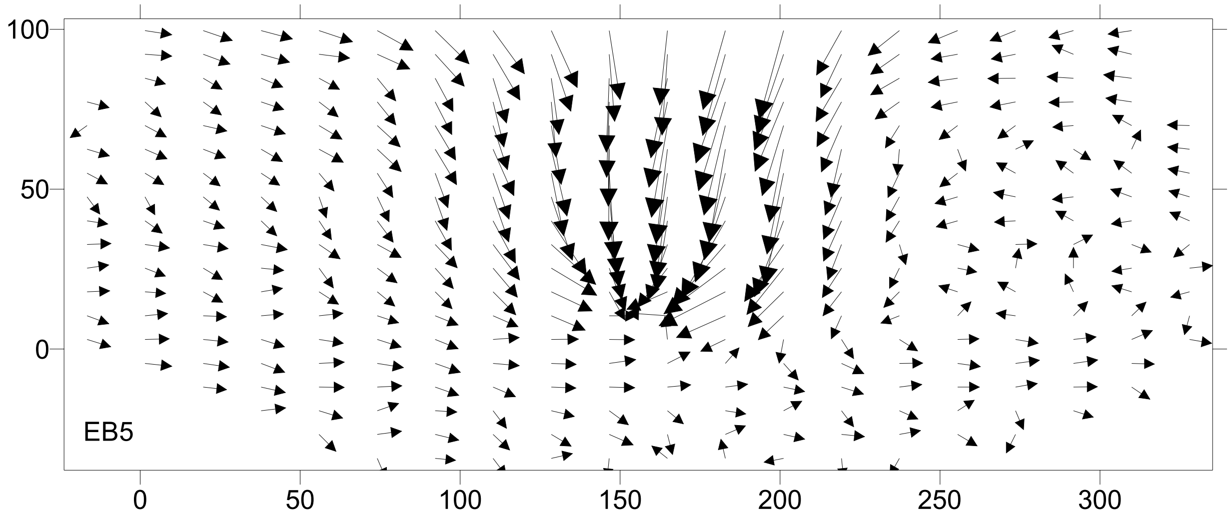
EB5
100
50
0
0
50
100
150
200
250
300

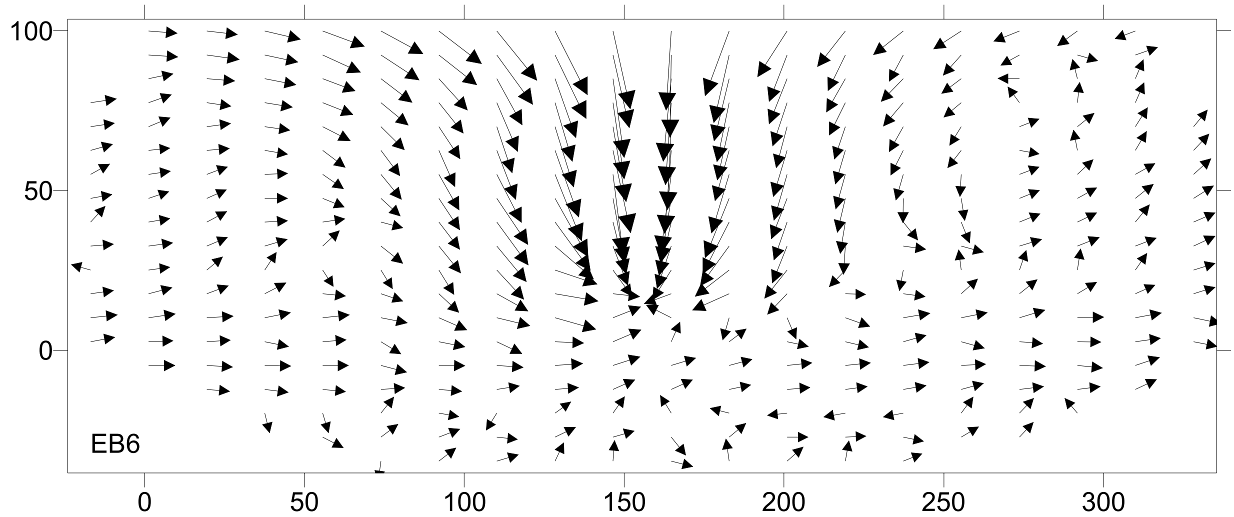
EB6
100
50
0
0
50
100
150
200
250
300

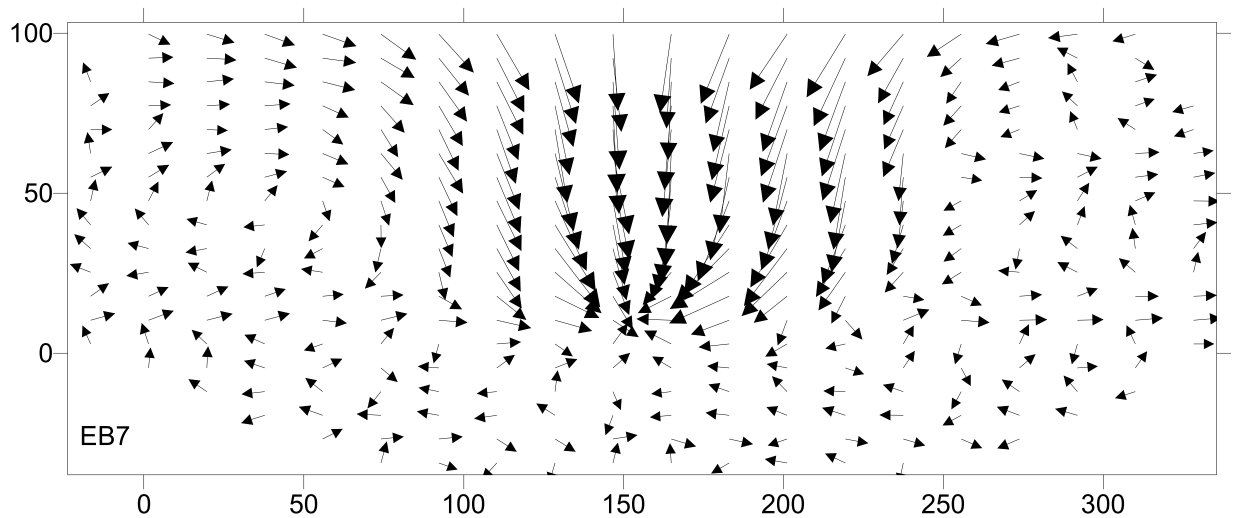
EB7
100
50
0
0
50
100
150
200
250
300

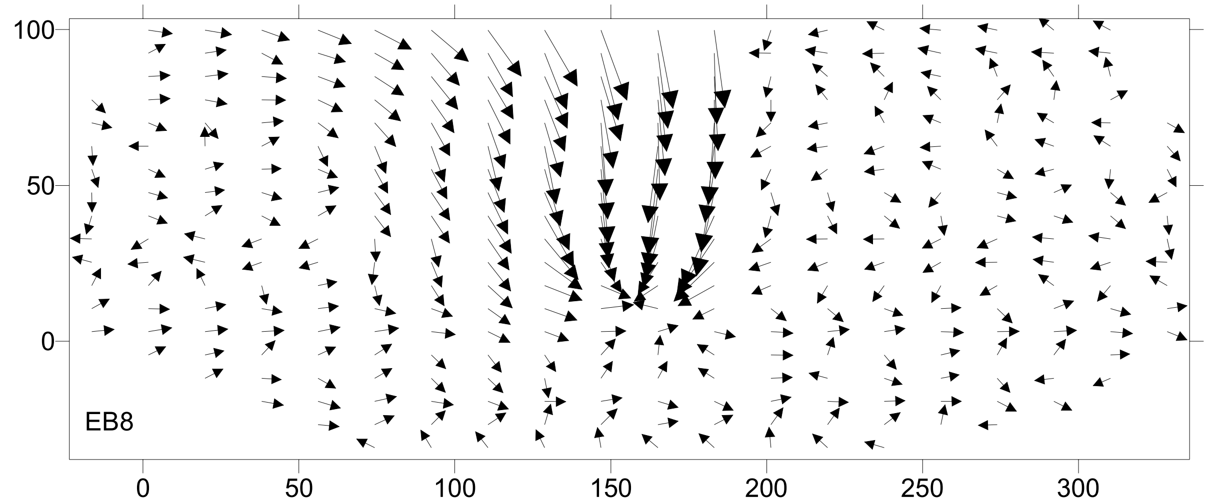

EB8
100
50
0
0
50
100
150
200
250
300

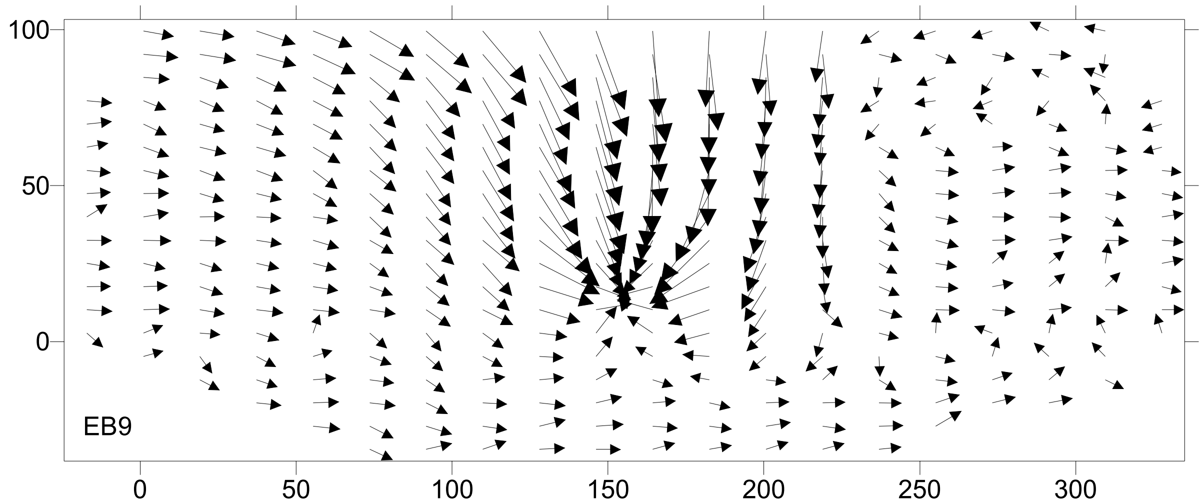

EB9
100
50
0
0
50
100
150
200
250
300

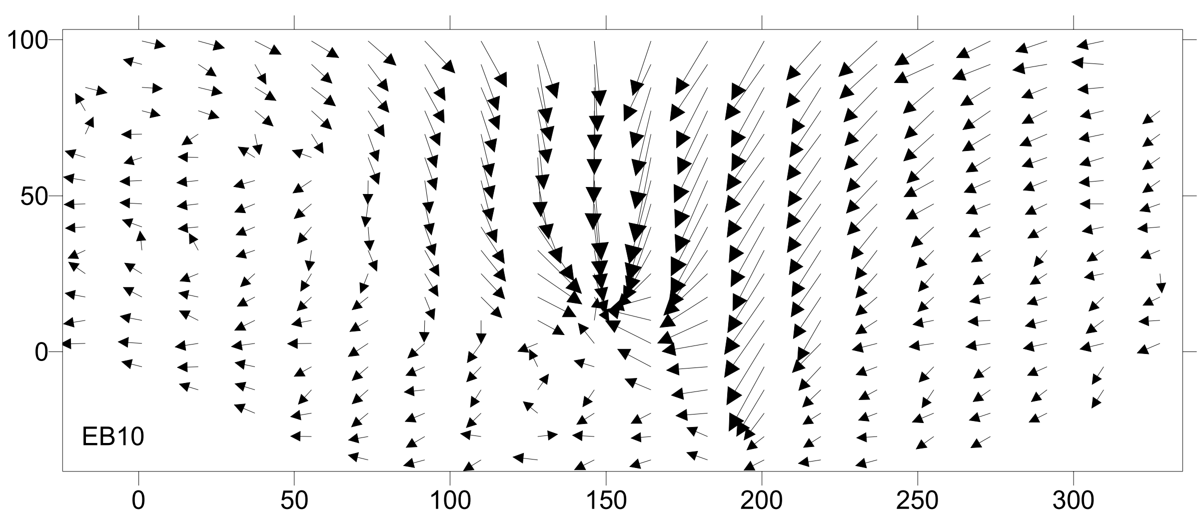

EB10
100
50
0
0
50
100
150
200
250
300

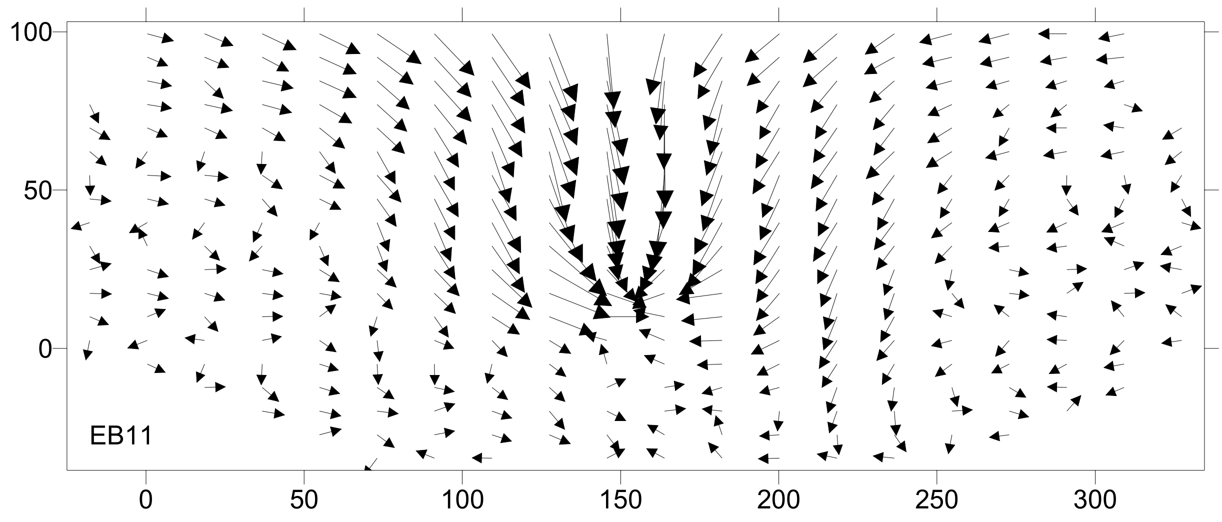
EB11
100
50
0
0
50
100
150
200
250
300

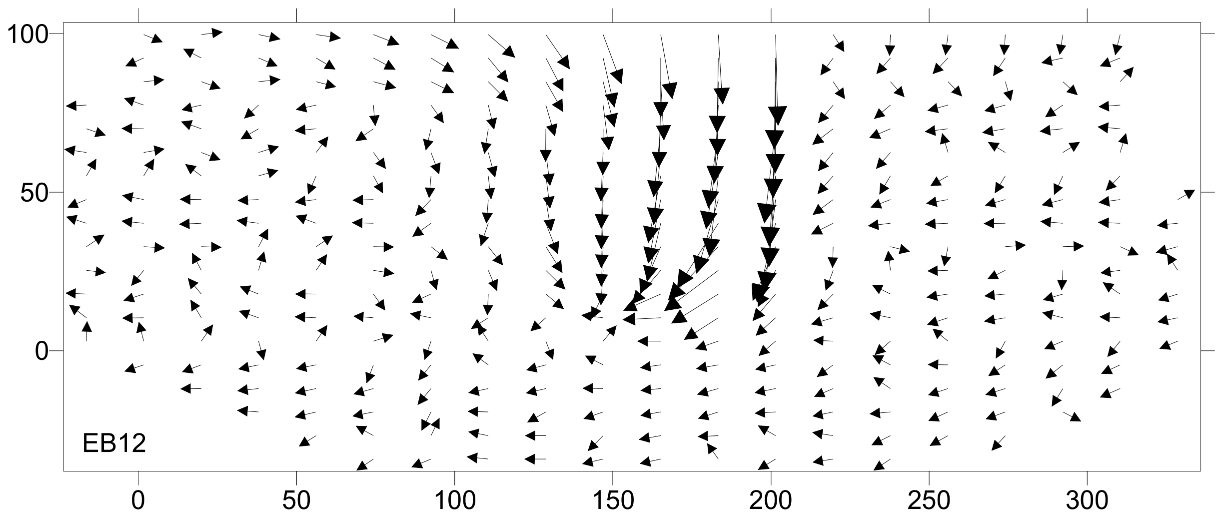
EB12
100
50
0
0
50
100
150
200
250
300

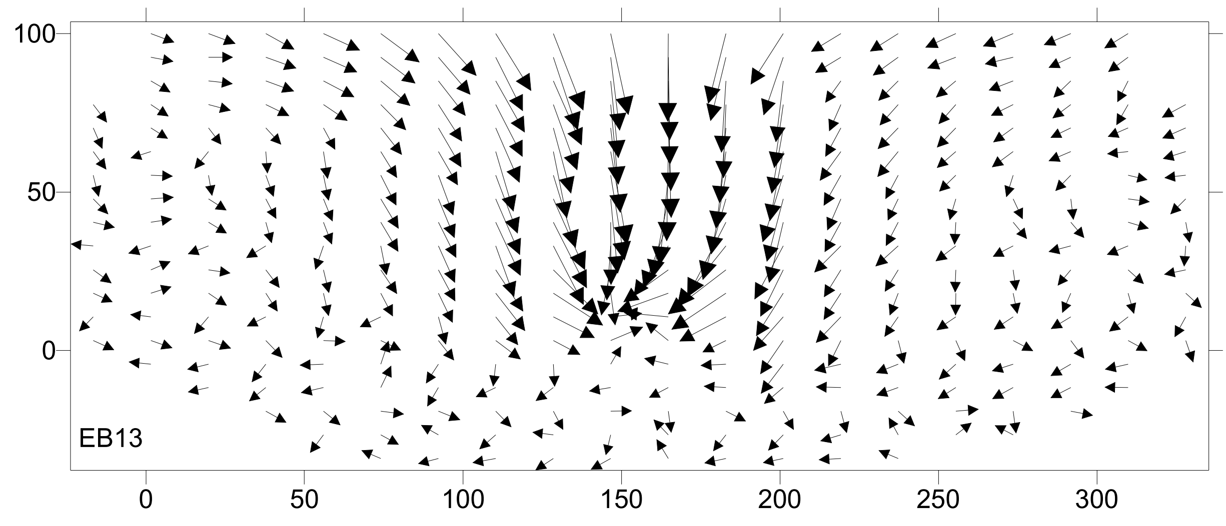
EB13
100
50
0
0
50
100
150
200
250
300

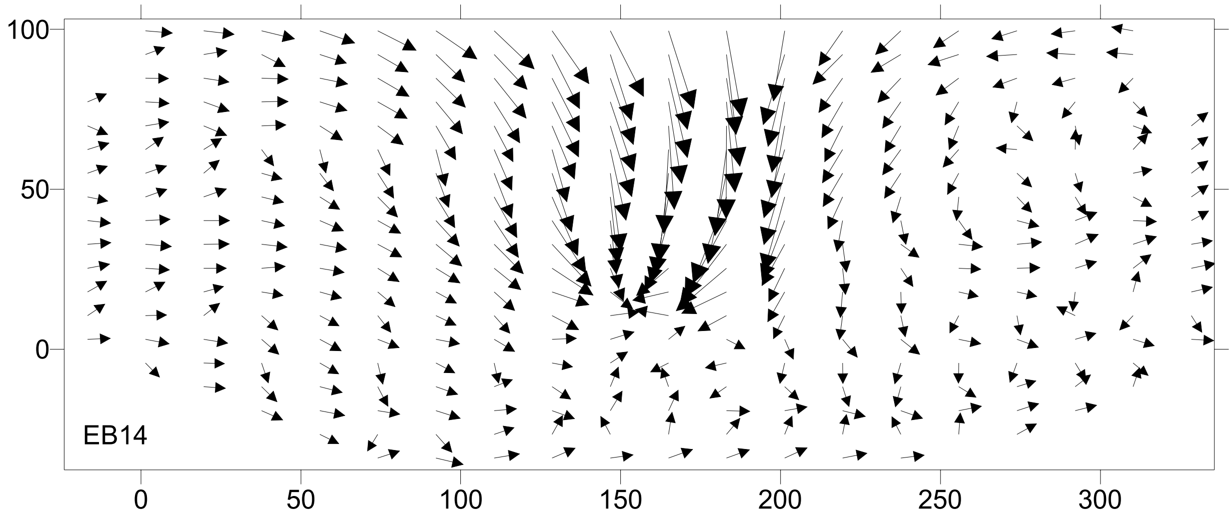
100
50
0
0
50
100
150
200
250
300
EB14

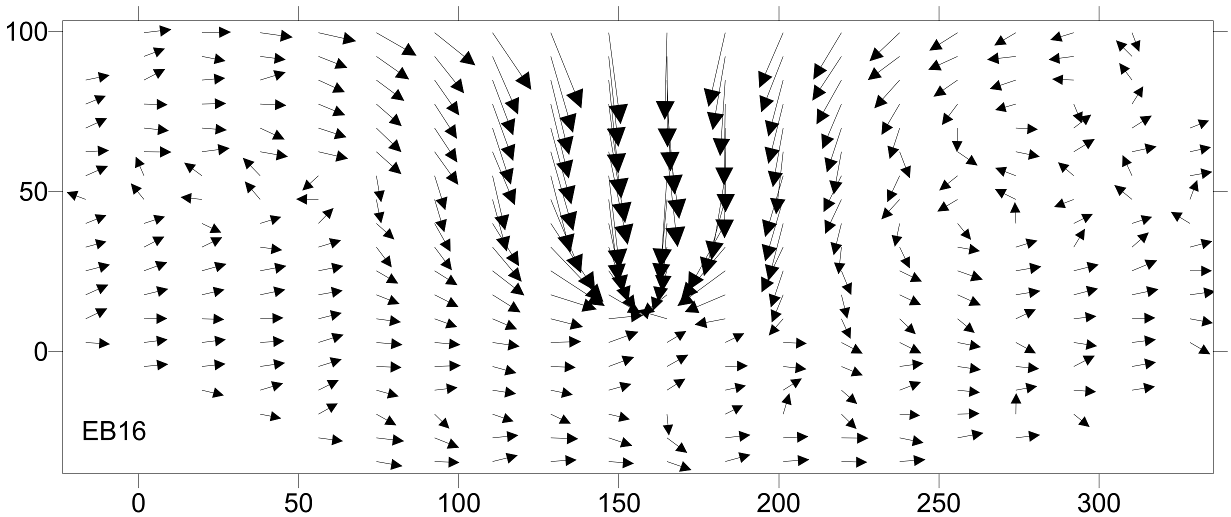
100
50
0
0
50
100
150
200
250
300
EB16

IV. Numerical analyses

Introduction

As aforementioned, in order to plan the centrifuge tests to be carried out at City University, a number of preliminary analyses have been performed to identify the main geometrical factors affecting the problem. These analyses were not specifically aimed to reproduce the behaviour of the models which have been tested afterward, because at that time the details of model preparation and test procedure were not established yet.

After that tests had been carried out, in order to gain a deeper insight of the experimental findings, a new set of numerical analyses has been performed. In this case the soil was modelled with two constitutive laws, which belong to the framework of the Critical State Soil Mechanics: the Modified Cam Clay (Roscoe & Burland, 1968) and the Three Surfaces Kinematic Hardening (Stallebrass, 1990).

In this chapter the results of the preliminary analyses will be briefly commented. Afterward the main set of numerical analyses will be presented and their results will be discussed.

Preliminary analyses.

Preliminary analyses have been carried out by the commercial numerical code PLAXIS.

The soil is modelled as Hardening Soil, a nonlinear elastic-plastic constitutive model with volumetric and deviatoric hardening, implemented in the code (Schanz *et al.*, 1999) and the values of the adopted mechanical parameters are typical of a soft soil but they are not referred to a specific one (see Tab. IV.1). Details on the constitutive law can be found in App. 3.

Table IV.1 – Soil parameters for Hardening Soil

Parameter	Value	
γ_{wet}	19	kN/m^3
γ_{dry}	18	kN/m^3
K	10^{-8}	m/s
E_{50}^{ref} (per p_{ref} = 100 kPa)	1×10^4	kN/m^2
E_{ur}^{ref} (per p_{ref} = 100 kPa)	1×10^5	kN/m^2
E_{oed}^{ref} (per p_{ref} = 100 kPa)	1.5×10^4	kN/m^2
Cohesion c	0	kN/m^2
Friction angle φ	25.4	°
Dilatancy angle ψ	0	°
Poisson's ratio ν_{ur}	0.2	-
Power m	1	-
K_0^{nc}	0.57	-
Tensile strength	0	kN/m^2
Failure ratio q_{fail}/q_{asy}	0.9	-

Plane strain analyses were performed. The mesh of linear strain 6-node triangles is 70 m wide and 37 m deep. The tunnel has a 10 m diameter, its axis being 15 m deep (D=10 m, C=10 m). The mesh sides are restrained from moving horizontally and free to settle, the bottom is restraint in both horizontal and vertical displacements. No ground water was introduced in the model.

A sketch of the mesh is shown in Fig. IV.1.

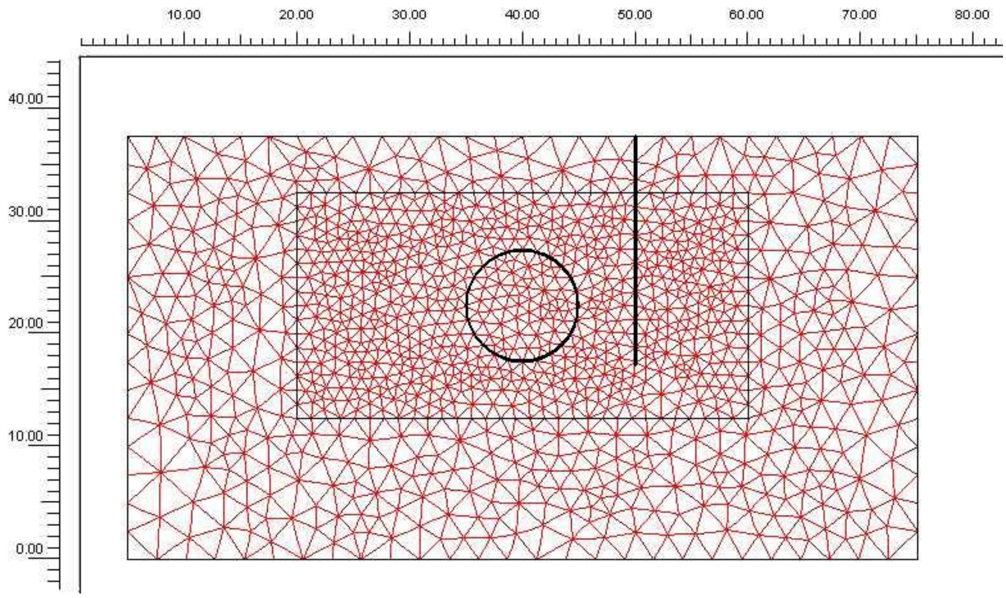

Figure IV.1 – Sketch of the Plaxis mesh.

The tunnel excavation is simulated by eliminating the corresponding elements and by substituting them with a system of stresses of the same entity and opposite sign of those exerted by the elements of the tunnel on its geometric contour. Each analysis has been subdivided in subsequent phases, associated to different percentages of stresses reduction. The excavation is continued up to failure. The numerical analyses are performed in drained conditions. This choice is not consistent with the undrained conditions which occurred in the following tests. At that time, in fact, the possibility to perform tests on sandy ground was considered and for this reason the preliminary analyses where performed in drained conditions. After the decision to test clayey models in undrained conditions, the preliminary analyses were not repeated as the tests were simulated afterward in the main set of numerical analyses.

A first reference analysis has been carried out without diaphragm wall, in order to obtain settlement troughs at different stresses reduction levels. It has been possible to relate the percent values of stress reduction M_{stage} to the settlement trough volume, expressed as a percentage of the tunnel volume (Fig.IV.2).

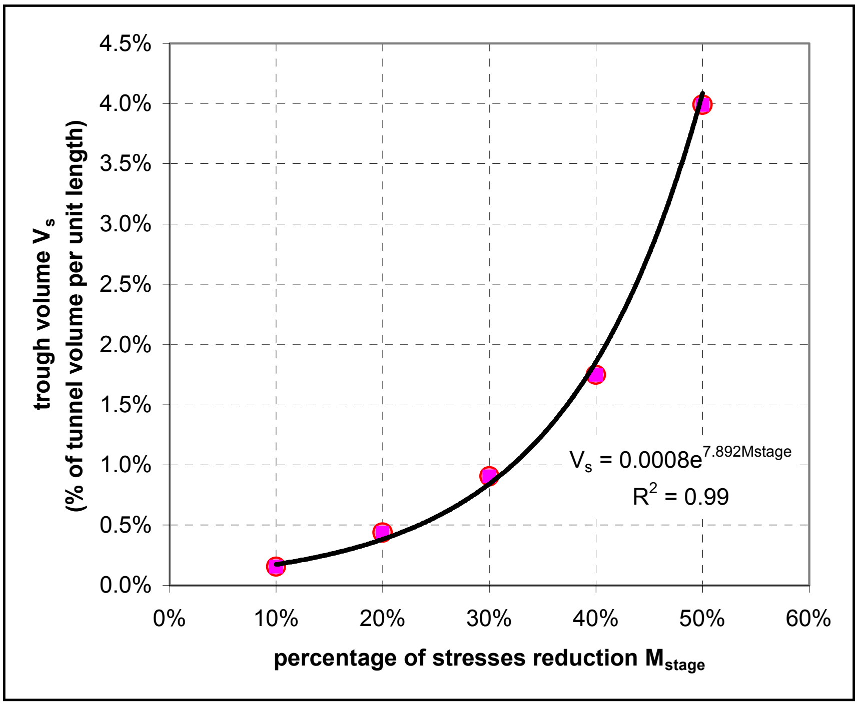

Figure IV.2– relation between the trough volume and the stress reduction

Since the analyses are not carried out at constant volume, this value V_s does not coincide with the volume loss V' as usually defined.

In Fig. IV.3 the normalised reference settlement profiles are compared to two Gaussian curves: the dashed line refer to K=0.5 which is a common assumption for normal consolidated clays in undrained condition, the continuous line is the best fitting of the computed data over a distance of ±*i* from the tunnel axis. As drained conditions occurs, it is convenient that the computed curves are wider than the Gaussian fitting with K=0.5; on the other hand, also the best fitting is not very close to the Gaussian curve.

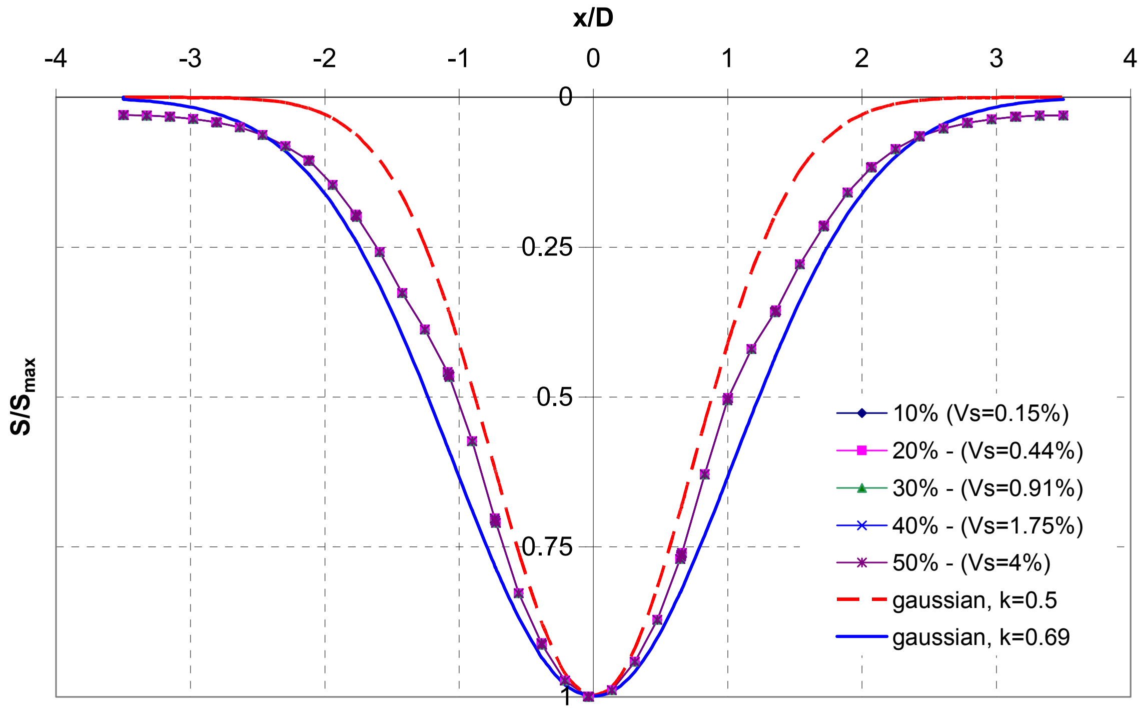

Figure IV.3 – normalised settlement profiles at different stress levels

Two more ‘no-wall’ analyses have been carried out to study the influence of the boundary conditions on the solution. In the first analysis the distance of the bottom of the mesh from the tunnel invert was increased from 17.5 m to 22.5 m; in the second one, the lateral distance of the sides of the mesh from the tunnel wall was increased from 30 m to 35 m. The corresponding settlement troughs are plotted in Fig. IV.4, for 40 % of stresses reduction, and compared to the previous ‘no-wall’ analysis.

It can be observed that, in the investigated range of sizes and mechanical properties, the influence of the mesh bottom depth is negligible, while the influence of the lateral distance of the boundary is very small and, in any case, it appears out of the area of applicative interest (d>3i).

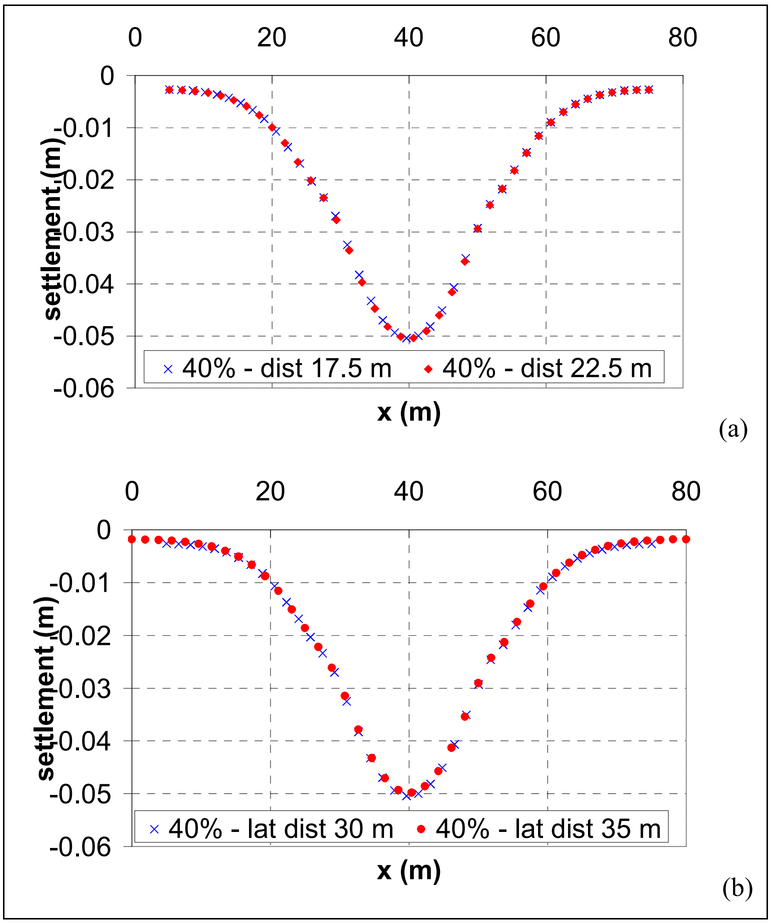

Figure 4 – comparing settlement trough of meshes with different bottom depth (a) and different lateral extent (b)

A series of analyses has been carried out with an aluminium diaphragm wall at a side of the tunnel. The wall length L, its distance from the tunnel axis d, its thickness t and the relative roughness of the interface R were varied, as shown in Tab. IV.2.

Table IV.2 –wall geometrical parameters

L (m)	d (m)	t (cm)	R
10; 20; 30	10	12.5; 100	1; 0.1
10; 25	15		

Aluminium was chosen as it is adopted in the centrifuge tests. In the numerical analyses the diaphragm self weight was neglected. The parameter R is a strength reduction factor for the interface: R=1 was used to model rough walls, R=0.1 to model slip walls. Before the interface strength is attained, the wall behaves elastically with parameters which depend on the soil stiffness and on the factor R; after an interface element attains its strength, it starts to slip. The interface elements are defined by three pairs of nodes with the same coordinates. They have a 'virtual' thickness necessary to define their stiffness which is equal to 0.1 times the average mesh element size.

The analyses results will be discussed in the followings by comparing the settlement profiles at surface and the horizontal displacement profiles along the diaphragm wall axis, in the different configurations at 40% of stress reduction. This value corresponds to V_s = 1.75% in the reference configuration.

In Figs. IV.5 and IV.6 the surface settlement curves have been subdivided into five classes and compared to the no-wall prediction. From an overall view, some remarks can be drawn about the influence of the varying parameters.

Influence of the length L:

- by increasing L the reduction of settlements at the back of the wall is greater;

- by increasing L the difference of behaviour between the stiff walls and the flexible ones becomes more evident;

- the diaphragm walls as deep as the tunnel invert, and preferably more, appear more effective.

Influence of the stiffness:

- Varying stiffness seems not to have a significant influence on the settlements trough.

Influence of the distance d:

- by increasing d for the shallow diaphragm walls there is almost no influence of the interface roughness and in general the effectiveness of the walls reduces;

- when d = 10 m the rough diaphragm walls, both flexible and stiff, produce a surface trough very close to the one without diaphragms walls;

- by increasing d, settlements on the back of the deeper walls (deep at least as the invert) do not vary sensibly, whilst that improves the behaviour on the front of the wall since settlements reduce.

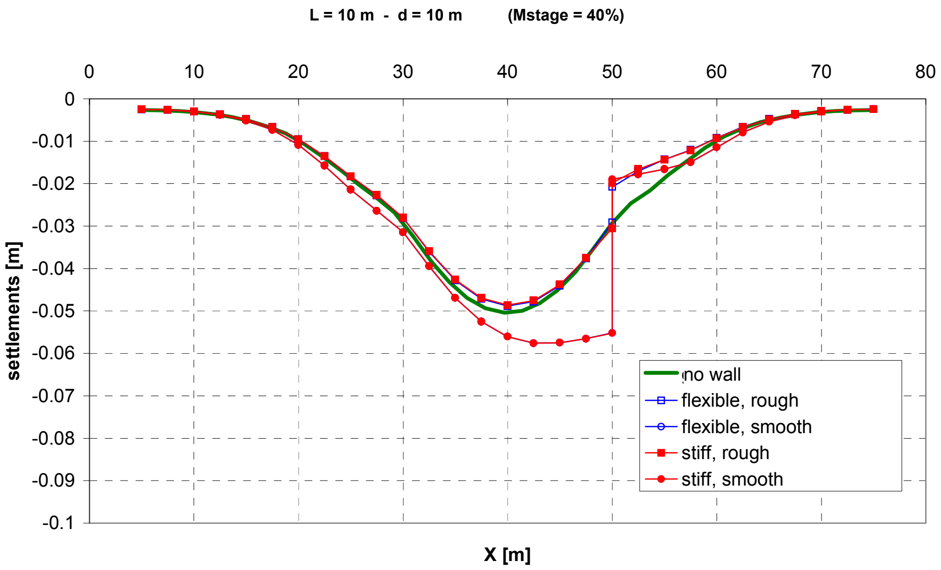
L = 10 m - d = 10 m (Mstage = 40%)
0 10 20 30 40 50 60 70 80
0 -0.01 -0.02 -0.03 -0.04 -0.05 -0.06 -0.07 -0.08 -0.09 -0.1
settlements [m]
X [m]
no wall
flexible, rough
flexible, smooth
stiff, rough
stiff, smooth

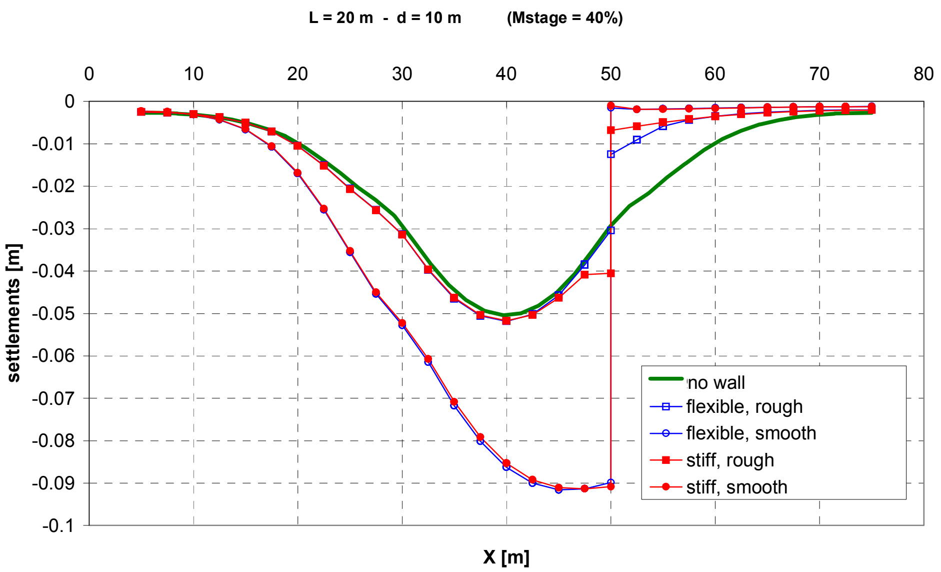
L = 20 m - d = 10 m (Mstage = 40%)
0 10 20 30 40 50 60 70 80
0 -0.01 -0.02 -0.03 -0.04 -0.05 -0.06 -0.07 -0.08 -0.09 -0.1
settlements [m]
X [m]
no wall
flexible, rough
flexible, smooth
stiff, rough
stiff, smooth

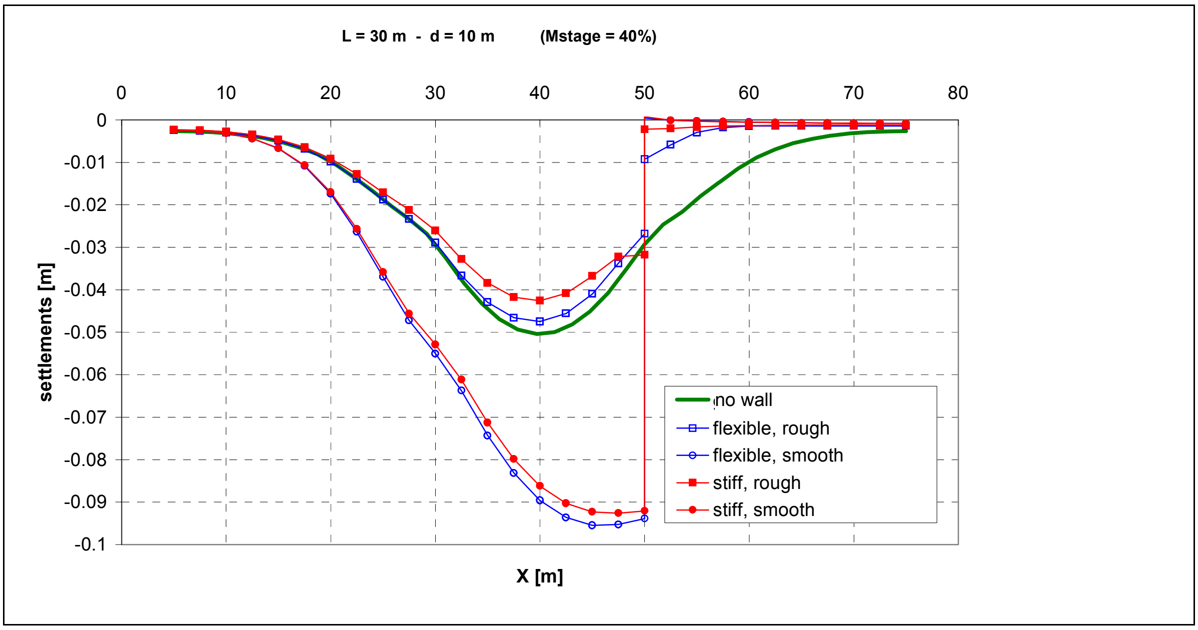

Figure IV.5 – settlement troughs of models with d=D

Influence of the roughness:

- roughness has a large influence in front of the diaphragm walls; on the back, settlements are always strongly reduced;

- smooth diaphragm walls increase the settlement of the tunnel cover.

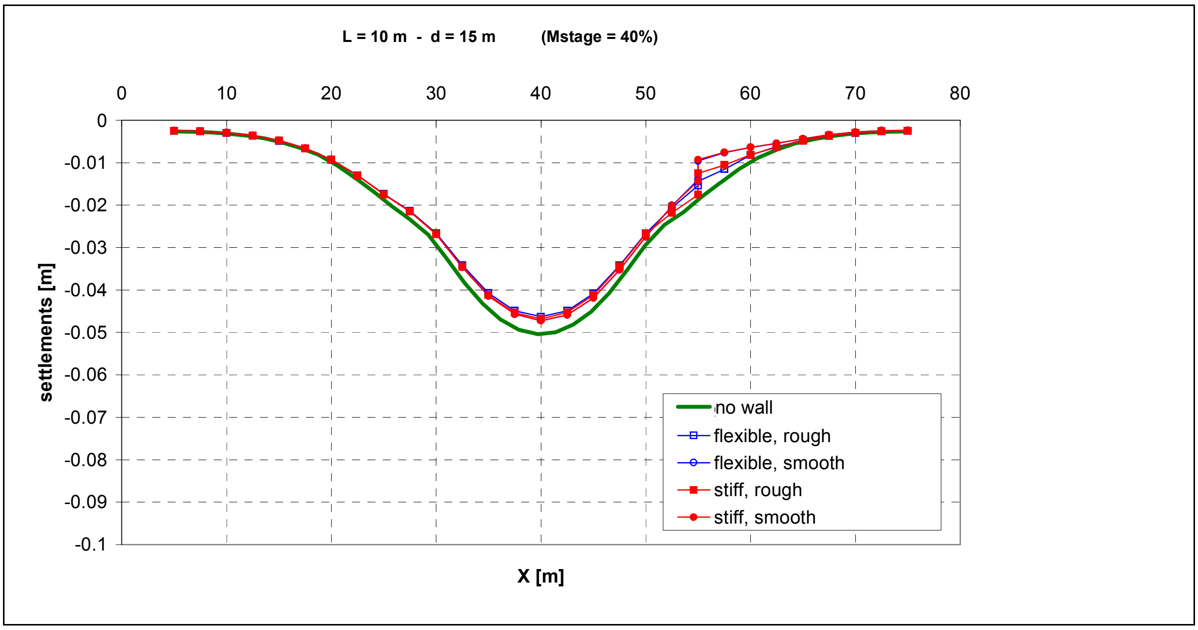

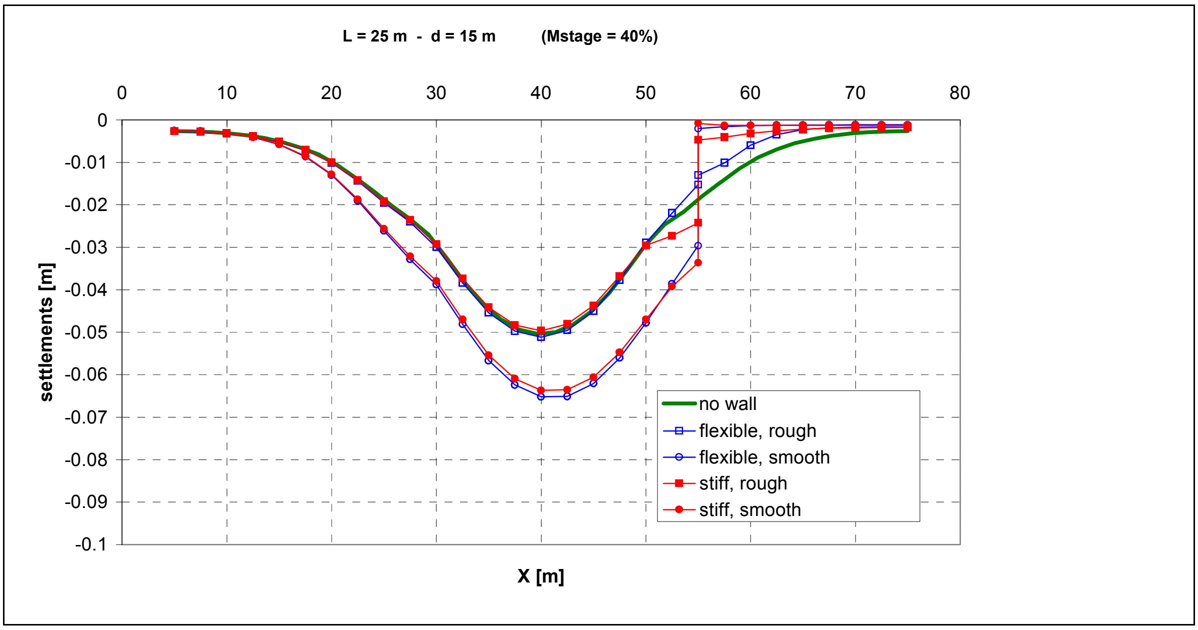

Figure IV.6 – settlement troughs of models with d=1.5D

In Fig. IV.7 the curves of the horizontal displacements of the diaphragm walls with depth are compared to the corresponding 'no wall' profile, which is also shown in Fig. IV.8. The four graphs correspond each to a distance d and a given wall stiffness.

Some possible comments to the figure are reported in the followings.

Influence of the length L:

- the length of the wall is a very important parameter: the diaphragm walls tend to rotate at the bottom as the 'no wall' displacement field invites to do. Then, the walls with L = 10 m appear to be very ineffective.

Influence of the stiffness:

- stiff walls are more effective than flexible ones if adequately deep. For L = 10 m no significant difference results when varying stiffness.

Influence of the distance d:

- the horizontal distance of the walls from the tunnel axis seems not to have a significant influence on their behaviour if looking to the magnitude of the horizontal displacement at the top of the wall. Nevertheless it could be noticed that the diaphragm walls closer to the point of maximum 'no-wall' horizontal displacement (see Fig. IV.8) are more effective.

Influence of the roughness:

- it seems that smooth walls tend to adapt themselves to the deformation pattern which the soil would have in ‘no-wall’ conditions. Then, their stiffness controls the shape of their inflexion.

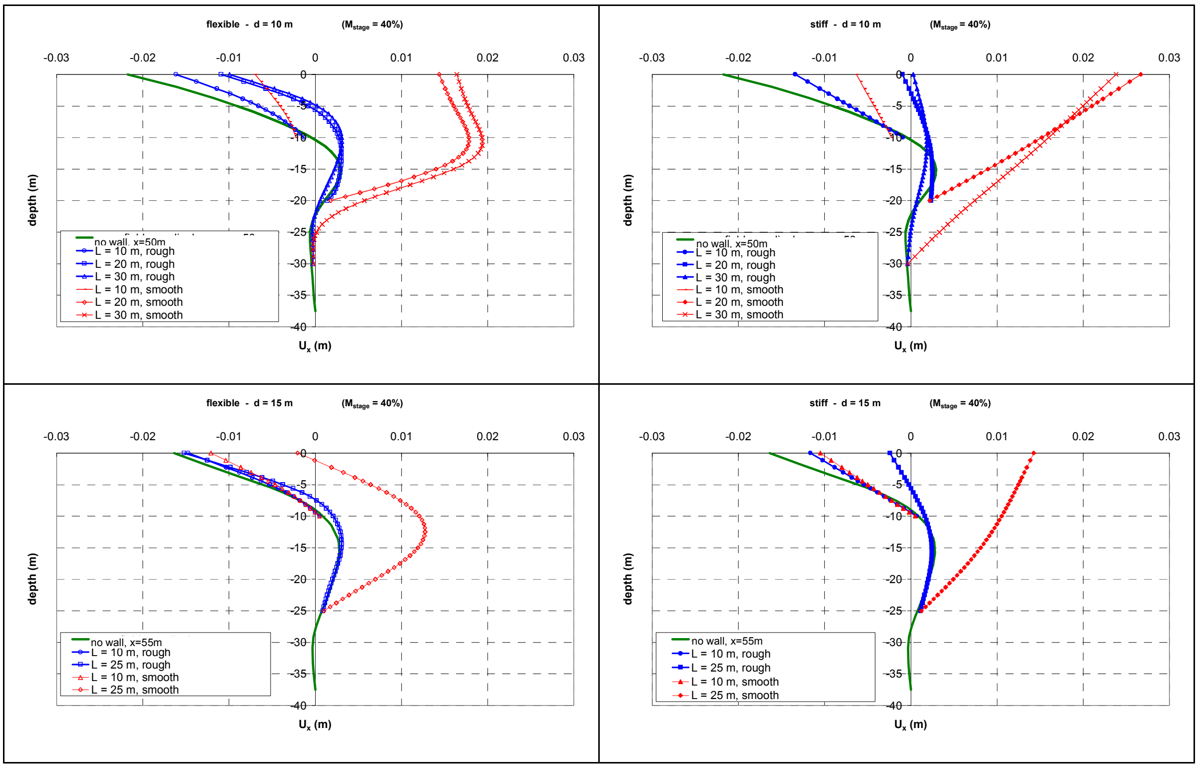

Figure IV.7 – wall horizontal displacements compared to the reference profile without wall

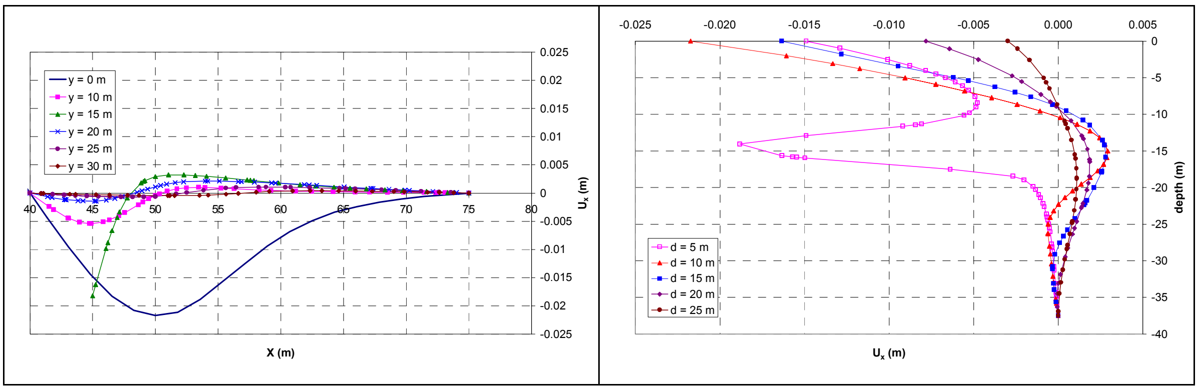

Fig. IV.7 – reference profiles of horizontal displacements

A few words deserves the pattern of horizontal movements close to the tunnel in the no-wall conditions. It can be observed that the ground horizontal displacements at the tunnel axis level are directed towards the tunnel up to a distance between 5 m (tunnel boundary) and 10 m (about one diameter away from the axis). This circumstance was not observed in a few more calculations with K_o=1, which were aimed to verify this issue: this suggests that the anisotropy of the initial stress state has to be carefully considered. The difference between the results between models of ground with a different degree of stress anisotropy could depend on the stress release procedure, which is always an approximation of the real excavation process. Among others, Boulon *et al*. (1996) showed that the classical method of simulating the excavation by reducing progressively the existing stress at the boundary of the tunnel is not always able to reproduce the measured pattern of displacements. In these preliminary analyses this aspect was neglected, even if some of the observed behaviours of the wall models could have been influenced by the no-wall displacement field. On the contrary, in the main set of numerical analyses the same procedure as in tests was adopted, hence the computed displacement fields should be more reliable.

Furthermore, in this preliminary stage, the ground movement fields have been compared at the same supporting pressure because this seemed obvious, as during experimental test the cavity supporting pressure was reduced.

It has to be noticed that the aforesaid remarks have not been all confirmed by the experimental results. This possibly depend on the different boundary conditions and soil characterisation. Nevertheless, these analyses gave indications which were taken into account when programming the tests. Length, thickness, roughness and distance of the wall from the tunnel axis were the geometrical factors on which the attention was focussed. The ratio C/D=1 was assumed to be representative of very shallow tunnels and it was not changed in the tests (apart from EB1-2-3 where C/D=0.9). The preliminary analyses showed the influence of the wall length and suggested to deepen the shorter wall at least to about the tunnel axis and the longer one below the tunnel invert. These analyses showed that the effect of stiffness was larger for deeper walls: in the test programme two model with long walls having different thickness were hence compared. Two wall thickness values were chosen to cover a wide range of stiffness. The importance of the wall roughness arose in this phase and led to perform couples of tests on models with the same wall size and location but different interface. Finally, as far as the distance of the wall is concerned, its influence on the problem seemed to be low. Furthermore, it is obvious that the variation of this parameter is constrained by the location of the area to be protected against large movements. However, two different locations for the wall were chosen in the tests, as detailed in Chapter III, in order to check this point.

Numerical analyses

The main set of numerical analyses was conducted by using SAGE CRISP, a Finite Element program (Britto & Gunn, 1987) in which both Modified Cam-clay and 3-SKH model are implemented.

For smooth walls, slip elements have been interposed between the wall and the soil. No specific tests have been carried out to determine the values of the soil constitutive parameters, because they are well characterised in literature (Stallebrass, 1990; Viggiani, 1992; Morrison, 1990). On the other hand, several analyses were run to set convenient values of the parameters of the smooth interface.

The shape and size of the numerical model was exactly the same of the physical model, that is 550 mm wide and 155 mm high. The numerical analyses were conducted in plane strain conditions. The boundary restraints were the same as in the tests. The ground table was fixed 2 mm below the ground level. A sketch of the mesh is shown in Fig. IV.9.

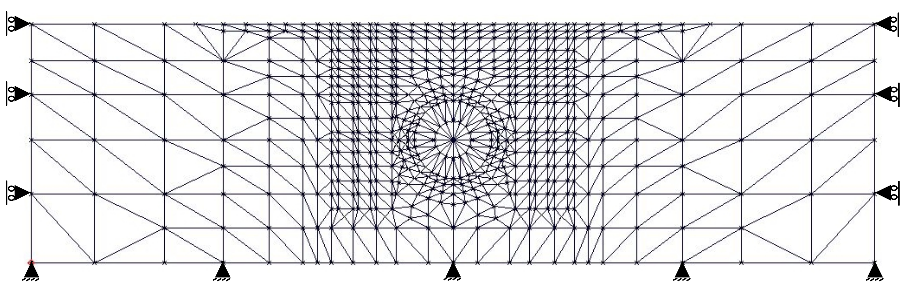

Figure IV.9 - Sketch of the mesh.

The mesh was constituted of 6-node linear strain triangles allowing excess pore pressure variations and it represented the whole model because when inserting the wall any possible symmetry was lost. The influence of this structured mesh on the solution of the problem has been also studied, as shown later.

Materials characterisation

The values for the parameters of Modified Cam-Clay and 3-SKH have been adopted as reported in literature and they are shown in Tabs. IV.3 and IV.4. These values descend from a careful calibration of the two models on a widespread laboratory testing programme on the same Speswhite kaolin. The unit weight of the soil is $\gamma = 17.44$ kN/m^3.

Table IV.3 - Soil parameters for Cam Clay (Morrison, 1994)

M	0.89	ν	0.3
λ	0.18		
e_{cs}	1.97	k_v	0.58E-6 mm/s
κ	0.035	k_h	1.58E-6 mm/s

Table IV.4 - Soil parameters for 3-SKH (Stallebrass, 1990; Viggiani, 1992)

M	0.89	T	0.25	A	1964 kPa
λ*	0.073	S	0.08	m	0.65
e_{cs}	1.994	ψ	2.5	n	0.2
κ*	0.005	k_v	0.58E-6 mm/s	k_h	1.58E-6 mm/s

The meaning of the 3-SKH parameters has been detailed in App. 3. The parameters λ* and κ* in Tab. IV.4 correspond, over an appropriate stress range, to the parameters λ and κ in Tab. IV.3 as soon as the normal compression line and the unloading-reloading lines are defined in the bi-logarithm $\ln e : \ln p'$ space, following Butterfield (1979).

The values of horizontal and vertical permeability have been calculated from the formulae (IV.1) given by Al-Tabbaa (1987) using the void ratio (IV.2) as calculated, by using the critical state parameters, at the initial mean effective stress ($\sigma'_{v,\max} = 350kPa$).

$$k_v = 0.5e^{3.25} \cdot 10^{-6} \quad (mm/s)$$
$$k_h = 1.43e^{2.09} \cdot 10^{-6} \quad (mm/s) \qquad \text{(IV.1)}$$

$$e = \exp\left[\ln N - (\lambda^* - \kappa^*) \ln p'_o - \kappa^* \ln p'\right] - 1 \qquad \text{(IV.2)}$$

In (IV.2) p'_o is the maximum mean effective stress in normal compression and defines the size of the bounding surface in both models at the initial state. N defines the location N-1 of the isotropic normal compression line in $e : \ln p'$ space.

The aluminium embedded walls have been modelled with 6-node non consolidating linear strain triangles with a linear elastic law (Tab. IV.5).

Table IV.5 – elastic parameters for the aluminum wall

E	7E7 kPa
ν	0.25
γ	27 kN/m^3

Analyses without wall

As in the experimental work, a reference analysis was necessary to model the ground movements in no-wall conditions before attempting to model the behaviour of a mesh with an embedded diaphragm wall.

The whole history of the model since the end of consolidation under the press was reproduced. The initial effective vertical stress was thus equal to 350 kPa and constant with depth as well as in the physical model. The initial horizontal effective stress was calculated through a constant value of K_o = 1-sinϕ.

A special procedure (Grant, 1998) was needed to assign the initial conditions, due to the impossibility of increasing the pore water self weight by increasing the gravity level when using CRISP. For this reason a pore pressure distribution had to be initially assigned to the mesh, which had the same gradient with depth as in the centrifuge at N times the earth gravity. Obviously, an equilibrating total stress distribution had to be created into the model in order to set the correct distribution of the effective stresses which was in the model after the consolidation in the press. Hence, total stresses were varied with the same gradient as the pore pressure: a fictitious acceleration N_s g was given to the model since the beginning in order to satisfy the condition (IV.3),

$$N_s \gamma = N \gamma_w \tag{IV.3}$$

which leads to $N_s = 90$. Then, by applying a vertical load $\sigma_s = p_{max} - N\gamma_w a$ on the top, where p_{max} is the consolidation pressure and a the water table depth, the resulting effective vertical stress in the model is constant with depth and equals p_{max}=350 kPa.

In Fig. IV.10 the applied stress distributions have been sketched.

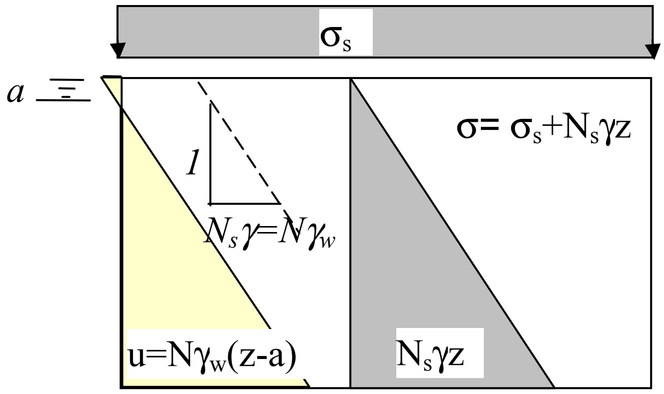

Figure IV.10 – Sketch of pore pressures and total vertical stresses

The analysis was then split in several blocks. In the first, the mesh was unloaded up to σ'_v = 150 kPa, thus modelling the extraction of the strong box from the consolidometer. In the following two blocks, the remaining 150 kPa were removed. At the same time the vertical acceleration was increased to the final value (160 g).

At that point, the elements of soil in the tunnel were removed and a pressure of 190 kPa was applied at the tunnel boundary, as it had been in the centrifuge test.

In all these phases a coupled analysis was performed, as consolidation occurred in the physical tests, and the duration of each block was high enough to ensure that at the final stage of a block the soil was completely consolidated.

In Fig. IV.11 the vertical effective stresses and pore pressure along the tunnel vertical centre line are shown, before and after removing the tunnel elements.

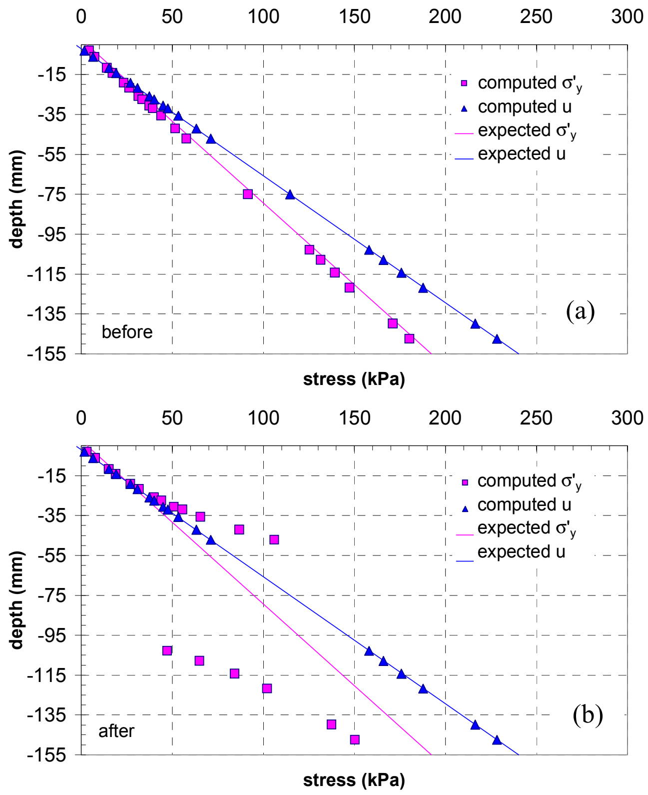

Figure IV.11 – Vertical effective stresses and pore pressure along depth before (a) and after (b) removing tunnel soil elements and applying supporting pressure (3-SKH)

In Fig. IV.11b it can be observed that the computed vertical effective stresses diverge from the linear distribution in the vicinity of the tunnel, as the soil elements corresponding to the cavity were removed and a uniform pressure was applied at the cavity boundary.

In Fig. IV.12 the variation along the tunnel vertical centre line at this stage of some quantities which can be used as input for numerical analyses which do not model the previous history of the model have been shown. They result from calculations performed with 3-SKH and Cam Clay. In Fig 12-a the profile of p'_c is shown: this represents the size of the boundary state surface. As Cam Clay does not allow for yielding during unloading, its value is constant with depth and equal to the initial one. It corresponds to the boundary surface passing at the point $\sigma'_v = p_{\max}$ on K_o-compression line. On the contrary, p'_c varies with depth in the 3-SKH analysis. As far as the profiles of void ratio e and earth pressure coefficient K_o are concerned, the largest difference between the two models seems limited to the cover. The undrained resistance c_u, which is a common input parameter in finite element analyses performed in total stresses and undrained conditions, has been calculated as (IV.4) from the void ratio e by using the critical state parameters:

$$c_u = \frac{1}{2} M \exp\left[\frac{\Gamma - e - 1}{\lambda}\right] \qquad \text{(IV.4).}$$

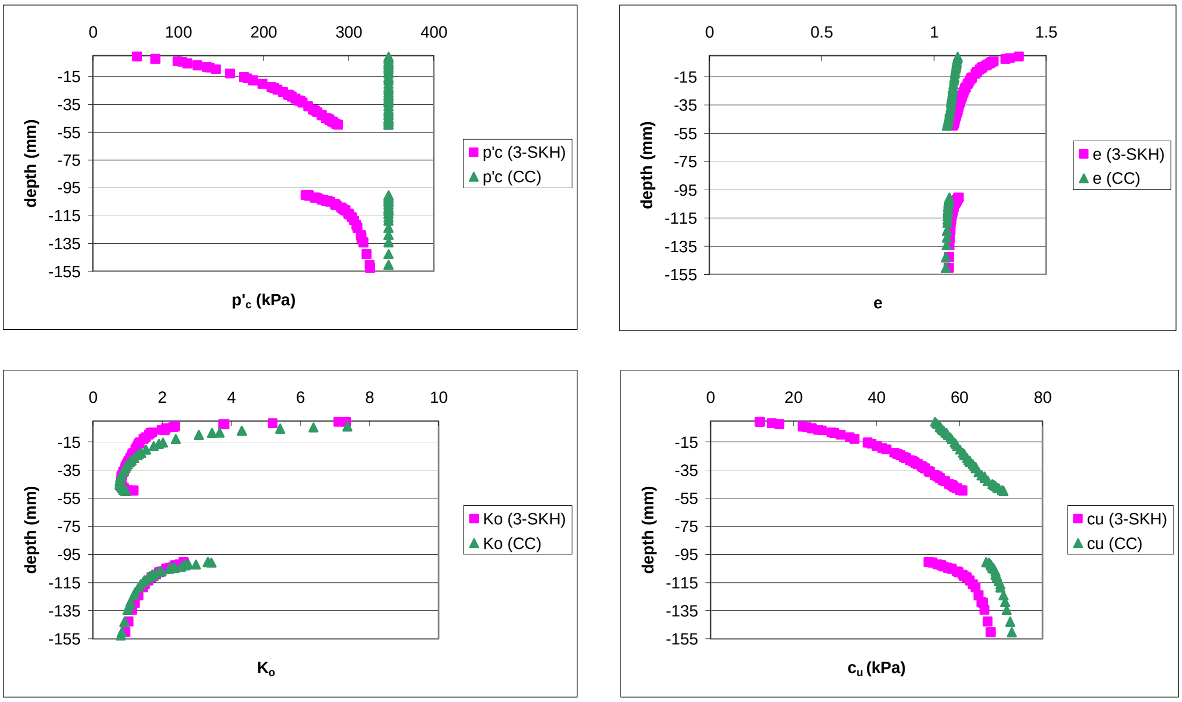

Figure IV.12 – Comparison between 3-SKH and Cam Clay no wall model before decreasing support pressure

As a term of comparison in Fig. IV.13 profiles of OCR, K_o and c_u with depth are shown as they are commonly calculated in practice.

The maximum effective vertical stress at the bottom of the model during flight can be calculated as: 160 x (17.44 x 0.155 – 9.81 x 0.153) = 192.36 kPa, the maximum consolidation stress is experienced by the sample under the press and it is p_{max} = 350 kPa. Hence OCR distribution has been calculated as:

$$OCR = \frac{350kPa}{\sigma'_v} \qquad \text{(IV.5)}$$

K_o has been hence calculated by using the (IV.6) proposed by Meyerhof (1976):

$$K_o = (1 - \sin\phi) OCR^{0.5} \qquad \text{(IV.6)}$$

The undrained shear strength c_u profile has been evaluated by using the expression (IV.7) proposed by Ladd and Edgers (1972) in which Mesri (1975) expression for normally consolidated soil has been integrated:

$$c_u = 0.22\sigma'_v OCR^{0.8} \qquad \text{(IV.7)}$$

In the figure, two scales have been reported along the depth axis, one is referred to the model an the other to the equivalent prototype.

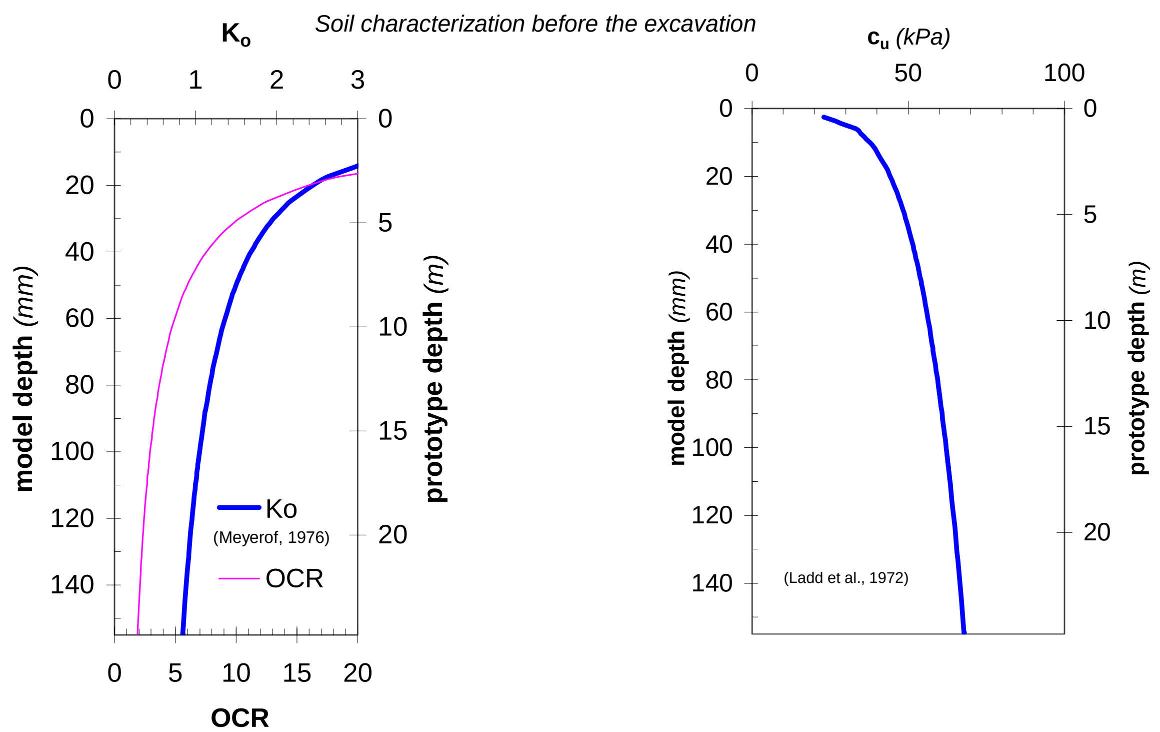

Figure IV.13 – Empirical characterisation of the soil before the excavation

It can be observed that the calculated K_o values are in the range of the empirical ones. In the first 15 mm (2.4 m in the prototype) below the surface the horizontal stress are significantly high.

The empirical prediction of c_u at surface is very close to that calculated by 3-SKH. On the contrary, Cam Clay largely overestimates the undrained shear strength of the cover.

In the last block of the analysis, the pressure inside the cavity was reduced to zero. The duration of this block was roughly equal to that in the corresponding phase of test, *i.e.* about 120 seconds. Hence, even if the analysis allowed the soil to consolidate, its actual behaviour was practically undrained, as in the tests.

Choice of the load increment size

When plasticity is involved in a finite element calculation, the equations to be solved become non-linear: this means that the boundary value problem needs to be solved in a series of calculation steps. A key issue of the solution procedure is thus the choice of the step size.

CRISP uses the incremental method of integration, which assumes that by sub-dividing the whole analysis into sufficiently small load increments, the difference between the piecewise linear function and the true soil response is negligible. This algorithm tends to move away from the true response of the soil if the load increments are too large. It is then necessary to use as many increments as possible in order to get a close approximation of the true behaviour of the soil. This number should not be too high in order to limit the computation time.

To ensure the accuracy of the solution, for each stage of the analysis without wall, the calculation has been repeated with an increasing number of load increments. When two computations produced very close results, the sufficient number of increments was established.

Plotted in Fig. IV.14 are the settlements of the surface nodes, as computed in a set of analyses of the same no-wall configuration at a support reduction stage when $-\Delta p/p_o$=40%.

The soil was modelled by using 3-SKH. The number of load increments was increased from 240 to 2400. It can be observed that the solutions for 1200 and 2400 increments coincide. Hence 2400 has been assumed as the number of increments for this stage.

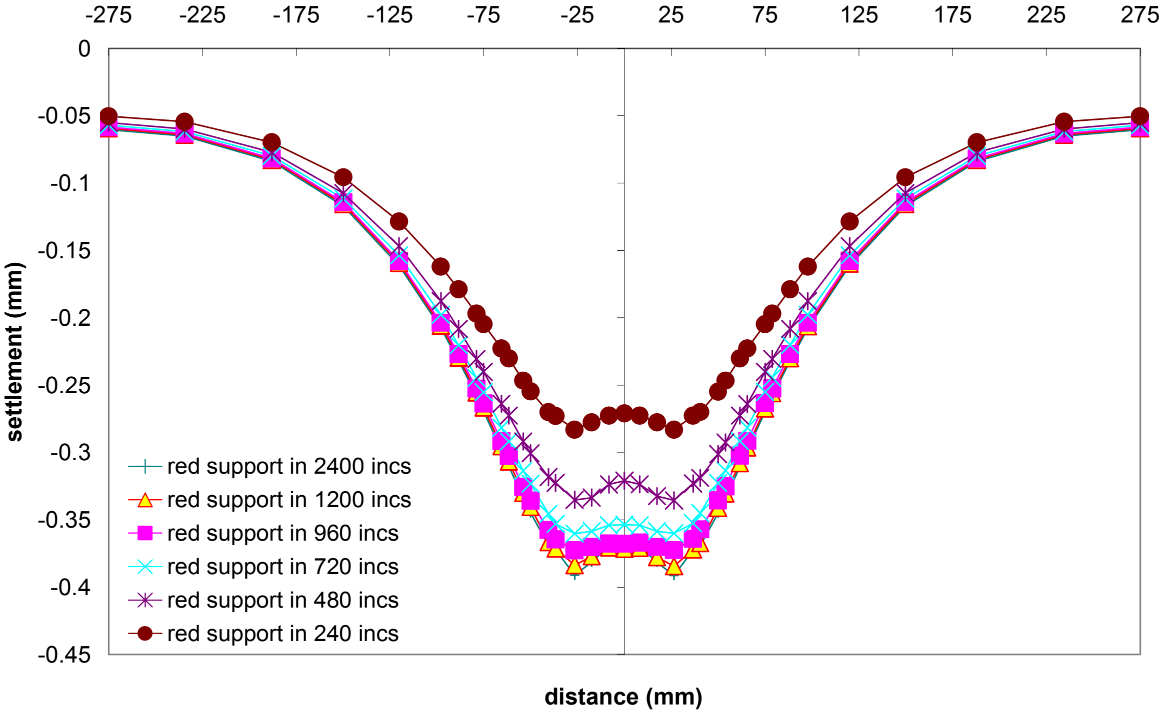

Figure IV.14 – Choice of the load increment size

The small amount of heave which can be observed around the centre line is limited to the first row of nodes and it was observed also by Stallebrass *et al.* (1994a) in analyses carried out on a model tunnel in London Clay, when the tunnel is excavated following anisotropic unloading without reloading stage. They attribute this behaviour to a general increase of stiffness at the tunnel crown where the soil is loaded in extension during the excavation, due to soil dilatancy in undrained conditions. In Fig. IV.15 contours are shown of the increment of p' from the start of the excavation stage to the point when $-\Delta p/p_o=40\%$ which show a local increase of p' in an area at about the mid cover around the tunnel vertical centre line. This could justify a local increase of stiffness and the corresponding surface settlement decrease.

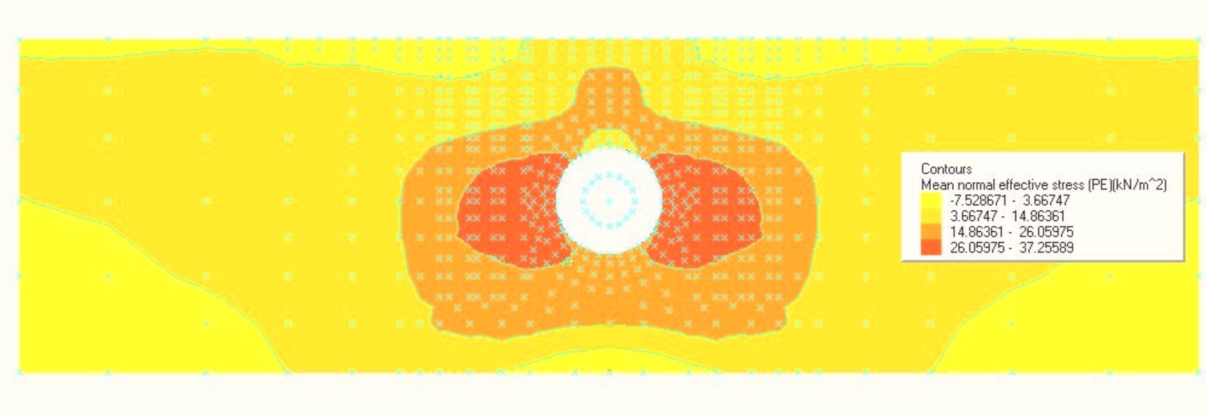

Figure IV.15 – Contours of mean effective stress p' variation for supporting pressure reducing from p_o to $0.6p_o$

Mesh dependence

As it can be observed in Fig. IV.9, the mesh adopted in the performed numerical analyses is regular. The subdivision pattern of that mesh was chosen having in mind the expected pattern of ground movements caused by the excavation. In order to check the influence of this choice on the solution, the no-wall analysis was repeated with an irregular mesh as shown in Fig. IV.16.

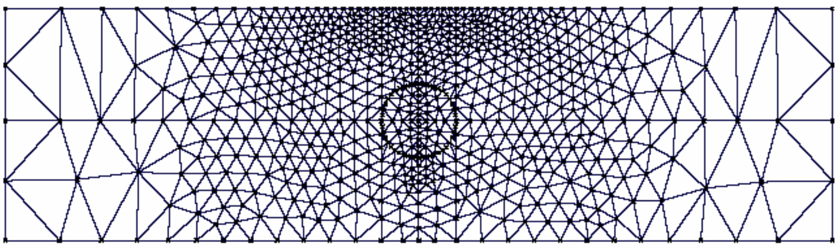

Figure IV.16– Mesh with irregular pattern

The results of the two meshes are very close each other, as it can be seen by comparing the computed settlement troughs in Fig. IV.17.

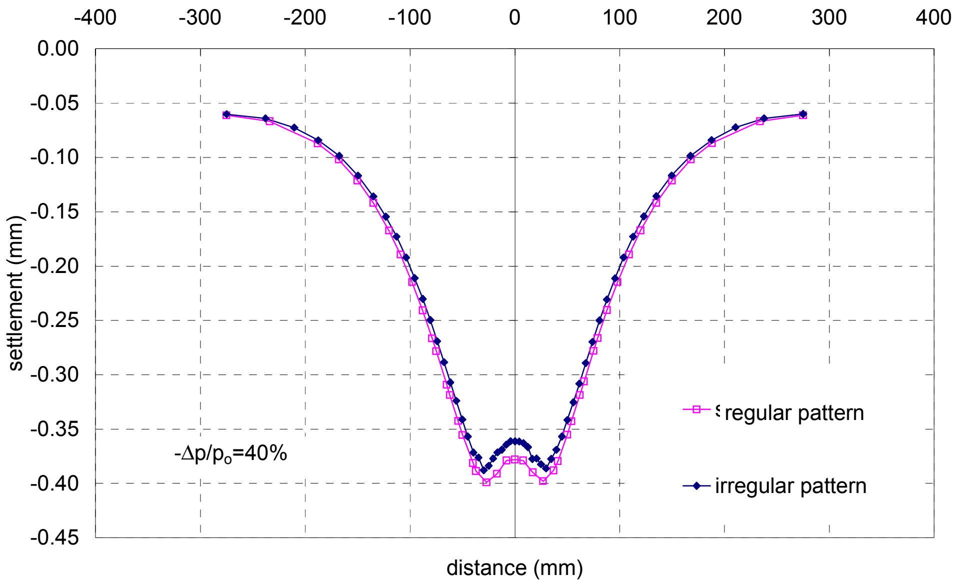

Figure IV.17– Comparison of computed settlement in the regular and irregular meshes

Soil-wall interface characterisation

Once a reference field of displacements without wall have been obtained, a set of numerical analyses with diaphragm walls were performed, which reproduce and integrate the centrifuge tests. It is worth remembering that in the experimental tests the surface of the rough walls was covered by a layer of medium coarse sand (and in one case it was tooth shaped) while the surface of the smooth walls was lubricated by some lithium grease. For these reasons, it was decided to model the rough interface simply by connecting the wall elements directly to the soil elements, thus not allowing any slip; on the other hand, interface elements were used to link the wall elements to the soil elements when modelling the smooth interface.

CRISP allows the use of interface slip elements. Such an element is a flat 8-noded quadrilateral element with two 'dummy' nodes at the midpoints of the narrow edges (that is, they are not used in the analysis but they are numbered). The displacement is assumed to be linear along the narrow side of the interface element and quadratic along the other side. For this reason they can be connected to the linear strain triangles only through the long sides, whilst each narrow side shall be connected to another slip element, thus forming a chain surrounding the wall.

The stress-strain law of the interface elements is elastic and described by two stiffness parameters: k_n and k_s are the initial normal and the shear stiffness respectively and their value shall be consistent with the continuum at either sides of the element. After a limiting shear stress has been reached, the shear stiffness is instantaneously reduced to a residual value $k_{s,res}$. The value of the limiting shear stress can be fixed by a Mohr-Coulomb criterion: $\tau_{\lim} = c + \sigma_n \tan\phi$, where c and ϕ are arbitrary and convenient constants. Should the normal stress in the element become negative, the normal stiffness is reduced by a factor 10^{-5}. In this way, slip and separation between the two surfaces at the side of the slip elements are modelled by using a very stretchable and deformable elastic interface elements. A further parameter to be assigned is the thickness of the interface element t.

In Tab. IV.6 the values adopted for the parameters of the interface elements are shown.

Table IV.6 – smooth interface parameters

c	1 kPa
ϕ	0°
k_n	$1*10^5$ kPa
k_s	$3*10^4$ kPa
$k_{s,res}$	0.1 kPa
t	0.1 mm

The values of c and $k_{s,res}$ were determined from a parametric analysis which will be shown later on. The value of ϕ was set to zero, assuming that the adhesion between the soil and the wall is constant with depth. The values of k_n and k_s were calculated as follows:

$$k_n = \frac{(1-\nu)}{(1+\nu)(1-2\nu)} E = \frac{2(1-\nu)}{1-2\nu} G \qquad \text{(IV.8)}$$

$$k_s = G \qquad \text{(IV.9)}$$

where ν = 0.3 and G was calculated from the expression by Viggiani (1992) at the depth corresponding to the mid length of the wall, using the same parameters adopted for the soil.

The value of t seems not to be very important, because the shear stiffness of the element can be varied by changing $k_{s,res}$. In any case, a classical literature indication about the slenderness of a finite element suggests to keep $10 < L/t < 100$.

In order to analyse how the way of modelling the interface was sensible to the variation of the main parameters c and $k_{s,res}$, several analyses were run by changing these two values. In these analyses the soil was modelled by 3-SKH and the wall was 9.8 mm thick and 70 mm long, 1D away from the tunnel axis. The results at $-\Delta p/p_o$ = 30% (far enough from the failure) are shown in Fig. IV.18.

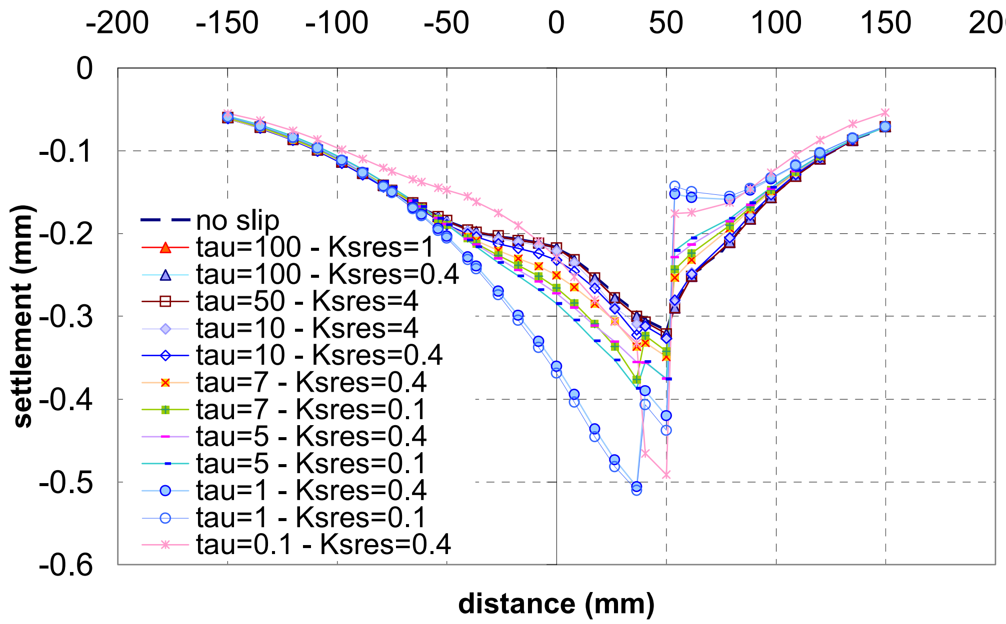

Figure IV.18 – Settlements of the nodes at depth –5mm for different values of the parameters τ (=c) and $k_{s,res}$ of the interface elements

In this figure the settlements at a depth z_m = 5 mm (z_p = 800 mm) are shown. It can be observed from an overall view that the curves appear to split into three groups. Several curves which do not show a clear discontinuity between the two sides of the wall belong to a first cluster: for comparison a dashed curve is also shown which refers to the analysis of a model with the same wall without slip elements (rough interface) and it can be seen that the curves of this first family are close to the 'no-slip' curve. In particular, the curves referred to $c > 10kPa$ coincide with the 'no slip' curve. On the other hand, when

$1kPa < c < 10kPa$ the relevant curves are clustered together in a second family and show a progressively increasing discontinuity between the two sides of the wall. The entity of the limiting shear stress τ_{lim} of the slip elements seems to be crucial for the wall to behave as a substantially rough or a completely smooth one: particularly, for values of $c = 1kPa$ (third group) there is a clear discontinuity between the soil and each side of the wall. Under this value, for $c = 0.1kPa$, the wall tends to punch the soil due to its own weight, but this behaviour was not observed in the tests. The influence of ϕ was not studied in depth because the reduction of the supporting pressure was practically undrained and the soil was overconsolidated, hence the possible dependence of the adhesion between the wall and the soil from the horizontal stress with depth was assumed to be negligible. The influence of the parameter $k_{s,res}$ was studied by varying its value between 4 kPa and 0.1 kPa (corresponding to about $k_s *10^{-4 \div -5}$) but the analyses which have been run did not lead to a clear indication of how much this value affects the generation of the gap between the two sides of the wall. This point was not examined furthermore as soon as it was observed that for the lower likely value of c (1 kPa) and low values of $k_{s,res}$ (0.1÷0.4 kPa), the gap was unaffected by changes in the residual shear stiffness of the slip element.

The results of this parametric study led to set in the analyses c=1 kPa and $k_{s,res}$=0.1 kPa, as shown before in Tab. IV.6, to model a completely smooth interface between the soil and the wall.

Results of the analyses: comparison between the two adopted constitutive laws

The results of the analyses of the reference model (without any diaphragm wall) are compared in this Chapter as performed by modelling the soil with Cam Clay and 3-SKH since its first consolidation under press.

In Figs. IV.19-IV.20, contours of the mean effective stress p' are reported as they result at various stages of reducing supporting pressure when soil is modelled with Cam Clay (Fig. IV.19) and 3-SKH (Fig. IV.20).

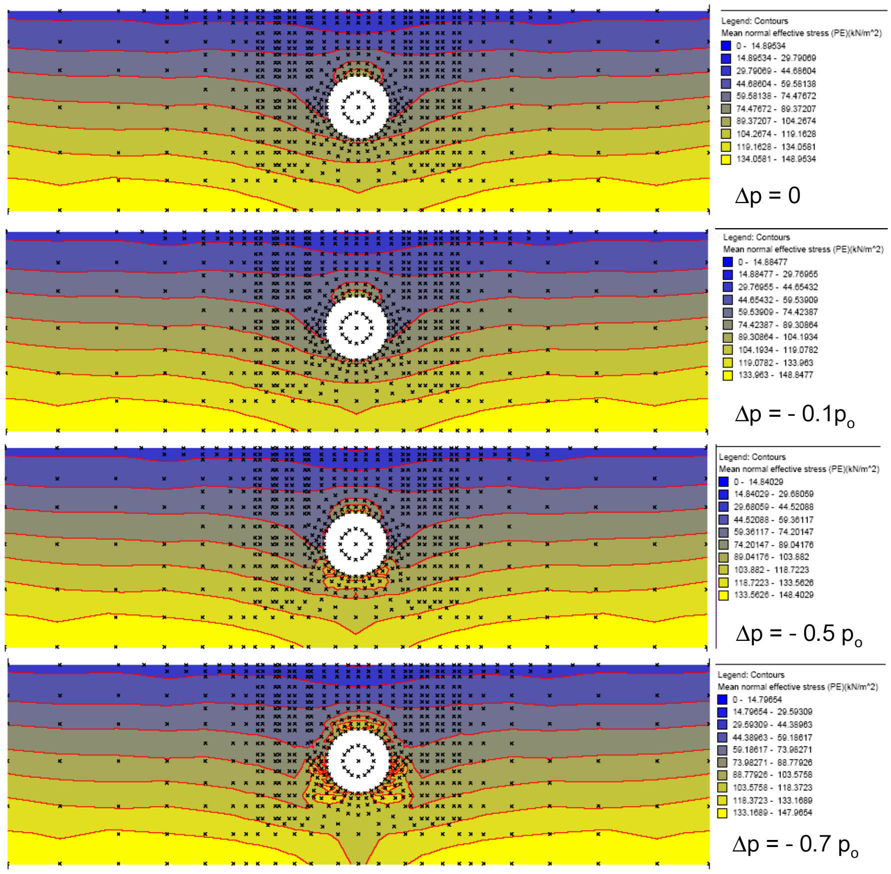

Figure IV.19 – contours of mean effective stress p' at various supporting pressures (Cam Clay)

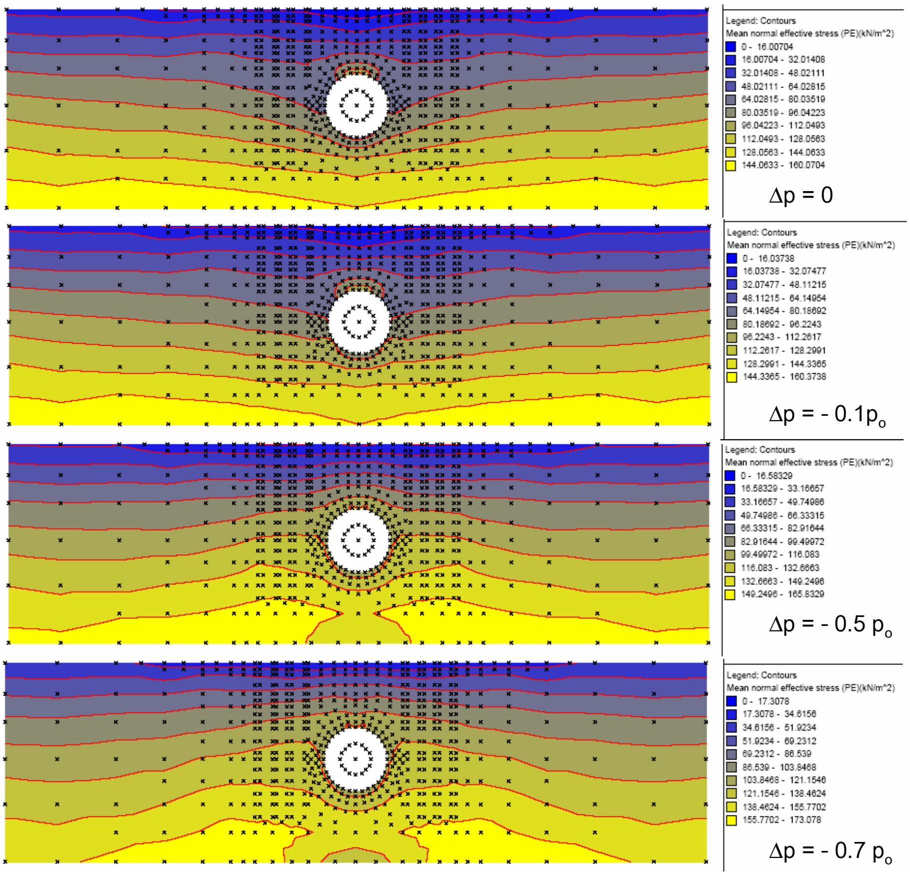

Figure IV.20 – contours of mean effective stress p' at various supporting pressures (3-SKH)

It can be observed in Fig. IV.20 that in the Cam Clay ground the changes in p' are localised around the cavity boundary. They start at the crown and affect the invert later on. The cover is practically not influenced by any change in the mean effective stress. With 3-SKH, on the contrary, the changes of p' are much more significant and they interest a wider area around the cavity. At first, only the crown is affected but as soon as the cavity support decreases, the mean effective stress increases over the whole tunnel cover.

The main differences between the two constitutive models are observed at $-\Delta p/p_o = 50\%$ in the cover: 3-SKH predicts p' varying from 15 kPa just below surface up to about 100 kPa at crown, whereas Cam Clay gives significantly lower values, between 60 and 75kPa, in a wide area around the upper arch from the mid-cover up to the axis level, a part from a narrow strip at crown where p' rapidly increases to about 100 kPa.

In Figs. IV.21-IV.22 the contours of the deviatoric stress $(\sigma_1 - \sigma_3)$ are shown.

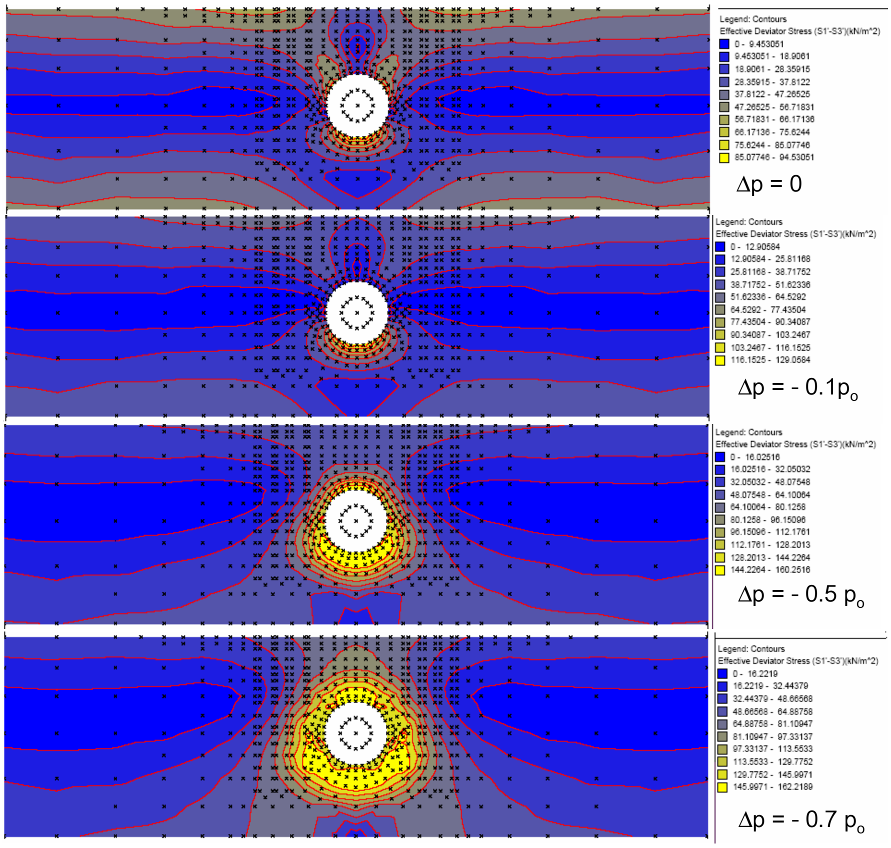

Figure IV.21 – contours of deviatoric stress $(\sigma_1 - \sigma_3)$ *at various supporting pressures (Cam Clay)*

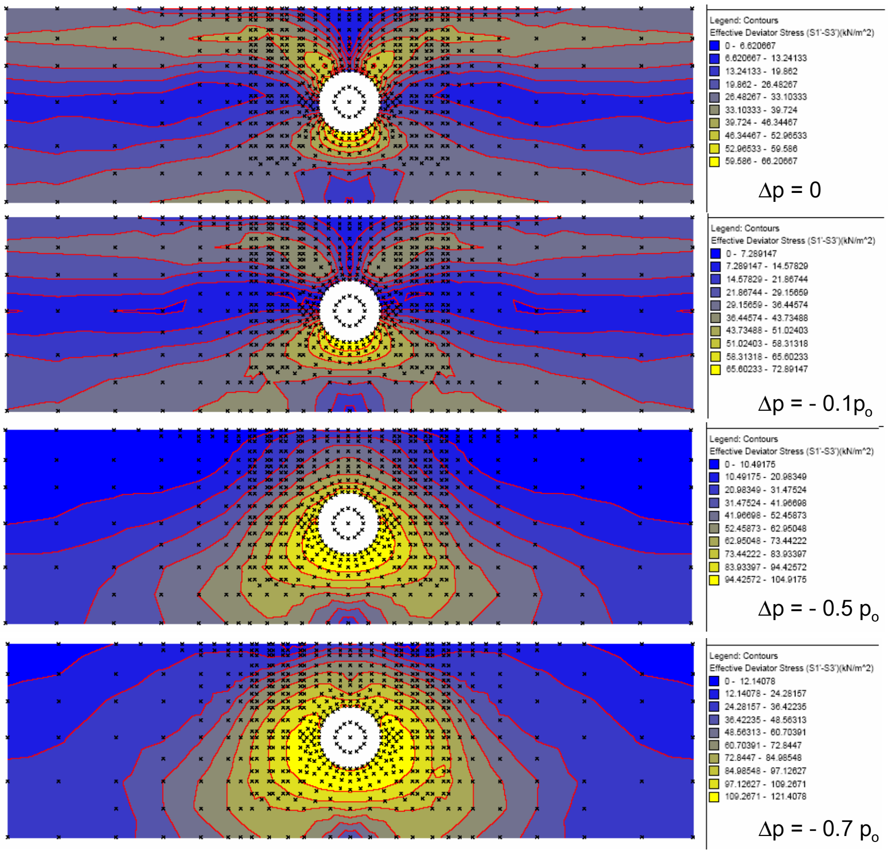

Figure IV.22 – contours of deviatoric stress $(\sigma_1 - \sigma_3)$ *at various supporting pressures (3-SKH)*

Before the tunnel support is reduced, the stress state follows from the internal supporting pressure which has been applied through the cavity boundary to the inertial stress distribution 'at rest'. Both models show an area around the tunnel axis level and about 1.5D away from the tunnel centre which has $(\sigma_1 - \sigma_3)$=0, because the principal stresses are close each other, hence K_o is close to 1, as it can be observed in Figs. IV.27-IV.28, which show the principal stress directions.

High values of $(\sigma_1 - \sigma_3)$ are computed at the tunnel invert by both models, even if Cam Clay predicts higher deviatoric stress (up to 95 kPa) than 3-SKH (up to 65 kPa). Also, a sort of ears where $(\sigma_1 - \sigma_3)$=50 kPa arise at both tunnel sides between the springlines and the crown, which bend horizontally in the 3-SKH model, where the deviatoric stress in the shallower ground is lower than in Cam Clay. This corresponds to lower horizontal stresses, consistently with the computed lower K_o values.

At lower support pressure (-Δp/p$_o$ = 50%), $(\sigma_1 - \sigma_3)$ tends to decrease from the cavity boundary outward. This happens with higher values and gradient in Cam Clay than in 3-SKH.

Moreover, at the same support pressure, the ground which is influenced by large changes in the deviatoric stress is limited around the cavity in the Cam Clay model, whereas it is widespread to the whole 3-SKH model.

Contours of the pore pressure changes during the undrained ‘excavation’ are shown in Figs. IV.23-IV.24. Cam Clay model predicts excess pore pressures almost close to zero all over the model, a part from a significant reduction of u at the tunnel invert. This corresponds to the observed larger variation of p’. At lower supporting pressures, the whole tunnel boundary is interested by a pore pressure gradient which is directed almost radially, but this affects a very narrow ring around the cavity. 3-SKH, on the contrary, gives rise to a large decrease of u around the tunnel, which begins at the invert. At -Δp/p$_o$ = 70% (close to the tunnel failure) the pore pressure gradient is directed almost radially, influencing the ground around up to about 1.5D from the tunnel centre.

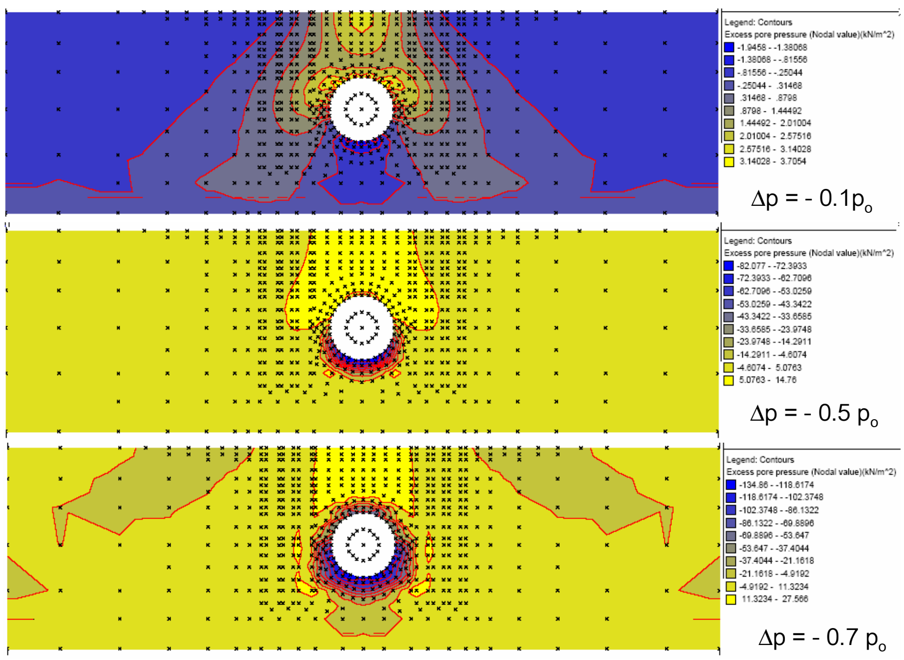

Figure IV.23 – contours of pore pressure changes at various supporting pressures (Cam Clay)

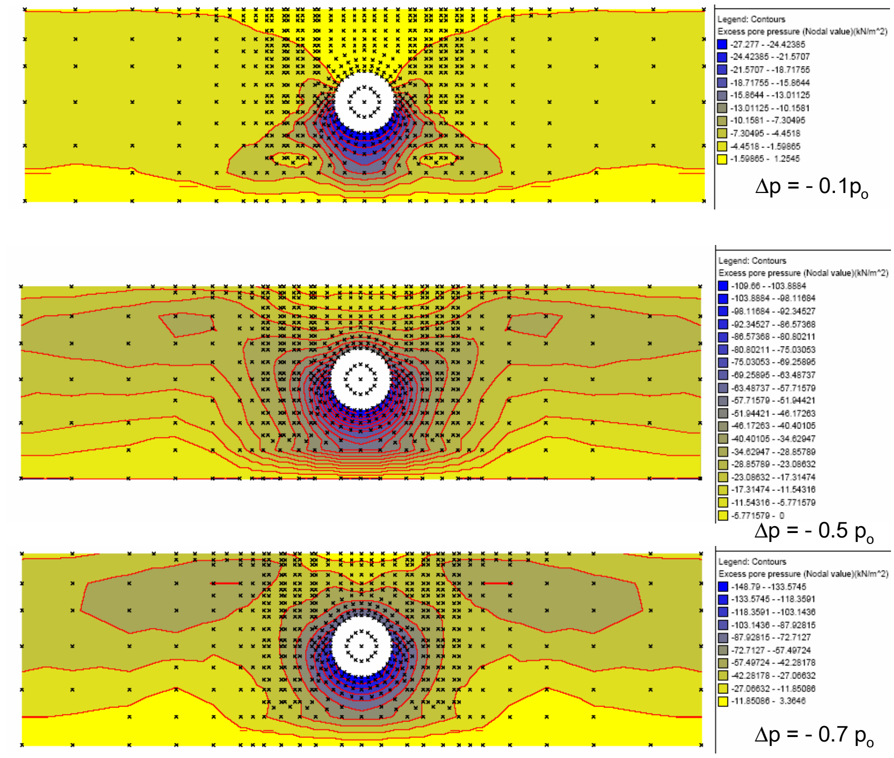

Figure IV.24 – contours of pore pressure changes at various supporting pressures (3-SKH)

These behaviours follow from the structure of the two constitutive laws. As a matter of fact, Cam Clay is elastic inside the boundary surface: this means that until the stress path does not reach the boundary surface, yielding does not start and pore pressure changes are not able to develop. On the contrary, 3-SKH can model yielding also inside the boundary surface, thus predicting pore pressure change in undrained conditions.

In Fig. IV.25-IV.26 contours of the deviatoric strain $\varepsilon_s = \dfrac{2}{3}\sqrt{\varepsilon_x^2 + \varepsilon_y^2 - \varepsilon_x \varepsilon_y + \dfrac{3}{4}\gamma_{xy}^2}$ are shown. It can be observed that the maximum deviatoric strain predicted at $-\Delta p/p_o = 10\%$ by using Cam Clay are about 0.4÷0.5% whereas they are 0.1÷0.2% by using 3-SKH. By looking at the stress state at the same pressure level, it has been noticed that whilst in Cam Clay all the integration points are in elastic state, in 3-SKH they are almost all in plastic conditions: the lower strain predicted by 3-SKH is attributable to the higher (non-linear) stiffness which is provided at low strain level.

At $-\Delta p/p_o = 50\%$ a narrow vertical area in Cam Clay can be observed where the deviatoric strain is higher than about 0.5% and increase up to about 2-3% at invert and crown. The soil is still in elastic state. At the same pressure, 3-SKH predicts a similar shaped region where the deviatoric strain is higher than about 0.5%, but it increases up to about 6% at the tunnel invert. As 3-SKH stiffness is non linear outside the small inner surface, this larger strain is justified.

Finally, at $-\Delta p/p_o = 70\%$, the deviatoric strain in Cam Clay increases until reaching locally almost 10% at the tunnel invert. The integration points in a ring around the whole cavity lie on the boundary (yielding) surface. In 3-SKH the deviatoric strain reaches values of about 12÷20% almost around all the cavity, apart from crown. At the same level no integration point lies on the boundary surface, most of them are on the history surface. Differently from Cam Clay, at this level the 3-SKH ground is collapsing.

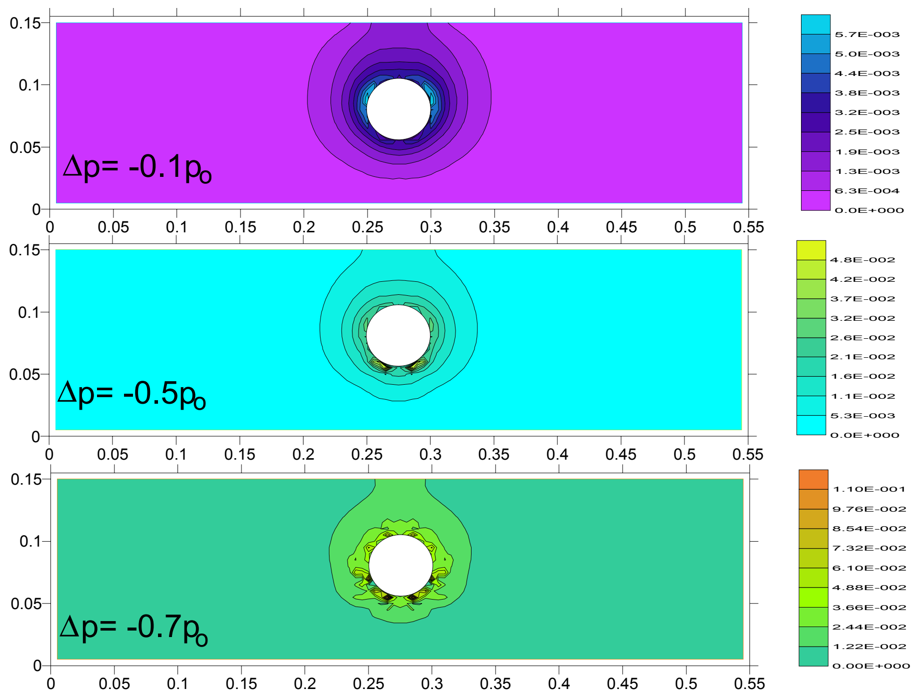

Figure IV.25 – contours of deviatoric strain ε_s at various supporting pressures (Cam Clay)

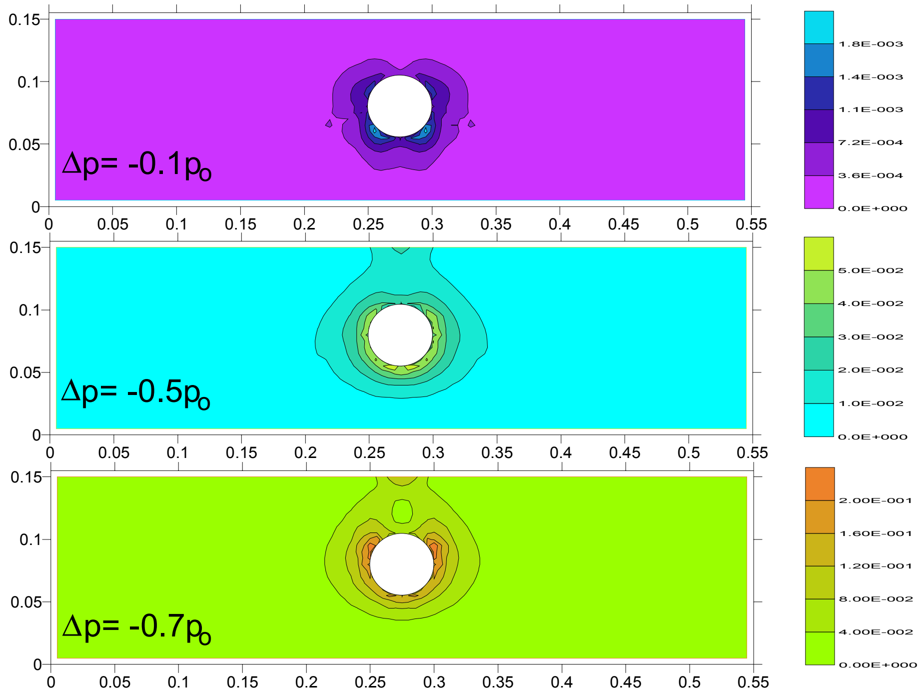

Figure IV.26 – contours of deviatoric strain ε_s at various supporting pressures (3-SKH)

In Fig. IV.27-IV.28 a plot of the stress directions are shown. It can be observed that initially $K_o>1$ above the tunnel axis model whereas $K_o<1$ below. At the end of the 'excavation' the first principal direction of stress are circumferential in a ring of ground over a span of about 1.5D from the tunnel centre; away from the tunnel, the first principal stress tends to be vertical. This condition occurs at $-\Delta p/p_o$ = 70% for 3-SKH, whereas for Cam Clay a higher pressure reduction has to be attained.

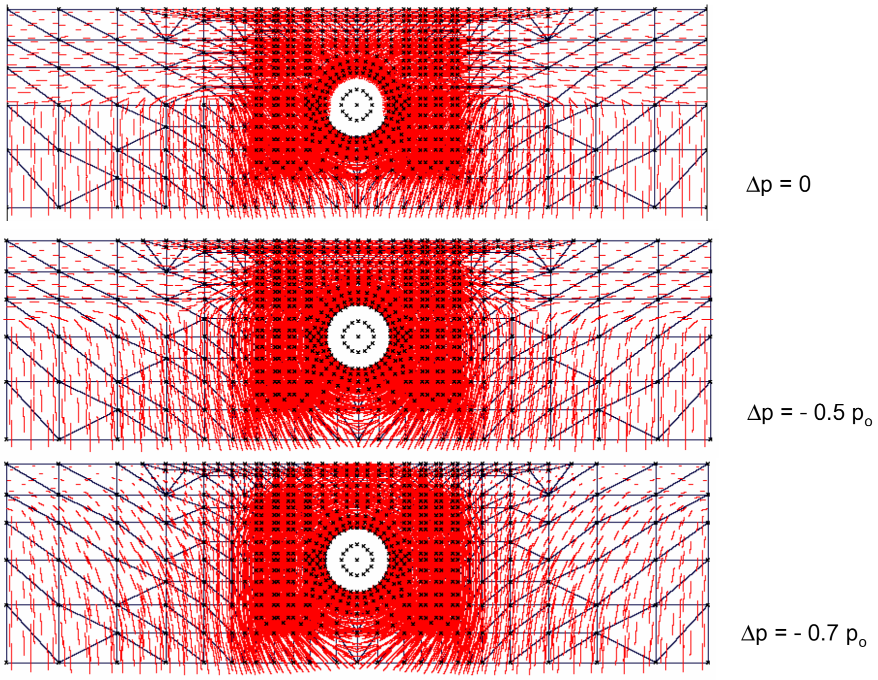

Figure IV.27 – principal stress directions at various supporting pressures (Cam Clay)

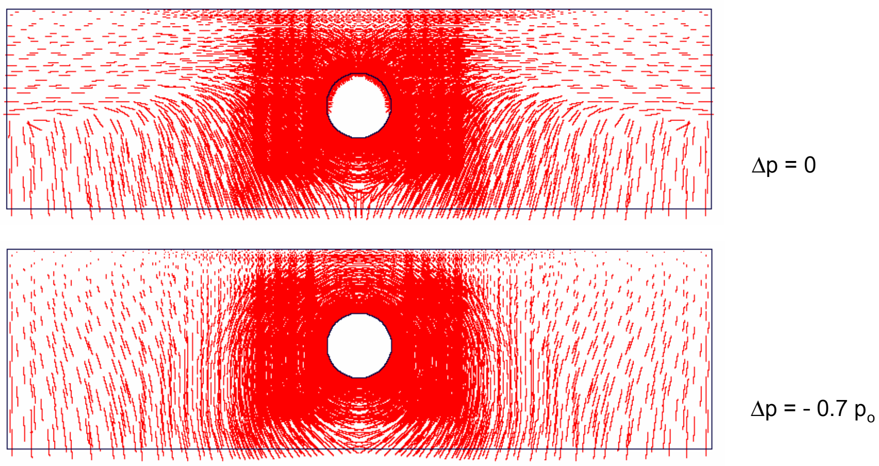

Figure IV.28 – principal stress directions at various supporting pressures (3-SKH)

Displacements fields predicted by the two models have been also compared at different stages.

In Fig. IV.29 the predicted ground movements at a supporting pressure reduction as little as 10% have been compared. At this level of supporting pressure, it can be expected that 3-SKH gives a much stiffer response than Cam Clay, as the strain level is low. As a matter of fact, 3-SKH computed displacements are lower than Cam Clay. Hence volume loss is also different: V'=0.3% is computed on the basis of 3-SKH prediction, V'=1% on the basis of Cam Clay. These values are close enough to those which usually occurs in practice. The difference between the two predictions is a consequence of different volume losses, which follows by different shear strains as computed at this level. Nevertheless, a major difference can be observed between the settlements and horizontal movements predicted above the tunnel. 3-SKH gives rise here to movements which are around one fifth of the corresponding Cam Clay predictions, whereas in the rest of the model the differences are lower.

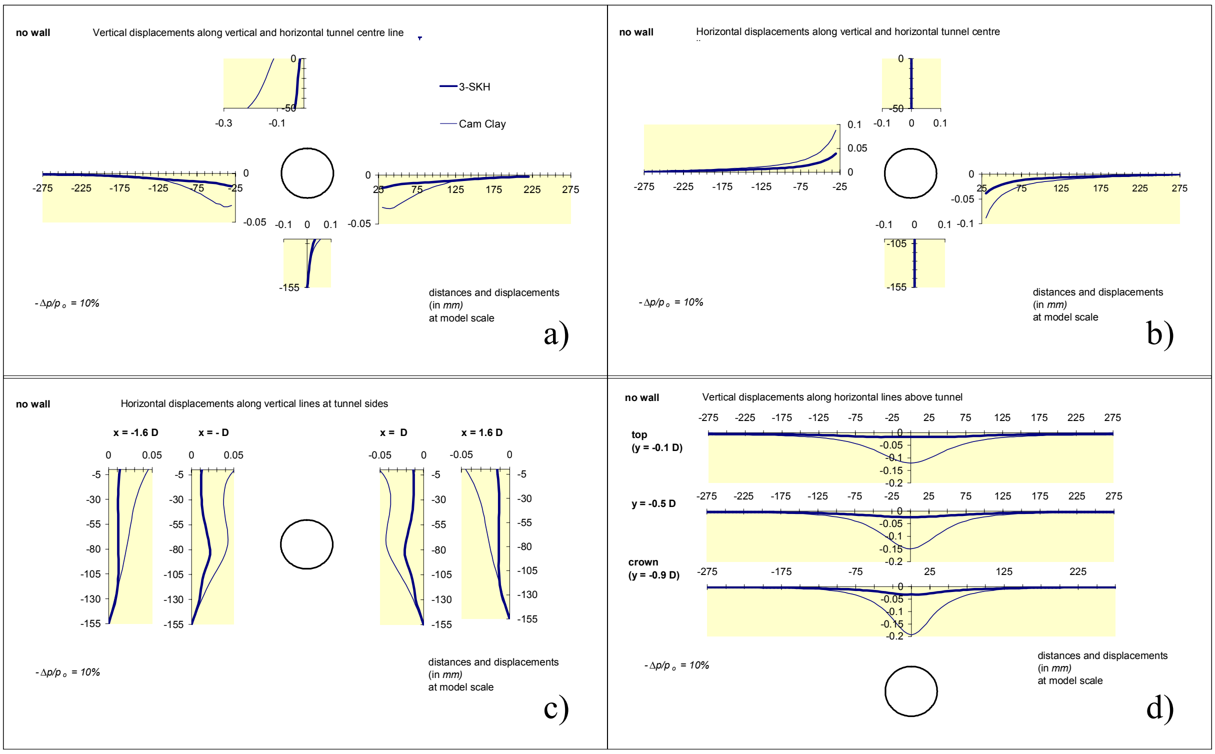

Figure IV.29 – comparison between the predicted ground movements at $-\Delta p/p_o = 10\%$

In Fig. IV.30 the predicted ground movements have been compared for a higher stress release. The supporting pressure in 3-SKH is higher (about $0.5p_o$) than in Cam Clay (about $0.3p_o$), but these values correspond to the same volume loss (V'≅10%), which is actually not very realistic in practice. It has been observed before that the two numerical model achieve the collapse at very different supporting pressures. If a load factor LF as defined by (III.1) is computed, it is equal to about 0.7 in both cases. This suggests that the amount of mobilised strength in the two models is the same and probably high enough to produce similar results: the behaviour of Cam Clay and 3-SKH at large strains, in fact, is ruled by the same set of mechanic parameters. By comparing the movements at this volume loss, it can be observed that they agree very well, apart from a slight difference on settlements above the tunnel.

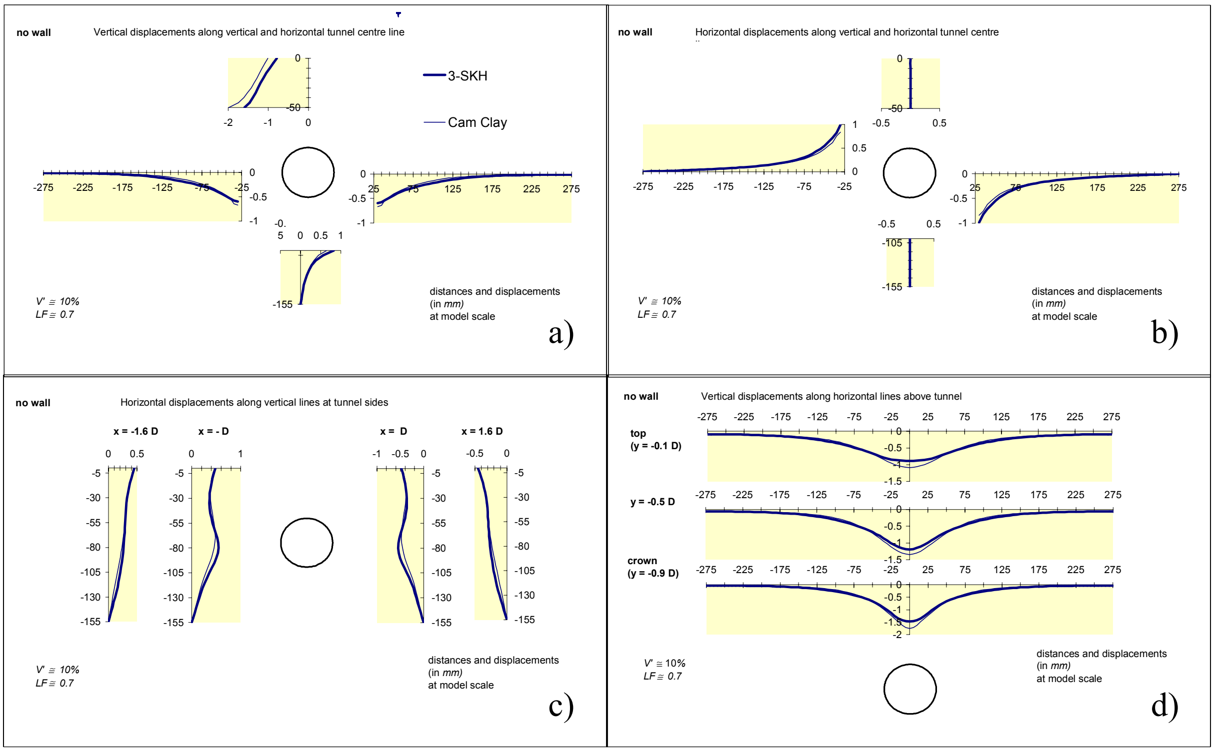

Figure IV.30 – comparison between the predicted ground movements at V' ≅ 10% (LF ≅ 0.7)

Some of the issues which have been observed above, will be considered and discussed in the next paragraph, where the numerical predictions are compared to the test measurements.

Comparison between numerical and experimental results

In the followings, the results of the numerical analyses performed with the two models will be compared to the tests results.

In Fig. IV.31 the maximum settlements $S_{v,max}$ at depth –5 mm, both numerically calculated and experimentally observed, are plotted for different percentages of pressure reduction.

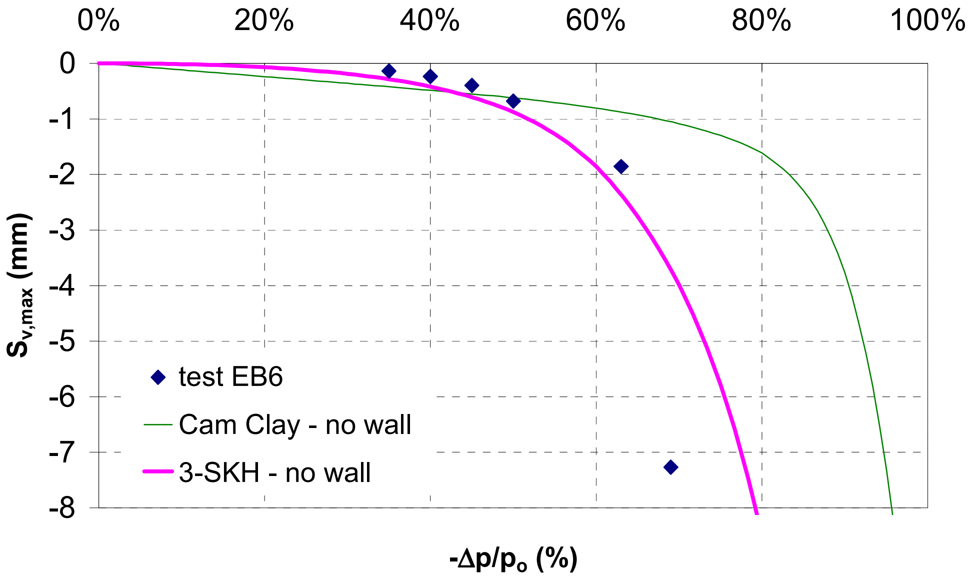

Fig. IV.31 - Maximum settlement at depth –5mm vs *percentage of supporting pressure change in both numerical and physical models without wall.*

The comparison between the two numerical models shows that Cam Clay predicts a quasi-linear variation of settlement with decreasing pressure until about $-\Delta p/p_o$=50%. On the contrary, the curve pertaining to the 3-SKH model appears clearly non-linear since the beginning. The value of pressure at which the cavity is collapsing is different between the two models: in the 3-SKH analysis at $-\Delta p/p_o$=80% the settlement is very large, denoting that the cavity is collapsing; on the other hand, at the same pressure the calculated settlement in the Cam Clay analysis is still low and the following curve is approaching an asymptote at about 95% of pressure reduction. These behaviours are consistent with the fact that in a large area around the tunnel the stress paths evolve inside the state boundary surface where Cam Clay computes only elastic strains with a constant stiffness whilst 3-SKH allows developing plastic strains with decreasing stiffness. By looking to the settlement as measured during the test, it is evident that the 3-SKH model is able to reproduce the physical behaviour much better than Cam Clay: the 3-SKH curve is very similar to the experimental curve until about $-\Delta p/p_o$=60%. After this point, in the test the cavity approaches collapse while the numerical model is still showing hardening: the numerical analysis appears not accurate enough at this stress level. Moreover, looking back to Fig. IV.12, the higher stress release allowed by Cam Clay is consistent with the higher available undrained strength predicted by Cam Clay before the 'excavation' stage.

In Fig. IV.32 the percentage of supporting pressure reduction inside the cavity is plotted against the calculated and measured volume losses.

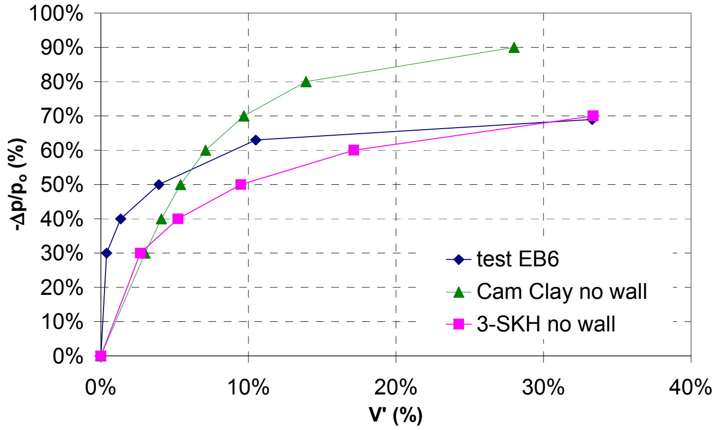

Figure IV.32 - Percentage of supporting pressure change vs *volume loss in both numerical and physical models without wall.*

The numerical and experimental values of the volume loss at the same pressure are rather different. The 3-SKH analysis tends to overestimate the 'volume loss' but the difference with the measured values decreases when a general failure is forthcoming. On the other hand, the volume loss as calculated by Cam Clay is close to the 3-SKH until 30%-40% of pressure decrease, after which this model is much 'stiffer', as observed before.

A similar chart is shown in Fig. IV.33 where the load factor is plotted along the volume loss. This chart hides the high underestimation of the collapse pressure by Cam Clay, but it highlight similarities and differences between the two models at the same level of 'global' mobilised strength, and in particular the linear behaviour of Cam Clay where 3-SKH is already non-linear.

The collapse pressure in the two numerical analyses has been computed by fitting an hyperbola to the points in the p:V' plane and assuming that collapse occurs at 90% of the asymptotic value: this gives p_{ult}=6 kPa in Cam Clay and p_{ult}=52 kPa in 3-SKH, whereas p_{ult}=59 kPa was assumed by the test results. This chart shows again that both models predict larger volume losses than measured and that they differ particularly at low load factors, where the prediction of 3-SKH is more accurate than Cam Clay.

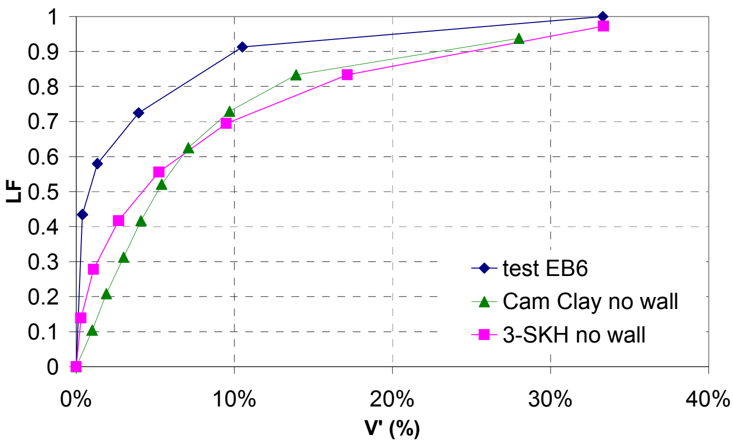

Figure IV.33 - Load factor vs *volume loss in both numerical and physical models without wall.*

In Fig. IV.34 the pore pressures as measured at the location of PPT1 and PPT2 in tests EB6 (no wall), EB5 (short, thick and rough wall) and EB12 (short, thick and smooth wall) have been plotted together with the numerical predictions. The kinks in the experimental curves correspond to tunnel failure.

It can be observed that 3-SKH predictions are usually much better than Cam Clay. As a matter of fact, Cam Clay does not predict significant pore pressure changes until yielding occurs: in fact, Cam Clay response is elastic until the clear kink in the curve which denotes yielding. After that, the pore pressure quickly decreases due to plastic dilatant behaviour. On the other hand, yielding is predicted very soon by 3-SKH. It is worth noticing that the initial decrease of pore pressure as predicted by 3-SKH is often higher than that observed in the measurements.

As a general comment, these diagrams indicate that 3-SKH model is more successful in predicting the actual paths of the effective stresses during the 'excavation' .

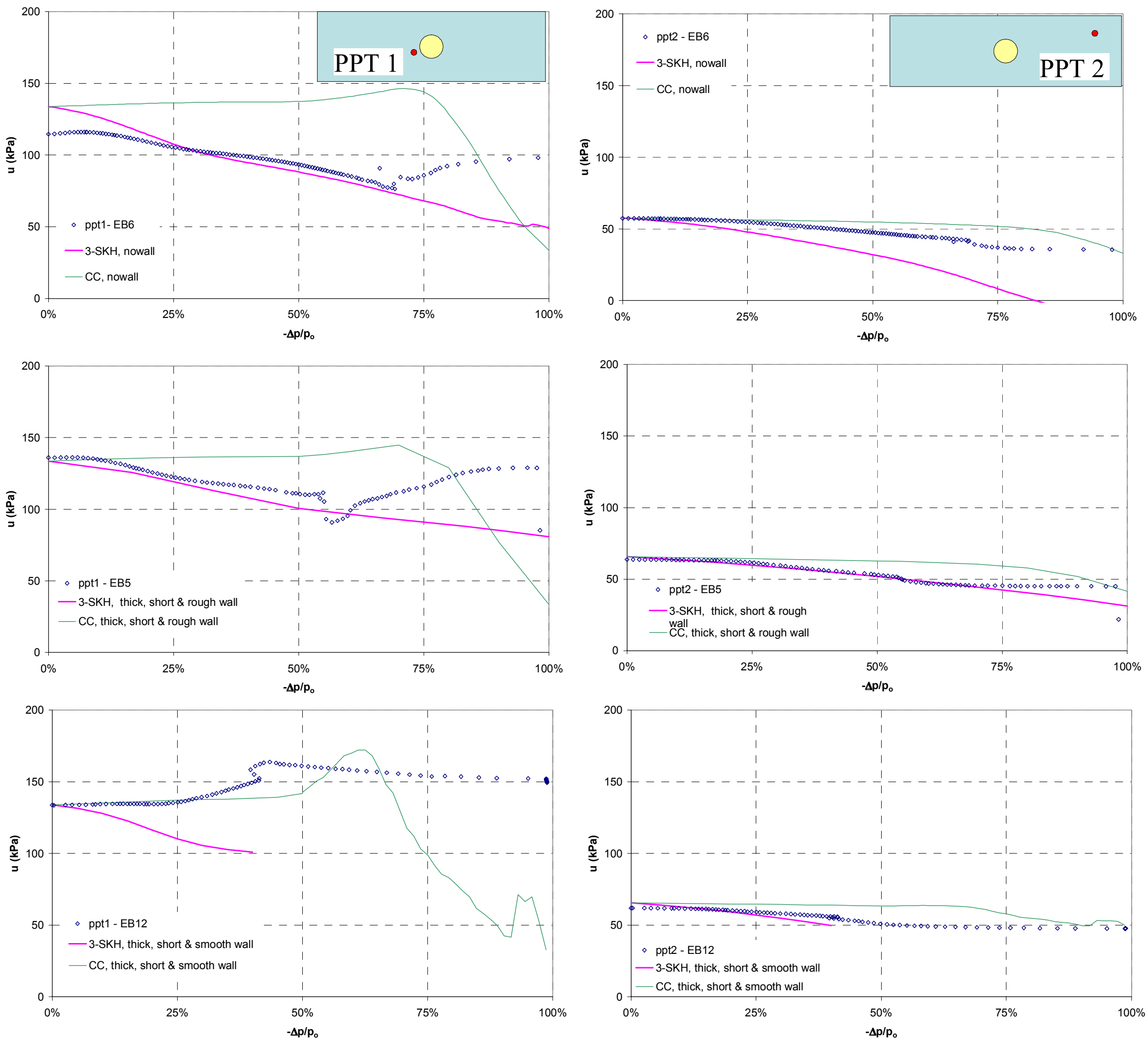

Figure IV.34 - Measured and predicted pore pressures at the locations of PPT1 and PPT2.

The normalised settlement profiles at –5mm from the surface are shown in Fig. IV.35, as measured and calculated in the configuration without wall at various levels of the cavity supporting pressure. Apart from some scatter in the data at the first stages of the test due to the already discussed errors in measurements, the subsequent normalised curves from the different stages of test superimpose each other. This indicates that the pattern of movements in the field is independent of the level of supporting pressure, at least in the explored pressure range (between 70% and 50% of the initial value) in which the observed volume loss varies between 0.5% and 4%. These latter values are in the range of the volume losses which can be commonly encountered in practice. A Gaussian curve has been fitted in the data as described in Chapter III.

In the computed settlement profiles, whilst the normalised curves from Cam clay are very close each other, but this does not happen to the 3-SKH curves: these tend to be narrower at larger strains. This behaviour was already observed by Grant (1998) in numerical analyses of centrifuge tests with deeper tunnels. At $-\Delta p/p_o$=60%, when large strains occur, the settlement profile computed by 3-SKH is close to that by Cam Clay, as it must be expected because the adopted parameters for the boundary surface in the two models are the same.

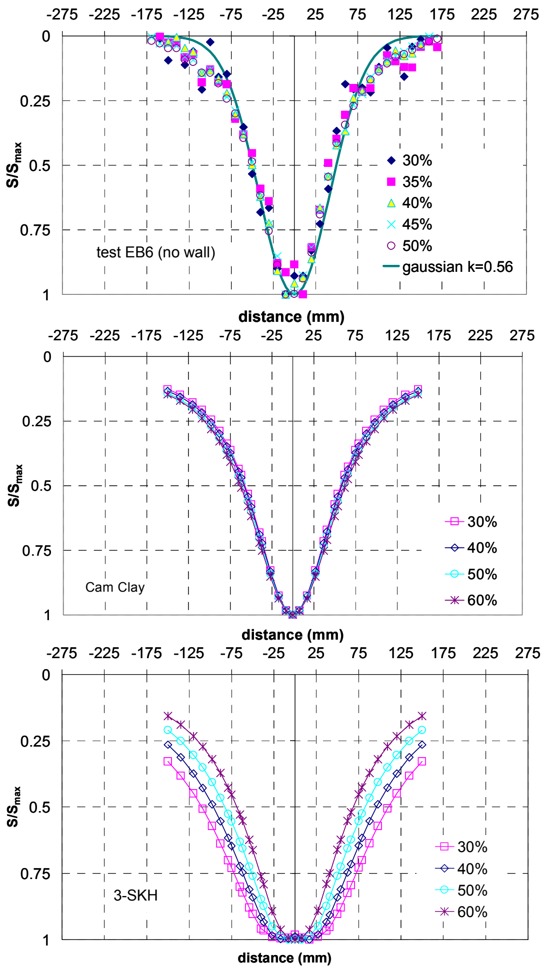

Figure IV.35 - Normalised settlement trough at different supporting pressures in the experimental and numerical analyses – configuration without wall.

The settlements and horizontal displacements as measured and calculated at $-\Delta p/p_o \cong 40\%$ in three different configurations (no wall, rough wall, smooth wall) at the depth –5 mm are compared with the relevant experimental measures in the Figs. IV.36-IV.38. For this comparison, a short and thick wall, one diameter away from the tunnel axis has been chosen, but the observed patterns are more general.

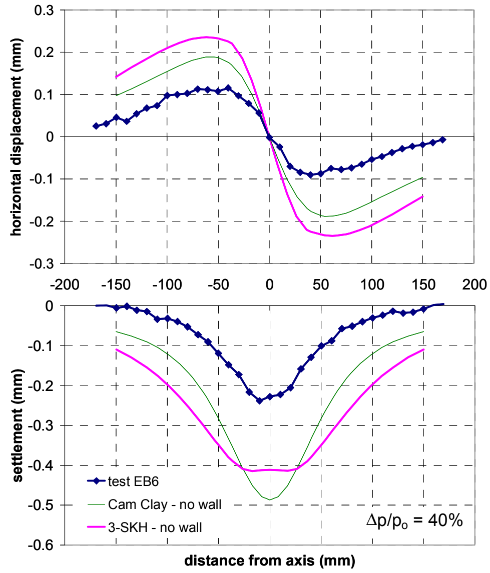

Figure IV.36 - Comparison between computed and measured displacements at depth –5mm in the model without wall

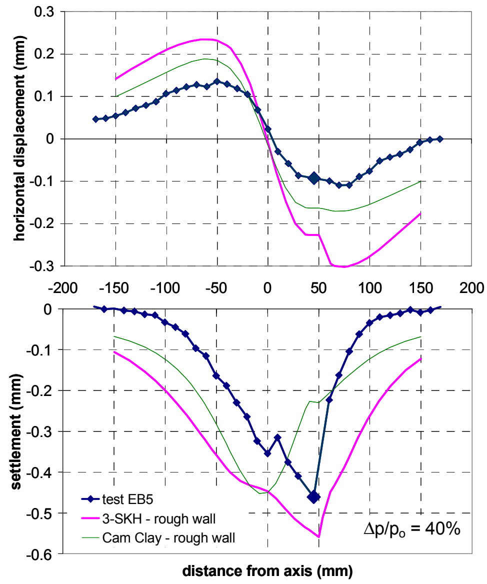

Figure IV.37 - Comparison between computed and measured displacements at depth –5mm in the model with a rough wall

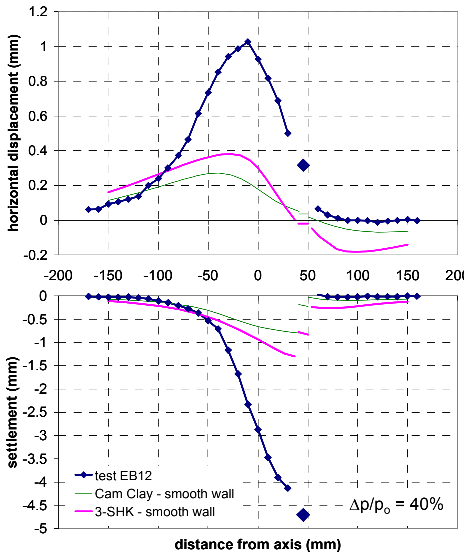

Figure IV.38 - Comparison between computed and measured displacements at depth –5mm in the model with a smooth wall

When comparing the curves related to the configuration without wall, it can be observed that both the numerical models overestimate the displacements at this pressure level, giving values of the maximum settlement twice as large as the measured ones. By looking again at Fig. IV.31 it can be seen that the predictions with the 3-SKH model improve noticeably at larger deformations, whilst the predicted maximum settlements with the Cam Clay model are much lower than the measured ones after the supporting pressure has been reduced at less than 50%.

The chart showing the settlement profiles of the models with a rough wall indicates that 3-SKH is able to reproduce the large vertical movement of the wall as it has been observed in the test: Cam Clay, on the contrary, predicts a completely different pattern. Looking back to Fig. IV.34, where the experimental results for rough walls are plotted, it can be observed that this large settlement affects not only the short and thick wall located one diameter away from the tunnel axis, but also the same wall at 1.5D and the long and thick wall at 1D. The numerical analyses with 3-SKH (which will be shown later) confirm the behaviour of both the short walls, whilst predict a different behaviour for the long wall. On the contrary Cam Clay is not able to describe in any case this phenomenon which is largely dependent on the stress state predicted in the area between the wall and the cavity.

In order to observe how the patterns of surface settlements are modified by the presence of an embedded wall, no matter their actual magnitude, in Fig. IV.39 the computed and measured settlements have been plotted after they were divided by their maximum value $S_{v,max}$.

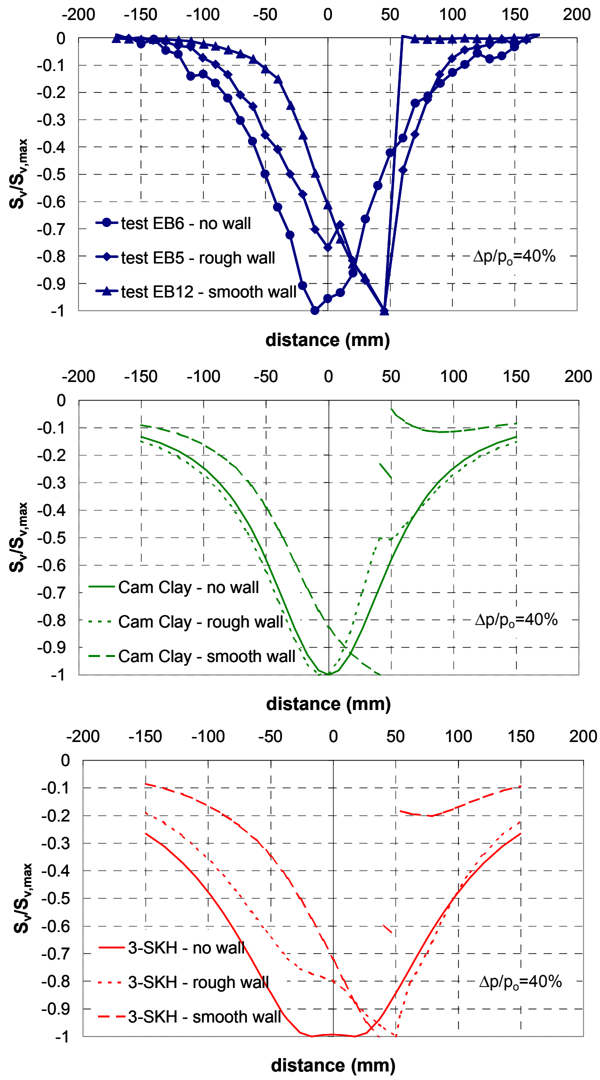

Figure IV.39 - Comparison between computed and measured normalised settlements at depth –5 mm

At a first glance the patterns of the calculated settlements are reasonably similar to the measured ones, even if some significant differences still persist. For the evidences discussed above, the test and the numerical patterns with Cam clay can be considered independent of the particular stage of test at which they are referred. On the contrary, the results with 3-SKH cannot be directly generalised to the whole development of the analysis.

In the following Figs. IV.40-IV.42 the ground movements as measured in tests EB6, EB5 and EB12 at the same amount of stress release ($-\Delta p/p_o$=30%) are compared to Cam Clay and 3-SKH predictions. This value has been chosen because it gives rise in both models without wall to the same amount of volume loss approximately (*cf.* Fig. IV.32). At lower pressure releases, the comparison with measurements would not have been possible, as they are not accurate enough.

Volume losses to which the measured and computed ground movements refer are shown in Tab.IV.7.

Table IV.7 – volume losses of ground movement fields shown in Figs. IV.40-IV.42

	volume loss V’		
	measured	computed (Cam Clay)	computed (3-SKH)
no wall	0.4%	3%	2.7%
rough wall	0.6%	2.8%	3.2%
smooth wall	1.2%	1.6%	0.9%

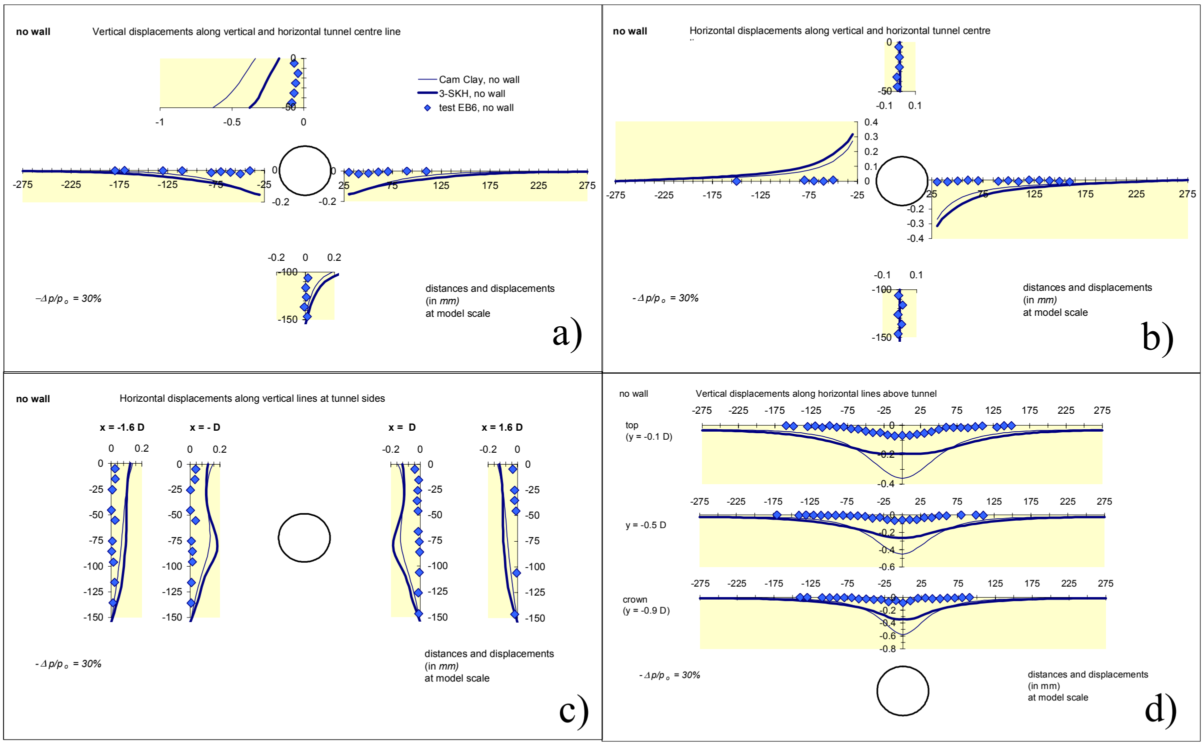

Figure IV.40 - Measured and predicted ground movements in models without diaphragm wall at-$\Delta p/p_o$=30%.

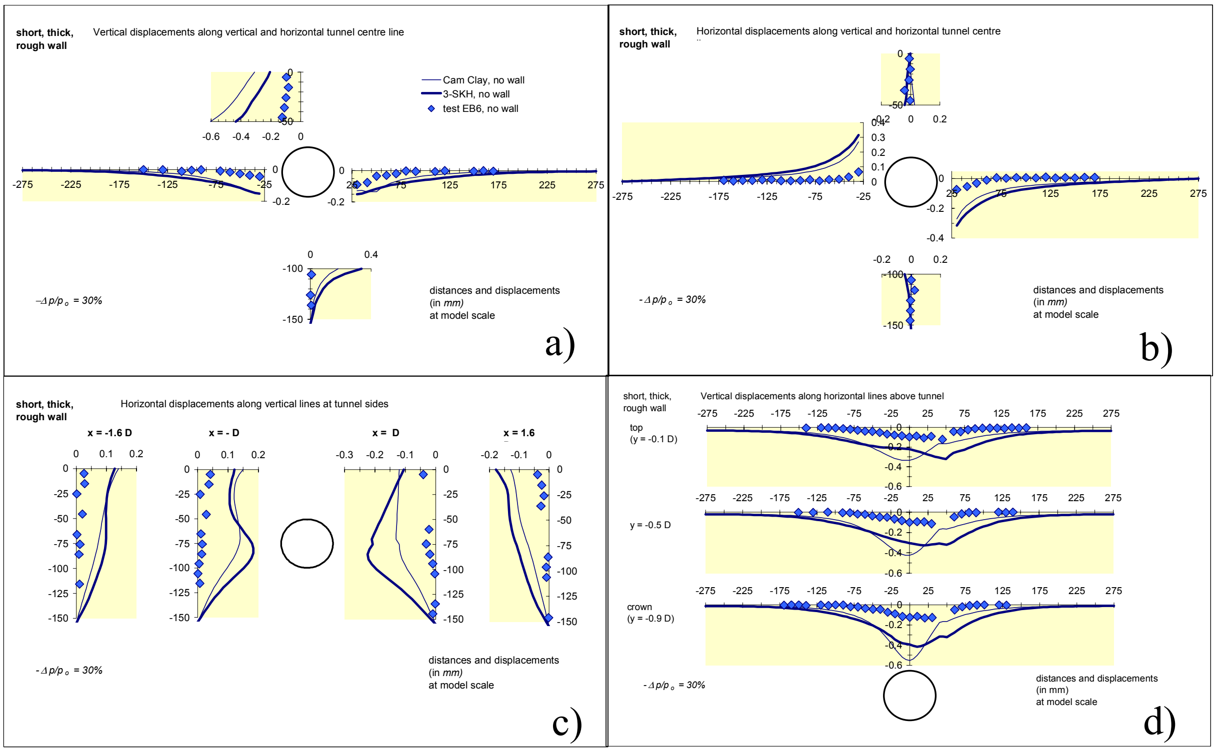

Figure IV.41 - Measured and predicted ground movements in models without a rough diaphragm wall at-$\Delta p/p_o$=30%.

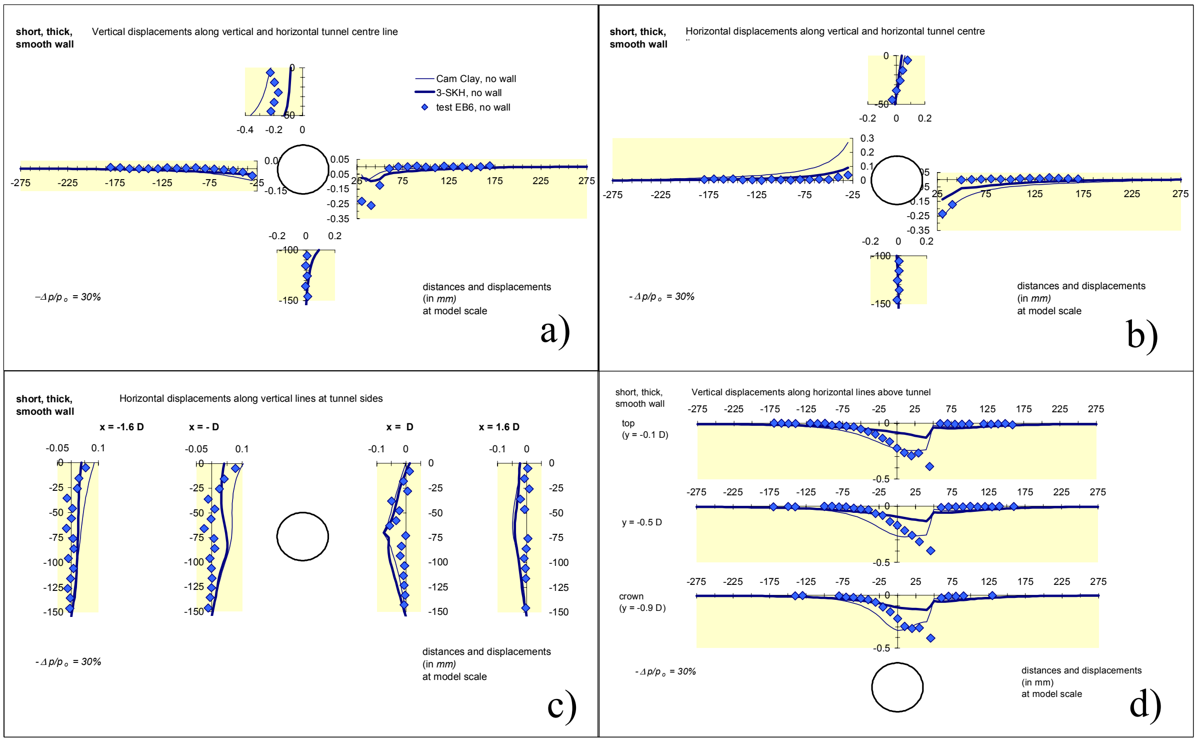

Figure IV.42 - Measured and predicted ground movements in models with a smooth diaphragm wall at-$\Delta p/p_o$=30%.

It can be observed that some aspects of the overall behaviour are reproduced by the numerical analyses, some others are not.

The magnitude of predicted movements, at least in the first two cases (Figs. IV.40 and IV.41), is higher than measured. This could be also deducted by observing the maximum settlement Fig. IV.31.

The main differences between ground movement predictions in the no wall case (Fig. IV.40) arise on the settlement troughs and they have been discussed before.

As far as the rough wall model is concerned, 3-SKH seems to overestimate the wall rotation (Fig IV.41-c, x=D), if compared to Cam Clay and to measurements. In general (*cf.* also no wall model in Fig.IV.40.) the horizontal movements predicted at the tunnel axis level are higher than in Cam Clay

The agreement between predicted and measured movements in Fig. IV.42 (smooth walls) seems higher. Still, the major difference between Cam Clay and 3-SKH arises in the settlement profiles above the tunnel. Even if Cam Clay prediction is closer to measured settlement at the top, at deeper levels it cannot be stated which model gives better predictions, as it depends on what particular point is observed.

Up to this point, comparison between measured and computed ground movements have been done at the same amount of supporting pressure. This seemed a natural consequence of the fact that in the performed tests the supporting pressure was controlled, whereas volume loss was only computed. Nevertheless, in practice volume loss is a design parameter, particularly used to predict field ground movements. Hence a comparison is shown in Fig. IV.43 between numerical and experimental results at V'≅3%. In Tab. IV.8 the relevant support pressures and load factors are shown. It can be noticed that the computed displacements are the same which are also shown in Fig. IV.40.

Table IV.8 – support pressures and load factors of ground movement fields shown in Fig. IV.43

	measured	computed (Cam Clay)	computed (3-SKH)
support pressure	101 kPa	133 kPa	133 kPa
pressure change	-47% p_o	-30% p_o	-30% p_o
load factor	0.68	0.31	0.42

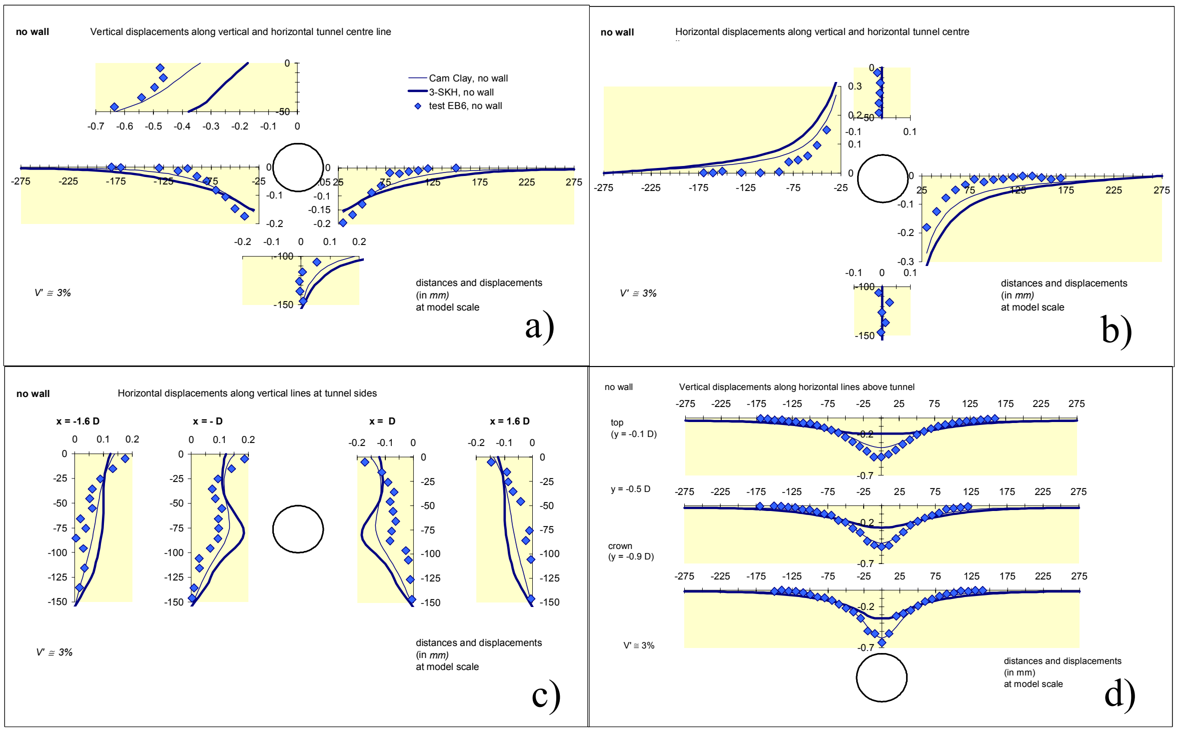

Figure IV.43 - Measured and predicted ground movements in models without diaphragm wall at V'≅3%

This comparison shows a better agreement between experimental data and numerical prediction than observed in Fig. IV.40 at the same supporting pressure. Particularly, Cam Clay settlement trough seems to be very satisfactory. But it is not surprising that by comparing the results at the same measured volume loss, the magnitude of displacements has to be very similar, if not the same. It seems more important to highlight that this kind of charts 'hides' the fact that the ground movement profile refers to different supporting pressures in the experimental and numerical models. This means that the stress levels in the experiment and in the corresponding numerical analysis are different, at the same V'. As far as the target is to model a centrifuge test, where a very specific stress state is induced, it seems thus obvious that comparing at the same V' is probably not very useful.

In general, if the reliability of the prediction is a matter of concern, particular care should be given to the capacity of extrapolating numerical results to different conditions. From this point of view, there is no doubt that 3-SKH is an improvement of Cam Clay for overconsolidated clays, even if, for this particular case, Cam Clay gives reasonable predictions of the pattern of vertical deformation above the tunnel. As a matter of fact, Cam Clay seems to be unable to predict the pattern of movements in the vicinity of the wall, which is a key issue for this problem.

At the end of this section, it seems hence possible to conclude that it appears more reliable to adopt 3-SKH to perform numerical analyses of boundary value problems which cannot be directly compared to measured ground movement fields.

Analysis of the numerical results

In the following, the main results of the set of numerical analyses defined in Tab. IV.9 will be discussed. The attention will be focussed on the analyses in which the 3-SKH model has been adopted: as discussed in the previous section, this model is more able than Cam Clay to capture some aspects of the problem which depend on the recent stress history and cannot be neglected in order to understand the observed behaviour in physical modelling.

Table IV.9 - Geometrical characteristics of the wall

length (mm)	thickness (mm)	distance (mm)	interface
70 – 120	0.8 – 9.5	50 - 75	rough – smooth

In Figs. IV.44-IV.47 the results from 17 analysed cases are shown. The settlements and the horizontal displacements at the soil surface in the zone of interest behind the wall (away from the tunnel) are reported together with the values of the slope θ and horizontal strain ε_h as calculated by differentiating polynomial functions fitted in the displacement profiles. These latter parameters are important when describing the damage to buildings affected by ground movements at the foundation level (Burland *et al*., 1977). The calculated slope θ of the settlement profiles is not often used as a direct indicator of the level of damage, but it can be used as a very conservative assessment of the distortion which affects an existing building. A reduction in slope should correspond to a reduction in distortion.

All the charts refer to a supporting pressure equal to 60% of the initial pressure p_o. The choice of comparing results at the same supporting pressure has been justified in the previous section. This pressure corresponds to that, which in the reference test without wall (EB6) gives rise to V'=1.35%, which is an average value in field.

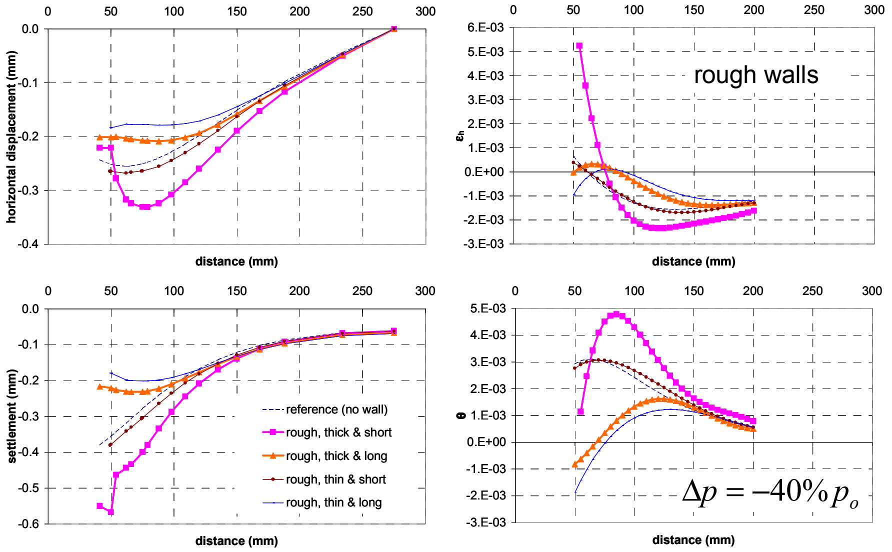

Figure IV.44 - Displacements, slopes and horizontal strains behind the wall – rough walls, 1D away.

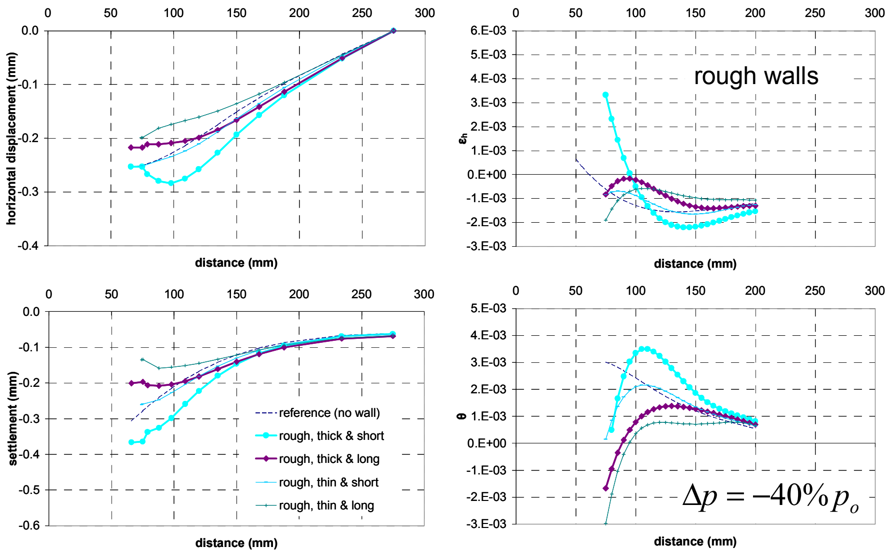

Figure IV.45- Displacements, slopes and horizontal strains behind the wall – rough walls, 1.5D away.

In Figs. IV.44-IV.45 the settlements behind the rough walls are shown together with the reference profile referred to the model without wall. Both thick and thin rough walls do not reduce settlements when they span from the surface until about the tunnel axis depth (short walls). This behaviour seems to be independent of the offset of the wall from the tunnel. The thicker (hence heavier) the wall the more the settlement behind it increases compared with its homologous in the configuration without wall. Very flexible short walls do not modify too much the reference profile. On the other hand, longer walls, both thick and thin, reduce settlements and horizontal displacements over an extent of about one diameter behind the wall. This reduction is larger immediately behind the wall and ranges between one half and one third of the reference settlement, respectively for the thinner and the thicker wall. The reduction on the horizontal displacement is lower.

Concerning the calculated slopes θ of the settlement profiles behind the rough walls, the influence of the wall covers an extent of about two diameters behind. The short and thick walls increase rotations in this area, except inside a very limited distance from the wall, while the short and thin ones do not change sensibly the reference values (which are between 10^{-3} and $3*10^{-3}$), except when located far away from the tunnel. On the contrary, long walls are able to reduce rotations up to zero and even to invert their sign. This means that an area which is subjected to hogging in the configuration without walls, is now sagging with beneficial effects on the possibly existing structures.

The maximum computed reference horizontal strain ε_h is tensile and equal to about $1.5*10^{-3}$: this value is not particularly high but it can require protective measures if combined with large distortions. Long and rough walls reduce this strain until zero at some points and generally provide a certain degree of reduction within a distance of about 2-2.5D behind the wall. Nevertheless, the effect in the zone immediately adjacent to the wall itself is negative because the horizontal strains are tensile and sometimes higher than the reference ones. Short and thin wall are practically ineffective on the horizontal strains, whilst short and thick are able to turn the horizontal strain from tension to compression in a zone of about 0.5D behind them.

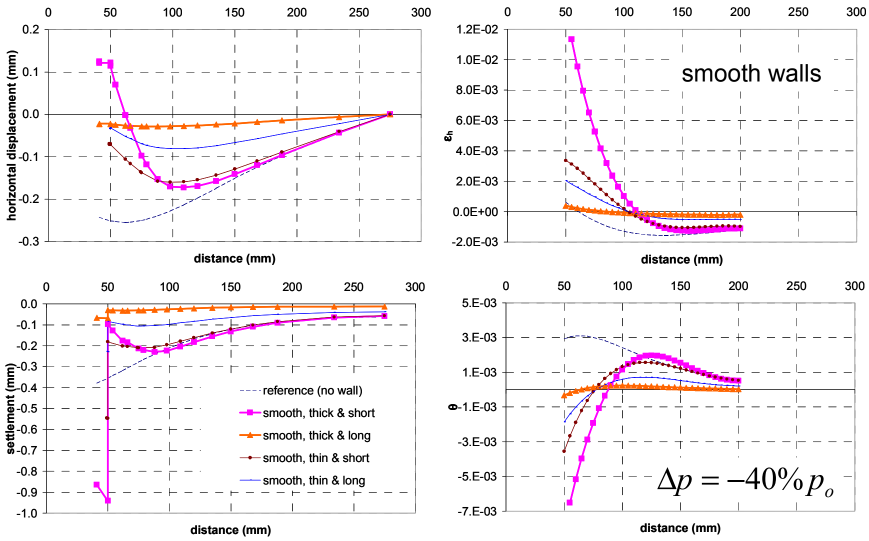

Figure IV.46 - Displacements, slopes and horizontal strains behind the wall – smooth walls, 1D away.

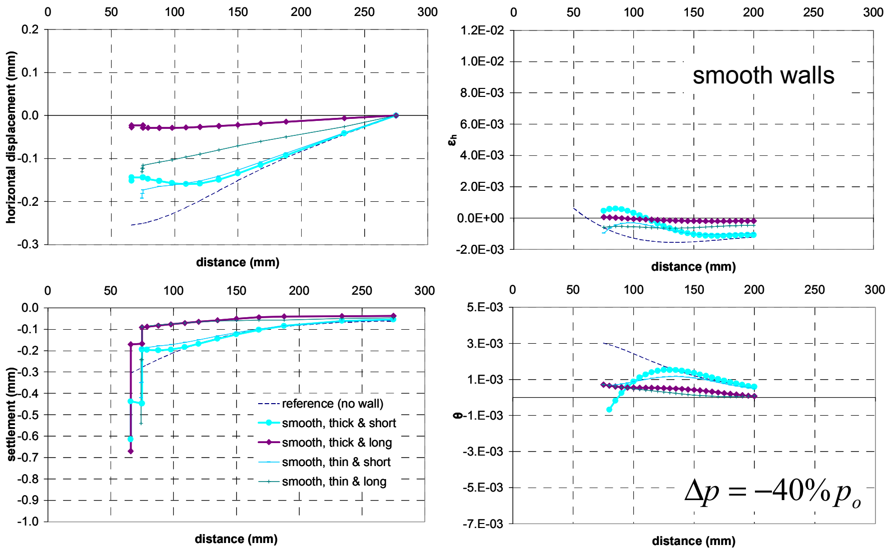

Figure IV.47 - Displacements, slopes and horizontal strains behind the wall – smooth walls, 1.5D away.

In Figs. IV.46-IV.47 the settlements behind the smooth walls are shown. It can be observed that all the walls provide a certain degree of reduction of settlement at their back. Both the entity of this reduction and its extent behind the wall seems to be less dependent on the thickness of the wall than on its length. The influence of the short walls, in fact, is limited to about one diameter behind them, whilst that of the long walls is still evident a few diameters far away. The longer walls provide a reduction in settlements up to about one tenth behind the walls closer to the tunnel, but this volume decreases when increasing the wall offset from the tunnel. The reduction of the horizontal displacements is generally much larger for the thicker walls.

As far as the slope θ is concerned, it can be observed that all the walls reduce its value at their back up to different distances. The shorter walls influence a smaller extent, nevertheless they are able in most cases to invert the sign of θ: a span which was interested by hogging in the reference model is now sagging. This phenomenon was observed above for rough and long walls: it has to be highlighted that the long walls, both smooth and rough, are able to invert the concavity of the trough approximately of the same entity and over the same extent, when their offset from the tunnel axis is small (one diameter). The long and thick smooth wall is even able to reduce to zero the slope value, along the whole surface profile at its back.

For the horizontal strains similar comments can be done as for the slopes. The long walls are able to reduce the ε_h to zero, particularly the thicker ones. The closer the wall, the more it is able to turn tensile strains into compression, over a span which is about one diameter behind all the walls located one diameter away from the tunnel axis.

Among all the results, the following evidences can be outlined.

Settlements and horizontal displacements. As far as the surface settlements behind the wall are concerned, it seems that the shortest walls are less effective than the longest ones in reducing ground displacements behind them. Furthermore, the rough walls are less effective than the smooth ones. On the other hand, the stiffness of the wall seems to influence the surface ground movements less than its length.

Slopes and horizontal strains. All the smooth walls and the long and rough walls provide a strong reduction of both these quantities up to a certain extent behind them. It can be observed that, depending on its location and length, the presence of the wall can induce a beneficial sagging where in the reference conditions without walls the ground was hogging.

V. Synthesis and discussion of the results

Introduction

In the previous chapters the results of an experimental campaign and a set of numerical analyses performed to reproduce and integrate the experiments were presented.

In this Chapter, an attempt has been made to summarise the results and to interpret the observed behaviour in a simple framework. In order to verify the limits of the study and to investigate the possibility of generalisation of the results, numerical modelling was used and the results will be discussed. Following the trends which appeared by comparing the Cam Clay and 3-SKH constitutive models and which were illustrated in Chapter IV, it was decided to perform all subsequent analyses by modelling the soil with 3-SKH.

Extensive discussion has been presented on the ability of the finite element analyses undertaken to capture the behaviour of the experimental models. Even though a quite sophisticated constitutive law was used for soil, which allowed reproduction of many aspects of the soil behaviour and which could predict with reasonable reliability some relevant quantities, a need for a further improvement in the constitutive modelling of this boundary value problem arose. in general, the experiments and the related computations gave similar responses, but the accuracy of the numerical predictions of the experimental observations was not always satisfactory.

As the numerical analysis allowed varying a larger set of geometrical factors than experiments, the discussion on the effectiveness of an embedded diaphragm wall as a mitigation measure against ground movements induced by shallow tunnelling has been based mainly on numerical results. Nevertheless, the experimental findings have been also reported in similar forms for comparison and validation every time it has been possible.

Scope and limits of the performed study

The numerical analyses of the centrifuge tests presented so far have boundary conditions that are consistent with the experimental apparatus.

Provided that the mesh boundaries are a reasonable representation of the centrifuge model boundaries, their influence on the problem can be studied by performing some numerical analyses where, for example, their location is varied.

In order to check the influence of the lateral boundaries on the problem, a numerical analysis of the no wall set-up was performed with the lateral sides of the mesh located up to 10 D away from the periphery of the tunnel, whereas they were 5D away in the experimental set-up. Comparison of the results in terms of computed stresses and strains indicated no significant difference between the two conditions.

Moreover, the influence of the distance from tunnel invert of the rigid bottom of the model was an issue of interest. This was investigated by extending the ground beneath the tunnel from about 1D (the experimental set-up) to about 6D and about 11D. The upper part of the mesh can be superimposed to the original smaller one. Fixities along the sides have been extended to the bottom, where displacements were restrained. Even if a new drainage boundary was provided at the bottom of the mesh, drainage was also permitted at the same distance below the tunnel invert as in the smaller mesh (and the experimental model). This condition did not influence the pore pressure distribution immediately before the 'excavation' stage, as the consolidation analysis was performed up to equilibrium conditions. But it allowed in the deeper mesh the same potential of dissipating the excess pore pressures as in the shallower mesh: this was particularly helpful to compare results during the 'excavation' phase. The initial stress conditions and the load sequence were adapted in order to reproduce in the shallower part of the new mesh the same recent stress history as in the previous small mesh. In this way the tunnel is 'excavated' in a ground which experienced the same history as in the centrifuge tests modelled by the previous analyses.

The comparison between the three new configurations, without the wall present, showed that similar stress distributions and displacement fields were predicted at the same level of support pressure in the tunnel. The analyses which have been performed on meshes without walls are summarised in Tab. V.1.

Table V.1 – Analyses performed to check the influence of the mesh boundary distance on the displacement field in no wall conditions.

analysis reference	C/D	distance from invert to base of mesh	lateral distance from tunnel periphery to edge of mesh
NW1	1	~D	5 D
NW2	1	~D	10 D
NW3	1	~6 D	10 D
NW4	1	~11 D	10 D

In Fig. V.1 the surface troughs have been plotted as they were computed by the analyses of the smaller and the larger meshes at $-\Delta p/p_o$=40%. From this it was concluded that the results of the performed analyses were not only representative of tunnel excavation in a layer lying on rigid bedrock, but they are also a good approximation of tunnelling in an ideal half plane.

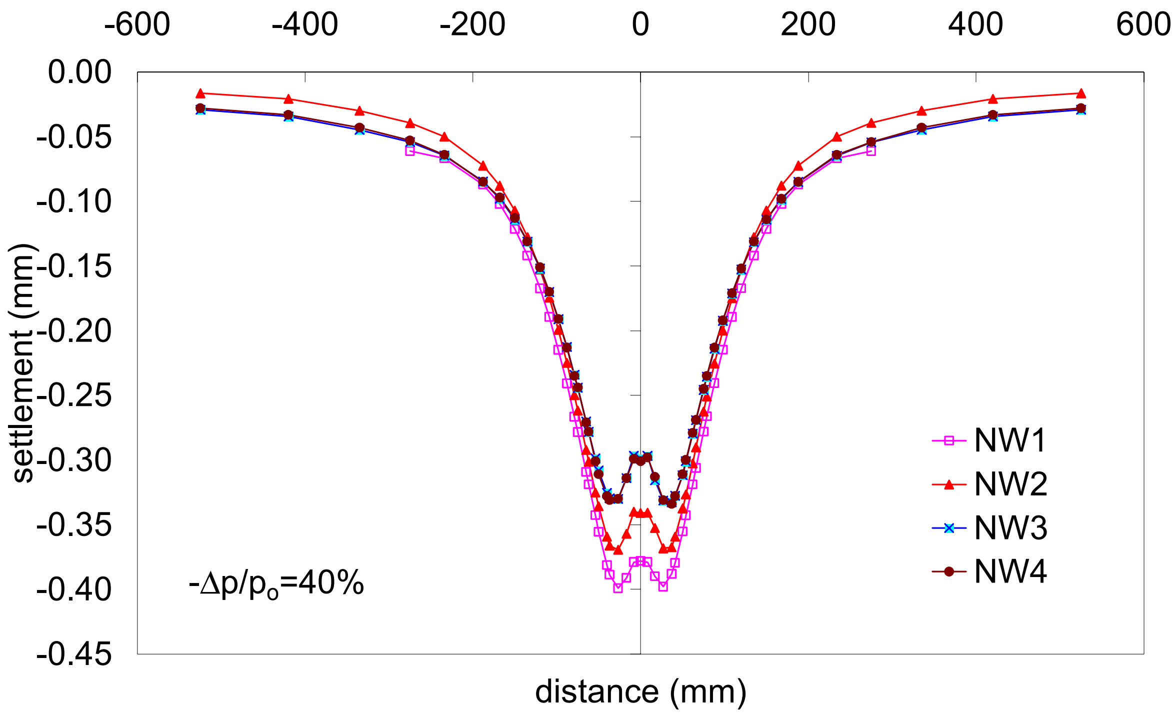

Figure V.1 – Influence of the mesh boundaries on the surface settlements in the reference configuration without wall

Nevertheless it has to be accounted for the influence of the distance from the wall toe of the base of the mesh. Some analyses were thus performed of a long wall configuration using the deeper mesh and these were compared to similar analyses using a smaller mesh. The wall was 120 mm long corresponding to the longest wall used in the tests (about 2.5D long). The details of the analyses are shown in Tab. V.2.

Table V.2 – Analyses performed to check the influence of the mesh boundary distance on the displacement field when the wall length was about 2.5D.

analysis reference	C/D	wall length	distance from invert to base of mesh	lateral distance from tunnel periphery to edge of mesh
LW1	1	~2.5D	~D	5 D
LW2	1	~2.5D	~6 D	10 D
LW3	1	~2.5D	~11 D	10 D

The results, as shown in Fig. V.2, show that in the analysis LW1 with a long and rough wall which extends up to about 1D below the tunnel axis in a mesh with a bottom boundary about 1D below the tunnel invert, the maximum settlement and the wall settlement are higher than in the analysis LW2 where the same wall was embedded in a mesh with a bottom located about 6D below the tunnel invert. Moreover, no difference can be observed on the computed surface settlements between the analyses LW2 and LW3, where the mesh bottom was deepened up to about 11D.

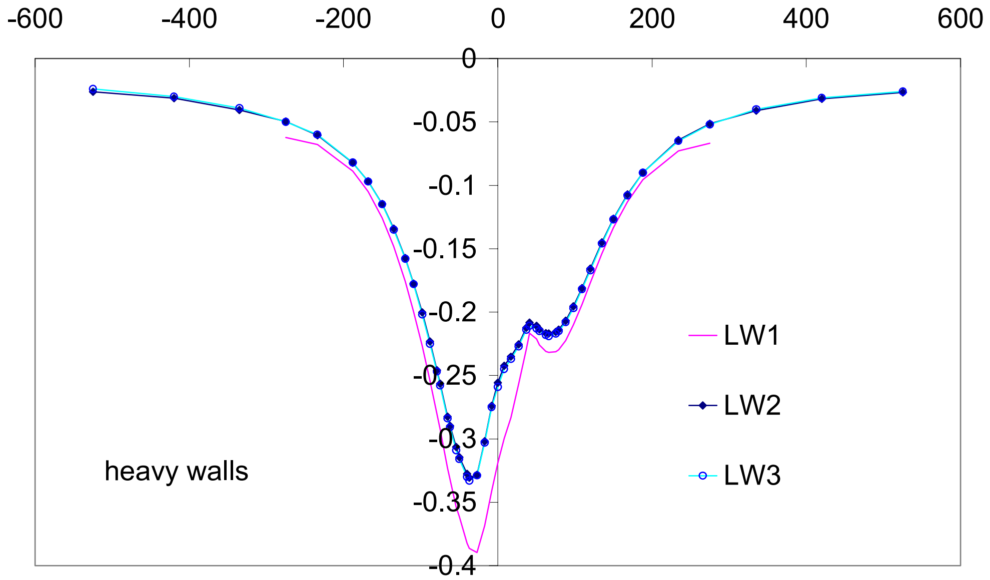

Figure V.2 – Influence of the mesh boundaries on the surface settlements in the configuration with a long wall

Both tests and numerical analyses have shown that, provided a given amount of interface roughness, the wall length is the main factor influencing the ground displacement field. It is questionable up to which point is worthwhile to deepen the wall below the tunnel invert instead of designing different mitigation measures. For this reason some analyses have been performed on the deeper mesh where the length of the wall was increased up to 1.5D below the tunnel invert. Moreover, a set of analyses was performed in which the tunnel axis was deepened at 2.5D below the ground level (C/D=2). This new tunnel depth was mainly studied to verify how much the prescribed tunnel depth C/D=1 was influencing the effectiveness of such a measure. In the following paragraphs the results of all the performed sets of numerical analyses will be discussed.

Definition of the efficiency of the protecting measure

In order to quantify the influence of a diaphragm wall in reducing ground movements induced by tunnelling, a dimensionless parameter can be introduced to represent the efficiency of such a measure.

Buildings founded in the vicinity of a shallow tunnel are mainly affected by the amount of surface settlements and horizontal displacements. As it has been observed in Chapter II, the amount of damage observed on buildings can be related to distortions and horizontal strains, which can be obtained by derivating the displacements profiles. Some comments were made on this at the end of Chapter IV with respect to the results of the numerical analyses corresponding directly to the centrifuge tests. Nevertheless, in this Chapter the attention will be focused on displacements and not on strains.

A dimensionless quantity has been defined by referring to a scheme of possible modifications of the settlement trough due to the wall which is shown in Fig. V.3. The reference settlement S_{ref} has been defined as the surface settlement in the no wall model at a distance d from the tunnel vertical centre line: this is the distance were the wall is embedded in the relevant model. The settlement of the wall S_w has been defined as the settlement of the top of the wall, whereas the settlement S_{bw} is computed as the settlement of the ground surface immediately behind the wall away from the tunnel. In case of a rough wall, where no relative displacement is allowed at the soil-wall interface, it can be assumed that $S_{bw} = S_w$. On the other hand, if a smooth interface is provided to the wall, these two settlements are different. The 'back-wall' settlement S_{bw} is not always the maximum settlement which can occur behind the wall, particularly if the wall is rough: in this case, in fact, a slightly higher settlement has been computed in some cases at a small distance behind the wall. Nevertheless, the criterion used is to assume $S_{bw} = S_w$ for all the cases with rough walls. This assumption does not lead to significant errors.

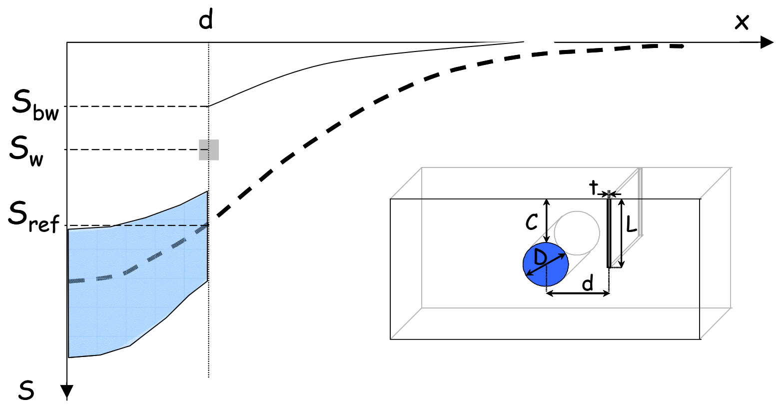

Figure V.3 – Definition of the settlement at the wall back, S_{bw}

The dimensionless quantity which has been assumed to represent the efficiency of the diaphragm wall in reducing the settlement behind the wall and away from the tunnel is the ratio:

$$\eta^v_{bw} = \frac{S_{ref} - S_{bw}}{S_{ref}} \tag{V.1}$$

When $\eta^v_{bw} = 1$, the embedded diaphragm wall is completely effective to eliminate all settlement at its back, and when $\eta^v_{bw} = 0$ the wall has no influence at all on settlement. In some tests and in the relevant numerical analyses it has been observed that the settlements behind the wall were higher than the reference settlements. In this case it can be computed $\eta^v_{bw} < 0$, which means that the wall effect is undesirable as it does not achieve the goal it has been designed for.

In a very similar manner, the following quantities can be defined, which describe in a synthetic and rather complete way the effects of the wall on the surface ground movements:

$$\eta_{fw}^{v} = \frac{S_{ref} - S_{fw}}{S_{ref}} \qquad \text{(V.2)}$$

$$\eta_{bw}^{h} = \frac{U_{ref} - U_{bw}}{U_{ref}} \qquad \text{(V.3)}$$

$$\eta_{fw}^{h} = \frac{U_{ref} - U_{fw}}{U_{ref}} \qquad \text{(V.4)}$$

$$\eta_{sym}^{v} = \frac{S_{sym,ref} - S_{sym}}{S_{sym,ref}} \qquad \text{(V.5)}$$

The quantity η_{fw}^{v} describes the effect of the wall on the surface settlements between the wall and the tunnel vertical centre line: S_{fw} is the 'front wall' settlement, that is the settlement of the ground surface immediately close to the wall on the tunnel side. As for rough walls it can be assumed $S_{fw} = S_w$, and it follows that for rough walls $\eta_{fw}^{v} = \eta_{bw}^{v}$.

The horizontal displacement U_{ref} is defined as the horizontal displacement in the no wall model at a distance d from the tunnel vertical centre line; the quantities η_{bw}^{v} and η_{fw}^{v} thus represent a degree of effectiveness of the diaphragm wall in reducing the horizontal displacements at the ground surface.

The last quantity η_{sym}^{v} is calculated from the values of S_{sym} which is the surface settlement at the symmetrical location of the wall to the tunnel vertical centre line: it gives an indication of the effect of the wall on the settlement trough on the other side of the tunnel.

A set of modification factors β can be also defined following the general formula:

$$S = \beta S_{ref} \qquad \text{(V.6)}$$

which links the reference displacement to the displacement in the configuration with wall.

It is easy to verify that:

$$\beta = 1 - \eta \qquad \text{(V.7).}$$

Efficiency of the diaphragm wall as observed in the centrifuge tests and the relevant back-analyses

It has been observed in the previous Chapter that the length of the wall is the main geometrical factor affecting its efficiency, once a certain degree of roughness has been provided to its interface with the soil. This will be investigated further by plotting the efficiency parameter η_{bw}^{v} calculated from both the tests and analyses as a function of the length of the wall.

In Fig. V.4 $\eta_{bw}^{v} = \eta_{w}^{v}$ for rough and thick walls has been plotted along the wall length. It has been computed from the settlement measured on the first row of targets in the tests (5 mm below the ground surface at the model scale) and in the corresponding point of the numerical analyses. The pertinent volume loss is V'=1.35%: the corresponding experimental settlement profiles have been shown in Fig. III.32. Two more lengths were considered in the numerical analyses than in tests. The chart presents the curves corresponding to two different offsets of the wall from the tunnel axis (d=D and d=1.5D).

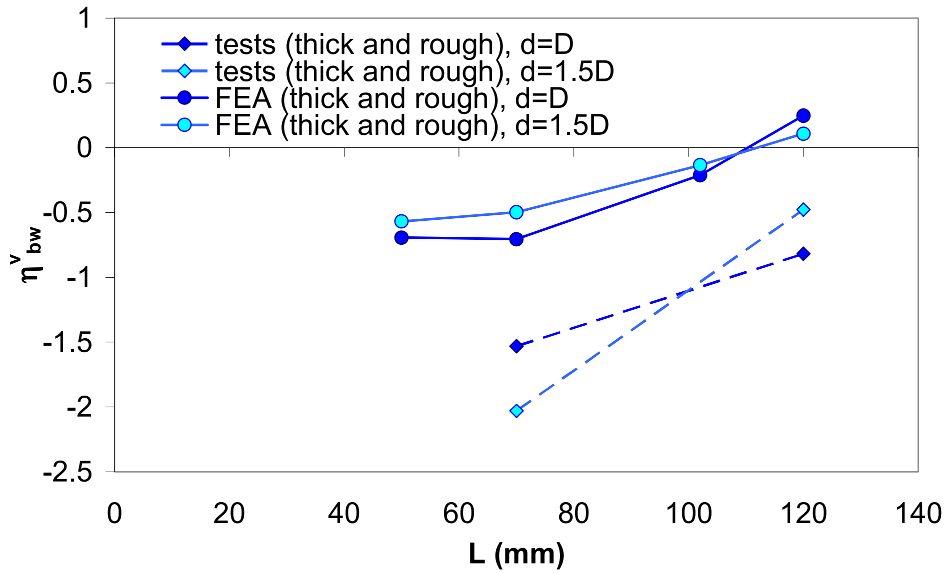

Figure V.4 – Efficiency parameter η_{bw}^{v} as computed in tests and numerical analyses on rough walls at V'=1.35%

It is evident in the figure that the efficiency of the tested rough walls is negative, hence their effect undesirable. Nevertheless, an increasing trend toward positive values can be recognised. The numerical results still give negative efficiencies, but lower in absolute magnitude than those measured experimentally. For the longer walls (L=120 mm, which corresponds to about one diameter below the tunnel axis) positive values of η_{bw}^{v} are predicted from the numerical analyses. On the other hand the shorter walls (L=50 mm corresponds to the toe at the crown level, L=70 to about the axis level) attain approximately the same efficiency. It is likely that for lower lengths their efficiency tends to zero, which is the attainable limit in no wall conditions. From these results it cannot be stated that by increasing the wall length its efficiency rises indefinitely. In order to explore this possibility, a deeper mesh has been analysed, as it will shown later. The profiles of η_{bw}^{v} with the wall length, suggest that the negative efficiency is a consequence of the wall weight. In order to validate this statement, similar analyses have been performed in which the unit weight of the wall was set equal to that of the soil, thus eliminating the influence of the extra weight on the problem: the corresponding η_{bw}^{v} profiles are compared in Fig. V.5.

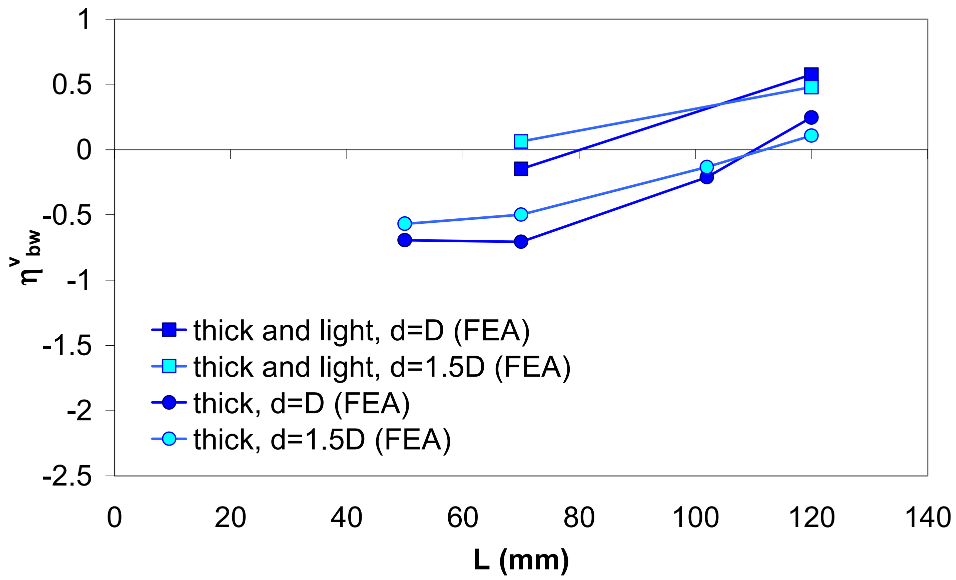

Figure V.5 – Efficiency parameter η_{bw}^{v} as computed in numerical analyses on 'heavy' and 'light' rough walls at V'=1.35%

It can be observed that the 'light' walls (density set equal to that of the surrounding soil) have a positive efficiency from a length which corresponds to about the tunnel axis level, whereas the corresponding 'heavy' walls have negative efficiency. Thus, it can be concluded that the wall self weight is an important parameter.

As far as the offset of the wall is concerned, both in the tests and the numerical analyses, it can be observed that its influence on the wall efficiency is negligible.

In Fig. V.6 the numerical analyses on thin and thick walls, with rough interface, have been compared.

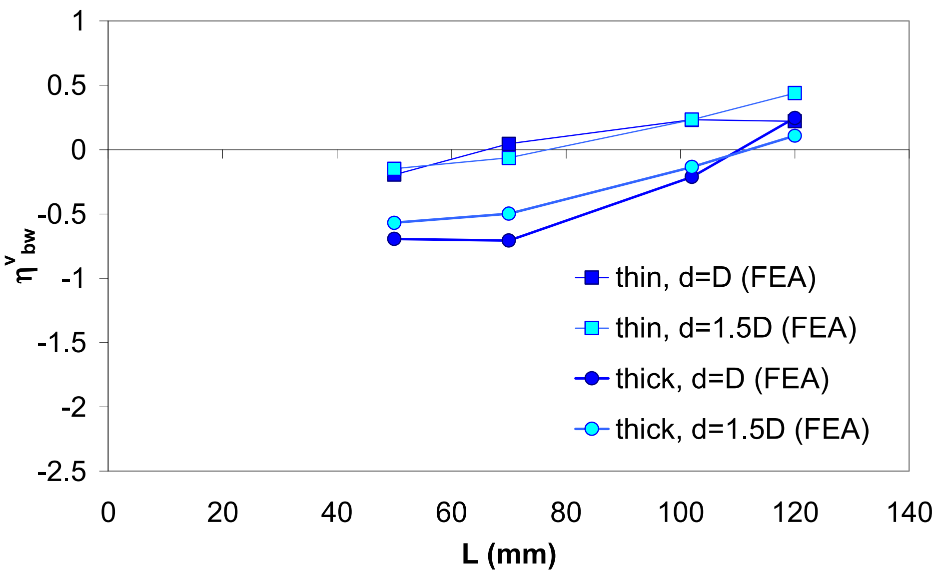

Figure V.6 – Efficiency parameter η^{v}_{bw} *as computed in numerical analyses on thin and thick rough walls at V'=1.35%*

From this chart it could be stated that the thinner the wall, the more effective in reducing settlements. In fact, it is worth noting that the thinner walls are not only more flexible than the thicker ones, but also lighter. Therefore, a comparison between thin and thick walls to highlight the influence of only the stiffness has to be performed using 'light' walls (same unit weight as the soil). The results of such analyses are plotted in Fig. V.7.

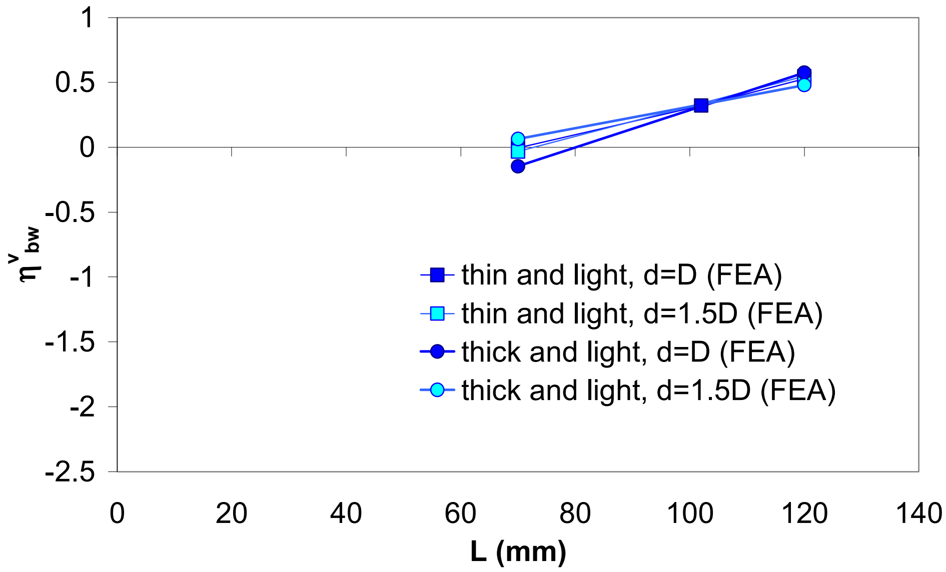

Figure V.7 – Efficiency parameter η_{bw}^{v} *as computed in numerical analyses on thin and thick 'light' rough walls at V'=1.35%*

There can be observed that the computed efficiencies are practically the same. This leads to the conclusion that the wall stiffness has a secondary role in this problem.

In a similar way, the η_{bw}^{v} values of smooth walls are plotted along their length in Fig. V.8.

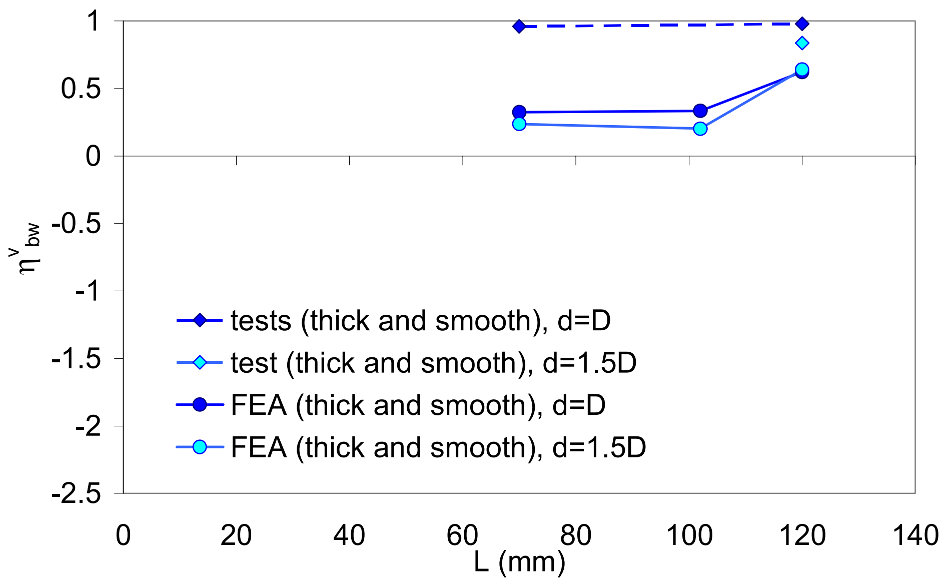

Figure V.8 – Efficiency parameter η_{bw}^{v} *as computed in tests and numerical analyses on smooth walls at V'=1.35%*

The efficiency of smooth walls is always positive, though in the tests the values are higher than in the corresponding numerical analyses and much closer to 1, which means that the settlements behind the wall are close to zero. From the experiments the trend of η_{bw}^{v} with the wall length seems to be zero, whereas in the numerical analyses this trend has been observed only in limited range of length. In fact, the efficiency seems to improve when the wall length increases from L=100 mm (tunnel invert depth) to L = 120. However, this results is not completely reliable because of the possible influence of the mesh bottom. Therefore, similar analyses have been performed on a deeper mesh, which will be discussed in the next section.

The influence of the wall offset is negligible as already shown for rough walls.

The influence of the wall self weight has not been studied, because in the case of smooth walls the 'back wall' settlement is independent of the wall settlement, due both to its definition and to the complete smoothness condition at the interface. In fact, smooth walls do not show negative efficiency.

The influence of the wall stiffness can be observed in Fig. V.9.

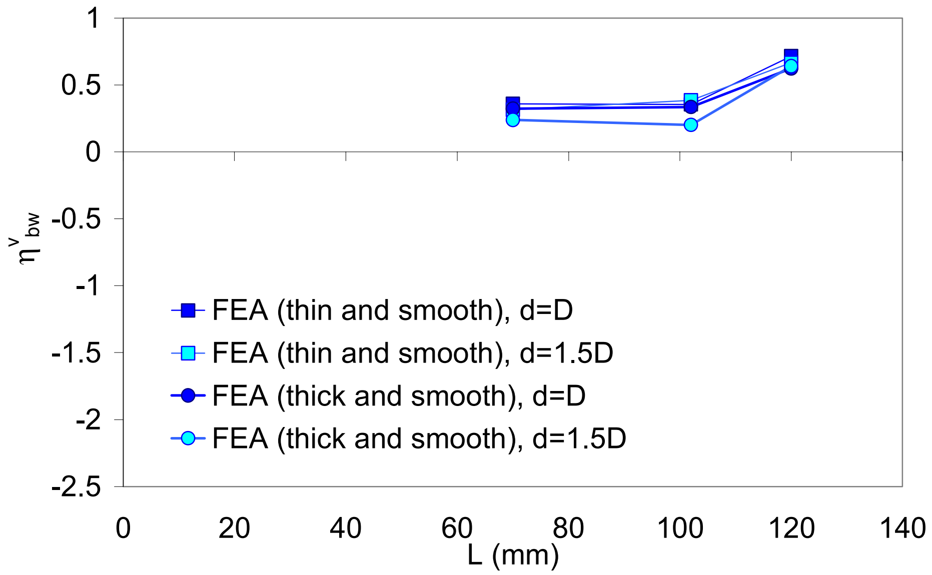

Figure V.9 – Efficiency parameter η_{bw}^{v} as computed in numerical analyses on thin and thick smooth walls at V'=1.35%

It can be observed that the efficiency of smooth walls in this problem, as that of rough walls, is substantially independent of their stiffness.

Efficiency of the diaphragm wall as computed in the complete set of numerical analyses

In order to extend the conclusions which have been drawn up to this point, a set of numerical analyses has been performed on a deeper and larger mesh and with two different values of C/D. The configurations which have been studied are summarised in Tab. V.3. In all the cases, the bottom distance below the invert tunnel was set to about 6D and the distance of the lateral boundaries from the tunnel side was 10D: as it has been discussed above, this mesh is representative of the problem in a half space.

In the same table, the cases are divided in classes and identified by a terminology which will be used in the following discussion. The lengths in square brackets relate to the equivalent prototype scale.

Table V.3 – New set of performed analyses

analysis reference	C/D	L/D	offset d	thickness (mm) *[m]*	interface	wall unit weight (kN/m^3)
reference no wall						
NW3	1	-	-	-	-	-
NW5	2	-	-	-	-	-
rough, thick, ‘heavy’ walls C/D=1, d=D						
W50	1	D	D	9 *[1.44]*	rough	27
W70	1	~1.5D	D	9 *[1.44]*	rough	27
W100	1	2D	D	9 *[1.44]*	rough	27
LW2	1	~2.5D	D	9 *[1.44]*	rough	27
W155	1	~3D	D	9 *[1.44]*	rough	27
W170	1	~3.5D	D	9 *[1.44]*	rough	27
rough, thick, ‘heavy’ walls C/D=1, d=1.5D						
FaW50	1	D	1.5D	9 *[1.44]*	rough	27
FaW70	1	~1.5D	1.5D	9 *[1.44]*	rough	27
FaW100	1	2D	1.5D	9 *[1.44]*	rough	27
FaW120	1	~2.5D	1.5D	9 *[1.44]*	rough	27
FaW155	1	~3D	1.5D	9 *[1.44]*	rough	27
FaW170	1	~3.5D	1.5D	9 *[1.44]*	rough	27
rough, thick, ‘light’ walls C/D=1, d=D						
LiW50	1	D	D	9 *[1.44]*	rough	17.44
LiW70	1	~1.5D	D	9 *[1.44]*	rough	17.44
LiW100	1	2D	D	9 *[1.44]*	rough	17.44

LiW120	1	~2.5D	D	9 *[1.44]*	rough	17.44
LiW155	1	~3D	D	9 *[1.44]*	rough	17.44
LiW170	1	~3.5D	D	9 *[1.44]*	rough	17.44
smooth, thick, 'heavy' walls C/D=1, d=D						
SliW50	1	D	D	9 *[1.44]*	smooth	27
SliW70	1	~1.5D	D	9 *[1.44]*	smooth	27
SliW100	1	2D	D	9 *[1.44]*	smooth	27
SliW120	1	~2.5D	D	9 *[1.44]*	smooth	27
SliW155	1	~3D	D	9 *[1.44]*	smooth	27
SliW170	1	~3.5D	D	9 *[1.44]*	smooth	27
rough, thin walls C/D=1, d=D						
ThinW50	1	D	D	1 *[0.16]*	rough	27
ThinW70	1	~1.5D	D	1 *[0.16]*	rough	27
ThinW100	1	2D	D	1 *[0.16]*	rough	27
ThinW120	1	~2.5D	D	1 *[0.16]*	rough	27
ThinW155	1	~3D	D	1 *[0.16]*	rough	27
ThinW170	1	~3.5D	D	1 *[0.16]*	rough	27
rough, thick, 'heavy' walls C/D=2, d=D						
W50-2	2	D	D	9 *[1.44]*	rough	27
W75-2	2	1.5D	D	9 *[1.44]*	rough	27
W100-2	2	2D	D	9 *[1.44]*	rough	27
W120-2	2	~2.5D	D	9 *[1.44]*	rough	27
W150-2	2	3D	D	9 *[1.44]*	rough	27
W170-2	2	~3.5D	D	9 *[1.44]*	rough	27
W205-2	2	~4D	D	9 *[1.44]*	rough	27
W220-2	2	~4.5D	D	9 *[1.44]*	rough	27
rough, thick, 'light' walls C/D=2, d=D						
LiW50-2	2	D	D	9 *[1.44]*	rough	17.44
LiW75-2	2	1.5D	D	9 *[1.44]*	rough	17.44
LiW100-2	2	2D	D	9 *[1.44]*	rough	17.44
LiW120-2	2	~2.5D	D	9 *[1.44]*	rough	17.44
LiW150-2	2	3D	D	9 *[1.44]*	rough	17.44
LiW170-2	2	~3.5D	D	9 *[1.44]*	rough	17.44
LiW205-2	2	~4D	D	9 *[1.44]*	rough	17.44
LiW220-2	2	~4.5D	D	9 *[1.44]*	rough	17.44

The displacements at the mesh top nodes have been computed at the stage when V'=1% and the relevant efficiency parameters have then been calculated as defined above.

Influence of the wall length and offset

In Fig. V.10 the vertical efficiency $\eta^v = \eta^v_{bw} = \eta^v_{fw}$ has been plotted along the wall length for the rough and thick walls located at d=D and d=1.5D from the tunnel axis (C/D=1).

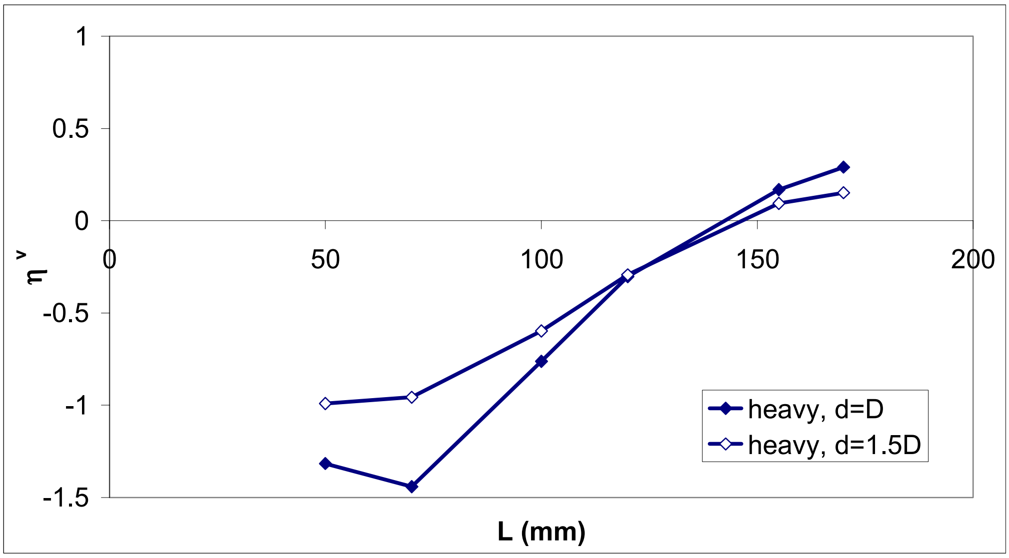

Figure V.10 – Efficiency parameter η^v *as computed in numerical analyses (C/D=1) on rough and thick walls at V'=1%*

These results, obtained on a deeper and larger mesh than the test model, confirm that the wall has to be deepened at least about one diameter below the tunnel invert, otherwise it is ineffective in reducing ground surface movements and its effect is, on the contrary, undesirable. This behaviour is substantially independent of the distance of the wall from the tunnel axis, but the larger settlements are predicted near the shortest walls when they are closer to the tunnel.

In Fig. V.11 the corresponding horizontal efficiency $\eta^h = \eta^h_{bw} = \eta^h_{fw}$ has been plotted.

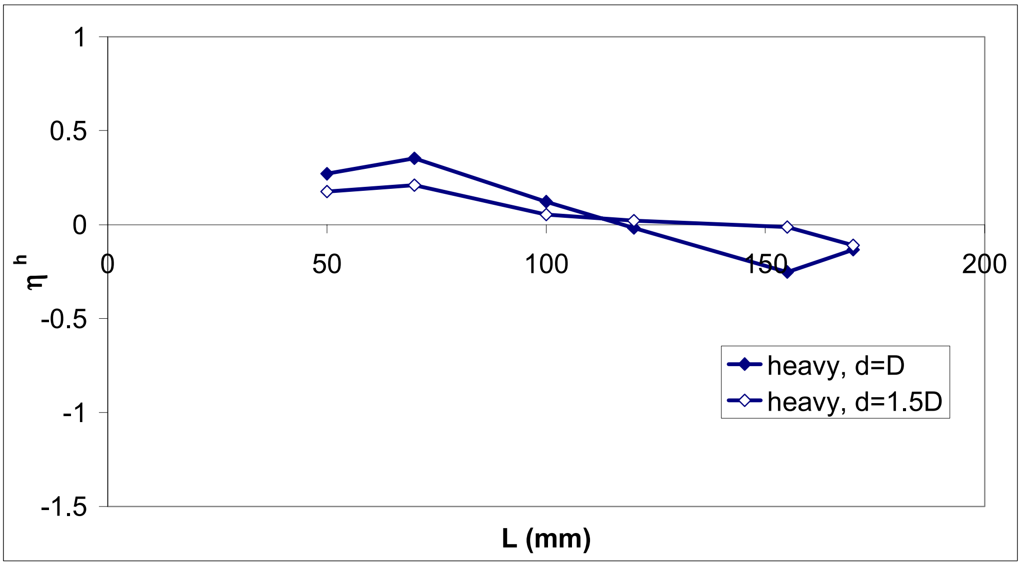

Figure V.11 – Efficiency parameter η^h *as computed in numerical analyses (C/D=1) on rough and thick walls at V'=1%*

This chart shows that the shortest walls have a positive effect in reducing the horizontal movements, but by increasing the wall length, the wall efficiency reduces and also becomes negative in some cases. However the influence of the walls on the horizontal displacements is much lower than their influence on settlements.

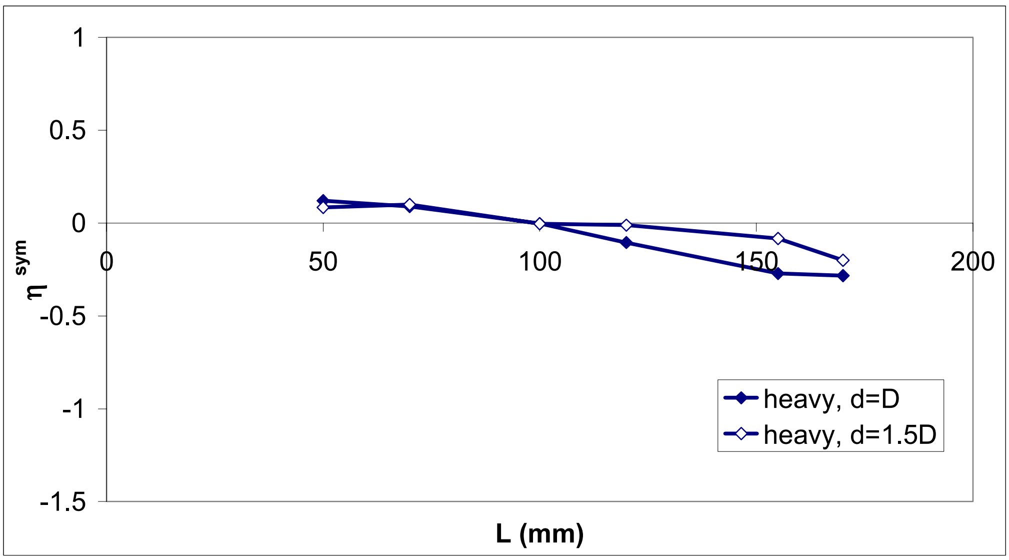

Figure V.12 – Efficiency parameter η^{sym} *as computed in numerical analyses (C/D=1) on rough and thick walls at V'=1%*

In Fig. V.12, the symmetrical efficiency η^{sym} has been plotted along the wall length.

This plot shows substantially that the influence of the wall on the ground surface settlements on the other side of the tunnel is limited. The trend towards negative efficiency is a dual effect of the increase in η^{v}. As a matter of fact, as relevant settlements are computed on settlement troughs having the same area (V'=1%), the more effective the wall on the right side, the more ineffective on the left one.

Influence of the wall self weight

The influence of the wall weight can be observed in the following Figs. V.12÷V.15, where the efficiency parameters as computed for thick and heavy rough walls (the same shown in Fig. V.10÷V.12) are compared with the corresponding parameters as computed for similar 'light' walls.

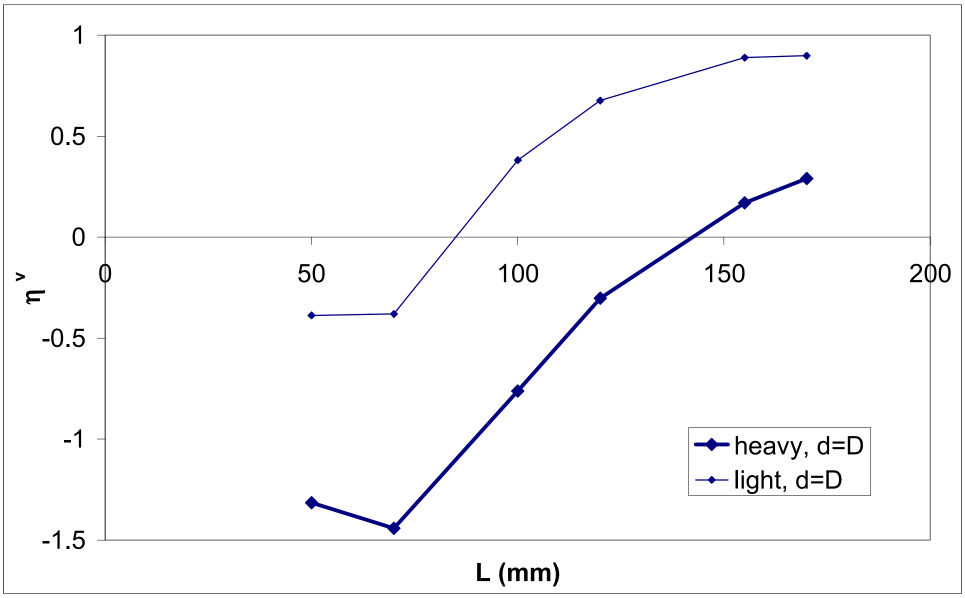

Figure V.13 – Efficiency parameter η^{v} as computed in numerical analyses (C/D=1) on 'heavy' and 'light' rough and thick walls at V'=1%

It can be observed in Fig. V.13 that the efficiency of 'lighter' walls is much higher than that of 'heavier'. It increases clearly with the wall length up to a level close to 0.9, where it has an asymptote. However, the shortest walls have still negative efficiency, which cannot be attributed only to the wall self weight.

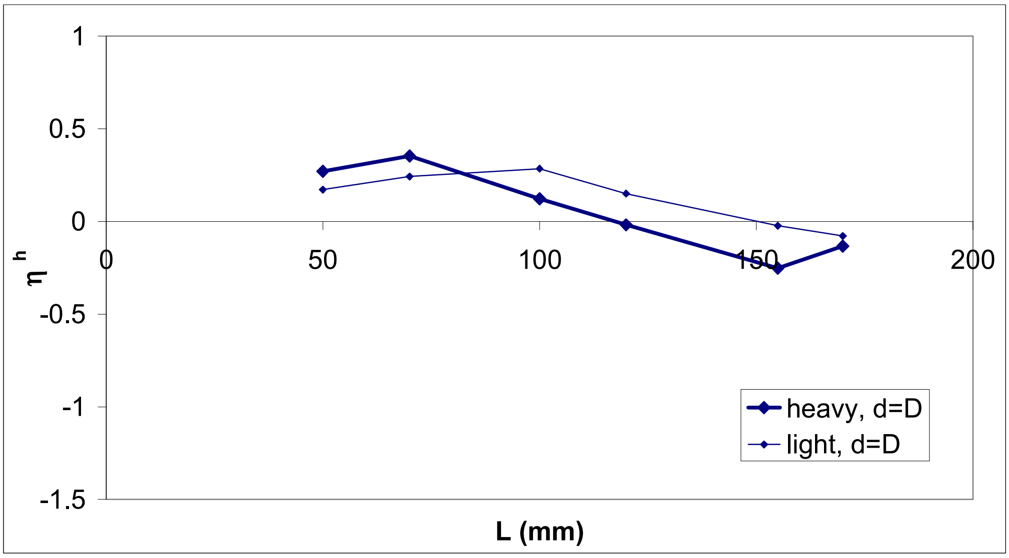

Figure V.14 – Efficiency parameter η^h *as computed in numerical analyses (C/D=1) on 'heavy' and'light' rough and thick walls at V'=1%*

As far as the parameter η^h is concerned, it can be observed in Fig. V.14 that for lighter walls compared to heavy walls there is a bigger range of walls lengths giving a positive efficiency.

The efficiency η^{sym} of lighter walls is on the contrary always negative but it has the same trend as that of heavier walls (Fig. V.15).

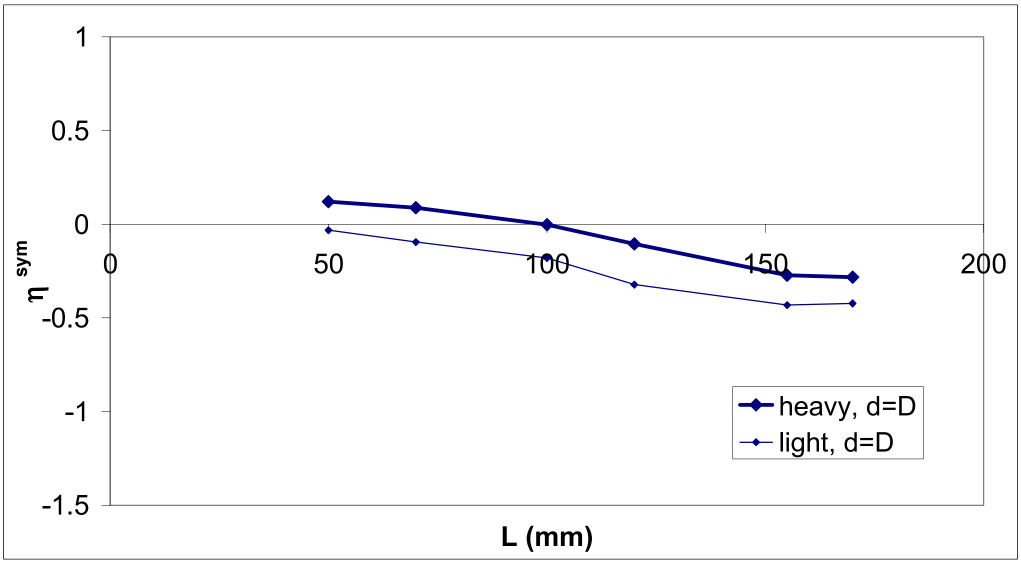

Figure V.15 – Efficiency parameter η^{sym} as computed in numerical analyses (C/D=1) on 'heavy' and'light' rough and thick walls at V'=1%

Influence of the wall thickness

The influence of the wall thickness on the parameter η^{v} can be deduced by Fig. V.16, where curves are compared referred to thick and thin rough walls. It can be observed that 'light' thick walls and thin 'heavy' walls have closer values of vertical efficiency. Nevertheless a difference persists, which can be in part attributed to the wall self weight and in part to its flexural rigidity. It is worth noticing (*cf.* Tab. V.3) that the ratio between thin and thick walls thickness is 1:9, which means a large difference in flexural rigidity, whereas the difference in efficiency is at most 30%. Therefore it is confirmed that the influence of the stiffness of the wall on this problem is not very high. In the following Figs. V.17-V.18 similar comparisons are shown for the horizontal and the symmetrical efficiency: the horizontal efficiency of thin walls is always positive and increasing with the wall length; the symmetrical efficiency of thin walls, on the contrary, has the same trend as for the other walls.

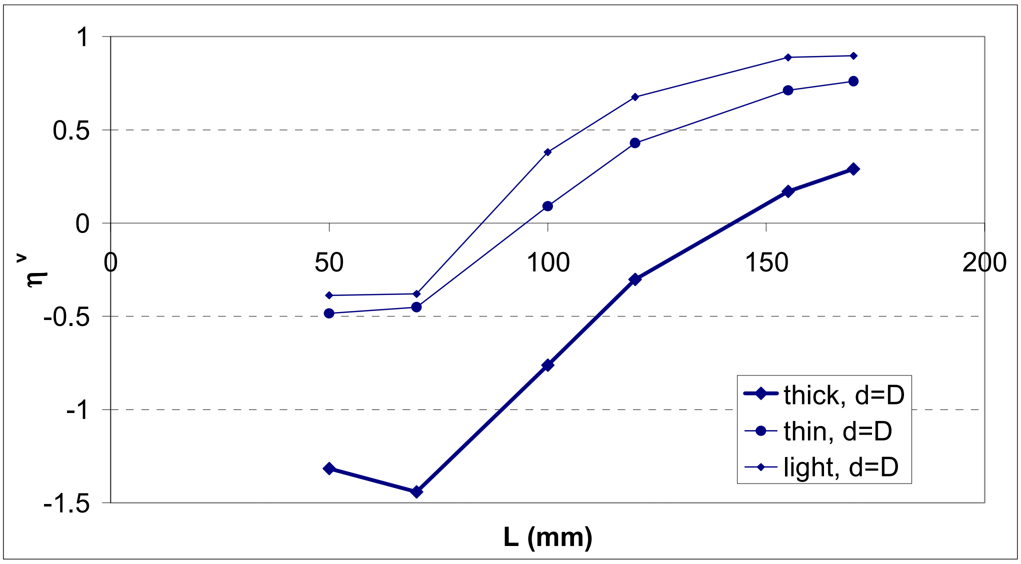

Figure V.16 – Efficiency parameter η^v as computed in numerical analyses (C/D=1) on thick and thin rough walls and 'light' thick rough walls at V'=1%

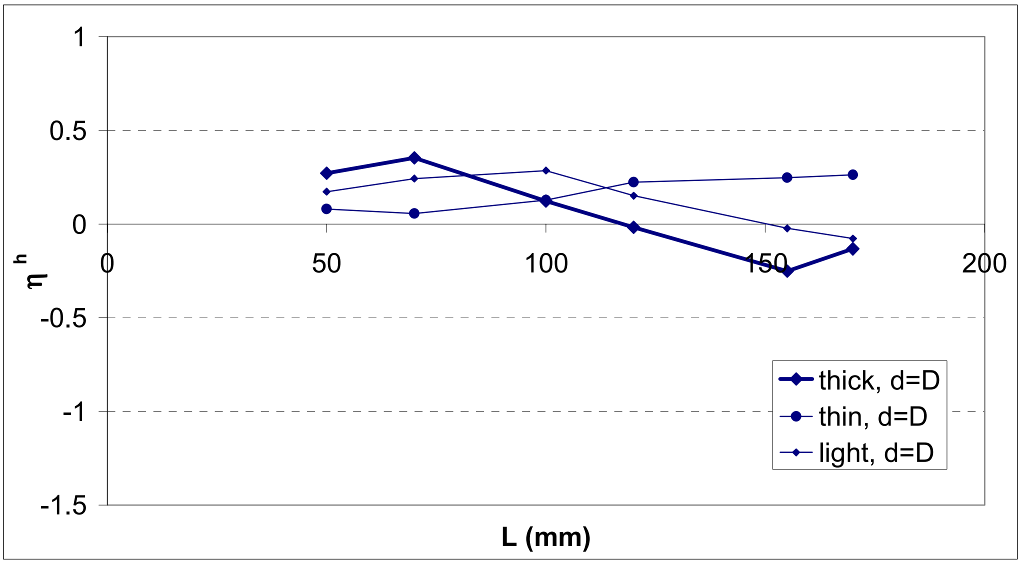

Figure V.17 – Efficiency parameter η^h as computed in numerical analyses (C/D=1) on thick and thin rough walls and 'light' thick rough walls at V'=1%

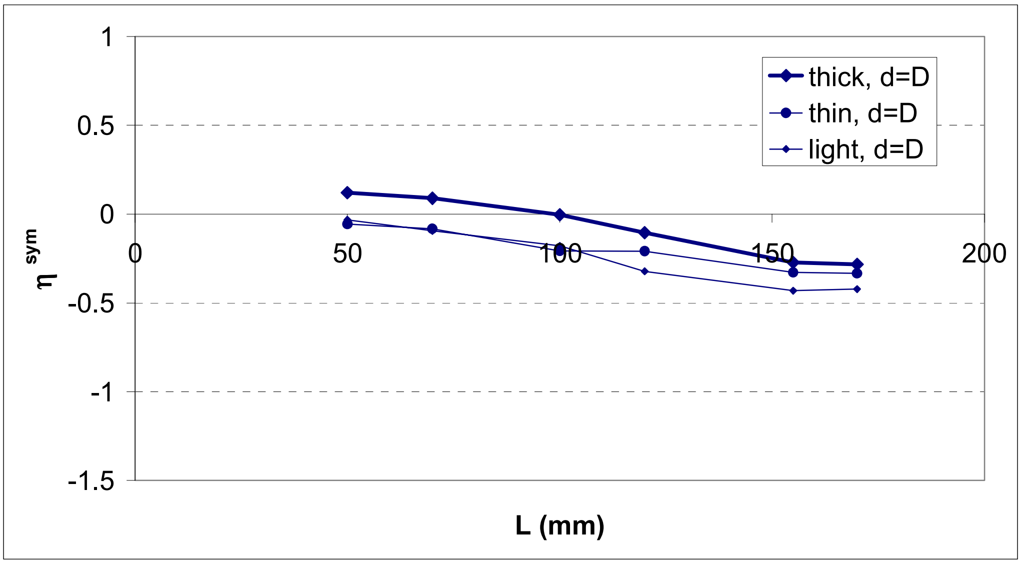

Figure V.18 – Efficiency parameter η^{sym} as computed in numerical analyses (C/D=1) on thick and thin rough walls and 'light' thick rough walls at V'=1%

Influence of the wall smoothness

In Figs. V.19÷V.21 the vertical, horizontal and symmetrical efficiencies are plotted along the wall length in the cases where the wall interface was allowed to slip.

The vertical efficiency parameters η^{v}_{bw} (back wall) and η^{v}_{fw} (front wall) are shown in Fig. V.19.

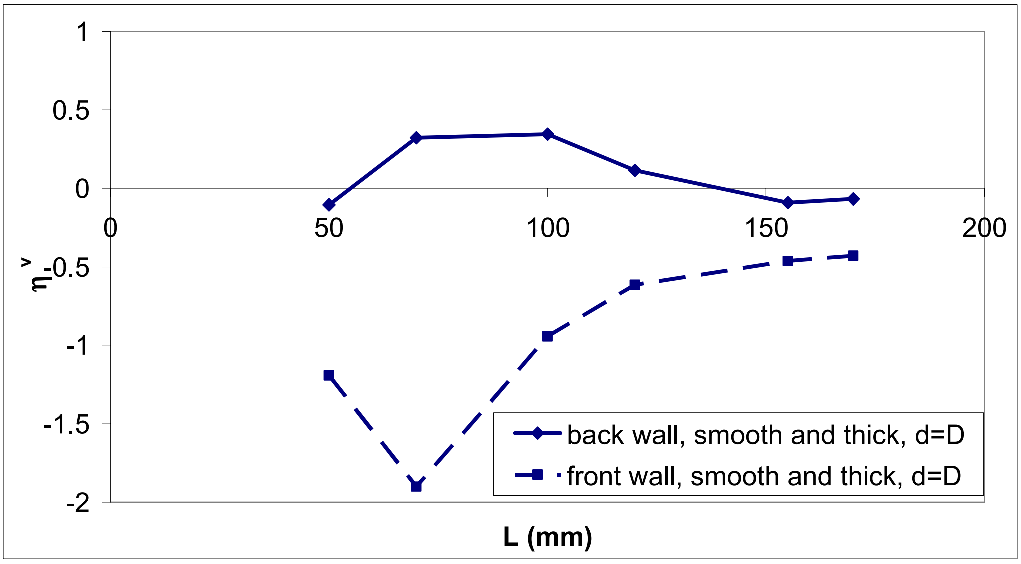

Figure V.19 – Efficiency parameters η^{v}_{bw} and η^{v}_{fw} as computed in numerical analyses (C/D=1) on smooth and thick walls at V'=1%

As far as η^{v}_{bw} is concerned, it can be observed that, consistent with the centrifuge tests, there exists a range of wall lengths where the vertical efficiency behind the wall is positive and almost constant but its value is much lower than observed in the experiments. By increasing the wall length, the efficiency η^{v}_{bw} behind the wall tends to zero: in fact, the soil behind the wall tends to settle more than the wall itself. This behaviour was not observed in the previous numerical analyses, where the mesh had the same size of the test model (*cf.* Fig. V.8): there, the wall always settled more than the soil at its back. Thus, it appears that the distance of the rigid boundary below the smooth wall plays an important role. Moreover, below a certain length (say, less than the tunnel cover) the wall is ineffective. It seems, in fact, that the discontinuity provided by the wall is not developed enough to influence significantly the ground movement field. This could explain also the initial part of the negative η^{v}_{fw} profile (front wall vertical efficiency) where the increase of settlement at the soil-wall interface on the tunnel side is lower than for longer walls. As a matter of fact, by further deepening the wall from about the axis level, η^{v}_{fw} increases towards a constant value of about -0.5.

In Fig. V.20 the horizontal efficiency parameters η^{h}_{bw} (back wall) and η^{h}_{fw} (front wall) are shown.

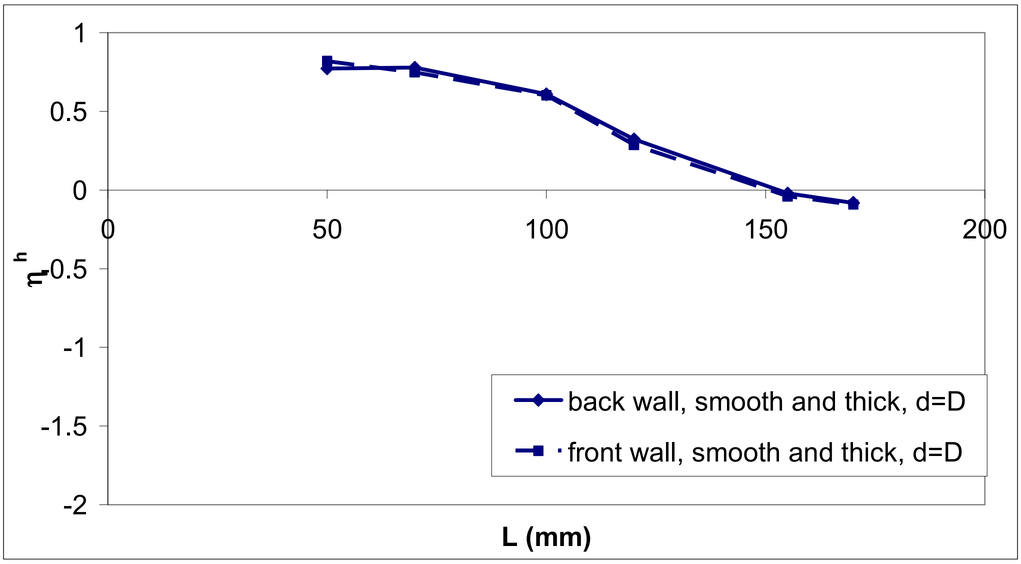

Figure V.20 – Efficiency parameters η^h_{bw} and η^h_{fw} as computed in numerical analyses (C/D=1) on smooth and thick walls at V'=1%

It can be observed that the two parameters are equal: this means that at this stage of the analyses no 'separation' between the soil and the wall at the interface occurred. However the reduction in horizontal displacements immediately behind and in front of the wall is very high ($\eta^h \cong 0.8$) when the wall toe is located between the crown and the axis level, then it tends to decrease to zero and below.

In Fig. V.21, the symmetrical efficiency parameter η^{sym} is shown.

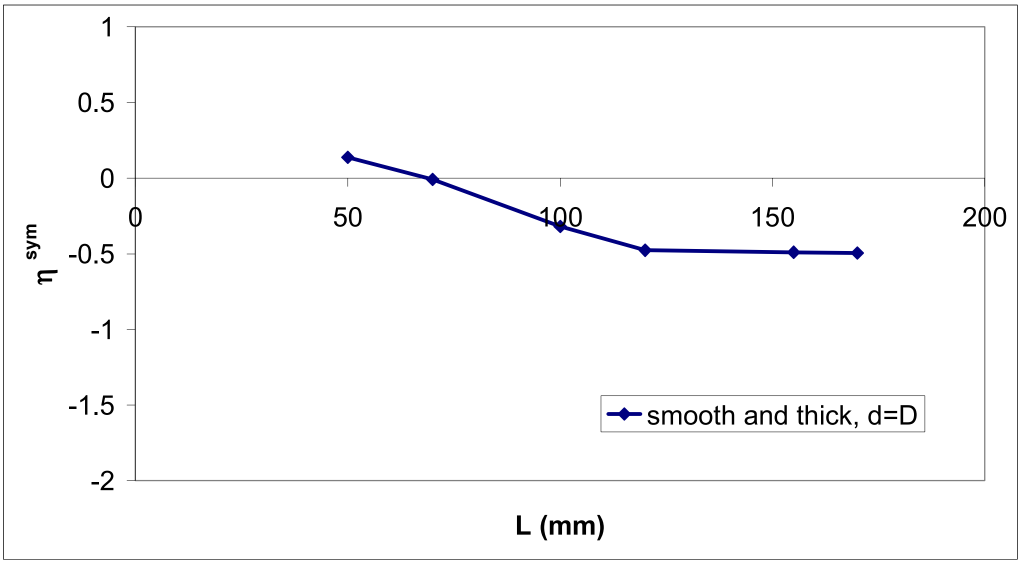

Figure V.21 – Efficiency parameter η^{sym} as computed in numerical analyses (C/D=1) on smooth and thick walls at V'=1%

Influence of the tunnel cover

In order to study the influence on the problem of the tunnel depth, a set of analyses has been performed where the C/D ratio was set equal to two.

In the following Figs. V.22÷V.24, the profiles of vertical, horizontal and symmetrical efficiency are shown for a set of rough and thick walls, located one diameter away from the tunnel axis (Tab. V.3). Both the case of 'heavy' and that of 'light' walls have been analysed.

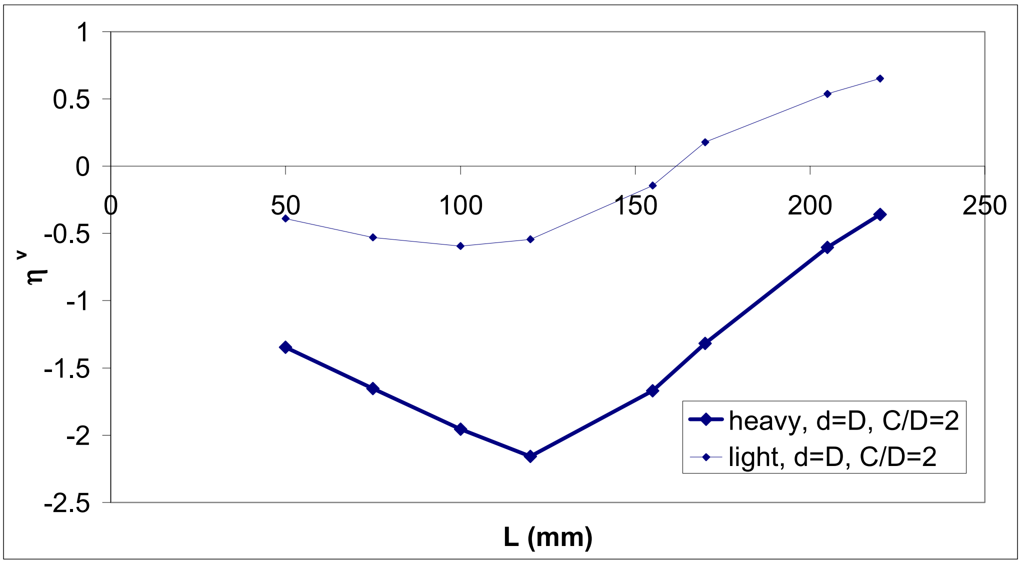

Figure V.22 – Efficiency parameter η^v *as computed in numerical analyses (C/D=2) on 'heavy' and 'light' rough and thick walls at V'=1%*

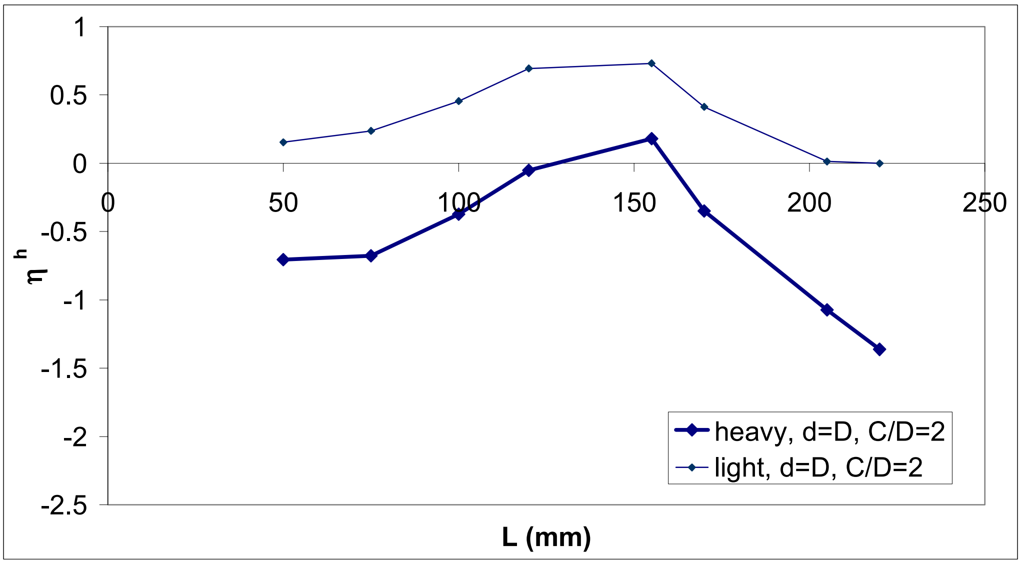

Figure V.23 – Efficiency parameter η^h *as computed in numerical analyses (C/D=2) on 'heavy' and'light' rough and thick walls at V'=1%*

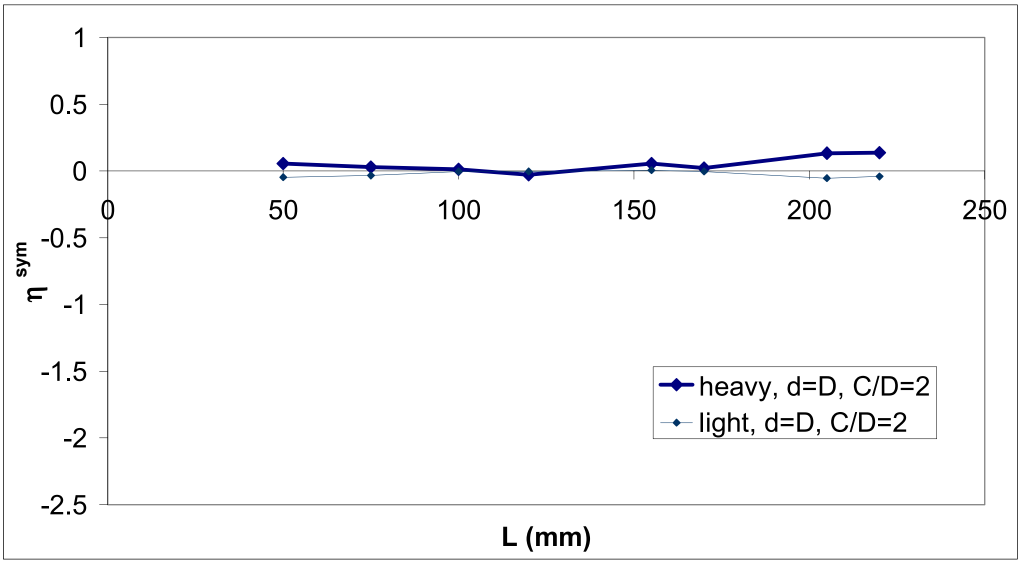

Figure V.24 – Efficiency parameter η^{sym} *as computed in numerical analyses (C/D=2) on 'heavy' and'light' rough and thick walls at V'=1%*

As a general comment, it can be observed that the influence of the wall self weight is confirmed also for the case of a deeper tunnel. In general the trend towards positive η^{v} starts only after the cover level has been reached: before, the increase of length corresponds essentially to an increase of weight and the efficiency η^{v} tends to more negative values. The negative values of η^{v}, which can be observed for the shortest walls, cannot be attributed only to the self weight of the wall, as they occur also for the 'light' walls. However, they were observed also for shallower tunnels.

The horizontal efficiency of the 'heavy' walls is generally negative, whereas the 'light' walls are always effective (*i.e.* positive efficiency). However, the profiles have similar shape and the 'light' walls reach a maximum of effectiveness when their toe rests between the tunnel axis and invert, as can be observed in Fig. V.23. This occurs also for shallower tunnels (*cf*. Fig. V.14)

The influence of the walls on the ground settlements at the symmetrical point is negligible (Fig. V.24).

In order to better highlight the influence of the cover on the wall effectiveness, the η^v and η^h have been plotted in Figs. V.25-V.26 along the normalised length L/C.

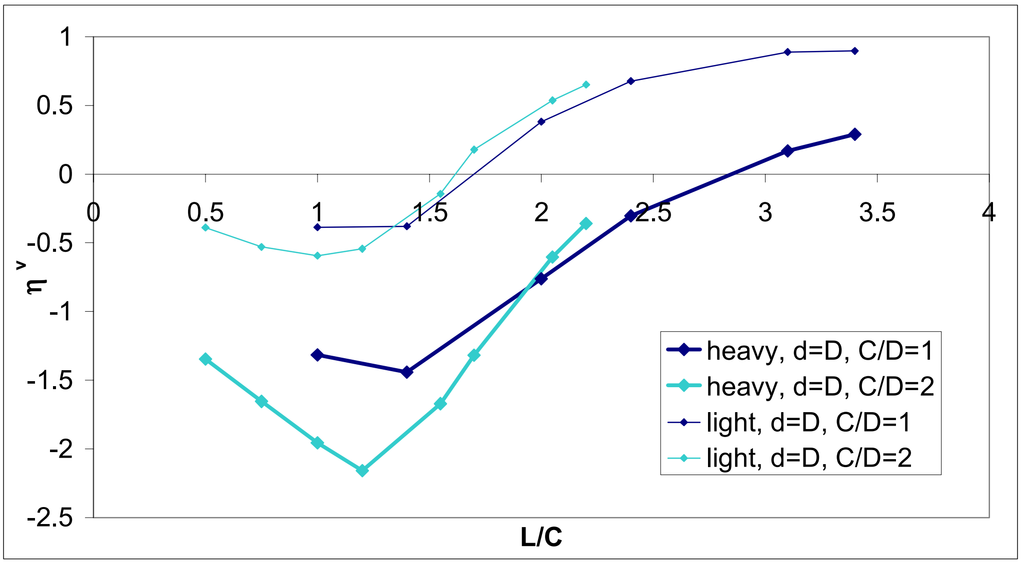

Figure V.25 – Efficiency parameter η^v as computed in numerical analyses on 'heavy' and 'light' rough and thick walls at V'=1%

It can be observed in Fig. V.25 that the vertical efficiency of the wall is substantially independent of the cover. The major differences between the corresponding profiles can be observed for the shortest 'heavy' walls. It is worth noticing that the normalisation 'hides' the fact that walls having the same normalised length L/C, in different C/D configurations, have actually different length, hence different weight. Therefore, the difference between the configuration C/D=1 and C/D=2 is more evident where the wall weight has a major role, that is for shorter walls.

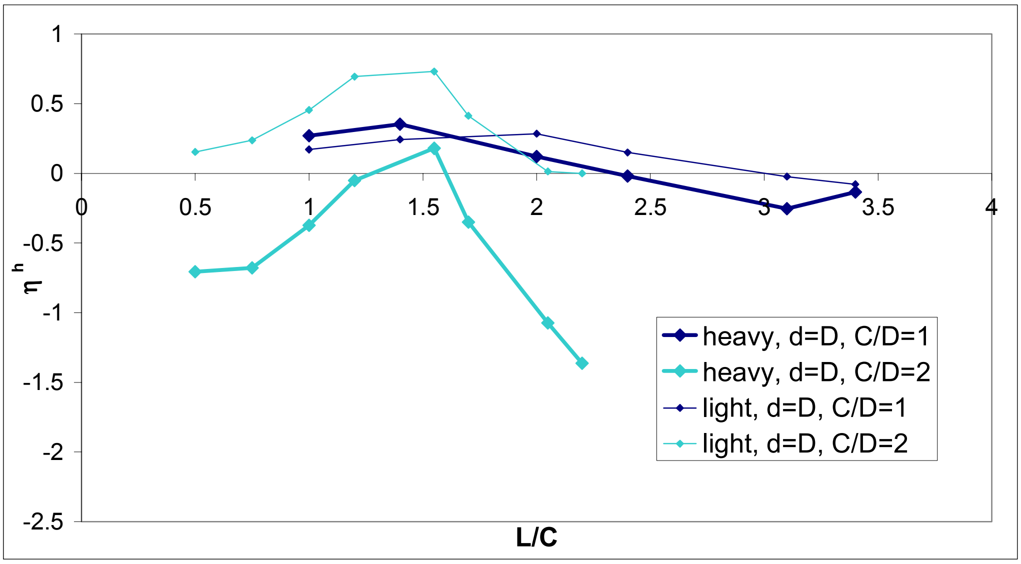

Figure V.26 – Efficiency parameter η^h as computed in numerical analyses on 'heavy' and 'light' rough and thick walls at V'=1%

In Fig. V.26, on the other hand, it can be observed that the cover has an influence on the horizontal efficiency, as the corresponding profiles are sensibly different.

Remarks

Provided that the ground loss during the construction is controlled, a diaphragm wall can be effective in reducing settlements, depending mainly on its length, weight and roughness.

A rough wall should be light enough. This can be achieved either by reducing its self-weight or by reducing its stiffness.

The vertical efficiency of a light enough, rough wall increases with its length tending to an asymptote:

- walls as light as soil and shorter than about 1.5C increase settlements rather than reduce them;
- walls as light as soil and longer than 3C do not provide further increase in vertical efficiency.

The vertical efficiency behind a complete smooth wall is generally positive, provided that the shear discontinuity is long enough, but not too long:

- the wall should reach and possibly overcome the crown level;
- it is not worth deepening the wall below the invert level.

The vertical efficiency in front of a complete smooth wall is always negative, but settlements reduce with the wall length.

The diaphragm wall can also be effective in reducing horizontal displacements, depending mainly on its roughness and length, but also on the tunnel cover.

A rough wall has a limited range of lengths were it is positively effective: light and stiff walls have a wider range and they needs a shorter length to become effective.

A smooth wall has a very high horizontal efficiency, but decreasing with length.

In conclusion of this Chapter, it seems important to stress on the fact that the proposed efficiency parameters are necessarily a simplification of the ground movement patterns which occur in front and at the back of the wall. Therefore, they give a useful but incomplete picture of the influence of such walls on the ground movements. Thus although the trends of these parameters are useful to understand a complex problem, the complete pattern of ground movements should always be kept in mind before drawing any definitive conclusion.

VI. Conclusions

Aims

Tunnelling in urban areas has become very common in recent years. As tunnel excavation induces ground movements, tunnelling beneath towns, usually in a shallow ground, could affect existing structures and induce damages of various magnitude to them. Therefore a large number of techniques can be adopted to limit the extent of the areas affected by movements and reduce their magnitude. In this research, the effect of one of this technique has been investigated. A vertical diaphragm wall can be embedded between the tunnel and the area to be protected, before tunnelling. Depending on its features it can modify the displacement field induced by tunnel excavation in a favourable way. The study has been performed with modelling techniques often adopted in soil mechanics and the results have been presented and discussed in this dissertation. In the following sections the methodology, the observations and the remarks will be summarised, the implications will be highlighted and the limitations discussed.

Methodology

The problem was investigated by physical modelling and numerical analysis. Reduced scale models were tested in centrifuge thus creating an inertial stress distribution in them which guarantees the mechanical equivalence with prototypes of full size.

A total of fourteen plane strain centrifuge model tests were successfully carried out.

Centrifuge modelling was used to measure the displacement fields occurring in different geometrical configurations of the problem. The tunnel was represented by a circular cavity under a ground cover equal to its diameter. The model soil was an overconsolidated kaolin. The excavation was simulated by reducing the air supporting pressure inside the cavity until collapse. The displacement field was determined by tracking the position of a set of plastic targets embedded in a regular grid on the exposed front of a model. In fact, a digital camera was able to capture images of the model front through a perspex window during centrifuge operation. After test, image processing allowed producing records of target co-ordinates in real space.

A test was performed in this configuration to produce a reference displacement field for comparisons. A series of tests were performed in which a diaphragm wall was embedded at a side of the tunnel. The main variables were: the location of the wall, its length, its thickness, the roughness of its interface. They were changed in a limited set of combinations following the indications of preliminary numerical analyses performed to this purpose. Therefore, a rich data base of 'case histories' was collected: this aspect seemed to be particularly important due to the lack in the technical literature of well documented cases in which similar techniques had been adopted.

A series of numerical analyses was carried out after the experimental work to compare the prediction potential of two constitutive laws with the experimental measurements and to integrate the set of configurations which had been studied in centrifuge with numerical simulation of configurations which had not been tested. The two constitutive laws were Modified Cam Clay and Three-Surface Kinematic Hardening.

After that some quantitative indications on the efficiency of the diaphragm wall had been obtained for the tunnel geometry above described, a further set of numerical analyses was performed to investigate the possibility of a limited generalisation of the results.

Observations and remarks

The integrated approach of physical modelling in centrifuge, and numerical analyses with FE, is a very powerful method of investigating geotechnical problems.

The experimental findings are summarised in the followings.

a. The measured displacement fields in no-wall models confirm what observed for similar soils in real cases. Besides the agreement of the surface settlement profile with a Gaussian distribution with the same approximation which is commonly observed, it has been observed that the measured ratio between the maximum settlement at surface and at the tunnel crown w_{max}/w_c can be predicted by using the empirical correlation proposed by Ng (1991) and based on a series of case histories.

b. In presence of a wall with a smooth interface with the soil, the displacement field induced by the tunnel excavation shows a clear discontinuity in correspondence of the wall.
c. The collapse pressure is influenced by the presence of the wall. In fact, the wall weight reduces the stability of the tunnel in the sense that collapse occurs for higher values of supporting pressure than in the no-wall model.
d. The calculated values of loading factor LF in the tests without wall, with slightly different C/D ratios and pre-consolidation pressures, when plotted as a function of the relative volume loss V' fall in a very narrow band. Mair *et al.* (1981) observed a relatively narrow band even for C/D ratios varying from 1.5 to 3.1.
e. The LF:V' curves corresponding to rough walls fall in a very narrow band together with the reference curve for the no-wall test and independently of the wall length and offset from the tunnel. The wall weight affects therefore the collapse pressure but it does not affect the loading factor.
f. The LF:V' curves corresponding to smooth walls also fall in a very narrow band (independently of the wall length, thickness and offset from the tunnel), but completely distinct from the reference curve: at the same relative volume loss V' correspond a higher loading factor LF than in the reference no-wall model. The effect of the discontinuity in shear stress transmission between the two sides of the wall is therefore very clear also in this plane.
g. The displacement fields can be compared at the same supporting pressure or at the same relative volume loss V'. As for a given tunnelling operation, hence for the same supporting pressure level, the presence of a wall changes volume loss, the choice of the criterion of comparison influences the conclusions. In fact, this difference is not very important for rough walls, whereas for smooth walls it is particularly evident in the settlement profiles on other side of the tunnel.

h. The shape of settlement distribution remains constant for a wide range of volume losses (V'=1÷10% and beyond) in tests without wall.
i. When a wall is embedded in the model, the global pattern of movements is the same at various volume losses but locally, in the vicinity of the wall, some differences arise.

The numerical analyses performed with Modified Cam Clay and 3-SKH allowed comparing the predictive potential of the two constitutive laws. Cam clay is a model which is now commonly adopted in the design practice and its parameters can be obtained by standard laboratory tests. On the other hand, 3-SKH was adopted to take into account that the strains mobilised in a tunnel construction process are usually very small and that the stress paths during the excavation have usually different directions from those which the soil has experienced during its deposition: for these reasons the deformation is ruled by a strongly non-linear stiffness which is dependent on the recent stress history of the soil. The results of calculation have been generally compared at the same supporting pressure level. This seemed a natural consequence of the fact that in the performed tests and numerical analyses the supporting pressure was controlled, whereas the volume loss only computed. Such a comparison of the numerical results with the experimental measurements led to the following remarks.

a. 3-SKH generally allows closer prediction than Cam Clay of the settlement on the vertical tunnel centre line in no-wall model.
b. It is also proved that 3-SKH is able to reproduce the non-linear behaviour at low unloading levels (or loading factors).
c. As far as the width of the settlement trough is concerned: 3-SKH overestimates *i* both compared to Cam Clay and to the experimental values; increasing the loading factor, 3-SKH predictions tend to Cam Clay: these are narrower, hence closer to the experimental values, and independent of the loading factor.
d. Both models tend to overestimate the volume loss V' compared to the measured values.

e. For a given supporting pressure, the stress state predictions of the two models are sensibly different.
f. It was possible to compare the evolution of the excess pore pressure during the test with the predicted one. 3-SKH appears generally more accurate than Cam Clay in this respect.
g. Some experimental evidences of the model with embedded wall, due to the wall weight, could not be reproduced by Cam Clay, whereas 3-SKH was successful. This is probably due to a better prediction of the stress state in the 3-SKH model.
h. The boundary effects of the mesh having the same size than the centrifuge model were investigated. The results have shown that the performed analyses were not only representative of tunnel excavation in a layer lying on rigid bedrock, but they are also a good approximation of tunnelling in an ideal half plane.

By examining the results of both tests and numerical analyses, some practical implications of this study can be outlined.
A set of efficiency parameters has been defined. They express how much the wall is able to modify the reference (without wall) profiles of settlements and horizontal displacements. When the efficiency is equal to unity, the embedded diaphragm wall is completely effective to reduce displacements, whereas when it is zero, the wall is useless to this purpose. In some tests and in the relevant numerical analyses of models with walls it was observed that the displacements in the zone of interest were higher than in the reference configuration: in this case, a negative efficiency can be computed. This means that the wall effect is undesired as it does not achieve the goal it has been designed for.
The test procedure, that is the model tunnelling operation, would have suggested to compute the efficiency parameters at a given supporting pressure. Nevertheless, the volume loss is a key design parameter because it is commonly used in the practice to predict settlements which occur for a given excavation technology. Hence, it seemed

convenient to compute efficiencies on displacement profiles pertaining to the same volume loss.

The analysis of the computed values of efficiency, together with a general picture of the whole set of experimental and numerical results, has allowed to draw the following remarks.

a. <u>Settlements</u>. Provided that the ground loss during the construction is controlled, a diaphragm wall can be effective in reducing settlements, depending mainly on its length, weight and roughness. A main distinction have to be operated between rough and smooth walls.

   a.1. *Rough walls.* A rough wall should be light enough. This can be achieved either by reducing its self-weight or by reducing its stiffness. The vertical efficiency of a light enough, rough wall increases with its length tending to an asymptote:

   - walls as light as soil and shorter than about one and half cover increase settlements rather than reduce them;
   - walls as light as soil and longer than three times cover do not provide further increase in vertical efficiency.

   a.2. *Smooth walls.* The vertical efficiency behind a complete smooth wall is generally positive, provided that the shear discontinuity is long enough, but not too long:

   - the wall should reach and possibly overcome the crown level;
   - it is not worth deepening the wall below the invert level.

   In front of a complete smooth wall, the vertical efficiency is always negative, but settlements reduce with the wall length.

b. <u>Horizontal displacements</u>. Diaphragm walls can also be effective in reducing horizontal displacements, depending mainly on roughness and length, but also on the tunnel cover.

   b.1. *Rough walls* have a limited range of lengths were they are positively effective. In general, light and stiff walls have a wider range and they need a shorter length to become effective.

   b.2. *Smooth walls* have a very high horizontal efficiency, but decreasing with length.

c. Slopes and horizontal strains. Depending on their location and length, the presence of walls can induce a beneficial sagging where in the reference conditions without walls the ground was hogging.

Limitations and further work

The applicability of the findings of this research should not be intended out of the scope of the work. Centrifuge modelling has been a powerful tool to produce reliable data, and numerical analyses, with a sophisticated constitutive model, have permitted to extend and improve the interpretation of the experimental results. Nevertheless, a rigorous assessment of the findings against field observations, in various ground conditions, would be a necessary step before giving a general validity to the conclusions which have been drawn.

Moreover, the overview of the results and the experience which has been gained during the research work, have suggested some indications for further investigation, as shown immediately next.

Experimental work.

- The effect of the wall self weight could be investigated in centrifuge, by changing the wall material. It would be important to verify that physical models with light walls confirm the positive effect of such walls in reducing ground movements.
- The effects of the wall installations have been completely neglected: the walls in the tests and numerical analyses performed can be intended as 'wished in place'. It seems necessary to find alternative ways to embed the wall in the model, in order to study the influence of installation. To this purpose, for instance, it would be useful to cast the wall during the centrifuge flight.
- Different soils or long term conditions, with the same model geometry, should be tested.
- The wall could be instrumented in order to measure the loads acting on it during excavation.

- A stiff lining could be provided to the cavity. This could be also specially designed to allow applying a given amount of contraction, as this is more likely in the case of closed shield tunnelling.
- Different linings with different flexural stiffness could be used and instrumented in order to study the effect of the diaphragm wall on the loads acting on the tunnel lining.

Numerical analysis.

Some of the abovementioned aspects (installation, soil characteristics, lining) could be investigated by finite element analysis. This would be useful also as a preliminary tool in planning the centrifuge activity and designing the relevant instrumentation. Moreover, the constitutive model could be improved or changed in order to take into account the constitutive issues which influence tunnel-induced deformation of soft ground, as discussed in Chapter II. In this study the effect of recent stress history and small strain stiffness have been considered. It would be interesting to calibrate on some of the performed tests a constitutive law allowing for soil anisotropy and use it for predictions. In this sense, some efforts would be useful to improve the prediction of the settlement trough width in greenfield conditions.

Protective measures.

An implication of the effect of the wall self weight is that alignments of jet-grouting columns, which can be assimilated to a light and rough wall, can be very effective in reducing settlements. Nevertheless, in this case the effect of high-pressure grouting very close to existing structures have to be carefully assessed.

From a technological point of view, some efforts could be spent to study a construction process able to provide a smooth discontinuity in the soil. The results of this research do not exclude the efficiency of plastic (bentonite) diaphragms, but the installation effects are in that case very important and need to be carefully considered.

Finally, this research was limited to the effects of a vertical diaphragm wall. But the wall could be inclined, propped or anchored. Different configurations of more than one wall can be used. These and other techniques, which are commonly adopted in practice, could be investigated with the same methodology in order to give further contributions to insert empirical solutions to the problem in a rational framework.

Appendix 1 – Construction aspects of soft ground tunnelling

Introduction

Tunnelling technology is a very important aspect of tunnel construction, as it largely affects the interaction between the construction process and the nearby environment. It is a crucial issue particularly when control and mitigation of ground movements has to be performed. Modelling construction processes, however, needs to identify the essential details which have to be modelled, whereas secondary factors have to be taken into account in a simplified way. Many reasonable approximations have been done in configuring both the centrifuge and the numerical models which have been studied in this research. Therefore, a short overview of the principal excavation techniques is proposed in this Appendix, in order to remark the differences between the simplified models which have been studied and the real cases.

The techniques which are usually adopted for tunnel excavation (*cf.* Mair and Taylor, 1997; Leca, Leblais and Kuhnenn, 2000) can be classified as:

- traditional methods
- shield tunnelling

Traditional methods

Excavation with conventional methods, which are sometime referred to as NATM (New Austrian Tunnelling Method), can be performed with either full or partial heading. A primary (provisional) lining can be adopted to sustain the excavation before the secondary (definitive) is finished, but a final lining can directly be installed if the ground around is preliminarily conditioned and improved (soil treatments and pre-lining techniques).

Traditionally, the excavation is immediately lined with steel ribs and sprayed (sometimes reinforced) concrete (SCL, ShotCrete Lining). The definitive lining is installed afterward, usually by cast-in-place reinforced concrete. In more recent years, many progresses have been done, which allowed developing more flexible tunnel support systems, thus reducing loads acting on lining. However, in urban areas it is important, on the contrary, reducing ground movements, hence SCL can be adopted only if accompanied by preventive measures to reduce movements below existing buildings.

If partial heading excavation is performed, as it is usual when the tunnel section is not circular, portions of tunnel section are excavated subsequently and each one is lined in order to ensure the stability of the excavation. The phase sequence is not univocally defined: very common is the 'top-heading and bench' excavation (Fig.1), in which the crown is excavated and lined before, then the bench and, finally, the invert; also common is the 'side drift excavation', where lateral drifts are excavated before, then crown, after bench and finally invert; sometimes a pilot tunnel of smaller diameter than the full tunnel is excavated before and enlarged afterward (Fig.2).

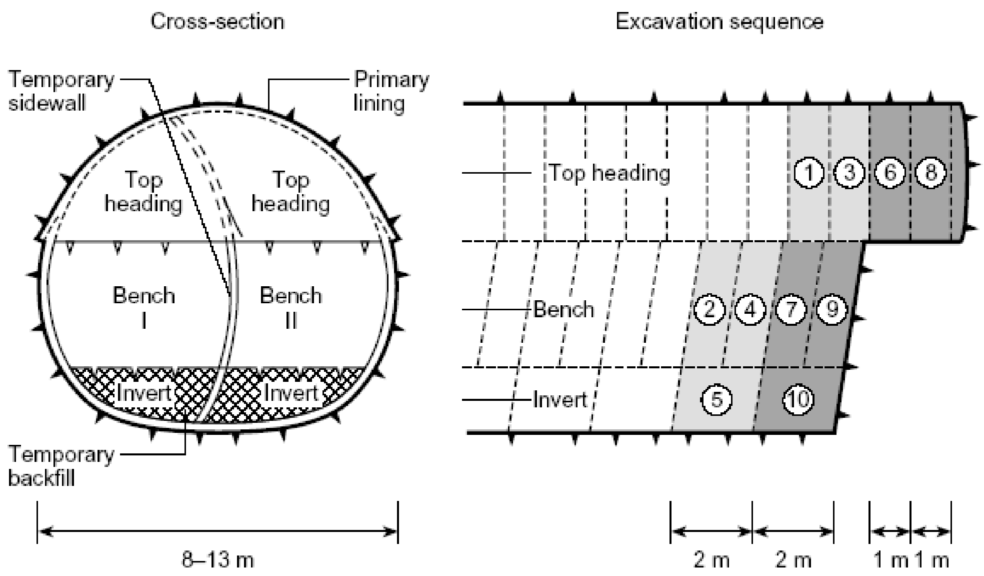

Fig. 1 – Use of divided face in NATM construction (after Mair and Jardine, 2001)

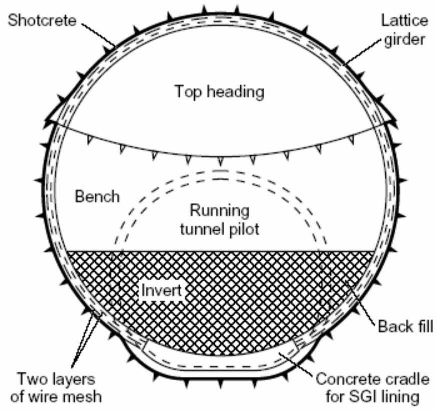

Fig. 2 – Use of pilot tunnel in NATM construction (after Mair and Jardine, 2001)

Several techniques have been developed in recent years to obtain a certain degree of structural support at the front before excavation: among the others, radial and face bolting, jet-grouting or micropiles umbrella or concrete pre-vaulting. Radial bolting is usually performed together with shotcrete lining, whereas the face bolting is usually needed when the excavation of the whole heading is performed. Usually these pre-lining and soil reinforcement techniques are used in combination and they should be accompanied by tunnel instrumentation, to verify the adequacy of design.

A recent report on geotechnical aspect of current underground construction in Japan (Akagi, 2002) shows that the use of traditional methods of excavation in soft ground increased in that country in the last decade. The so called 'Urban NATM' was seldom adopted before, due to the small amount of documented case histories in alluvial soil. It is now commonly assumed that it can be performed if the undrained shear strength c_u is equal at least to 50 kPa and the 'elastic modulus' E not lower than 10 MPa (Akagi, 2002). However, this method is not used in difficult ground water conditions and it needs to adopt auxiliary protections against ground movements, as mentioned above.

Shield tunnelling

The need for a faster tunnel construction led to adopt excavation techniques which allowed installing the long-term lining soon after the excavation. Shields are used to this purpose, also in open face excavations (Fig.3), but in the last decades many progresses have been done in constructing and using closed-face shields. TBMs (Tunnel Boring Machines) are able to pressurise the front and to sustain with their shields the lateral boundary of the cavity up to their tail. The provisional lining can be therefore avoided provided that the definitive one is installed just after the TBM: this is usually a pre-cast concrete (but also cast-iron or steel) segmented lining.

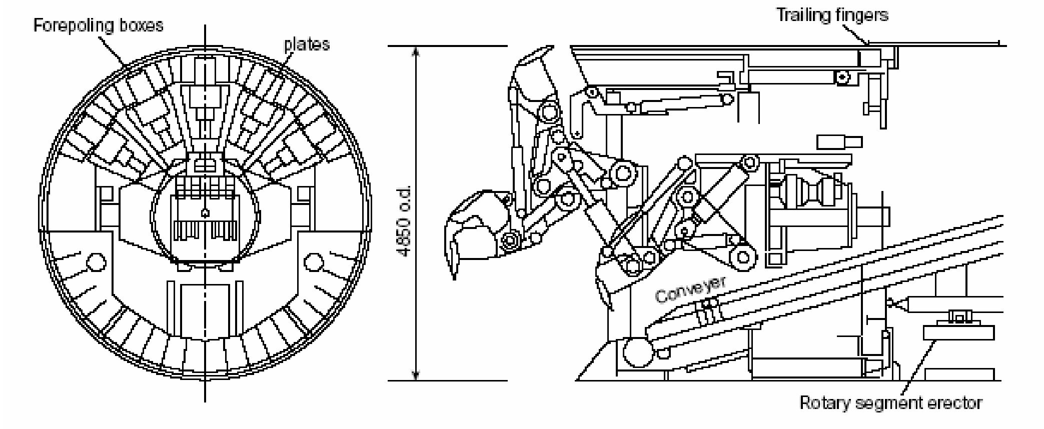

Fig. 3 – Kind of open shield and back-hoe machine used in Jubulee Linee Extension (after Mair and Jardine, 2001)

This kind of tunnellers is nowadays extensively used in the excavation of circular tunnels beneath urban areas and in difficult ground conditions. The most common are the slurry shields (Fig. 4) and the Earth Pressure Balance (EPB) shields (Fig.5).

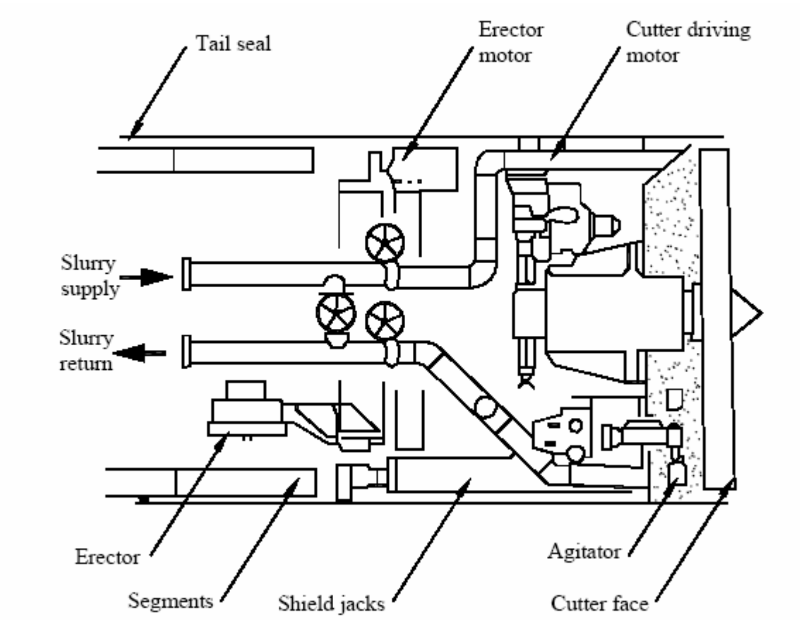

Fig. 4 – Sketch of a slurry shield machine(after Fujita, 1989)

The slurry shields use bentonite (or polymer based) slurry to stabilise the working face of the tunnel and they were introduced in the early 1960s in the UK. They are commonly used in water bearing granular soils. The EPB shields were introduced a decade after and they can be used for every kind of soil. They provide face support by retaining the spoils in a chamber until a sufficient confining pressure is reached which balances the earth and water pressure in the ground. Compressed air has also been used to support the face, but this technique is effective in soils with low permeability.

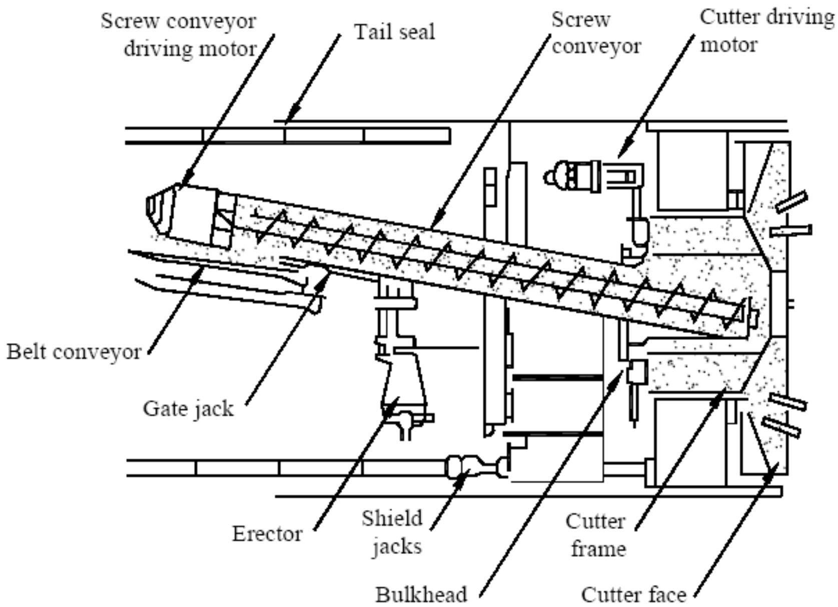

Fig. 5 – Sketch of a EPB shield machine(after Fujita, 1989)

The shield construction industry is now devoted to design sophisticated shields which are able to change their configuration during the excavation in order to face different types of soils, which is a very important issue of concern in a very heterogeneous subsoil.

The progress in shields technology and the increased experience of workmanship nowadays allowed lower tunnel-induced ground movements than in the past, but still they are variables which influence a lot the potential of predicting accurately such induced movements.

In Fig. 6 is shown a sketch of the main components of ground movement caused by tunnelling with a shield. Depending on the kind of adopted shield, these components have a different relative weight on the total amount of ground loss around the excavation.

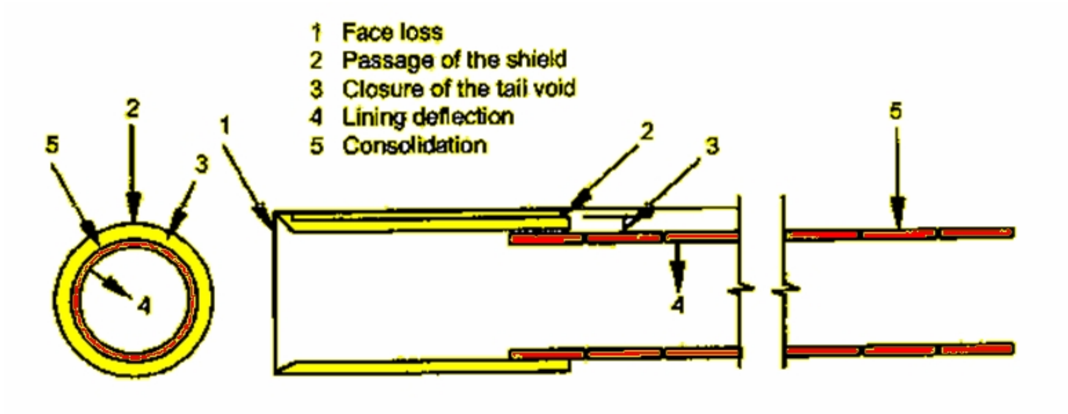

Fig. 6 – Components of ground movements induced by shield excavation (after Cording, 1991)

It can be observed clearly that the deformation processes occurring during tunnelling are a very complex three-dimensional problem which is rather difficult to reproduce completely in modelling.

The problem becomes more complex when the excavation interacts with existing excavations or structures in the vicinity. Therefore simplifications, like those which have been done in the experiments and numerical analyses which are at the basis of this dissertation, are necessary and inevitable.

Appendix 2 – Principles of Centrifuge Modelling

Introduction

Even if already in the 19th century the Anglo-French engineer Edouard Phillips proposed centrifugal force as a means for carrying out tests in reduced-scale models (Craig, 1989), the first centrifuge tests dates back to the 1930's when the first rudimental centrifuge tests were carried out simultaneously by Davidenkov and Pokrovskii in USSR and Bucky in the USA. The first publication in a geotechnical context was at the First International Conference on Soil Mechanics and Foundation Engineering in 1936. Between 1930 and 1970 a number of centrifuges were installed in the USSR, but the isolation of the Soviet Bloc after the second world war caused a general neglecting of the method in the western bloc. Only in the late 1960's, the centrifuge was rediscovered and papers on centrifuge testing appeared at the 7th ICSMFE. A strong boost to the centrifuge testing came then from the UK and particularly from Andrew Schofield at the University of Cambridge. The first International Conference on Geotechnical Centrifuge Modelling was held in Paris in 1988. In Italy, the first and only operating centrifuge was designed and developed for geotechnical purposes by ISMES.

The experimental work at the basis of this dissertation was carried out at the City University London which was the third centre in the UK to have a geotechnical centrifuge testing facility, in 1989.

Principles and scaling laws

The centrifuge is a powerful tool for testing reduced scale models in which the appropriate scaling laws are respected (Schofield, 1980; Taylor, 1995). The main point concerning centrifuge testing is that a stress distribution can be created in the model in such a way that the stress level in every point is the same as in the homologous point in the prototype:

$$\sigma_{vm} = \sigma_{vp} \qquad (1)$$

This feature is very useful in geotechnical models, as the mechanical behaviour of soil is stress dependent, and it is particularly important in problems dominated by self-weight effects, as is the case of movements induced by tunnel excavation. When the model size is equal to 1/N of the prototype size, the model has to be accelerated to N times Earth's gravity in order to achieve the stress distribution which guarantees the mechanical equivalence between the model and the prototype.

As Newton's laws of motion state, by pulling a mass in a radial path, a radial acceleration is imposed to it:

$$a = \omega^2 r \qquad (2)$$

where ω is the angular velocity (rad/s)

r is the radius from centre of rotation (m)

The small model in a centrifuge is hence at rest in an inertial force field N times stronger than the Earth's gravity g, where:

$$N = \frac{a}{g} \qquad (3)$$

The basic scaling law for centrifuge models follows from the need to ensure a mechanical equivalence with the prototype, hence, from (1):

$$\rho g h_m = \rho N g h_p \qquad (4)$$

Where ρ is the density of the material; if the same material is used in the model as the prototype, then the scaling law for length is:

$$h_m = h_p N^{-1} \qquad (5)$$

and the scaling factor (model:prototype) for linear dimensions is 1:N.

Therefore, the 1:N scale model must be accelerated to N times gravity to simulate the prototype stress distribution (Fig. 1).

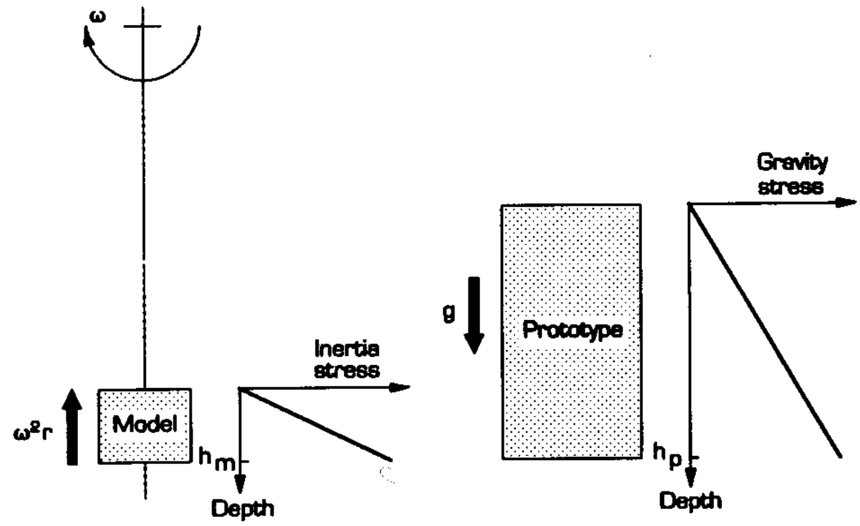

Fig.1 – Inertial stresses in a centrifuge model induced by rotation about a fixed axis correspond to gravitational stresses in the corresponding prototype (Taylor, 1995)

As strains are dimensionless, this sole scaling law provides that the same part of the soil stress-strain curve is mobilised in a prototype point and its homologous in the model.

Other scaling laws can be derived, depending on the problem. In the problem presented in this dissertation, the time of consolidation is a relevant variable and its scaling law can be easily determined by using dimensional analysis. In fact, the time factor T_v, which is used to describe the degree of consolidation, is a dimensionless parameter, hence:

$$T_{vm} = T_{vp} \tag{6}$$

or

$$c_{vm}\frac{t_m}{H_m^{\ 2}} = c_{vp}\frac{t_p}{H_p^{\ 2}} \qquad \text{(6bis)}$$

where c_v is the coefficient of consolidation, t is the time and H is a distance related to a drainage path length.

Since (5) applies to H, then the scaling law for the time of consolidation is:

$$t_m = \frac{1}{N^2}\frac{c_{vp}}{c_{vm}}t_p \tag{7}$$

Hence, if the prototype soil and the model soil are the same, then the scale factor for consolidation time is 1:N^2.

Inherent errors

Variability of acceleration along the model depth

An error which is usually acceptable in centrifuge modelling is to assume that the acceleration a is constant along the model depth, whereas it slightly increases with the radius. As it is shown in Fig. 2 if the prototype and model vertical stresses are equated at a depth $\frac{2}{3}h$, the maximum under-stress occurs at $\frac{h}{3}$, whereas the maximum over-stress is at depth h. Moreover, in this case the relative under-stress and over-stress are equal, therefore the error is minimised.

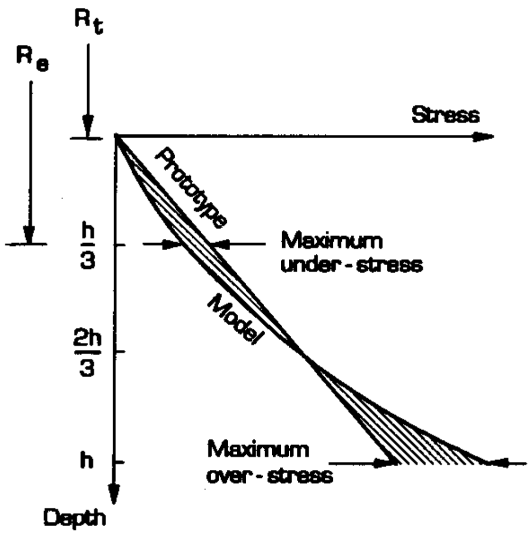

Fig.2 – Comparison of stress variation with depth in a centrifuge model and its prototype (Taylor, 1995)

In practice, by introducing in (2) an equivalent radius

$$R_e = R_t + \frac{h_m}{3} \qquad (8)$$

where R_t is the radius of the top of the model and h_m the model height, the exact correspondence in stress between model and prototype occurs at two-thirds model depth and, by assuming an usual ratio $h_m / R_e \leq 0.2$, the error in the stress profile is approximately 3% (Taylor, 1995).

Lateral component of acceleration

A second source of error is the fact that the acceleration field is directed towards the axis of rotation. This means that the acceleration vectors are radial, hence assuming that they are vertical in the model reference frame is correct only along the model centre line: in all the other points a lateral acceleration arises, which increases the more the considered point is far from the centre line. In order to minimise this component, it is important that the major vertical plane of the model lies in the vertical radial plane. In the tests conducted in this research, this maximum lateral acceleration was about 0.6% of the vertical one and occurred at the boundaries of the model top surface.

Coriolis acceleration

The Coriolis acceleration a_c is related to the angular velocity ω of the centrifuge and the velocity v of a mass within the model as:

$$a_c = 2\omega v \tag{9}$$

It is a spurious component of acceleration which arises when there is a movement in the model in the plane of rotation and acts in that plane, perpendicularly to the velocity v. As $a = \omega^2 r$, it can be shown that until $v \leq 0.05\omega r$, the ratio a_c/a is less than 10% hence, as generally assumed, the Coriolis effect is negligible. In the tests carried out in this research, all the events were undoubtedly slower than this limit.

Particle size effect

It is not easy to answer the question whether or not the scaling laws should be applied to the particle size. It is generally accepted that as far as the model soil behaves as a continuum, the particle size should not be scaled: hence it can be used the in the model the same soil which is in the prototype. In order to verify the continuum-like behaviour, the grain size should be compared to some important dimension in the model. In this study, the most important dimension appears to be the tunnel diameter, which is thousands times larger than the particles size. Therefore, the effects of the grain size on the problem are negligible.

Appendix 3 – Constitutive laws

Introduction

In this Appendix some constitutive laws will be shortly presented. They have been adopted to model the soil in the finite element analyses. They are: Modified Cam Clay (Roscoe and Burland, 1968), Three-Surfaces Kinematic Hardening (Stallebrass, 1990), Hardening Soil Model (Schanz, 1999). The main characteristics of the last two models will be outlined, whereas the Cam Clay model will not be presented here, as it is discussed in details in every Soil Mechanics textbook.

Modified Cam Clay

The meaning of the model parameters is outlined in Tab. 1.

Table 1 – Cam Clay parameters

symbol	description
λ	*slope of isotropic compression line in* v:lnp' *plane*
κ	*slope of unload-reload lines in* v:lnp' *plane*
e_{cs}	*reference void ratio on critical state line when p'=1 kPa*
M	*slope of critical state line in* q:p' *plane*
ν	*Poisson's ratio*

Three-Surfaces Kinematic Hardening (3-SKH)

The 3-SKH Model was originally defined in the triaxial space. Two kinematic surfaces were added to the Modified Cam Clay boundary surface (Fig.1a). They lye inside the state boundary surface, which is not anymore a yielding surface as in Cam Clay. The outer surface is defined by

$f_o = 0$, where:

$$f_o = \frac{q^2}{\mathrm{M}^2} + \left(p' - p'_o\right)^2 - p'^2_o \tag{1}$$

In Eq. (1) p'^2_o is half the isotropic pre-consolidation pressure p'_c: the bounding surface is symmetric about the p' axis and passes through the origin.

Inside the boundary surface, the two kinematic surfaces have the same shape but a smaller size.

The intermediate surface, or history surface, is defined by $f_a = 0$, where:

$$f_a = \frac{(q - q_a)^2}{\mathrm{M}^2} + \left(p' - p'_a\right)^2 - T^2 p'^2_o \tag{2}$$

The centre of the history surface is defined by (p'_a, q_a), whereas T is the ratio between its size and the size of the boundary surface.

Inside the history surface, the yield surface is defined by $f_b = 0$, where:

$$f_b = \frac{(q - q_b)^2}{\mathrm{M}^2} + \left(p' - p'_b\right)^2 - T^2 S^2 p'^2_o \tag{3}$$

The centre of the yield surface is defined by (p'_b, q_b), whereas S is the ratio between its size and the size of the history surface.

Inside the yield surface the behaviour of the soil is isotropic elastic:

$$\begin{bmatrix} \delta\varepsilon^e_v \\ \delta\varepsilon^e_s \end{bmatrix} = \begin{bmatrix} \kappa^*/p' & 0 \\ 0 & 3G_e \end{bmatrix} \begin{bmatrix} \delta p' \\ \delta q \end{bmatrix} \tag{4}$$

The elastic shear modulus G_e can be expressed following Viggiani (1992) as:

$$\frac{G_e}{p_r} = A\left(\frac{p'}{p_r}\right)^n R_o{}^m \tag{5}$$

where R_o is the overconsolidation ratio and p_r a reference pressure.

The swelling parameter κ^* is derived from a ln$v$:lnp' graph (Butterfield, 1979).

The hardening law is the same as in Modified Cam Clay:

$$\delta p'_o = \frac{p'_o}{\lambda^* - \kappa^*} \delta\varepsilon^p_v \tag{6}$$

The three surfaces expand and contract at the same time, keeping constant their size ratios, depending on the changes in plastic volumetric strain. As well as κ^*, the compression parameter λ^* is derived from a ln*v*:ln*p'* graph (Butterfield, 1979).

Plastic flow on the kinematic yield surface is associated, hence the relative magnitudes of shear and volumetric strain are governed by the normality rule.

Two translation rules control the movement of the two kinematic surfaces: they are dragged by the current stress state during loading and the translation rules ensure that they do not intersect and they meet each other with a common outward tangent.

Each kinematic surface has two components of translation: one is related to the expansion or contraction of the three surfaces, which causes itself a displacement of the centre point; the second is caused by the displacement of the stress state point when it lies on the surface and drags it along its path. This translation must occur along the vector which joins the stress state with its conjugate on the surface the stress state is approaching to. That is, if the stress state lies on the yielding (inner) surface, the vector γ is defined as that joining it to its conjugate point on the history (intermediate) surface; if the stress state lies on the history surface, the vector β is defined as that joining it to its conjugate point on the bounding (outer) surface (Fig. 1b).

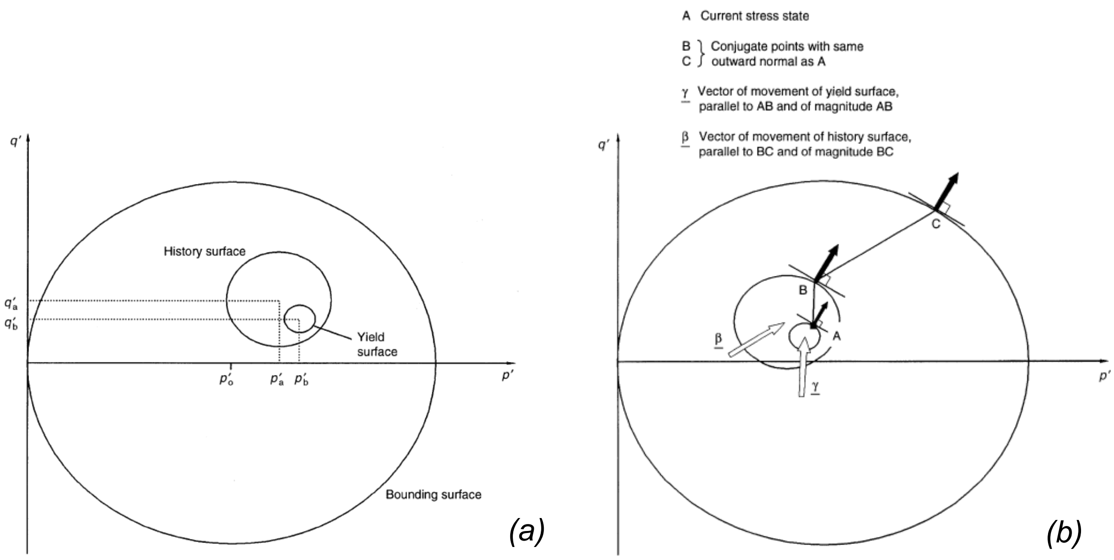

Fig.1 – Three surfaces of 3-SKH model and principles of the translation rules (Stallebrass & Taylor, 1997)

Therefore, the full expressions of the two translation rules are the following:

$$\begin{bmatrix} \delta p'_a \\ \delta q_a \end{bmatrix} = \frac{\delta p'_o}{p'_o}\begin{bmatrix} p'_a \\ q_a \end{bmatrix} + W\begin{bmatrix} \dfrac{p'-p'_a}{T} - (p'-p'_o) \\ \dfrac{q-q_a}{T} - q \end{bmatrix} \tag{7}$$

$$\begin{bmatrix} \delta p'_b \\ \delta q_b \end{bmatrix} = \frac{\delta p'_o}{p'_o}\begin{bmatrix} p'_b \\ q_b \end{bmatrix} + Z\begin{bmatrix} \dfrac{p'-p'_b}{S} - (p'-p'_a) \\ \dfrac{q-q_b}{S} - (q-q_a) \end{bmatrix} \tag{8}$$

respectively for the yield and the history surface. The values W and Z can be determined by imposing the consistency condition on the surfaces:

$$\delta f_a = 0 \tag{9}$$

$$\delta f_b = 0 \tag{10}$$

When two surfaces are in contact each other, the translation rules simplify as follows:

$$\begin{bmatrix} \delta p'_a \\ \delta q_a \end{bmatrix} = (1-T)\begin{bmatrix} \delta p' \\ \delta q \end{bmatrix} + T\begin{bmatrix} \delta p'_o \\ 0 \end{bmatrix} \tag{11}$$

$$\begin{bmatrix} \delta p'_b \\ \delta q_b \end{bmatrix} = (1-S)\begin{bmatrix} \delta p' \\ \delta q \end{bmatrix} + S\begin{bmatrix} \delta p'_a \\ \delta q_a \end{bmatrix} \tag{12}$$

The hardening modulus is developed for the special case when all the surfaces are in contact and then generalised. By combining the hardening rule and the normality rule (plastic flow is associate) the following equation can be derived:

$$\begin{bmatrix} \delta \varepsilon_v^p \\ \delta \varepsilon_s^p \end{bmatrix} = \frac{1}{h}\begin{bmatrix} (p'-p'_b)^2 & (p'-p'_b)\dfrac{(q-q_b)}{\mathrm{M}^2} \\ (p'-p'_b)\dfrac{(q-q_b)}{\mathrm{M}^2} & \left(\dfrac{(q-q_b)}{\mathrm{M}^2}\right)^2 \end{bmatrix}\begin{bmatrix} \delta p' \\ \delta q \end{bmatrix} \tag{13}$$

where

$$h = h_o + H_1 + H_2 \tag{14}$$

In the special case when all three surfaces are in contact, $H_1 + H_2 = 0$ and

$$h = h_o = \frac{(p'-p'_b)}{(\lambda^* - \kappa^*)}\left[p'(p'-p'_b) + q\frac{(q-q_b)}{\mathrm{M}^2} \right] \tag{15}$$

In the general case H_1 and H_2 were added to solve a problem of instability (the function predicts infinite strains) at a number of points on the kinematic surfaces. They were defined so that they guarantee continuity in stiffness when two or more surfaces are in contact. They cannot be negative, because plastic strains have to be lowest when the stress state lies on the yield surface ($H_2 \geq 0$) and greatest when it lies on the bounding surface ($H_1 \geq 0$). Moreover, $H_2=0$ when the stress state lies within the bounding surface on the history and yield surface, so that both these surfaces are predicting the same strains.

The functions H_1 and H_2 are defined by the following equations:

$$H_1 = S^2 \left(\frac{b_1}{b_{1\max}} \right)^{\psi} \frac{1}{\lambda^* - \kappa^*} p'^3_o \tag{16}$$

$$H_2 = \left(\frac{Tb_2}{b_{2\max}} \right)^{\psi} \frac{1}{\lambda^* - \kappa^*} p'^3_o \tag{17}$$

Where b_1 is the degree of approach of the history surface to the bounding surface, and b_2 the degree of approach of the yield surface to the history surface. They are defined when the stress state is on the yield surface only, b_1 as the scalar products of the vector β and the normal at the conjugate point on the history surface, divided by T, and b_2 as the scalar products of the vector γ and the normal at the current stress point, divided by S. The maximum values that the two functions can assume are:

$$b_{1\max} = 2p'_o(1-T) \tag{18}$$

$$b_{2\max} = 2Tp'_o(1-S) \tag{19}$$

The exponent ψ controls the decay of stiffness inside the bounding surface.

The meaning of the model parameters is outlined in Tab. 2.

Table 2 – 3-SKH parameters

symbol	**description**
λ^*	*slope of isotropic compression line in* lnv:lnp' *plane*
κ^*	*slope of unload-reload lines in* lnv:lnp' *plane*
e_{cs}	*reference void ratio on critical state line when p'=1 kPa*
M	*slope of critical state line in* q:p' *plane*
G_e	*elastic shear modulus (also given as A, m, n)*
T	*ratio of the size of the history surface to the size of the bounding surface*

S	*ratio of the size of the yield surface to the size of the history surface*
ψ	*exponent in the hardening function defining the rate of decay of stiffness inside the bounding surface*

Hardening Soil Model (HS)

At the basis of the model is the hyperbolic relationship between the axial strain and the deviatoric stress in the primary triaxial loading.

$$\varepsilon_1 = \frac{q_a}{2E_{50}} \frac{(\sigma_1 - \sigma_3)}{q_a - (\sigma_1 - \sigma_3)} \qquad \text{for } q < q_f \qquad (20)$$

In (1) the ultimate deviatoric stress q_f and the asymptotic value q_a are defined as:

$$q_f = \frac{6\sin\phi_{pk}}{3 - \sin\phi_{pk}}\left(p + c\cot\phi_{pk}\right) \qquad (21)$$

$$q_a = \frac{q_f}{R_f} \qquad (22)$$

where ϕ_{pk} is the peak friction angle , c the cohesion, as defined in the Mohr-Coulomb failure criterion and R_f a failure ratio which is used to fit the experimental data in the hyperbolic relationship and it is smaller than unity. (Fig. 2)

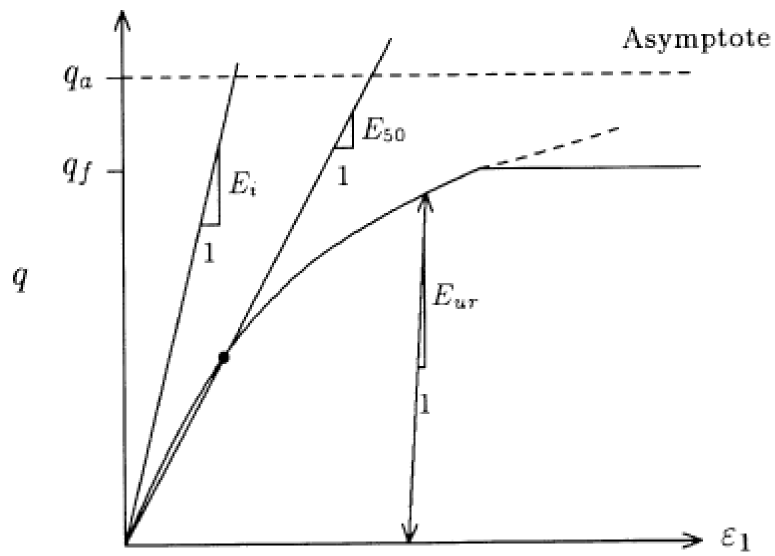

Fig. 2 - Hyperbolic stress-strain relationship in primary loading for a drained triaxial test (Schanz et al.*, 1999)*

The parameter E_{50} is the stress dependent secant stiffness modulus for primary loading at 50% of the maximum shear strength q_f and it is given by:

$$E_{50} = E_{50}^{ref} \left(\frac{\sigma_3 + c\cot\phi_{pk}}{p^{ref} + c\cot\phi_{pk}} \right)^m \tag{23}$$

where E_{50}^{ref} is a reference modulus corresponding to the reference pressure p^{ref}. The amount of stress dependency is given by the power m.

Unloading-reloading stress paths are modelled as elastic through another stress dependent stiffness modulus:

$$E_{ur} = E_{ur}^{ref} \left(\frac{\sigma_3 + c\cot\phi_{pk}}{p^{ref} + c\cot\phi_{pk}} \right)^m \tag{24}$$

and a Poisson's ratio ν_{ur}.

For the triaxial case, the yield function is defined as:

$$f = \frac{1}{E_{50}} \frac{q}{1 - q/q_a} - \frac{2q}{E_{ur}} - \gamma_p \tag{25}$$

where $\gamma^p = \varepsilon_1^p - \varepsilon_2^p - \varepsilon_3^p$ (26)

For a given value of the hardening parameter γ^p the yield condition f=0 defines a shear yield surface as shown in the plane p':q in Fig. 3.

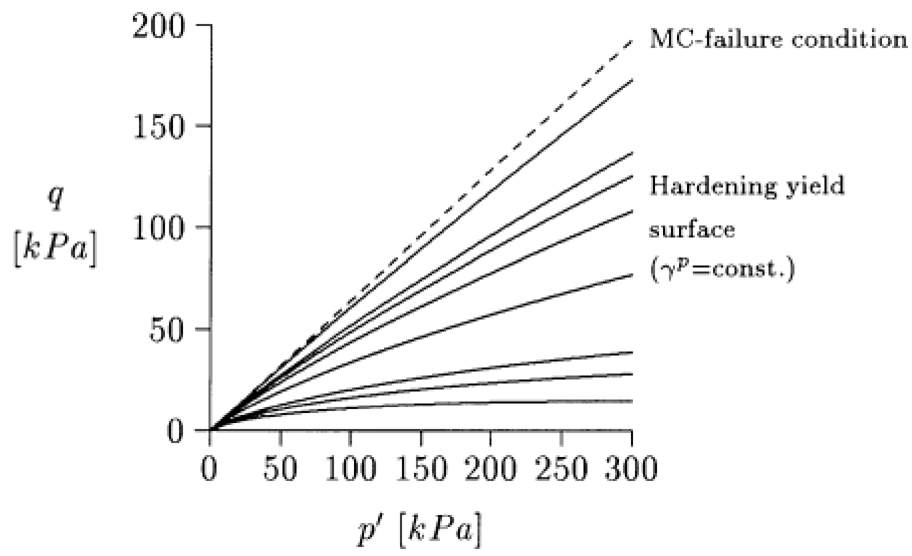

Fig. 3 - Successive yield loci for various values of the hardening parameter γ_p up to failure (Schanz et al., *1999)*

In order to extend the model to general 3D states of stress, the following general yield function is adopted:

$$f = \tilde{q} - \tilde{\mathrm{M}}\left(p + c\cot\phi_m\right) \tag{27}$$

where:

$$\tilde{q} = \sigma'_1 + (\alpha - 1)\sigma'_2 - \alpha\sigma'_3 \tag{28}$$

$$\alpha = \frac{3 + \sin\phi_m}{3 - \sin\phi_m} \tag{29}$$

$$\tilde{\mathrm{M}} = \frac{6\sin\phi_m}{3 - \sin\phi_m} \tag{30}$$

The flow rule which links the plastic volumetric strain rate $\delta\varepsilon_v^p$ to the plastic shear strain rate $\delta\gamma_v^p$ is:

$$\delta\varepsilon_v^p = \sin\psi_m \delta\gamma^p \tag{31}$$

The mobilised dilatancy angle ψ_m is defined as a function of the mobilised angle of shearing resistance ϕ_m, its value at peak failure ϕ_{pk} and the parameter ψ_{pk} which is the peak (maximum) dilatancy angle.

Following the framework of Schanz and Vermeer (1996) the following expression can be derived:

$$\sin\psi_m = \frac{\sin\phi_m\left(1 - \sin\phi_{pk}\sin\psi_{pk}\right) - \sin\phi_{pk} + \sin\psi_{pk}}{1 - \sin\phi_{pk}\sin\psi_{pk} - \sin\phi_m\left(\sin\phi_{pk} - \sin\psi_{pk}\right)} \tag{32}$$

The above definition of the flow rule is equivalent to the definition of a plastic potential which in the general 3D stress state has the following expression:

$$g = q^* - \mathrm{M}^*\left(p + c\cot\psi_m\right) \tag{33}$$

where:

$$q^* = \sigma'_1 + (\beta - 1)\sigma'_2 - \beta\sigma'_3 \tag{34}$$

$$\beta = \frac{3+\sin\psi_m}{3-\sin\psi_m} \tag{35}$$

$$\mathrm{M}^* = \frac{6\sin\psi_m}{3-\sin\psi_m} \tag{36}$$

The deviatoric hardening law implicitly expressed by the yield condition f=0 (shear yield surfaces) is not able to reproduce the plastic volume strains which is observed in isotropic compression. Hence, a second type of yield surface, a so-called 'cap', is defined to limit the elastic region in the direction of the p' axis.

The cap yield surface is defined as:

$$f_c = \frac{\tilde{q}^2}{M^2} + \left(p + c\cot\phi_m\right)^2 - \left(p_c + c\cot\phi_m\right)^2 \tag{37}$$

where p_c is the isotropic pre-consolidation stress and M is an auxiliary model parameter which is not directly assessed, as it will be discussed later.

The cap hardening law is defined in isotropic compression as:

$$\delta\varepsilon_v^c = \frac{\delta p_c}{H} \tag{38}$$

where H is an hardening modulus which express a relation between the elastic swelling modulus and the elasto-plastic compression modulus.

The flow rule on the cap is assumed associate, therefore the plastic potential coincides with the yield surface:

$$g_c = f_c \tag{39}$$

By combining (37), (38) and (39) with the consistency condition $\delta f = 0$, the following expression for the cap volumetric strain can be derived:

$$\varepsilon_v^c = \frac{H}{m+1}\left(\frac{p_c}{p_{ref}}\right)^{m+1} \tag{40}$$

Both H and M are auxiliary material parameters but they are not directly used as input parameters. Instead, they are defined through relationships:

$$K_o^{NC} = K_o^{NC}(\ldots, M, H) \tag{41}$$

$$E_{oed}^{ref} = E_{oed}^{ref}(\ldots, M, H) \tag{42}$$

Therefore K_o^{NC} and E_{oed}^{ref} are used, at the place, as input parameters: K_o^{NC} can be easily assessed as $K_o^{NC} = 1 - \sin\phi_{pk}$, whereas E_{oed}^{ref} is calculated on an oedometer primary loading curve as a tangent stiffness at a reference vertical stress. The oedometer stiffness dependency on the stress level can be hence expressed by:

$$E_{oed} = E_{oed}^{ref}\left(\frac{\sigma_1 + c\cot\phi_{pk}}{p^{ref} + c\cot\phi_{pk}}\right)^m \tag{43}$$

The meaning of the model parameters is outlined in Tab. 3.

Table 3 – Hardening Soil parameters

symbol	**description**
E_{50}^{ref}	*reference secant stiffness modulus corresponding to the reference confining pressure p_{ref}*
E_{ur}^{ref}	*reference Young's modulus for unloading and reloading, corresponding to the reference confining pressure p_{ref}*
E_{oed}^{ref}	*reference tangent stiffness modulus for primary oedometer loading at the reference pressure p_{ref}*
c	*cohesion*
ϕ_{pk}	*friction angle*
ψ_{pk}	*angle of dilatancy*
ν_{ur}	*Poisson's ratio for unloading-reloading*
m	*power for stress-level dependency of stiffness*
K_o^{nc}	*K_o value for normal consolidation*
R_f	*failure ratio q_f/q_a*

References and bibliography

Addenbrooke, T.I. (1996), Numerical analysis of tunnelling in stiff clay, *PhD Thesis*, Imperial College of Science, Technology and Medicine, London

Addenbrooke, T.I., Potts, D.M. and Puzrin, A.M. (1997), The influence of pre-failure soil stiffness on the numerical analysis of tunnel construction, *Geotechnique*, 47 (3), 693-712

Akagi, H. (2002), Geotechnical aspects of current underground construction in Japan*, Proc. 3rd international symposium on geotechnical aspects of underground construction in soft ground (Kastner, Emeriault, Dias, Guilloux eds.) – IS-Toulouse 2002*, 3-14.

Al Hallak, R., Leca, E., Magnan, J.P., Garnier, J. (2000), Etude expérimentale et numérique du renforcement du front de taille par boulonnage dans les tunnels en terrains meubles, *Etudes et Recherches des Laboratoires des Ponts et Chaussées,* Paris.

Al-Tabbaa, A. (1987), Permeability and stress-strain response of Speswhite kaolin, *PhD Thesis,* University of Cambridge.

Atkinson, J.H., Potts, D.M., Schofield, A.N. (1977), Centrifugal model tests on shallow tunnels in sand, *Tunnels and tunnelling*, 9 (1), 59-64

Attewell, P.B. and Farmer, I.W. (1974), Ground deformations resulting from shield tunnelling in London Clay, *Canadian Geotechnical Journal*, 11, no.3, 380-395.

Attewell, P.B. and Woodman, J.P. (1982), Predicting the dynamics of ground settlement and its derivatives caused by tunnelling in soil. *Ground Engineering*, vol.15, no.7, 13-22.

Baker, W.H., MacPherson, H.H. and Cording, E.J. (1980), Compaction grouting to limit ground movements: instrumented case history evaluation of the Bolton Hill Subway Tunnels, Baltimore, MD*., Technical report,* US Dept. of Transportation.

Boscardin, M.D., Cording, E.J. (1989), Building response to excavation-induced settlement, *Journal of Geotechnical Engineering (ASCE)*, vol.115, no.1, 1-21.

Boulon, M., Armand, G., Flavigny, E., Roy, M. (1996), Modélisation en éléments finis du phasage des travaux de creusement et de soutènement d'un tunnel urbain band les alluvions, *AFTES – Journées d'études internationale de Chambery*, 1996.

Britto, A.M. and Gunn, M.J. (1987), Critical State Soil Mechanics via Finite Elements, Ellis Horwood, Chichester.

Burd, H.J., Houlsby, G.T., Augarde, C.E. (2000), Modelling tunnelling-induced settlement of masonry buildings. *Proc. ICE Geotechnical Engineering*, 2000, 143, January, 17-29.

Burland, J.B., Broms, B.B and De Mello, V.F.B. (1977), Behaviour of foundations and structures, *State of the art report, Session 2, Proc. 9th Int Conf SMFE, Tokyo,* 2, 495-546

Burland, J.B., Broms, B.B., de Mello, V.F. (1977), Behaviour of foundations and structures, 9th ICSMFE, Tokyo, vol.2, 495-546.

Burland, J. B. and Puzrin, A. S (1997). Non-linear model of small strain behaviour of soils. Geotechnique, (in press for publication in 1998).

Burland, J.B., Standing, J.R., Jardine, F.M. (eds.) (2001), Building response to tunnelling, vols.1 & 2, CIRIA - London

Burland, J.B. and Wroth, C.P. (1974), Settlement of building and associate damage, *Proc. Conf. on Settlement of Structures*, Cambridge, 611-654.

Butterfield, R. (1979), A natural compression law for soils, *Geotechnique* 29, No.4, 469-480.

Chambon, P., Corté, J.F., Garnier, J.I., Koenig, D. (1991), Face stability of shallow tunnels in granular soils, *Centrifuge '91*, 99-105

Chambosse, G. and Otterbein, R. (2003), Central Station, Antwerp – Compensation grouting under heavily loaded foundations, *Proc. Int. Conf. On Response of buildings to excavation-induced ground movements*, London, CIRIA, 207-212

Chen, X.L., Liu, Y.H., Cao, W.H. and He, Z.F. (1998), Protection for the former observatory during construction of the Yan An Dong Lu Tunnel, *Tunnels and Metropolises,* Negro Jr & Ferreira (eds.), 1083-1088

Clough, G.W. and Schmidt, B (1981), Design and performance of excavations and tunnels in soft clay. *Soft Clay Engineering*, Elsevier, 569-634.

Cording, E.J. (1991), Control of ground movements around tunnels in soil, General report, *Proc. 9th Pan American Conf. Soil Mechanics and Foundation Engineering*, Buenos Aires, 571-632.

Cording, E.J. and Hansmire, W.H. (1975), Displacements around soft ground tunnels. *General report 5th Pan American Conference on Soil Mechanics and Foundation Engineering*, Buenos Aires, Session IV, 571-632.

Craig, W. H. (1989), Centenary Biography: Edouard Phillips (1821-89) and the idea of centrifuge modelling, *Géotechnique*, 39, no. 4, 697-700.

Davis, E.H., Gunn, M.J., Mair, R.J., Seneviratne, H.N. (1980), The stability of shallow tunnels and underground openings in cohesive material, *Géotechnique*, 30, no. 4, 397-416.

Forbes, J. and Finch, A.P. (1996), Application of compensation grouting to the St. Clair River Tunnel project, *Proc. Int. Symp. on Geotechnical Aspects of Underground Construction in Soft Ground*, London (Mair & Taylor eds.), 343-348.

Fujita, K. (1989), Underground construction, tunnel, underground transportation, Special Lecture B, *Proceedings 12th International Conference on Soil Mechanics and Foundation Engineering*, Rio de Janeiro, vol. 4, 2159-2176.

Gens, A. (1995), Prediction, performance and design, *Proc. Int. Symp. Pre-failure Deformation of Geomaterials* (Shibuya, Mitachi & Miura eds.), Sapporo, vol.2, 1233-1247.

Grant, R.J. (1998), Movements around a tunnel in 2-layer ground, *PhD Thesis,* City University, London.

Grant, R.J. (1998), Prediction of pre-failure ground movements due to tunnelling: physical and numerical modelling, *Proc. Int. Workshop on Prediction and Performance in Geotechnical Engineering*, Napoli, 329-356.

Grant, R.J. and Taylor, R.N. (1996), Centrifuge modelling of ground movements due to tunnelling in layered ground. *Proc. Int. Symp. on Geotechnical Aspects of Underground Construction in Soft Ground*, London (Mair & Taylor eds.), 507-512.

Hansmire, W.H. and Cording, E.J. (1985), Soil tunnel test section: case history summary. *Journal of Geotechnical Engineering (ASCE)*, vol.111, no.11, 1301-1320.

Harris, D.I. (2001), Protective measures, in *Building response to tunnelling,* Burland, Standing and Jardine (eds.), vol.1, 135-176

Honda, T., Hibino, T., Kuwano, J (2001), Centrifuge model tests on deformation mechanism of nail reinforced sand ground around shallow tunnel, *Geotechnical Engineering in Soft Ground, Proc. Reg. Conf. Shanghai 2001*, 554-559

Jardine, R. J., Potts, D. M., Fourie, A. B. & Burland, J. B.(1986), Studies of the influence of non-linear stress-strain characteristics in soil-structure interaction, *Geotechnique*, 36 (3), 377-396.

Kerry Rowe, R. and Kack, G.J. (1983), A theoretical examination of the settlement induced by tunnelling: four case histories, *Canadian Geotechnical Journal*, 20, 299-314.

Kerry Rowe, R., Lo, K.Y., Kack, G.J. (1983), A method of estimating surface settlement above tunnels constructed in soft ground, *Canadian Geotechnical Journal*, 20, 11-22.

Kimura, T. and Mair, R.J. (1981), Centrifugal testing of model tunnels in soft clay, *Proc. 10th ICSMFE,* Stockholm, vol.1, 319-322.

Ladd, C.C. and Edgers, L. (1972), Consolidated-undrained direct-simple shear tests on saturated clays, *MIT, Dept. of Civil Eng. Research report*, R72-82.

Leca, E., Leblais, Y., Kuhnhenn, K. (2000), Underground works in soils and in soft rock tunneling. *Proc. GEOEng 2000*, Melbourne, vol.1, 220-268.

Lee, K.M., Kerry Rowe, R., Lo, K.Y. (1992a), Subsidence owing to tunnelling. I. Estimating the gap parameter, *Canadian Geotechnical Journal*, 29, 929-940.

Lee, K.M., Kerry Rowe, R., Lo, K.Y. (1992b), Subsidence owing to tunnelling. II. Evaluation of a prediction technique, *Canadian Geotechnical Journal*, 29, 941-954.

Lee, S.W., Dasari, G.R., Mair, R.J., Bolton, M.D., Soga, K., Sugiyama, T., Ano, Y, Hagiwara, T., Nomoto, M. (1999), The effects of compensation grouting on segmental tunnel linings, *Geotechnical Aspects of Underground Construction in Soft Ground,* Kusakabe,Fujita & Miyazaki (eds), 257-262.

Lembo-Fazio, A. and Ribacchi, R. (1986), Stato di sforzo e deformazione intorno ad una galleria, MIR 86, n.11, 1-36.

Littlejohn, S. (2003), The development of practice in permeation and compensation grouting. A historical review (1802-2002), *Proc. ASCE 3rd Int. Conf. on Grouting and Ground treatment,* vol. 1, 100-144

Lunardi, P. and Focaracci, A. (1998), Mechanical pre-cutting for the construction of the 21.5 m span arch of the 'Baldo degli Ubaldi' Station on the Rome Underground, *Tunnels and Metropolises,* Negro Jr & Ferreira (eds.), 1001-1007

Maiorano, R.M.S. and Viggiani, G.M.B. (2003), Observed movements above a tunnel in pyroclastic ground, *Proc. Int. Conf. On Response of buildings to excavation-induced ground movements,* London, CIRIA, 375-386

Mair, R.J. (1979), Centrifugal modelling of tunnel construction in soft clay, *PhD Thesis,* Cambridge University

Mair, R.J. (1993), Unwin Memorial Lecture 1992. Developments in geotechnical engineering research :application to tunnels and deep excavations, *Proc. ICE, Civ. Engng,* 93, Feb., 27-41

Mair, R.J., Gunn, M.J., O'Reilly, M.P. (1981), Ground movements around shallow tunnels in soft clay, *Proc. 10th Int. Conf. Soil Mechanics and Foundations Engineering*, Stockholm, Vol. 1, 323-328.

Mair, R.J. and Taylor, R.N. (1993), Prediction of clay behaviour around tunnels using plasticity solutions, *Predictive Soil Mechanics. Proc. Wroth Memorial Symposium*, Oxford, 449-463.

Mair, R.J. and Taylor, R.N. (1997), Bored tunnelling in the urban environment, *Theme lecture, 14th ECSMGE – Hamburg*, 2353 – 2385

Mair, R.J., Taylor, R.N., Burland, J.B. (1996), Prediction of ground movements and assessment of risk of building damage due to bored tunnelling, *Proc. Int. Symp. on Geotechnical Aspects of Underground Construction in Soft Ground*, London (Mair & Taylor eds.), 713-718

Melis, M., Trabada, J., Oteo, C., Sola, P. (1998), Crossing of an underground tunnel bored in clayey sand under an old railway tunnel in Madrid, *Tunnels and Metropolises,* Negro Jr & Ferreira (eds.), 1041-1046

Melis, M.J., Oteo, C., Sola, P.R, Monroe, A. S. (2003), Compensation grouting for the Madrid Metro, *Proc. Int. Conf. On Response of buildings to excavation-induced ground movements,* London, CIRIA, 537-544

Mesri, G. (1975), Discussion: New design procedure for stability of soft clays, *Proc. ASCE, Journal of the Geotechnical Engineering Division*, 101(GT4), 409-12.

Meyerhof, G.G. (1976), Bearing capacity and settlement of pile foundations, 11th Terzaghi Lecture, *Proc. ASCE, Journal of the Geotechnical Engineering Division*, 102(GT3), 417-30.

Miliziano, S., Soccodato, F.M., Burghignoli, A. (2002), Evaluation of damage in masonry buildings due to tunnelling in clayey soils, *Proc. 3rd Int. Symp. Geotechnical Aspects of Underground Constructions in Soft Ground* – Toulouse. pp

Morrison, P.R.J. (1994), Performance of foundations in a rising groundwater environment, *PhD Thesis,* City University, London.

Muir Wood, A.M. (1975), The circular tunnel in elastic ground, *Géotechnique*, 25, no.1, 115-127.

Muir Wood, D. (1990), Soil Behaviour and Critical State Soil Mechanics, Cambridge University Press.

Ng, R.M.C. (1991), A procedure for prediction of settlement due to tunnels in clays, *Proc. 9th Pan American Conf. Soil Mechanics and Foundations Engineering*, Vina del Mar, Chile, vol. 3, 1413-1430.

O'Reilly, M.P. and New, B.M. (1982), Settlements above tunnels in the United Kingdom – their magnitude and prediction, *Proc. Tunnelling '82 Symp.,* Institution of Mining and Metallurgy, London, 55-64

Oteo, C.S., Arnaiz, M, Trabada, J., Melis, M., Mendana, F., (1999), Experiences in the subsidence problems in Madrid Subway Extension, *Geotechnical Aspects of Underground Construction in Soft Ground,* Kusakabe, Fujita & Miyazaki (eds), 275-280

Panet, M. & Guenot, A. (1982), Analysis of convergence behind the face of a tunnel, *Proc. Tunnelling 82*, IMM, London, 197-204.

Peck, R.B. (1969), Deep excavations and tunnelling in soft ground, *Proc. 7th ICSMFE*, Mexico City, State of the Art Volume, 225-290.

Polshin, D.E. and Tokar, R.A. (1957), Maximum allowable non-uniform settlement of structures, *Proc. 4th ICSMFE*, London, vol.1, 402-405.

Pototschnik, M.J. (1992), Settlement reduction by soil fracture grouting, *Proc. ASCE Conf. on Grouting, Soil Improvement and Geosynthetics,* vol 1, 398-409

Potts, D.M. (1976), Behaviour of lined and unlined tunnels in sand, *PhD Thesis,* Cambridge University

Potts, D.M. and Addenbrooke, T.I. (1997), A structure's influence on tunnelling-induced ground movements, *Proc. ICE Geotechnical Engineering*, 1997, 125, April, 109-125

Quick, H., Michael, J. and Arslan, U. (2003), About the effect of preliminary in-tunnel measures on ground movements due to tunnelling, *Proc. Int. Conf. On Response of buildings to excavation-induced ground movements,* London, CIRIA, 503-512

Roscoe, K.H. and Burland, J.B. (1968), On the generalised stress-strain behaviour of a 'wet' clay, in *Engineering plasticity,* Heyman & Leckie (eds.), 535-609

Sagaseta, C. (1987), Analysis of undrained soil deformation due to ground loss, *Géotechnique*, 37, no.3, 301-320.

Samarasekera, L. & Eisenstein, Z. (1992), Pore pressure around tunnels in clay, *Cananadian Geotechnical Journal*, 29, 819-831.

Schanz, T. and Vermeer, P.A. (1996), Angles of friction and dilatancy of sand, *Géotechnique*, 46, no. 1, 145-151.

Schofield, A.N. (1980), Cambridge geotechnical centrifuge operations, *Géotechnique*, 30, no. 3, 227-268

Simpson, B., Atkinson, J. H. & Jovicic, V. (1996), The influence of anisotropy on calculations of ground settlements above tunnels, *Proceedings of the international symposium on geotechnical aspects of underground construction in soft ground*, London (Mair & Taylor eds.), Balkema, pp. 511-514.

Sola, P.R., Guardia, A.C., Monroe, A.S. (2003), Underpinning with compaction grouting in gypsum karst under two buildings in the south east of Madrid, *Proc. Int. Conf. On*

Response of buildings to excavation-induced ground movements, London, CIRIA, 525-530

Sola, P.R., Monroe, A.S., Garces, J (2003), Ground treatments using grouting for the extension of the metro in Lisbon, *Proc. Int. Conf. On Response of buildings to excavation-induced ground movements,* London, CIRIA, 531-536

Sola, P.R., Monroe, A.S., Martin, L., Blanco, M.A., San Juan, R. (2003), Ground treatment for tunnel construction on the Madrid Metro, *Proc. ASCE 3rd Int. Conf. on Grouting and Ground treatment,* vol. 1, 1518 – 1533

Stallebrass, S.E. (1990), Modelling the effect of recent stress history on the deformation of overconsolidated soils, *PhD Thesis,* City University, London.

Stallebrass, S.E., Jovičić, V. and Taylor, R.N. (1994a), The influence of recent stress history on ground movements around tunnels, *Proc. Int. Symp. Pre-failure Deformation of Geomaterials* (Shibuya, Mitachi & Miura eds.), Sapporo, 615-620.

Stallebrass, S.E., Jovičić, V. and Taylor, R.N. (1994b), Short term and long term settlements around a tunnel in stiff clay, *Proc. 3rd European Conf. Numerical Methods in Geotechnical Engineering – ECONMIG 94,* (Smith ed.), Manchester, 235-240.

Stallebrass, S.E. and Taylor, R.N. (1997), The development and evaluation of a constitutive model for the prediction of ground movements in overconsolidated clay, *Géotechnique* 47, No.2, 235-255.

Standing, J. R., Nyren, R. J., Longworth, T. I. & Burland, J. B. (1996), The measurement of ground movements due to tunnelling at two control sites along the Jubilee Line Extension, *Proceedings of the international symposium on geotechnical aspects of underground construction in soft ground*, London (Mair & Taylor eds.), Balkema, 751-756

Taylor, R.N. (1995), Geotechnical centrifuge technology, Blackie Academic & Professional.

Taylor, R.N., Grant, R.J., Robson, S., Kuwano, J. (1998), An image analysis system for determining plane and 3-D displacements in soil models, *Centrifuge '98*, Kimura, Kusakabe & Takemura (eds), Balkema, 73-78.

Timoshenko, S. (1957), Strength of materials, Part I - D. Van Nostrand inc., London

Verruijt, A. & Booker, J.R. (1996), Surface settlements due to deformation of a tunnel in an elastic half plane, *Géotechnique*, 46, no.4, 753-756.

Viggiani, G.M.B. (1992), Small strain stiffness of fine grained soils, *PhD Thesis*, City University, London.